COMBUSTION OF CS_2/O_2 IN A LAMINAR MIXING LAYER AND PROCESSES IN THE CO CHEMICAL LASER

Thesis by

William Mark Grossman

In Partial Fulfillment of the Requirements

for the Degree of

Doctor of Philosophy

California Institute of Technology

Pasadena, California

1979

(Submitted September 5, 1978)

ACKNOWLEDGMENTS

Professor F.E.C. Culick has my deepest appreciation for the help, patience, and criticism he willingly afforded as my advisor. The suggestions and cooperation of Dr. Alan Vetter helped mold this work on a daily basis. Thanks go to Professor E. E. Zukoski for his concern and advice during this work, and Mark Kushner with whom discussions clarified many points in this thesis.

Much of the experimental apparatus was constructed with the help of Ty Linton, who cleverly made things work a little better.

The encouragement through the years by my parents, Vivienne and Eli, is most dearly appreciated.

Thanks also go to Ruth Stratton who typed the manuscript.

This work was funded in part by AFOSR 74-2694.

ABSTRACT

The combustion of CS_2 and O_2 in a free burning laminar mixing layer at low pressure was investigated using emission spectroscopy. The temperature fields, CO vibrational distributions, and CO concentrations were measured. The data indicate that vibrationally excited CO was produced in the mixing layer flames, but that there were no vibrational population inversions. In comparison with the CS_2/O_2 premixed flames, the mixing layer flames favored greater production of COS and CO_2. Computer modeling was used to study the mechanisms responsible for the production of COS and CO_2, and to study how the branching chain mechanism responsible for production of CO affects the behavior of the mixing layer flame. The influences of the gas additives, N_2O, COS, and CNBr, were also investigated.

Summary

Free burning CS_2/O_2 laminar mixing layer flames were investigated using emission spectroscopy. Typically, the pressures were about .01 atm, and the flow velocities about 1m/sec. The mixing was laminar. One product of CS_2/O_2 flames is vibrationally excited CO, which can be used as the active medium in a chemical laser. In this study, the effect of the mixing on the combustion was studied. In a mixing layer flame, the reactants diffuse toward each other opposing outward diffusion of products. The reactants do not meet until they have nearly reached the adiabatic flame temperature for the flame burning at the stoichiometric ratio. In premixed flames, the reactants are in continual contact, and reactions commence at lower temperatures.

The CS_2/O_2 laminar mixing layer flames were found to produce vibrationally excited CO just downstream of the leading edge of the flames, but population inversions were not found. The CO vibrational distributions equilibrated within a few centimeters of the leading edge of the mixing layer flames.

A blue-white visibly luminescing zone extended downstream over 10 centimeters. This region was often skewed toward the CS_2 stream more sharply as the relative velocity of the CS_2 stream decreased. Temperature measurements using spectroscopic means and thermocouples indicated that the maximum temperatures were in excess of 2500°K. The maximum temperatures were found displaced a few centimeters toward the side of the O_2 stream from the region of brightest visible emission.

Computer predictions and experimental evidence imply that the species concentrations are stratified across the flame. CS is found

toward the CS_2 stream and O toward the O_2 stream with the remaining intermediates and products nested more symmetrically between the reactant streams.

A few centimeters downstream of the leading edge of the mixing layer flame, COS and CO_2 were found. Their concentrations were larger in the mixing layer flame than in premixed flames. Computer modeling indicated that the COS and CO_2 production was dominated by the reactions, $CS_2 + O \rightarrow COS + S$ and $COS + O \rightarrow CO_2 + S$. Because the production of CO_2 must await the buildup in the concentrations of COS and O, it is delayed slightly downstream. At elevated temperatures the reaction path $CS_2 + O \rightarrow COS + S$ competes more favorably with the reaction path $CS_2 + O \rightarrow CS + SO$; this second path leads to the production of vibrationally excited CO. The COS producing path has a greater probability in the mixing layer flame than in the premixed flame, because the reactants are at elevated temperatures before meeting in the mixing layer flame.

Using the computer modeling, predictions were made of the CO production as a function of the position in a mixing layer flame. The production maximum occurred between 1 and 1.5 cm downstream of the start of the mixing layer, and decreased further downstream. The reactions and CO production in the CS_2/O_2 flame burning by a branching chain mechanism are predicted to proceed far more rapidly than in a mixing layer flame with the same upstream conditions, but burning by a contrived straight chain mechanism.

The additives N_2O, CNBr, and COS were investigated, of which only N_2O produced strong effects. N_2O was added to premixed CS_2/O_2 fuel lean flames. N_2O has the well-known effect of selectively depopulating the

lower vibrational levels of CO, which is beneficial to CO chemical laser performance. Two additional effects were observed: increased CO_2 formation and a reduction in the laminar flame speeds.

NOMENCLATURE

a	parameter describing the deviation of the heat transfer rate from a predicted value
A	spontaneous emission coefficient
A_k	pre-exponential factor for the reaction rate constant k
$A_{vv'}$	spontaneous emission coefficient for the transition from level v to v'
$A_{(v,J)\rightarrow(v',J')}$	spontaneous emission coefficient for the transition from level (v,J) to (v',J')
α	constant determining the mean flow in the y direction in a mixing-layer flame
α_+	constant determining the mean flow in the y direction for $y > 0$, in a mixing-layer flame
α_-	constant determining the mean flow in the y direction for $y < 0$, in a mixing-layer flame
b	constant equaling $(d_2/d_1)^{1/2}$
B	rotational constant
c	speed of light
C	a constant
C_{BB}	a constant
C_p	heat capacity at constant pressure
C_v	heat capacity at constant volume
$CO(v)$	carbon monoxide in vibrational level v
$CO(v,J)$	carbon monoxide in vibrational level v, rotational level J
$[CO]$	concentration of carbon monoxide

d	diameter of a thermocouple wire
d_i	diameter of a thermocouple wire number i
$\mathcal{D}$	diffusion coefficient
$\mathcal{D}_0$	diffusion coefficient at y = 0
$\mathcal{D}_\infty$	free stream diffusion coefficient
$\mathcal{D}_i$	diffusion coefficient for species i in ambient gas
$\mathcal{D}_{ij}$	binary diffusion constant for species i and j
$\mathcal{D}_{PF}$	binary diffusion constant for product gas and fuel
$\mathcal{D}_{POx}$	binary diffusion constant for product gas and oxidant
δ	one-dimensional flame thickness
δ_S	flame thickness for species diffusion flame
δ_T	flame thickness for thermal conduction flame
E_J	energy of rotation, rotational level J
$E(v,J)$	energy of molecule in vibrational level v, rotational level J
ΔE_a	activation energy
ε	surface emissivity
η	similarity variable
$\eta(\lambda)$	optical system efficiency
f	oscillator strength
f^*	stoichiometric ratio
$f(r)$	dependence of reaction rates on r
ΔF	change in free energy in a reaction
g_{vJ}	degeneracy of level (v,J)
$g(\nu)$	lineshape

$\gamma(\nu)$	gain
Γ_i	flux of species i in the y direction
h	Planck's constant; enthalpy
ΔH_o	difference between the heat of formation of reaction products and reactants
i	formal species name
I	intensity
$I_c(\lambda)$	corrected intensity as a function of λ
$I_c(v)$	corrected intensity due to the transition from level v to v-2
$I_c(v:z,y)$	corrected intensity at (z,y) due to the transition from level v to v-2
$I_{BB}(\lambda)$	theoretical black body intensity
$I_{OBB}(\lambda)$	observed black body intensity
$I_O(\lambda)$	observed spectral intensity
$I_{vP}(J)$	intensity on P branch transition from upper level (v,J)
$I_{vR}(J)$	intensity on R branch transition from upper level (v,J)
j	formal species name
J	rotational quantum number
$J^{(n)}$	n^{th} order correction to solution for J
J_m	upper rotational level for the transition with maximum gain
k	reaction rate constant
k_α	rate constant for a unimolecular reaction

$k_{\alpha\beta}$	rate constant for a bimolecular reaction
k_B	Boltzmann's constant
$k_{vv'}$	rate constant for CO going from level v to v'
k_v^d	rate constant for deactivation from level v
K	thermal conductivity
K_G	thermal conductivity of gas
K_W	thermal conductivity of thermocouple wire
ℓ	length along thermocouple wire
ℓ_E	equilibration length in flow
Le	Lewis number
λ	wavelength
λ_o	wavelength to which monochromator is tuned
$\lambda_P(v,J)$	wavelength of P branch overtone transition from upper level (v,J)
$\lambda_R(v,J)$	wavelength of R branch overtone transition from upper level (v,J)
$\Delta\lambda$	full width at half maximum of slit function $s(\lambda)$
M(v)	species M in vibrational level v
μ	viscosity
n	index of refraction
N	number density
N_{CO}	carbon monoxide number density
N*	excited state number density
$N^{(o)}$	ground state number density

N_D	diluent number density
N_F	fuel number density
N_{Ox}	oxidant number density
N_{Ox_I}	oxidant number density prior to substituting diluent
N_P	product number density
N_0	number density at y = 0
N_{ov}	normalization constant for rotational distribution in vibrational level v
N_v	number density of carbon monoxide in level v
$N_v(J)$	number density of carbon monoxide in level v as a function of rotational level
N_{vJ}	number density of carbon monoxide in level (v,J)
$N_v(z,y)$	number density of carbon monoxide in level v at (z,y)
ΔN_v	error bound associated with measured N_v
ν	frequency; kinematic viscosity
ν_o	line center frequency
ν_∞	free stream kinematic viscosity
p	pressure
p_I	initial pressure
Pr	Prandtl number
q	heat release of reaction
$\dot{Q}$	heat generation rate
Q_r	rotational partition function
r	ratio of CS_2 mole fraction to O_2 mole fraction
r_B	radius off the optical axis

R	reaction rate
Re_d	Reynolds number with respect to d
$R_{v \rightarrow v'}$	rate for vibrational exchange associated with rate constant $k_{v,v'}$
R_v^a	rate of chemical addition of CO in level v
R_v^p	pumping rate of CO in level v by vibrational transfer
ρ	density
ρ_i	density of species i
ρ_o	density at y = 0
$s(\lambda-\lambda_o)$	transmittance efficiency
Sc	Schmidt number
σ	Stephan-Boltzmann constant
t	time
t_C	characteristic time for chemical processes
t_D	characteristic time for diffusion processes
t_{spont}	spontaneous emission lifetime
T	temperature
$T^{(n)}$	n^{th} order correction to solution for temperature
T_G	gas temperature
T_F	adiabatic flame temperature
T_o	temperature at y = 0
T_S	temperature of surrounding surfaces
T_W	thermocouple wire temperature
T_{W_n}	thermocouple wire temperature, wire number n
τ	characteristic time for a process

τ_E	characteristic time for equilibration
u,U	velocity along the z axis, parallel to the flow
U_o	U at y = 0
$U_{\pm\infty}$	U at y = $\pm\infty$
v	vibrational quantum number; mean velocity along the y axis; the laminar flame speed
v_i	mean velocity of species i along y
v_{iD}	diffusion velocity of species i along y
v_S	flame speed in the approximation of a species diffusion flame
v_T	flame speed in the approximation of a thermal conduction flame
V(z)	v at z = 0
w_B	beam radius
W	species production rate
W_i	species production rate for species i
X_i	mole fraction of species i
X_v	mole fraction of CO in level v
χ	similarity variable
y	coordinate normal to the direction of the free stream flow
y_D	characteristic distance for diffusion processes
Y_i	mass fraction of species i
Y_F	mass fraction of fuel
Y_{Ox}	mass fraction of oxidant

z	coordinate in the direction of the free stream flow

TABLE OF CONTENTS

Chapter I

A. The Motivation for Study of the CS_2/O_2 Laminar Mixing Layer Flame

Carbon monoxide chemical lasers produce stimulated emission with wavelengths in the 4.7 to 5.8 μm spectral range. Emission is due to vibrational-rotational transitions of CO. The vibrational bands on which laser output is observed vary with the device, and are among the $16 \rightarrow 15$ to $1 \rightarrow 0$ bands.

The performance of a chemical laser depends greatly on the gas processes in the laser medium. One process that is important in many continuously operating chemical lasers is mixing. The free burning CS_2/O_2 laminar mixing layer flame offers an excellent arrangement for studying the interaction of the mixing and chemical processes in a chemical laser system. CS_2/O_2 free burning flames can generate the active medium of a chemical laser. Comparison between the previously unstudied CS_2/O_2 free burning mixing layer flame and the well studied CS_2/O_2 premixed free burning flame have allowed us to isolate effects due to the mixing layer configuration.

The reaction step $CS+O \rightarrow CO(v) + S$ pumps CO chemical lasers with vibrationally excited CO [I.1]. These chemical lasers are fueled by CS_2, O_2, or their more reactive decomposition products, O, CS, and S. We will call all these systems "CS_2/O_2 systems." The laser pumping reaction $CS+O \rightarrow CO+S$, must be fed by CS and O. In free burning CS_2/O_2 flames, CS and O are generated chemically by intermediate reaction steps in the flames. Some chemical lasers are directly fueled by CS and O generated in separate dissociating devices. Predissociating the reactants results

in a more rapid chemical reaction mechanism; generally this effect is beneficial for enhanced laser power [I.2,I.3]. If the reactants, CS_2 and O_2, are predissociated, they will vigorously react upon mixing. Vibrationally excited CO is produced and proceeds to equilibrate with time. Consequently, it is advantageous for the reactants to mix and react directly upstream of, or in, the laser cavity.

Laser systems in which mixing is important include CS_2/O_2 chemical lasers in which CS_2, O_2 or both are predissociated and many of the hydrogen-halide and deuterium-halide chemical lasers. These lasers motivated our interest in mixing layer processes in chemical lasers. The question we addressed is: What is the interaction of the mixing and the chemistry in a mixing layer chemical laser as it relates to the performance of the laser?

The CS_2/O_2 flames studied to date can be separated into two categories: those in which one or both of the reactants (CS_2 and O_2) were predissociated, and those in which CS_2 was burned in a free burning flame. In all the studies on free burning CS_2/O_2 flames, the gases were either premixed or they mixed after the confluence of narrow, finely spaced streams; in both of these experimental arrangements there have been no reports of important chemistry taking place prior to the mixing. In our work, we have examined the importance of mixing on the chemistry in a CS_2/O_2 free burning mixing layer flame.

The mixing layer is a common and useful combustion configuration. It eliminates the possibility of the flame striking back upstream, and it offers a stable configuration which can be scaled to larger dimensions.

A large, optically active medium can be obtained for use in a chemical laser by lengthening the mixing layer through the use of a longer burner, or by sandwiching multiple rows of mixing layer gas injection slots. The two-dimensional mixing layer flames offer a long, optically uniform path which is convenient for diagnostics. This differs from mixing jets which lack two-dimensional uniformity. These considerations dictated our choice of the two-dimensional configuration for studying the effects of mixing in a CS_2/O_2 flame. We chose to study a laminar rather than a turbulent flame, largely for simplicity. Also, many of the currently operating chemical lasers utilizing reactive mixing are run in the laminar regime.

Several differences are anticipated between the mixing layer and the premixed CS_2/O_2 flames. The flow fields will differ because the geometries of the gas injectors differ. The spatial distribution of chemical heat sources will differ, also causing the flow fields to differ. In the mixing layer flame the reactant gases will heat prior to coming into contact with each other. This may favor different reaction mechanisms than are dominant in the premixed CS_2/O_2 flames, influencing the production of vibrationally excited CO, and affecting the environment of the product CO. Hence, for a chemical laser, the utility of the mixing layer configuration may be influenced by the interaction of the mixing layer geometry and the chemistry. It is this interaction we chose to study.

Lasers from the CS_2/O_2 system have been reported to yield nearly 500 W CW [I.4,I.5]. The hydrogen-halide and deuterium-halide chemical

laser systems have been much more successful in achieving high power, particularly those systems lasing on HF and DF. HF and DF chemical lasers are pumped by the reactions $F+H_2 \rightarrow HF+H$ and $F+D_2 \rightarrow DF+D$, respectively. The active medium consists of vibrationally excited HF or DF. The higher power attained in the HF and DF systems can be attributed in part to the relative ease in producing the oxidant, free radical fluorine, for the pumping reactions of these systems. Dissociating F_2 into F+F requires about one-third the energy needed to dissociate CS_2 into CS+S or O_2 into O+O. The HF and DF systems consequently have more rapid pumping rates, resulting in more power.

Although the HF(DF) laser systems achieve higher power, the CS_2/O_2 systems offer some distinct operating advantages. These include using safer, more easily disposed of gases; operation using free burning flames at low Mach number; and less costly operation. These are additional reasons why we found it expedient to use the CS_2/O_2 system to study the effects of mixing in a chemical laser, effects which may be common to chemical lasers in general.

The vibrational deactivation rates for HF and DF are orders of magnitude higher than for CO in their respective chemical laser environments. The combustion of H_2 and F_2 in a low, pressure-free burning flame has been studied [I.6] and inversions have not been found. However, with CS_2/O_2 combustion we can make a comparison between premixed and mixing layer free burning flames, and both may generate nonequilibrium laser media.

The chemical processes in CS_2/O_2 flames are considerably more complex than in H_2/F_2 flames because there are more elements present, and because CS_2/O_2 combustion takes place via a branching chain mechanism [I.7],

whereas H_2/F_2 combustion does not. Consequently, we were also interested in the qualitative differences, due to the distinct CS_2/O_2 chemistry, between our CS_2/O_2 mixing layer flames and H_2/F_2 and D_2/F_2 mixing layer flames of other studies.

B. Literature Survey and Discussion of Mixing Layer Flames

Introduction

In the past decades there has been a large amount of research done on flames. In this section, a brief survey of the conclusions of that work will be presented, as they are relevant to the CS_2/O_2 reacting mixing layer. The flames that will be discussed range in pressure from atmospheric to 10 torr, and were all laminar. In these flames, the Reynolds numbers with respect to the downstream distance from the burners and the free stream gas velocities range from 100 to 10,000. Emphasis will be on the differences between the mixing layer and premixed laminar flames. Mixing layer flames are often referred to as "diffusion flames" in the literature, and we use the terms interchangeably. The reader interested in a general discussion of combustion is directed to the texts [I.8- 1.12].

The Wolfhard-Parker Burner

In 1949, H. G. Wolfhard and W. G. Parker published the results of a study on NH_3-O_2 and H_2-O_2 laminar mixing layer flames [I.13]. Particular attention will be paid here to the conclusions of their work and to that of others using similar burner configurations. This emphasis is appropriate because the Wolfhard-Parker burner configuration was adopted for our study of the CS_2/O_2 mixing layer flames.

The Wolfhard-Parker burner constrains the fuel and oxidant gases to mix and react downstream from a splitter plate. The gases react in a nearly two-

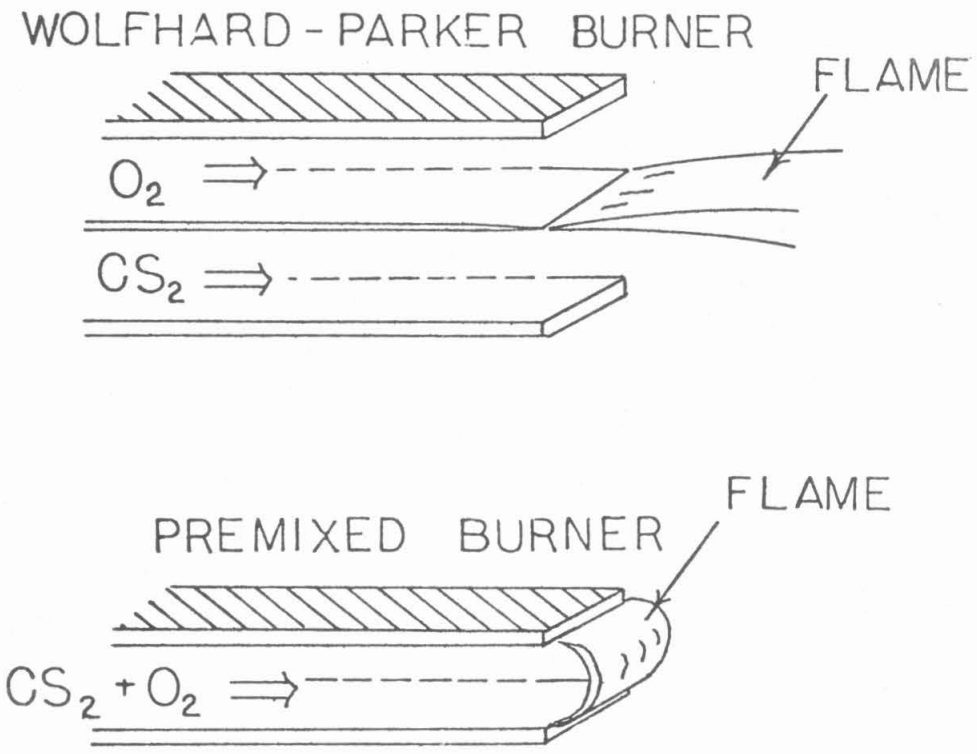

Figure I-B-1 The Wolfhard-Parker burner and the premixed gas burner

dimensional free burning flame. The Wolfhard-Parker burner and premixed flame burners are shown in Figure I-B-1. The advantages of the mixing layer flame over a premixed flame are twofold: It affords a long uniform optical path for flame studies, and it eliminates the possibility of the flame striking back upstream. With the advent of the chemical laser, a long optical path became of practical importance, as well as a convenience for diagnostics.

Various other mixing configurations have been used in chemical lasers; for examples see References I.4 and I.14. Many of the mixing and chemical reaction processes in the two-dimensional laminar mixing layer are common to more complex mixing situations. The Wolfhard-Parker burner provides a representative mixing configuration that easily accommodates spectroscopic investigation. Consequently it was chosen for most of the experimental work reported here.

Visible Flame Emission

Visible radiation is often observed from mixing layer flames. The cause of the emission varies; it may be due to ion-recombination [I.15], black body emission [I.16], or chemiluminescence; the latter is thought to dominate in CS_2/O_2 flames [I.17,I.18]. Many of the flames reported in the literature [I.13,I.15,I.16,I.19,I.20] show a strong similarity in appearance to the CS_2/O_2 flames observed in this study, in spite of the fact that the visible radiation results from different causes.

Skewing of Mixing Layer Flames

A skewing of the visibly radiating portion of mixing layer flames into one reactant stream has often been noted [I.13,I.15,I.16,I.19,I.20].

In our work we have observed a pronounced skewing in the CS_2/O_2 mixing layer toward the CS_2 stream. The severity and direction of skewing can be related to the relative diffusion constants of the reactants, the relative flow velocities of the reactants, the properties of diluents accompanying the reactants, and the stoichiometric ratio for the reaction. In most cases the CS_2/O_2 mixing layer flames observed in our studies were skewed into the CS_2 stream, probably due to the lesser CS_2 flow velocities commonly employed.

Diffusion Limited Reactions

In our flame the chemical reaction rates limit the rate of fuel consumption. We generally expect a smaller fuel consumption per unit length along the direction of flow in the mixing layer flame than in the premixed flame [I.15]. This is because the fuel consumption in a mixing layer flame is additionally limited by the diffusion processes normal to the flow direction, an influence not present in the premixed flame. The reduced production rates, with no directly linked reduction in deactivation rates for vibrationally excited CO, is likely to be detrimental when a mixing layer is used in a chemical laser.

Heat generated in a one-dimensional premixed CS_2/O_2 flame causes the flow to expand and accelerate. This causes increased convection of the equilibrated combustion products away from the region in which CO is produced in vibrational nonequilibrium. On the other hand, the expansion of chemically heated gases in a mixing layer flame may be normal to the flow direction, with the flow velocity nearly constant. This difference between the premixed and mixing layer flames favors premixed flames for use in chemical lasers.

HF and DF Chemical Lasers

The literature contains reports of many studies of hydrogen-halide and deuterium-halide mixing layer flames and chemical lasers. An excellent survey of this experimental and modeling work is presented in the review articles in Reference I.3. There are major differences between the flames in hydrogen-halide and deuterium-halide mixing layer chemical lasers and the CS_2/O_2 free burning flames. The hydrogen-halide and deuterium-halide flames often have predissociated oxidants (fluoride) and the reaction is often strictly mixing limited. The chemistry and vibrational exchange processes are considerably simpler and better understood than those in the CS_2/O_2 flames. The efforts to model the hydrogen-halide and deuterium-halide chemical lasers have progressed to the stage where there is more concern with the dynamics of mixing in high velocity, low pressure nozzles than with the details of the chemistry.

Differences between Mixing Layer and Premixed Flames

The reaction mechanisms and localization of reactions in mixing layer flames may differ from those in premixed flames [I.13]. In premixed flames the oxidant and reactant are in contact throughout the combustion process. They begin to react well before they reach the maximum flame temperature. In mixing layer flames, the reactants meet and react only after they have diffused towards each other through a region containing hot reaction intermediates and products. Characteristically, the reactants do not meet until they have nearly reached their adiabatic flame temperature [I.13]. As a result, the reaction mechanism in the mixing layer flame may differ significantly from the mechanism of the

premixed flame; for example, a reaction mechanism that is favored when the reactant temperatures are high may be more important in a mixing layer flame than in a premixed flame. Another possibility is that the fuel may thermally decompose as it diffuses toward the oxidant in a mixing layer flame, while in a premixed flame it may be decomposed only when attacked directly by the oxidant, to which it is continually exposed.

In a mixing layer flame, different reactions may occur in separate regions. The cause of this stratification may be that pyrolysis reactions occurring in the fuel precede the oxidation reactions. References I.13, I.15, I.19, and I.21-I.25 document observations of stratified chemistry across mixing layer flames using Wolfhard-Parker burners. Similar results obtained using other burner configurations are described in References I.26 and I.27. These observations of stratification in the chemical processes suggest that the chemical reaction mechanisms dominant differ from those in the corresponding premixed flames.

In ethylene-air and propane-air two-dimensional flames, the color of emission has been observed to be stratified normal to the plane of mixing [I.19]. These flames have distinct oxidizing and reducing zones, unlike premixed flames (see Figure I-B-2). This stratification does not extend all the way to the edge of the splitter plate where the flames attach; rather, in the region by the splitter plate the color of emission varies little.

If the reaction mechanism in a mixing layer flame differs from the reaction mechanism in a premixed flame, which appears to be the case for

ethylene-air and propane-air flames, the difference is minimal near the splitter plate, and greatest downstream (see Figure I-B-2). The chemical mechanism of the mixing layer flame is the same as that of a premixed flame in regions in which the characteristic time for the chemical processes greatly exceeds the characteristic time for mixing, i.e., if the gas mixes thoroughly before reacting. This is the case near the splitter plate. There, streams of pure fuel and oxidant mix. Due to the enormous concentration gradients just beyond the edge of the splitter plate, diffusive mixing is rapid and can proceed before any appreciable chemical reactions progress. Downstream, the reactants diffuse toward each other, driven by more shallow concentration gradients. The reactants, while diffusing through an environment of heated product gases, may undergo chemical reaction prior to meeting.

The degree to which a mixing layer flame may exhibit chemical mechanisms distinct from the premixed flame is pressure dependent [I.15]. Any difference between the chemical mechanisms of the mixing layer and premixed flames diminishes at lower pressures. Bimolecular chemical reaction rates increase with increasing pressure, roughly as p^2, and the bimolecular diffusion constants decrease with increasing pressure, roughly as p^{-1}. At sufficiently low pressure, or sufficiently close to the splitter plate, the mixing layer flame will exhibit the same chemical mechanism as the premixed flame, because the reactants will have been thoroughly mixed preceding any chemical reactions.

In the following pages this behavior is predicted by estimates based on known gross characteristics of reacting flows.

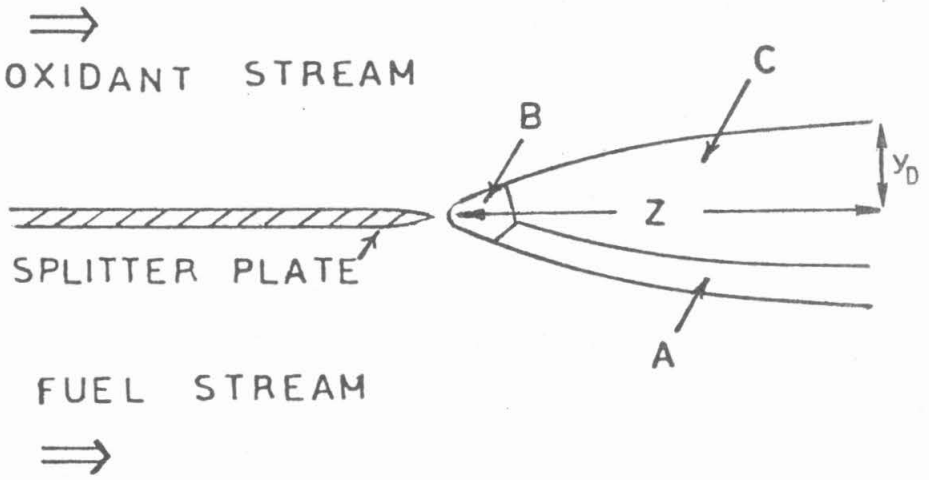

Figure I-B-2 A stratified mixing layer flame, as in Reference I.19; Region A is a pyrolysis zone; Region B is a zone in which fuel and oxidant have mixed prior to reacting; and Region C is an oxidizing zone

An Estimate of Reaction and Mixing Times

The size of the zone in which the reactants are thoroughly mixed prior to reacting can be estimated by comparing the characteristic times for diffusive mixing t_D, and the characteristic times for chemical reactions, t_C. In Figure I-B-2, the flame thickness is y_D. In Appendix A it is shown that y_D can be approximated:

$$y_D \simeq \sqrt{\mathcal{D}\, t_D}$$

where $\mathcal{D}$ is the diffusion constant. The characteristic time for the diffusion of the reactants toward each other is

$$t_D \simeq z/U$$

and the characteristic time for their chemical reaction is

$$t_C \simeq 1/(k[N])$$

respectively, where k is the rate limiting chemical reaction constant, and [N] is the molar density of the gas. U and z are the downstream velocity and distance. The characteristic time of diffusion t_D is not a function of $\mathcal{D}$ because the diffusion velocity, v_D, and the diffusion length, y_D, vary as $\sqrt{\mathcal{D}}$; consequently $t_D = y_D/v_D$ is independent of $\mathcal{D}$.

The chemical mechanism of the mixing layer flame will never differ from that of the premixed flame if the gas is thoroughly premixed prior to reacting:

$$t_D \ll t_C$$

Choosing k to be the rate for the reaction step, $SO+O_2 \rightarrow SO_2+O$, the slowest step in the 4-reaction branching chain mechanism for CS_2/O_2 combustion [I.27,I.7,I.28] and T to be 2000°K,

$$k \simeq 10^{-10} \text{ cm}^3/(\text{mole-sec})$$

and

$$[N] \simeq p \cdot 10^{-5} \text{ mole}/(\text{cm}^3\text{-sec-atm}) ,$$

consequently,

$$t_C \simeq 10^{-5} \text{ (sec-atm)}/p \quad .$$

To have $t_D \ll t_C$ with $U \simeq 100$ cm/sec requires

$$z/U \ll 10^{-5} \text{ (sec-atm)}/p \quad ,$$

hence

$$zp \ll 10^{-3} \text{ cm-atm} \quad .$$

The region in which the CS_2/O_2 mixing layer flame must have the same chemical mechanism as the premixed flame extends less than 1 cm downstream of the splitter plate at a pressure of 10^{-2}atm. Downstream, the mixing layer flame may, but need not, have a different chemical reaction mechanism from the premixed flame.

The preceding discussion based on dimensional analysis delineates the conditions under which differences in chemistry between the CS_2/O_2 mixing layer flame and the premixed flame are possible. Additionally, in the mixing layer flames, chemical reactions may occur involving reaction products that are not fully oxidized, such as CS, with reaction intermediates. This is because in a premixed flame the most reactive intermediates tend to be confined to a narrow reaction zone, while in a mixing layer flame the reactive intermediates are produced in the reaction zone, which extends downstream. Consequently in the mixing layer, the products may have prolonged contact with intermediate species, while in the premixed flame the contact is more brief. The net effect of these differences on the performance of the CS_2/O_2 chemical laser was not a priori clear.

C. History of the CO Chemical Laser

The progress in understanding and construction of CO chemical lasers spans roughly the past 12 years. In most CO chemical lasers, CS_2, O_2, or their decomposition products react to form vibrationally excited CO. The reactions were generally at low pressures, typically 3 to 60 torr. The flow velocities ranged from less than a meter per second in free burning flames, to supersonic in mixing layers using predissociated reactants. A brief history of the CS_2/O_2 systems follows. Emphasis is on the developments relevant to our study of the CS_2/O_2 laminar mixing layer flame, and many fine studies have therefore been omitted.

The First CO Chemical Lasers

Following the construction of the first electrical CO laser in 1964 [I.29], CO lasers whose energy was supplied by the exothermicity of a chemical reaction were investigated. By far the most studied and important of the CO chemical lasers have been those in which CS_2 and O_2 or their decomposition products were the reactants. Laser emission has been observed over the vibrational bands $1 \rightarrow 0$ to $16 \rightarrow 15$ [I.30], with rotational transitions typically involving rotational levels 5 to 35. Both P and R branch laser emission have been observed. Emission from these lasers has wavelengths in the range 4.7 to 5.8 μm.

The first CO chemical laser was developed in 1966. Laser emission followed the flash photolysis induced reaction of CS_2 and O_2 [I.31]. In

1969, a CO chemical laser was reported in which laser emission followed the electrically pulsed initiation of the reaction between CS_2 and O_2 [I.32]. Further studies of pulsed CO chemical lasers [I.30] showed that CO is selectively produced in high vibrational levels, with a maximum production near level v = 13. With increasing time after the CO is formed, the CO molecules vibrationally equilibrate, and the stimulated emission occurs on successively lower vibrational transitions.

The Free Burning CS_2/O_2 Flame Laser

In 1970, a vibrational inversion was reported in a free burning CS_2/O_2 flame [I.33]. This result suggested that a continuously operating CO chemical laser might be possible. Shortly after, a transversely flowing CO chemical laser was operated [I.34]. In this laser, the oxidant was atomic oxygen.

A free burning CS_2/O_2 flame was first used to provide the active medium for a CO chemical laser in 1971 [I.35]. This marked the first time that CO was used as the active molecule in a "purely chemical" laser. No energy was supplied to induce the chemical reactions; only the vacuum pumps, exhausting combustion products, required an external energy supply. The power output was approximately 1 mw.

In the same year, 1971, the chemical reaction $CS+O \rightarrow CO(v)+S$ was established as the mechanism responsible for the production of vibrationally excited CO in the CS_2-O_2 system [I.1]. The most rapid mechanism by which vibrationally excited CO is produced is the following 4 reaction chain [I.7]

$$CS_2 + O \rightarrow CS + SO$$
$$CS + O \rightarrow CO(v) + S$$
$$S + O_2 \rightarrow SO + O$$
$$2(SO + O_2 \rightarrow SO_2 + O)$$

This mechanism is a branching chain because, through each cycle, an extra chain carrier, O, is generated. The interested reader will find a comprehensive survey of CO chemical lasers including details of the chemical reactions in References I.3, I.28, and I.36. Information on the chemical aspects of a premixed free burning CS_2/O_2 flame may be found in Reference I.28. There, the chemical kinetics and their relation to the laminar flame speeds are discussed.

CO vibrational cascading, a shifting of the vibrational populations to lower levels, was examined with a Q switched laser cavity and a CS_2/O_2+O flame [I.36]. The vibrational levels participating in laser emission were found to shift, favoring lower levels, further along the flow direction after the vibrationally excited CO had been formed.

The addition of N_2O or vibrationally cold CO will, under many conditions, enhance the output power of a CO chemical laser [I.37]. The beneficial effect of these additives was stated in Reference I.37 to be selective depopulation of portions of the CO vibrational population via near resonant exchange. This selective transfer increases the inversions on the laser transitions. A free burning $CS_2/O_2/N_2O$ flame has been used to produce a continuous laser output of 25 watts on the 14 → 13 through 1 → 0 vibrational bands [1.38]. In these experiments and others [I.39-I.42), N_2O has been shown to be the most effective additive for laser

power enhancement. Reference I.38 contains the speculation that N_2O may chemically participate in the free burning $CS_2/O_2/N_2O$ flame by acting as a donor for atomic oxygen. COS, in general, has been found to be particularly detrimental to laser performance [I.37,I.39].

Burner Configurations for CO Chemical Lasers

Many CS_2/O_2 burner configurations have been examined, both to increase the laser output power and to gain understanding of the processes in these lasers; a few different configurations will be mentioned to give a flavor for their variety. CS_2 and O_2 have fueled an electrically initiated chemical laser using a TEA (Transversely Excited Atmospheric) laser configuration [I.43] and a longitudinal discharge configuration [I.44,I.45]. References I.46 and I.47 report studies of shock initiated CS_2/O_2 combustion and shock tube CS_2/O_2 chemical lasers. In these works, strong shocks were passed through a premixed CS_2+O_2 gas mixture. The shocks heated the gases and initiated the chemical reactions leading to the production of vibrationally excited CO.

High Power CO Chemical Lasers

The highest output power from a CO chemical laser to date was obtained from combustion of CS_2 in atomic oxygen [I.48]. The atomic oxygen was generated by injecting O_2 into an arc heated Ar jet. The atomic oxygen so formed then mixed and reacted with CS_2 in a supersonic nozzle. The laser cavity pressure was approximately 40 torr. 34 watts cw power was extracted.

In an effort to achieve higher power, CS has been used as a fuel instead of CS_2 [I.2]; atomic oxygen was the oxidant. As compared with

fueling with CS_2, fueling with CS was found to enhance the output power. Reasons for the beneficial effect of replacing CS_2 by CS include the fact that CS has more rapid and more simple chemistry than CS_2. More rapid chemistry implies increased production rates for the vibrationally excited CO without increased CO vibrational depopulation rates. In this case simplifying the chemistry means eliminating reactions involving CS_2; these would additionally heat the flow and would contribute molecules which rapidly depopulate vibrationally excited CO, such as COS.

The largest reported power levels for stimulated emission in CO chemical lasers are 84 watts [I.4] and 450 watts [I.5]. These results were obtained from devices in which CS_2 and O_2 were both dissociated before they were allowed to mix and react. However, in these lasers, no power was output coupled. The power was measured by calorimetry on the mirrors.

Conclusions

The research on CO chemical lasers has led to an understanding of the basic chemical mechanism by which the laser is pumped. Many of the reaction steps in the CS_2/O_2 flames are recognized, although all of their rate constants are not accurately known. A variety of CO chemical laser devices incorporating many flow configurations and combustion initiation mechanisms have been explored.

Predicting the utility of a burner configuration is a desirable, yet difficult, goal. As with other types of chemical lasers, CO chemical lasers produce higher power in systems in which the reactants are predissociated. Predissociating the reactants causes them to react more rapidly;

the chemical production rates for vibrationally excited CO increase relative to the deactivation rates. This permits larger flow rates of the excited species through the laser cavity. In chemical lasers in which predissociated reactants are used, the combustion occurs simultaneously with mixing. Both the mixing and the chemical processes affect the performance of the device. With CS+O, $F+H_2$, and $F+D_2$combustion models, the chemistry is often assumed known; there is a great deal of research continuing to understand the mixing processes.

The preceding section presented examples of mixing layer flames that behave differently than their corresponding premixed flames. This motivated us to investigate the CS_2/O_2 free burning mixing layer flame and to compare it with the premixed CS_2/O_2 flame. This study provided a means to gauge the interaction of the mixing and the chemical processes in one chemical laser flame.

Chapter I References

I.1 G. Hancock and I.W.M. Smith, "Infrared Chemiluminescence from Vibrationally Excited CO, Part 1.--The Reaction of Atomic Oxygen with Carbon Disulphide," Transactions of the Faraday Society 67, 2586-2598 (1971).

I.2 W. Q. Jeffers, C. E. Wiswall, J. D. Kelley, and R. J. Richardson, "CW CO Chemical Laser Directly Fueled by Carbon Monosulfide," Applied Physics Letters 22, 586-589 (1973).

I.3 R.W.F. Gross and J. F. Bott, Handbook of Chemical Lasers (Wiley and Sons, New York, 1976).

I.4 W. Q. Jeffers, H. Y. Ageno, and C. E. Wiswall, "CO Chain-Reaction Chemical Laser Research," Final Technical Report, AFWL-TR-75-227, McDonnel Douglas Corp (1976).

I.5 R. J. Richardson and T. J. Menne, "Combustor-Driven CO Laser," Laser Focus 14, 50-53 (1978).

I.6 D. I. MacLean and G. W. Tregay, "Spectroscopic Studies of Low-Pressure Hydrogen Fluorine Flames," 14th Symposium (International) on Combustion, The Combustion Institute, Pittsburgh, PA, pp. 157-165 (1973).

I.7 D. W. Howgate and T. A. Barr, Jr., "Dynamics of a CS_2-O_2 Flame," Journal of Chemical Physics 59, 2815-2829 (1973).

I.8 B. Lewis and G. Von Elbe, Combustion Flames and Explosions, 2nd edition (Academic Press, New York, 1961).

I.9 A. G. Gaydon and H. G. Wolfhard, Flames, Their Structure, Radiation, and Temperature (Chapman and Hall, Ltd., London, 1960).

I.10 Fristrum and Westenberg, Flame Structure (McGraw-Hill, New York, 1965).

I.11 I. Glassman, Combustion (Academic Press, New York, 1977).

I.12 F. A. Williams, Combustion Theory (Addison-Wesley, Reading, Mass., 1965).

I.13 H. G. Wolfhard and W. G. Parker, "A New Technique for the Spectroscopic Examination of Flames at Normal Pressures," Proceedings of the Physical Society A-62, 722-730 (1949).

I.14 A. B. Witte, et al.,"Aerodynamic Reactive Flow Studies of the H_2/F_2 Laser II," TRW Systems Group, Final Report, AFWL-TR-74-78 (1974).

I.15 H. G. Wolfhard and W. G. Parker, "A Spectroscopic Investigation into the Structure of Diffusion Flames," Proceedings of the Physical Society A-65, 2-19 (1952).

I.16 H. F. Sullivan and I. Glassman, "Vapor Phase Diffusion Flames in the Combustion of Magnesium and Strontium," Combustion Science and Technology 4, 241-256 (1972).

I.17 R. J. Richardson, "CS_2-O_2 Flame Chemistry," Journal of Physical Chemistry 79, 1153-1158 (1974).

I.18 E. M. Bulewicz and P. J. Padley, "A Cyclotron Resonance Study of Ionization in Low-Pressure Flames," Ninth Symposium (International) on Combustion, pp. 639-646 (1963).

I.19 P. Dearden and R. Long, "Soot Formation in Ethylene and Propone Diffusion Flames," Journal of Applied Chemistry 18, 243-251 (1968).

I.20 U. Bonn, "Radiative Extinguishment of Diffusion Flames at Zero Gravity," Combustion and Flame 16, 147-159 (1971).

I.21 S. R. Smith and A. S. Gordon, "Studies of Diffusion Flames. I. The Methane Diffusion Flame," Journal of Physical Chemistry 60, 795-763 (1956).

I.22 S. R. Smith and A. S. Gordon, "Studies of Diffusion Flames. II. Diffusion Flames of Some Simple Alcohols," Journal of Physical Chemistry 60, 1059-1062 (1956).

I.23 S. R. Smith, A. S. Gordon, and M. H. Hunt, "Studies of Diffusion Flames. III. The Diffusion Flames of Butanols," Journal of Physical Chemistry 61, 553-557 (1956).

I.24 A. S. Gordon, S. R. Smith, and J. R. McNesby, "Study of the Chemistry of Diffusion Flames," Seventh Symposium (International) on Combustion, pp. 317-324 (1959).

I.25 G. H. Markstein, "Structure of Low Pressure Trimethylaluminum-Oxide Flat Diffusion Flames," Combustion and Science Technology 3, 245-253 (1971).

I.26 T. Kinbara and J. Nakamura, "Diffusion Flames and Carbon Formation," Fifth Symposium (International) on Combustion, pp. 285-289 (1955).

I.27 J. A. Barnard and C. F. Cullis, "The Rates of Chemical Reactions in the Diethyl-Ether Diffusion Flame," Eighth Symposium (International) on Combustion, pp. 481-486 (1961).

I.28 A. A. Vetter, Ph.D. thesis: "Kinetics and Structure of the CS_2/O_2 Flame Laser," California Institute of Technology (1975).

I.29 C. K. Patel and R. J. Kerl, "Laser Oscillations on $X^1\Sigma^+$ Vibrational-Rotational Transitions of CO," Applied Physics Letters 5, 81-83 (1964).

I.30 D. W. Gregg and S. J. Thomas, "Analysis of the CS_2/O_2 Chemical Laser Showing New Lines and Selective Excitation," Journal of Applied Physics 39, 4399-4404 (1968).

I.31 M. A. Pollack, "Laser Oscillation on Chemically Formed CO," Applied Physics Letters 8, 237-239 (1966).

I.32 S. J. Arnold and G. H. Kimbell, "Chemical Laser Action in Electrically Pulsed Flowing CS_2-O_2 Mixtures," Applied Physics Letters 15, 351-353 (1969).

I.33 K. D. Foster and G. H. Kimbell, "Vibrational Population Inversion of CO in a Free Burning CS_2-O_2 Flame," Journal of Chemical Physics 53, 2539-2540 (1970).

I.34 W. G. Jeffers and C. E. Wiswall, "A Transverse Flow CO Chemical Laser," Applied Physics Letters 17, 67-69 (1970).

I.35 H. S. Piloff, S. K. Searles, and N. Djeu, "CW Laser from the CS_2-O_2 Flame," Applied Physics Letters 19, 9-11 (1971).

I.36 C. J. Ultree and P. A. Bonczyk, "Performance and Characteristics of a Chemical CO Laser," IEEE Journal of Quantum Electronics QE-10, 105-110 (1974).

I.37 R. D. Suart, S. J. Arnold, and G. H. Kimbell, "Power Enhancement by the Addition of Vibrationally Cool Gases," Chemical Physics Letters 7, 337-340 (1970).

I.38 M. J. Linevsky and R. A. Carabetta, "CW Laser Power from Carbon Bisulfide Flames," Applied Physics Letters 22, 288-291 (1972).

I.39 G. Hancock and I.W.M. Smith, "Quenching of Infrared Chemiluminescence. 1: The Rates of CO ($4 \leq v \leq 13$) by He, CO, NO, N_2, O_2, OCS, N_2O, and CO_2," Applied Optics 10, 1827-1843 (1971).

I.40 S. K. Searles and N. Djeu, "Characteristics of a CW CO Laser Resulting from a CS_2-O_2 Additive Flame," Chemical Physics Letters 12, 53-56 (1971).

I.41 W. Q. Jeffers and C. E. Wiswall, "Experimental Studies of the $O/O_2/CS_2$ CW CO Chemical Laser," IEEE Journal of Quantum Electronics QE-10, 860-869 (1974).

I.42 W. Q. Jeffers, C. E. Wiswall, and H. Y. Ageno, "Gas Additive Effects in CO Chemical Lasers," IEEE Journal of Quantum Electronics QE-12, 693-697 (1976).

I.43 J. L. Ahl and W. R. Binns, "A CS_2/O_2 Electrochemical, Pulsed T.E.A. Laser," IEEE Journal of Quantum Electronics QE-12, 26-29 (1976).

I.44 W. Q. Jeffers and H. Y. Ageno, "CO Chain Reaction Chemical Laser," Applied Physics Letters 27, 227-229 (1975).

I.45 N. A. Nielson, Jr., Ph.D. thesis, "An Electrically Discharged Carbon Disulphide-Oxygen Chemical Laser," Cornell University (1975).

I.46 R. Dibble, Ph.D. thesis: "Laser Probing of Excited CO Products from Shock Wave Initiated Oxidation of Carbon Disulfide," University of Wisconsin-Madison (1975).

I.47 J. Hardy, Ph.D. thesis: "A Shock Tube Study of Carbon Disulfide," University of Texas at Austin (1976).

I.48 L. R. Boedecker, J. A. Shirley, and B. R. Bronfin, "Arc-Heated Flowing CO Chemical Lasers," Applied Physics Letters 21, 247-249 (1972).

Chapter II

EXPERIMENTAL STUDIES OF CS_2/O_2 FLAMES

A. Experimental Aims and Apparatus

The experimental objective of this study was to investigate the behavior of CS_2/O_2 laminar mixing layer flames. We are interested in the effect of the mixing layer configuration on the suitability of the product carbon monoxide for use as the active medium in a chemical laser. We measured the vibrational level population distributions of the carbon monoxide and the temperature fields in CS_2/O_2 laminar two-dimensional mixing layer flames. This information is essential for evaluating the gain of the combustion product on the vibrational rotational lines of CO. In the course of this experimental program, our measurements have led us to a better understanding of the mixing, chemical, and CO vibrational kinetic processes in these flames.

Infrared emission spectroscopy was performed on CS_2/O_2 laminar mixing layer flames. From the data of these experiments, vibrational population distributions of carbon monoxide and temperature fields were deduced. The data reduction technique and results will be discussed in Chapter II, Section D. The components of the main experimental apparatus are shown in Figure II-A-1. They are the gas supplies, the vacuum chamber, the gas injector, the pumping system, the optical system, and the supporting electronics. These will be individually described. Some of the apparatus was adapted from that described in Reference II.1.

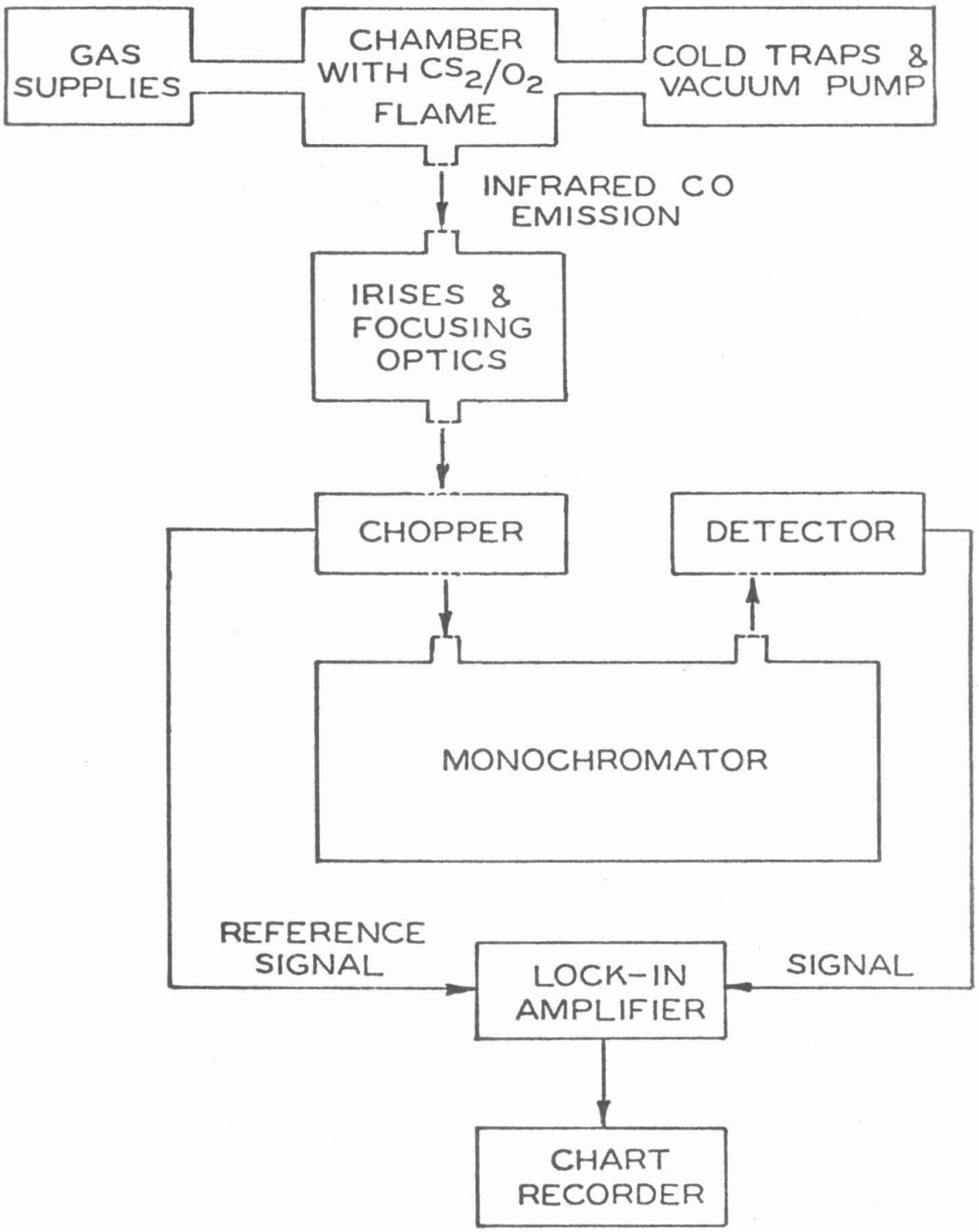

Figure II-A-1 Block diagram of the experimental system

Gas Supplies

Details of the gas supply system may be found in Reference II.1. A summary of the gases used is presented in Table II.A.1. The CS_2, O_2, and additive gas flows were regulated and metered; flow rates between .02 and 10.0 millimoles/sec were attainable for most gases. The individual species were regulated, metered, and then mixed as desired. The gases then flowed approximately 4 meters to the chamber in tubing of diameter .7 cm or less. The tubing used was tygon, Imperial-Eastman Poly-Flo, or aluminum. During the 4-meter journey to the chamber, there was ample opportunity for thorough mixing.

TABLE II.A.1. Gases Used; Acquired in Gaseous Form unless Otherwise Noted

Molecule	Source (Purity Minimum)
CS_2	Baker Analyzed Reagent (liquid) (99%)
O_2	Big 3 Gas Supply Co. (99.5%)
N_2	Matheson Extra Dry (99.9%)
Ar	Big 3 Gas Supply Co. (99.998%)
He	Big 3 Gas Supply Co. (99.997%)
N_2O	Matheson (97.5%)
H_2S	Matheson Technical Grade (99%)
CO	Matheson (P. Grade (99.5%)
CO_2	Victor Welding Grade
CNBr	Baker (solid)

The Pumping System

The chamber in which the flames were studied is pumped to low pressure, 2 to 20 torr, by a Cenco model Hyvac 45 constant volume vacuum pump, capacity 7.5 L/sec. The exhaust gas is drawn through dual liquid nitrogen

cold traps, in series, prior to entering the pump. The cold traps are present to reduce the quantity of noxious combustion products fouling the pump oil. Each cold trap has a cylindrical profile, 12.5 cm in diameter with .25 cm thick glass walls. Gas enters each cold trap through a centered 5 cm i.d. tube and is drawn out from the channel between the outer wall and the centered gas entry tube. Over 30 cm of each trap is immersed in the liquid nitrogen.

The cold traps are connected to the pump by metal pipe and heavy rubber 3 cm i.d. tubing. About .5 m of this tubing joining the traps and the pump serves to decouple pump vibrations from the chamber. After passing through the pumps, the exhaust is vented into the atmosphere via a fume hood. After each day's run, the traps and chamber are purged of their disgusting contents by flushing with air. The purge air flows through the chamber under a slight positive pressure, bypassing the pump and venting into the atmosphere.

The Chamber

Preliminary tests of the first small double-slotted injector were conducted in the glass vacuum chamber described in Reference II.1. The bulk of the experiments, including all the two-dimensional flame studies reported here, were carried out in a large aluminum vacuum chamber, as shown in Figure II-A-2. The chamber contained the gas injector. The chamber walls are 1.27 mm thick, and of aluminum. The dimensions of the chamber are 30 cm x 45 cm x 110 cm. The side walls and bottom are welded together and the top is bolted to a lip on the side walls. The seal is made with a 3.2 mm thick neoprene gasket.

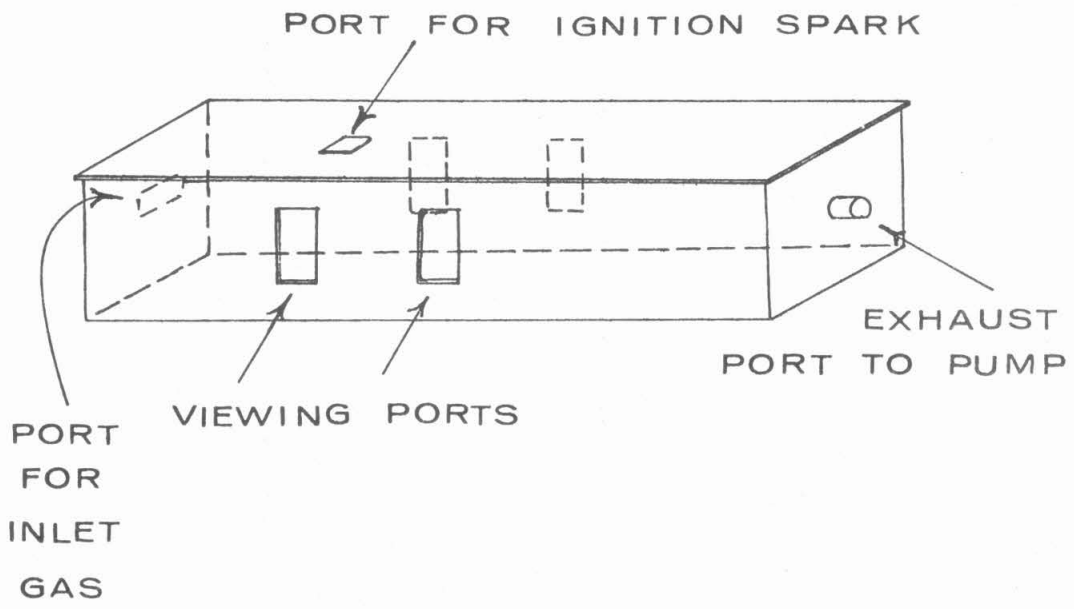

Figure II-A-2 The aluminum low pressure chamber

There are 7 major ports. Four measure 10 cm x 15 cm and are in the side walls. Over each, a 1.27 cm thick Plexiglass plate is bolted with gasket seal. The Plexiglass plates serve as bases into which optical windows are mounted. Purging gas inlets are mounted in the plexiglass plates next to the optical windows. Normally the viewing windows were sapphire flats, measuring 1 mm thick and 25 mm in diameter. Sapphire was chosen for its excellent durability and moderate infrared transmission losses below 6 μm. Lower optical losses were attained, when needed, by using NaCl optical flats measuring 6 mm thick and 50 mm in diameter. For some of the photographic work, 75 mm diameter Pyrex glass windows were used.

Four 1/4" o.d. Swagelok feed-throughs mounted in a 1.27 cm thick Plexiglass plate covering a 5 cm x 15 cm port carry the gas supply into the chamber. On the downstream end of the chamber, the gas is exhausted to the cold traps and pump through a centered hole of 5 cm diameter. The remaining port measures 10 cm x 10 cm, and is in the top of the chamber. A 1.27 cm thick Plexiglass plate is bolted over this port with a gasket seal. A high voltage feed-through is mounted in the center of the plate. This is used to strike a discharge in the chamber, igniting the flames.

Flame Photography

Photographs were taken of the flames through the side windows of the chamber. The windows used were either of 2.5 cm diameter sapphire or 7.5 cm Pyrex. An Olympus OM-1 35 mm single lens reflex camera was used, shooting Kodachrome or Ektachrome color slide film. The camera had a 50 mm f 1.8 lens and time exposures from 1 to 1/60 sec were typical; often

the lens was stopped down to expand the depth of field. The camera was typically mounted about 45 cm off the centerline of the gas injector.

The Gas Injectors

Four different gas injectors (or "burners") were used at different times. They are shown in Figures II-A-3 through II-A-7. Two different double-slot injectors were used in the mixing layer studies. Both had porous brass plates separating their plenum sections from their exit ducts. These are shown in Figures II-A-3 through II-A-5. Other than the porous plates, the injectors were constructed of aluminum. The exit slots of the smaller injector measure 10 mm x 70 mm. The exit slots of the larger injector measure 20 mm x 200 mm. An aluminum block 13 mm x 200 mm x 75 mm can be inserted into either slot of the large double-slot injector, partially blocking one slot and causing the two slots to have unequal dimensions. This arrangement is shown in Figure II-A-4.

The flow speeds at the exit slots could be varied between zero and about 5 m/sec by adjusting the chamber pressure and inlet-back pressures. The chamber pressure was typically between 2 and 20 torr. In this pressure and flow velocity range, the Reynolds number with respect to slot height is less than 200 for either double-slot injector. The flow in the gas injector is laminar and the flow field at the exit slot will be approximated by the well known parabolic velocity profile, typical of this nearly incompressible Couette flow.

A triple-slot injector, shown in Figure II-A-5, was constructed for examining sandwiched CS_2, O_2, CS_2 or O_2, CS_2, O_2 flows. Again, porous brass plates separate the gas inlet plenum from the exit ducts. The rest of the

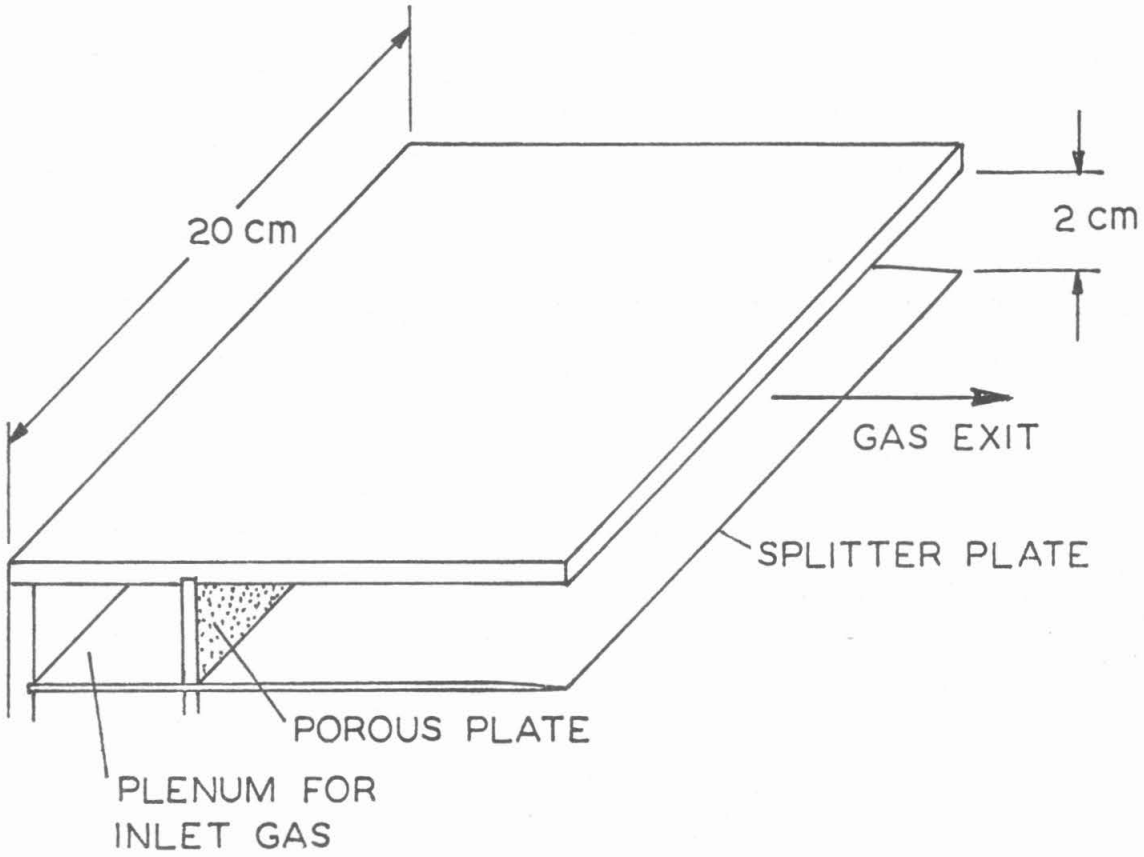

UPPER HALF OF THE TWO STREAM GAS INJECTOR,
SIDE WALLS REMOVED

Figure II-A-3 Cut-away of the large double-slot injector

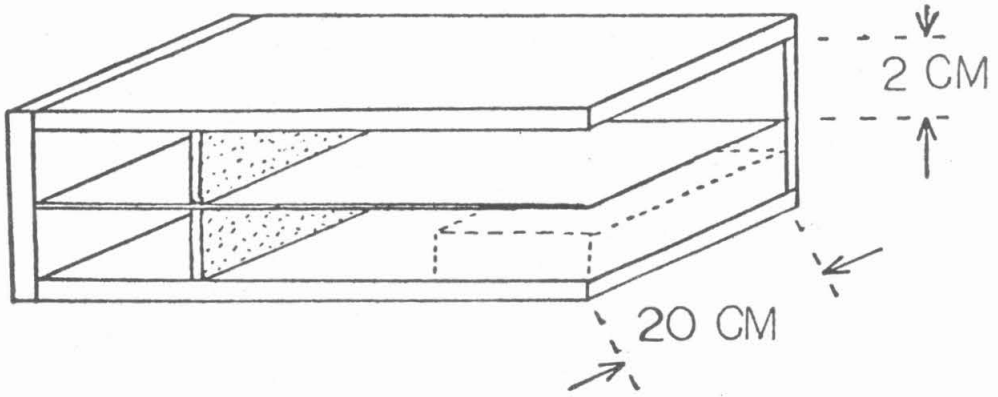

Figure II-A-4 Large double-slot gas injector

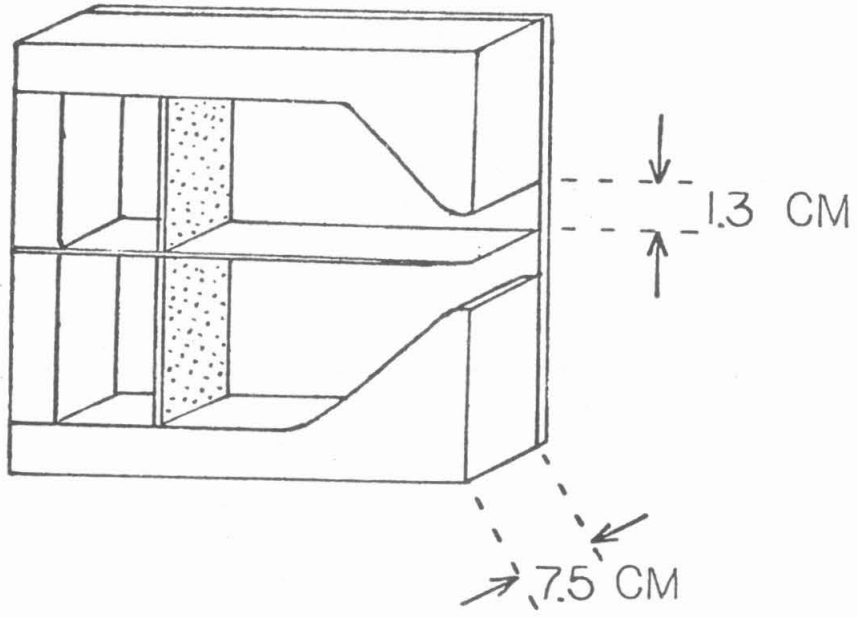

Figure II-A-5 Small double-slot gas injector

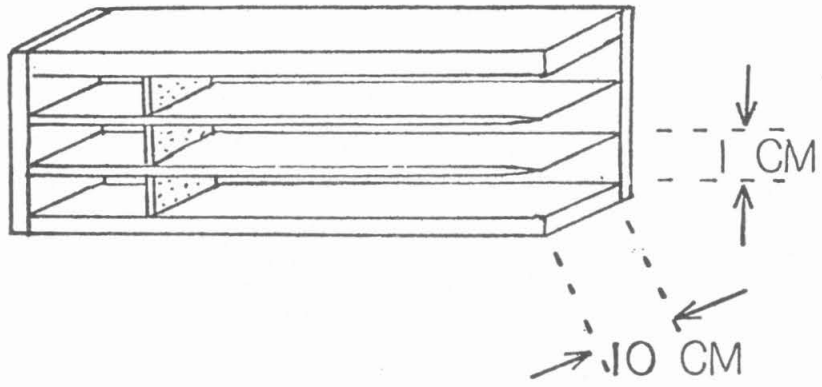

Figure II-A-6 Triple-slot gas injector

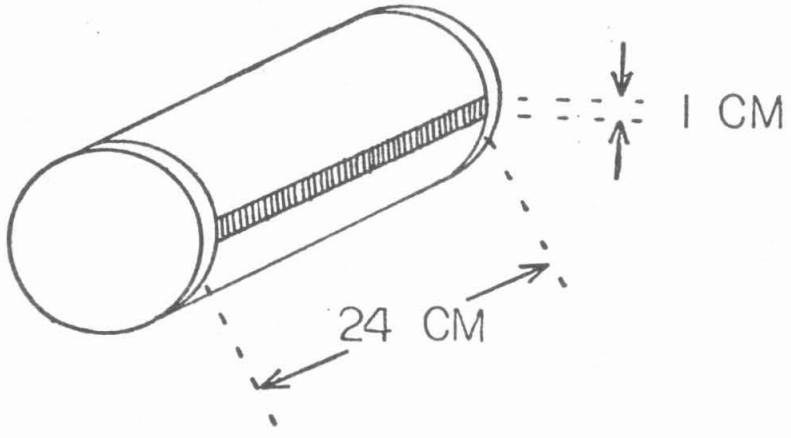

Figure II-A-7 Alternating-slot gas injector

injector is aluminum. Each exit slot measures 10 mm x 100 mm.

An injector was built especially for studying premixed flames; it was designed by V. A. Dudkin [II.2], and is shown in Figure II-A-7. This injector delivered the two reactants from alternating slots measuring .4 mm wide for CS_2 and 1.2 mm wide for O_2. The slots were separated by .4 mm wide aluminum spacers. The injector was comprised of 100 identical segments, each segment consisting of an O_2 slot, an aluminum spacer, a CS_2 slot, and another spacer. Each segment was a 2.4 mm long section of the 240 mm long, 7 mm high gas outlet face. This alternating slot injector was used to study flames in which the gases mix immediately after leaving the injector. Normally, the combustion occurs in what is essentially a one-dimensional free burning flame. The injector design prevented the flame from striking back upstream.

Moving an Injector

The gas injectors were mounted in the chamber on a mechanism which allowed them to be moved with two degrees of freedom, while the optics and chamber remained stationary, as shown in Figure II-A-8. The mechanism for horizontal translation was a screw driven sled on Teflon tracks. The drive screw was coupled to a universal joint and then through a vacuum rotary feed to a manually driven knob outside of the chamber. The injector was mounted atop a scissors jack resting on the screw driven translator just described. A telescoping rod of rectangular cross section connected the screw drive for the scissors jack to a second universal joint, and the driving torque was applied manually to a rod which entered the chamber via a vacuum feed, and fastened to the other side of the universal joint. This

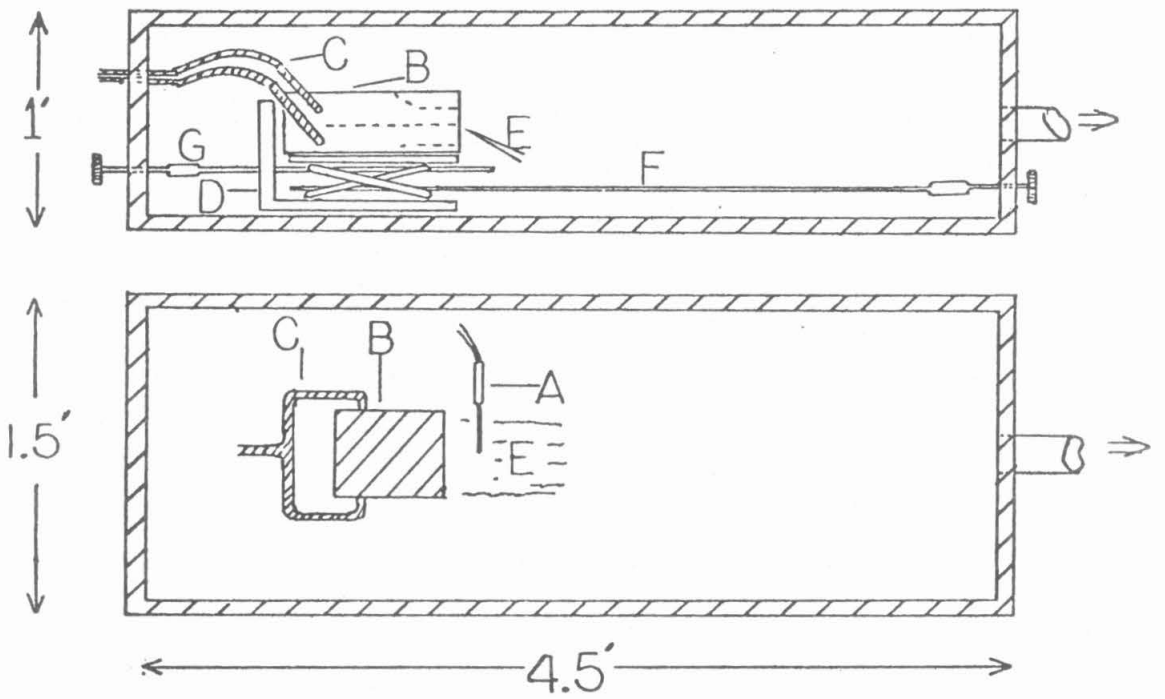

Figure II-A-4 Mechanism for moving the gas injectors inside the chamber: (A) thermocouple and mount (when present); (B) gas injector; (C) gas inlet tubes; (D) sled on which injector rests; (E) flame; (F) drive rod to elevator mechanism; (G) drive rod to horizontal drive screw.

translation mechanism could be used to generate independent motion in two dimensions.

The gas injectors were mounted on the sled-jack mechanism. Each could be moved over a 7.5 cm range vertically, transverse to the flow, and over a 30 cm range along the flow. Tygon tubing of 1/4" diameter, which was protected by additional layers of larger diameter Tygon tubing, provided flexible feeds for the inlet gases to the injector.

Electronics and Infrared Optics

Infrared emission spectroscopy was performed on the flames. The emission was detected through the side windows of the chamber and an iris was mounted just outside the window. Stopping the iris down narrowed the field of view; however, there was an accompanying reduction in signal. The iris was about 30 cm off the centerline of the injector. About 20 cm from the iris an f 8, 2.54 cm diameter, BaF_2 lens was mounted, so as to optimize the signal reaching the monochromator which was another 20 cm away. In between the BaF_2 lens and the inlet slits of the monochromator, the optical signal was physically chopped for phase synchronous detection.

The monochromator was a McPhearson model 2501. One of two gratings could be used, a 300 line/mm grating blazed for 3 μm or a 150 line/mm grating blazed for 4 μm. Either a lead sulfide detector or a gold-doped germanium detector could be attached to the monochromator. The lead sulfide detector operated at ambient temperature and was sensitive to the CO overtone band, 2.3 μm to 3.0 μm. The liquid-nitrogen-cooled Ge:Au detector was sensitive to the CO fundamental emission band, 4.5 μm to 6.0 μm. These detectors are described more fully in Reference II.1.

The efficiency of the optical system was calibrated by measuring the response of the system to a black body source. A Weller fixed temperature soldering iron tip at 644°K, coated with carbon black from candle soot, was used as the black body calibration source. The calibration signal was time averaged, and then the response of the system was calculated by the method presented in Chapter II, Section D.

The signal from the infrared detector was synchronously detected. The optical signal was modulated by a chopper, and the signal from the detector along with a reference signal from the chopper was fed into a Princeton Applied Research model 124A lock-in amplifier, preamp model 117. The output of the lock-in amplifier was recorded with an Omniscribe Houston Instruments single track chart recorder.

During thermocouple measurements of the flame temperatures, voltages off the thermocouples were obtained with a Data Precision model 3500 digital voltmeter. CO laser power measurements were made with a Scientech model 360001 power meter.

When the flame was used as a laser medium, the optical cavity was comprised of two 2.5 cm diameter mirrors, a flat gold-coated fully reflecting mirror (conservativity > 99% reflecting) and a 2 m radius, partially transmitting dielectric coated mirror. The maximum reflectivity of the output mirror, 98.5%, was at a wavelength of 5.4 μm, and its flat backside was antireflection coated. The active optical path in the flame was 20 cm. The mirrors were internally mounted, 80 cm apart. From these dimensions the beam width, w_B, was calculated using the formulas in Reference II.3 to be between 1 and 2 mm throughout the cavity. The laser beam intensity fell off as $e^{-r_B^2/w_B^2}$, where r_B is the radius off the optical axis.

B. Visual Observations of the CS_2/O_2 Laminar Mixing Layer Flame, and Comments on the Flame Chemistry

Before presenting the carbon monoxide vibrational population profiles for CS_2/O_2 mixing layer flames, a qualitative description of the flame based on the results of visual observations will be given. When viewed with the naked eye, the most prominent feature of this flame was a sheet of blue-white emission beginning at or near the splitter plate and extending 10 to 30 cm downstream, as shown in Figures II-B-1 through II-B-3. The location of the visible emission gave evidence of location of flame reactions, although important reactions might be occurring outside the visibly emitting region.

A summary of the conclusions of this section follows. The CS_2/O_2 mixing layer flame emitted in the visible. The region of brightest emission was blue-white. In the O_2 stream there was blue emission from SO_2, and on the side of the CS_2 stream there was faint yellow emission, probably C_2 Swan band emission. The region of blue-white emission broadened with decreasing pressure, and detached from the splitter plate at sufficiently low pressure, about 3.5 torr. We will argue that the flame detached due to the increasing importance of cooling and reactive species quenching at the splitter plate at reduced pressures. We also expect that increasing the flow velocity will drive the flame off. The blue-white flame skewed into the CS_2 stream, making an angle with the plane of the splitter plate of between 0° and about 70°. The skewing was most pronounced when the ratio of the velocity of the CS_2 stream to the velocity of the O_2 stream was small and least pronounced, zero degrees, when the ratio exceeded one.

The Shape of the CS_2/O_2 Mixing Layer Flame

The appearance of the CS_2/O_2 mixing layer flame varied with pressure. As the pressure exceeded about 20 torr, the flame showed the onset of unsteadiness. Under these conditions, the Reynolds number with respect to a downstream distance of 10 cm was about 20; the velocity was approximately 200 cm/sec; and the temperature was approximately 2000°K, so that the kinematic viscosity was approximately 100.

With increasing pressure, the effect of buoyancy on the flame became pronounced. Below 15 torr, the form of the flame was merely reflected about the plane of the splitter plate upon switching the CS_2 and O_2 streams. With increasing pressure, above 15 torr the flame lifted progressively more upward, as shown in Figure II-B-1.

The color and shape of the flame varied with pressure. Below 2 torr, if the gas velocity leaving the injector was about 150 cm/sec, the flame ceased to exist as a compact sheet; rather, a large reaction zone marked by a diffuse blue glow filled the volume downstream of the injector. This region was as wide as the injector (20 cm), over 10 cm thick, and extended about 10 cm in the direction of flow.

At pressures in the range of 2.5 to 3.5 torr, with flow velocities of about 1 m/sec, the visible blue luminescence appeared in a single thick sheet, as pictured in Figure II-B-2. As the pressure was increased above about 4 torr, the flame thinned and attached to the splitter plate. The region of brightest visible emission appeared blue-white rather than purely blue. A thin zone on the side of the flame adjoining the CS_2 stream displayed a faint yellow tint. The entire O_2 stream, adjoining the bright flame region, faintly emitted a deep blue hue; the correspond-

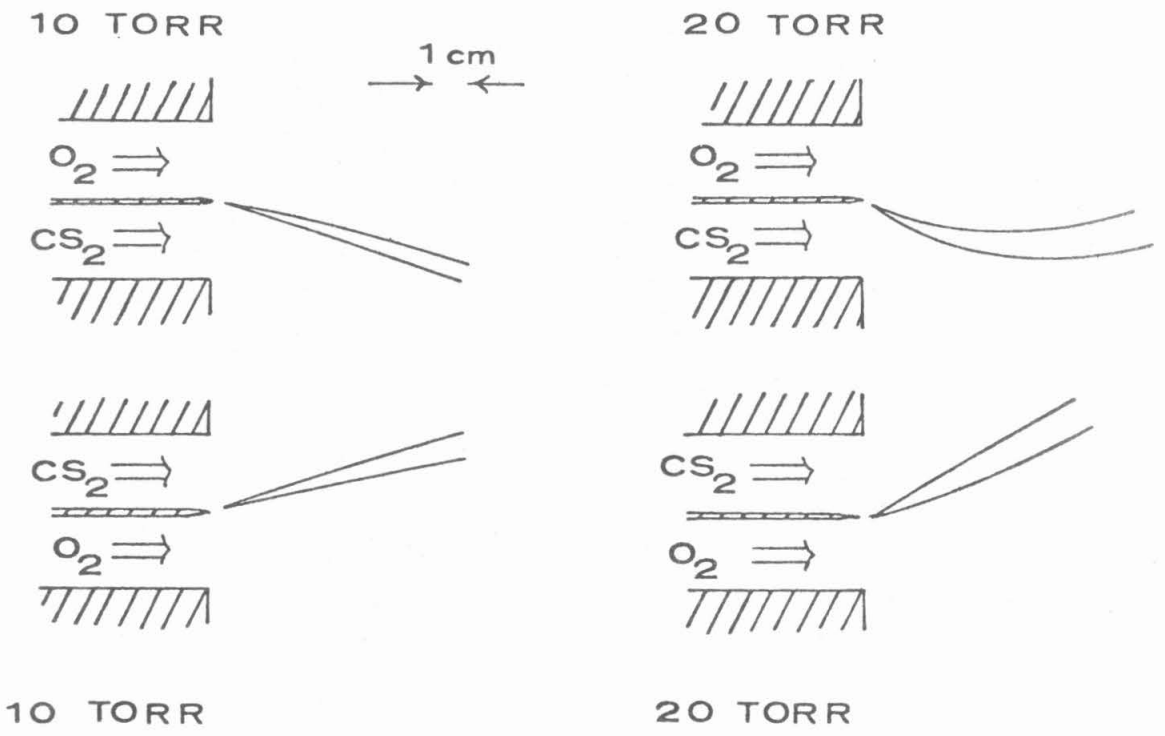

Figure II-B-1 The effect of buoyancy on CS_2/O_2 laminar mixing layer flames: the form of the region of brightest visible emission at 10 and 20 torr. Exit port velocities: $U_{CS_2} \simeq .5$ m/sec, $U_{O_2} \simeq 1.5$ m/sec

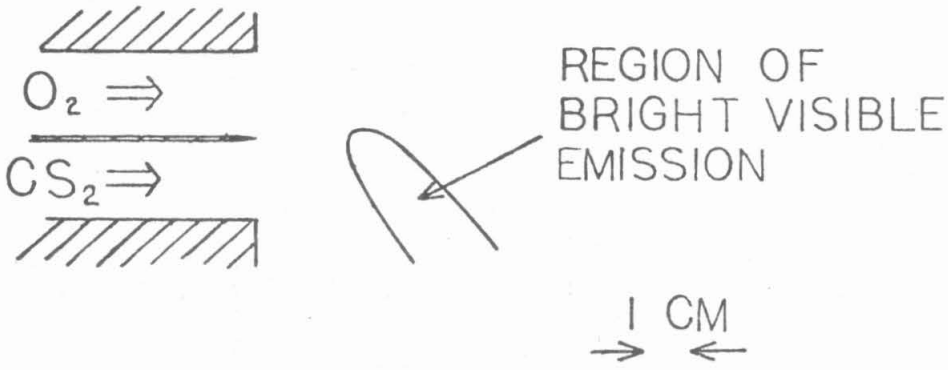

Figure II-B-2 A 3 torr CS_2/O_2 mixing layer flame. Exit port velocities: $U_{CS_2} \simeq .5$ m/sec, $U_{O_2} \simeq 1.5$ m/sec

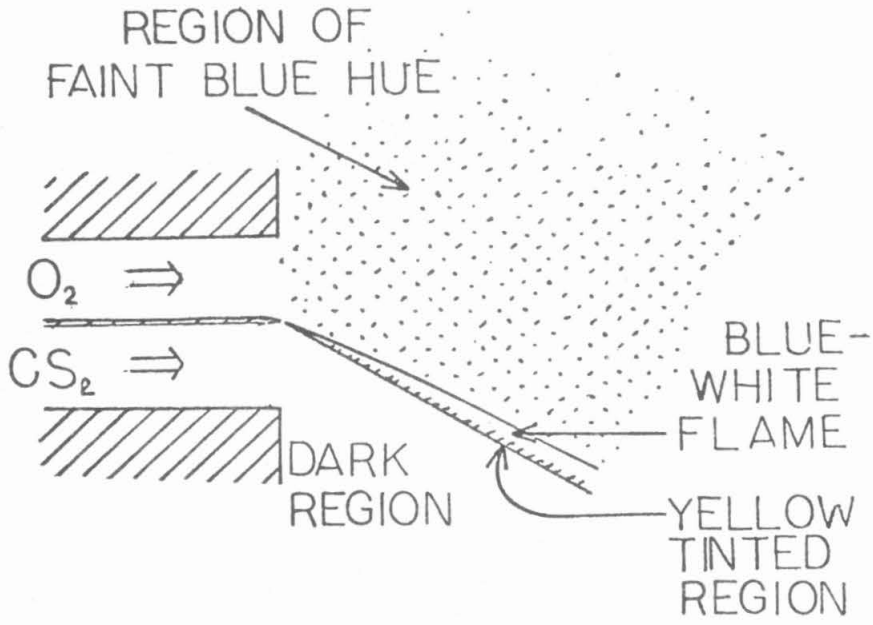

Figure II-B-3 A 6 torr CS_2/O_2 mixing layer flame. Exit port velocities: $U_{CS_2} \simeq .5$ m/sec, $U_{O_2} \simeq 1.5$ m/sec

ing region in the CS_2 stream did not emit. This is pictured in Figure II-B-3.

Any differences between the chemical reaction mechanisms dominant in the mixing layer CS_2/O_2 flames and the premixed CS_2/O_2 flames diminished as the pressure was lowered; this was established in Chapter I, Section C. Below 2 torr the reactions in the CS_2/O_2 flame occurred downstream of the splitter plate subsequent to thorough mixing. Flames burning at pressures from 2 to 3 torr did not attach to the splitter plate. At the upstream edge of these flames the reactants were thoroughly mixed prior to reacting.

The detachment of the flame from the splitter plate was not simply due to the reduction of bimolecular reaction rates at lower pressures. The laminar flame speed was indicative of the overall rate at which the chemical reactions progressed. Simple dimensional analysis showed that decreasing the pressure in a gas mixture increased the bimolecular diffusion constants; the thermal conduction did not vary, while the heat content decreased linearly with the decrease in density. These effects compensated for reduced reaction rates, and the flame speed remained constant [II.4]. This result is approximate; it is derived for flames in which bimolecular reactions dominate, and neglects variations in the dominant chemical mechanisms with pressure.

In our experiments, the volumetric pumping capacity was nearly independent of pressure. Increasing the molar flow of the reactants increased the pressure without appreciably changing the flow velocities. Because neither the flame speed nor the flow velocity varied strongly with pressure, the detachment of the flame from the splitter plate was

not a direct result of the dependence of the reaction rates on pressure.

The quenching effect of the splitter plate increased with decreasing pressure; the bimolecular diffusion constants increased, increasing the importance of intermediate species losses at the plate. There was also increased loss of heat at the plate relative to the heat production in the flame. These effects caused the flame to detach from the plate.

In some situations, flames stabilize in the low velocity wakes of splitter plates. However, the velocity profiles in the gas injector upstream of the edge of the splitter plate are the familiar parabolic profiles for duct flow; their form doesnot vary with pressure [II.5], nor do the flame speeds [II.4]. Consequently it is unlikely that the attachment of the flame to the splitter plate accompanying increased pressure was due to changes in the wake of the splitter plate.

The splitter plate played a passive role in the chemistry at high pressures, above about 5 torr, serving only to define the beginning of the mixing layer. It may also have served to stabilize the flame in the wake formed by its boundary layer. As the pressure was reduced, with the importance of conduction and diffusion increasing relative to convection, the splitter plate had more influence on the flame chemistry. It offered a relatively cold surface which conducted heat away from the flame and acted as a quenching site for free radicals in the flame. As the pressure decreased these quenching effects eventually became dominant; the flame detached and stabilized where the flow and flame velocities matched.

Skewing of the CS_2/O_2 Mixing Layer Flame

Appendix A contains an analysis of the skewing of a mixing layer flame into one reactant stream, a phenomenon that has been observed in many flames [II.6 - II.9]. Three possible causes for this skewing in the CS_2/O_2 flame are: CS_2 and O_2 have unequal constants for bimolecular diffusion opposing the reaction products; the stoichiometric ratio in which CS_2 and O_2 are consumed differs from one; and the CS_2 and O_2 streams often have unequal flow velocities.

The CS_2/O_2 laminar mixing layer flame was observed to skew from 0° to about 70° into the CS_2 stream. To find the cause of this, we examined flames with a variety of flow rates, pressures, gas additives, and gas injectors. Skewing into the CS_2 stream(s) was observed with all the gas injector configurations tested; the small double-slot injector, the large double-slot injector with equal and unequal slot heights, and the triple-slot injector run with $CS_2/O_2/CS_2$ and $O_2/CS_2/O_2$ flows.

When the CS_2 molar flow rates were increased to equal the O_2 molar flow rates, the flame straightened, i.e., 0° skewing. Simultaneously, sulfur deposition on the windows, caused by the presence of CS_2 in excess of the stoichiometric ratio, rapidly made it impossible to view into the chamber. Reducing the CS_2 and O_2 flow rates, while increasing the diluent flow across the windows, never completely overcame this difficulty. To achieve equal velocities in the CS_2 and O_2 streams with reduced CS_2 flow, the exit area of the CS_2 stream in the large double-slot injector was reduced. This permitted higher CS_2 flow velocities, with less sulfur deposition in the chamber. Using this flow configuration, increasing the velocity of the CS_2 stream straightened the flame. However, the

flame never skewed into the O_2 stream, even when the O_2 stream velocity was considerably less than the CS_2 stream velocity. In one experiment, using the large double-slot injector with unequal exit slot areas, the velocities at the duct exits of the CS_2 and O_2 streams were 3.2 m/sec and 0.6 m/sec, respectively.

To see whether the skewing was due to the unequal stream velocities only, the CS_2 flow rate was matched to the O_2 flow rate by adding an inert diluent, N_2, He, or Ar, to the CS_2 stream. This failed to affect the skewing. The skewing was often still 45° or more into the CS_2 stream.

The effect on the direction of flame skewing of a stoichiometric ratio favoring larger consumption of O_2 than CS_2 has the opposite effect of having larger bimolecular diffusion constants for the reaction products with O_2 than with CS_2. In Appendix A an estimate based on flame-sheet chemistry predicts that if the CS_2 and O_2 streams have equal velocities, the flame will skew into the O_2 stream.

Normally, the flow velocity of the O_2 stream was greater than that of the CS_2 stream. The areas of the CS_2 and O_2 exit ports on the gas injectors were equal in most experiments. This construction was chosen because prior to our experiments we did not know if we would be interested in having larger flows of CS_2 or O_2. The stoichiometric ratio in a flame depends on the dominant chemical mechanism, and we did not know whether the mechanisms in the mixing layer and premixed flames would be identical.

When the flow rate of the CS_2 stream was increased by adding inert gas, the velocity of the stream was increased relative to the O_2 stream, but the skewing remained. The amount of gas required to diffuse into the

mixing layer from the diluted CS_2 stream was larger than the amount of pure CS_2 required to support the same chemical reactions. Hence, diluting the CS_2 with an inert gas changed the ratio in which the flame consumed gas from the two reactant streams. This will be called the effective stoichiometric ratio. Both the relative flow velocities in the two streams and the effective stoichiometric ratio varied when an inert gas was added to one stream. Consequently, this experiment was not conclusive with respect to skewing.

The flame appeared straight when the CS_2 and O_2 flow rates were matched. This was evidence that the skewing was due to differing stream velocities. However, the flame did not skew into the O_2 stream when the velocity of the CS_2 stream exceeded the velocity of the O_2 stream using the injector with reduced CS_2 stream exit area. This may indicate that the skewing was due in part to the flame chemistry, or it may be that for this particular experiment the skewing was a result of the flow fields of this asymmetrical gas injector.

In summary, the CS_2/O_2 mixing layer flame exhibited a skewing which varied with the relative velocity of the CS_2 and O_2 streams, the region of brightest visible emission sloping toward the slower stream. However, skewing was never into the O_2 stream. The flame either appeared to project parallel to the plane of the splitter plate or to be skewed into the CS_2 stream. Quantitative agreement was not reached between the skewing angles predicted by the flame-sheet analysis in Appendix A and experimental observations.

Visible Emission

Spectra of radiation in the visible range from CS_2/O_2 laminar mixing layer flames were taken using the available low resolution, intensity uncalibrated, monochromator-photomultiplier. Emission was detected over the continuous spectrum from blue to red. This fact was corroborated by simply photographing the flame through a prism. A He-Ne laser beam (6328Å) was passed through the flame, and we visually examined for particle scattering. None was observed. This is qualitative evidence that the emission was not black body emission from particles, a common source in hydrocarbon flames.

The chemiluminescence following the reaction $SO+O \rightarrow SO_2(\tilde{a}^3B_1)$ is believed to be a source of blue emission from CS_2/O_2 flames [II.10, II.11]. This is consistent with our observation of a faint deep blue hue emanating from the O_2 stream and none in the CS_2 stream. Sulfur oxide can diffuse into either the CS_2 or the O_2 streams, but only in the O_2 stream is it likely to meet atomic oxygen. The modeling calculations in Chapter III predict that atomic oxygen reacts too vigorously with CS_2 and that CS is plentiful in the CS_2 stream. The lack of blue SO_2 chemiluminescence in the CS_2 stream is therefore understandable.

There was a thin region in the flame emitting faintly in the yellow. This region was on the edge of the region of bright visible emission adjoining the CS_2 stream. The yellow emission was observed when the pressure was about 5 torr or above. A second observation that may be related to this fuel-rich chemistry is that chamber walls on the side of the CS_2 stream consistently accumulated a solid yellow coating. This solid was identified as sulfur by its color and its distinctive odor when a sample was burned.

C_2 and CS have been identified as sources of visible emission in CS_2/O_2 flames [II.10]. The C_2 Swan bands have their origin at 5160Å and are shaded toward both the red and violet [II.12]. CS and C_2 will be shown to be the most likely candidates for the source of the yellow emission. The origin of CS $A'\Pi \rightarrow X'\Sigma^+$ band is at about 2580Å, and shaded to the red [II.12]; it does not appear yellow. Examining the spectroscopic constants found in References II.12 and II.13 for the molecules O_3, CS_2, S_2O, SO_2, COS, CO_2, S_2, O_2, C_2, SO, CO, and CS, only C_2 has a low-lying transition which produces emission in the yellow. Emission from ions is unlikely because, in a sensitive study, the total ion concentration in CS_2/O_2 flames was found to be below the detectable limit of 10^8/cc at pressures in the range of 8 to 200 torr [II.14].

The yellow emission being on the side of the CS_2 stream suggests that the emission source was an unoxidized molecule containing C or S. C_2 is such a molecule, and a yellow region of carbon formation is typical of the fuel side of hydrocarbon mixing layer flames [II.15]. A small fraction of the carbon remaining after sulfur was lost on the walls may be incorporated into C_2 by an unknown mechanism. These arguments are for the plausibility of observed yellow emission being due to C_2; however, C_2 Swan band emission is characteristic of CS_2 lean flames [II.10]. The identification of the source of the yellow emission cannot be made with certainty without high resolution spectroscopy. The yellow emission as well as the white emission may be due to C_2 or other more complex molecules that have not been considered.

The visible emission from the CS_2/O_2 mixing layer flame included chemiluminescence from electronically excited SO_2 and C_2. The character-

istically blue SO_2 emission was not observed on the side of the CS_2 stream, but was found elsewhere. The yellow emission, which was probably C_2 Swan band emission, was seen on the edge by the CS_2 stream of the region of brightest emission. The stratification of the visible emission across the mixing layer suggests that the chemical composition of the gas varied across the mixing layer.

C. CN and Its Energy Transfer with CO

It is well known that some molecules strongly affect the CO vibrational populations in CS_2/O_2 free burning flames, N_2O and COS, for example. CN (cyanogen monomer) has been reported to depopulate the upper vibrational levels of CO in electric discharges [II.16, II.17]. The following discussion explores the effects of CN addition on the CS_2/O_2 flame.

The visible sidelight emission from electrically excited CO lasers employing the flow-tube configuration is from electronically excited CO and CN [II.16]. A flow-tube configuration is one in which the laser cavity is downstream of the discharge. In discharge-tube configuration CO lasers, CO, C_2, CO^+, and CN are emission sources in the visible [II.16]. In both configurations the gas mixture input was a mixture of CO, N_2 and He in ratios of about 1:2:10. Since no CN was introduced into these tubes, the CN must have been formed in the discharges. Traces of CN may also have been formed in CS_2/O_2 flames. The carbon source was CS_2 and the nitrogen source was either N_2, used as an additive, or N_2 from small air leaks.

For both flow-tube and discharge-tube configuration CO lasers, the addition of O_2 to a mole fraction of .003 quenched the CN sidelight emission [II.16]. This quenching effect of O_2 has been well established [II.17]. The CN emission was probably quenched when the CN was chemically consumed, reacting with the oxygen to form CO and N_2 [II.16]. If so, the CN mole fraction can be estimated to be less than the mole fraction of O_2 added, .003.

Energy may be transferred from vibrationally excited CO to CN by reactions II.C.1 and II.C.2

$$CO(v \geq 12) + CN(X^2\Sigma^+) \rightarrow CO(v\text{-}12 \text{ or } v\text{-}13) + CN(B^2\Sigma^+) \qquad (II.C.1)$$

$$CO(v) + CN(v')(X^2\Sigma^+) \rightarrow CO(v\text{-}1) + CN(v'+1)(X^2\Sigma^+) \qquad (II.C.2)$$

There is disagreement in the literature over the importance of these processes in CO lasers. References II.16 and II.17 contain arguments that deactivation of CO by CN is substantial, while Reference II.18 contains arguments that it is not. Reaction II.C.1 produces CN in the $B^2\Sigma^+$ state; this CN may spontaneously decay, emitting radiation in the visible.

To test for an influence of CN on CS_2/O_2 flames, we added CNBr into the CS_2 stream in our mixing layer flames. In CS_2/O_2 flames, CNBr should be broken down due to the reactive high temperature environment, producing some free CN as well as further combustion products of CN including CO and N_2. We observed the overall visible emission intensity of the flame increased when the minimum measurable CNBr flow was added to the CS_2 stream. The CNBr:CS_2 ratio was 1:50 and the ratio of the CNBr and O_2 flow rates was about 1:200. An increase in emission intensity by a factor of 1.4 was indicated by a light meter used while photographing the flame. The photos support the measurement of this increase. An infrared spectrum of the flame did not vary with the addition of CNBr.

Because the infrared spectrum of the CS_2/O_2 flame did not vary with CNBr addition, we were able to conclude by the technique discussed in Section D that the populations in the vibrational energy levels of CO did not vary with the CNBr addition. Either there is negligible energy transfer to the CN from CO, or the CO vibrational energy pool is

sufficiently large so as to show no variation when a small amount of energy is transferred to CN. Because of the failure of the addition of CNBr to alter the CO vibrational level populations, we must conclude that there is little effect due to CN on the CO vibrational energy kinetics in a CS_2/O_2 flame. The brightness enhancement is either a result of combustion of CNBr or due to some undetermined energy transfer process in the flame, exciting a visible emitter.

D. Interpretation of Spontaneous Emission Spectra of Carbon Monoxide

Introduction

Low resolution CO spontaneous overtone spectra were taken from CS_2/O_2 two-dimensional laminar mixing layer flames under a variety of flow conditions. The spectral data were used to deduce the rotational temperature of the CO, the relative populations in each CO vibrational level, and the relative CO concentration profiles in the flame. In interpreting the spectra, the following assumptions are used: The medium is optically thin; the Einstein coefficients are known for the transitions observed; the emitting molecule is CO; the CO is in rotational equilibrium at the kinetic temperature; and the response of the optical system is linear with signal intensity. The data reduction and theoretical predictions presented in this section were accomplished using a number of computer codes written by Alan A. Vetter.

The field of view in the CS_2/O_2 mixing layer flames was partially masked by irises in order to attain spatial resolution, typically 1 cm. The flames were moved, with the optics stationary, to obtain spatial spectral profiles. The CO vibrational populations and temperatures were determined from the spectra; the technique is similar to those used in References II.19 through II.21. CO vibrational populations and CO concentrations were found relative to a normalization constant that could not be determined from these measurements. In the following pages, we will discuss the techniques used to deduce the CO vibrational populations, CO concentrations, and temperature profiles.

CO Molecular Spectra

In the combustion of CS_2, the exothermic reaction which produces the bulk of the vibrationally excited CO is CS+O → CO+S [II.21-II.28]. The CO is formed in a neutral electronic ground state, the only state that will be considered. The vibrational energy levels of CO are nearly evenly spaced. Each level is designated by a vibrational quantum number, v. The CO spontaneous emission band starts at 4.6 μm for the fundamental transitions (v → v-1), and 2.3 μm. for the first overtone transitions (v → v-2), see Figure II-D-1. CO spontaneous emission on the fundamental transitions has a greater probability than emission on the overtone, but available detectors for the overtone emission have a larger signal-to-noise ratio than those for the fundamental emission. The signal-to-noise ratio is better than an order of magnitude larger when observing overtone emission; consequently, the spectral measurements were taken of overtone emission.

The rotational energy levels are finely spaced in comparison to the vibrational energy levels. During a CO radiative vibrational transition, the rotational quantum number, J, has an extremely low probability to change by more or less than one unit. In emission, the vibrational-rotational transitions in which J decreases by one are designated R branch transitions, and those transitions in which J increases by one are designated P branch transitions. The transitions in which J is unchanged are designated Q branch transitions; for CO Q branch transitions are improbable, and will be given no further consideration. An abbreviated energy level diagram for CO is shown in Figure II-D-1, illustrating P and R branch transitions.

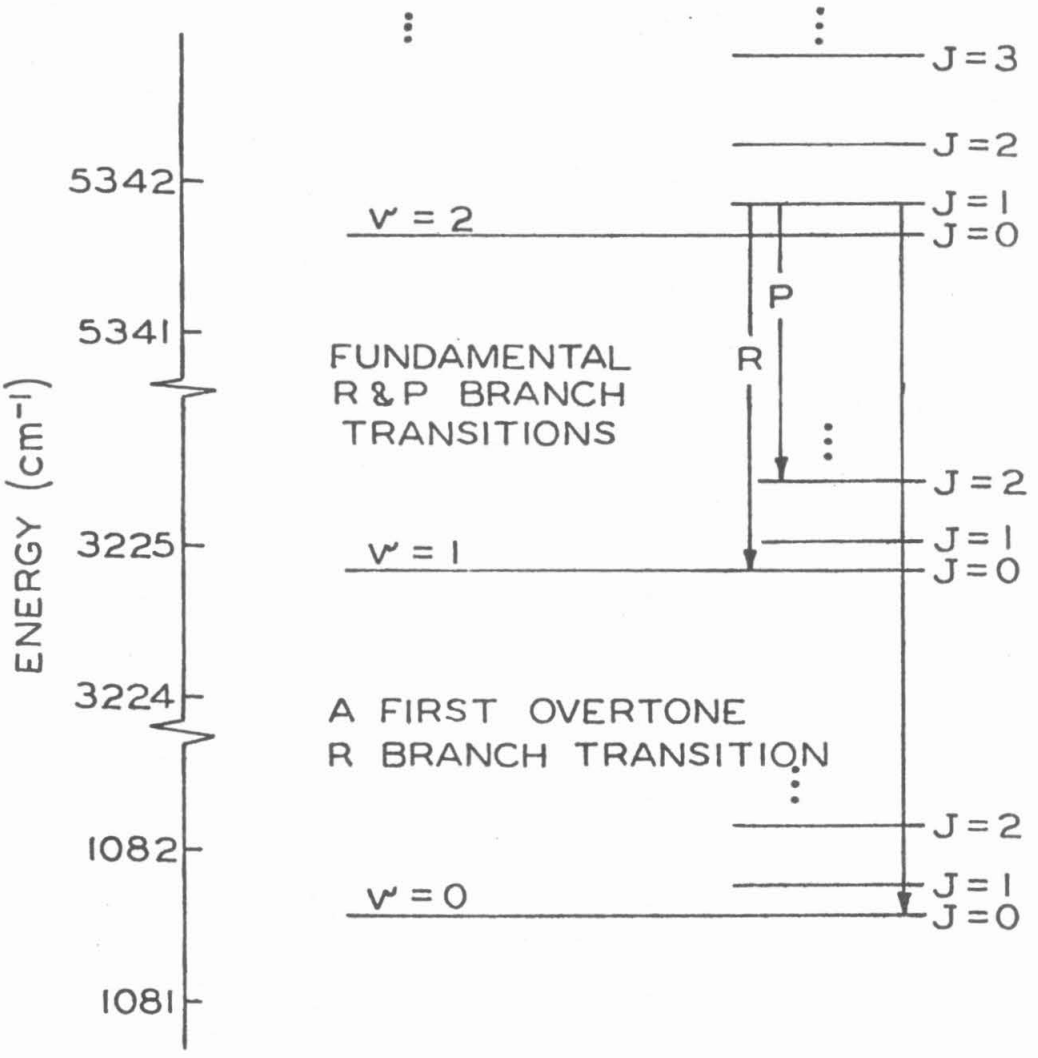

Figure II-D-1 Lowest energy levels of CO showing P and R branch transitions

The vibrational-rotational energy structure for CO is approximated by equation II.D.1 [II.29]. This equation includes terms that describe the anharmonicity of the CO molecule.

$$E(v,J) = \omega_e(v+\tfrac{1}{2})^{*} - \omega_e x_e(v+\tfrac{1}{2})^{2**} + \omega_e y_e(v+\tfrac{1}{2})^3 + \omega_e z_e(v+\tfrac{1}{2})^4$$
$$+ [B_e^{*} - \alpha_e(v+\tfrac{1}{2})^{\dagger} + \gamma_e(v+\tfrac{1}{2})^2]\, J(J+1)^{*}$$
$$- [D_e - \beta_e(v+\tfrac{1}{2})]\, J^2(J+1)^2 + H_e\, J^3(J+1)^3 \qquad \text{(II.D.1)}$$

where

$\omega_e = 4.3103193 \times 10^{-20}$ joules
$\omega_e x_e = 2.64081 \times 10^{-22}$ joules
$\omega_e y_e = 2.28 \times 10^{-25}$ joules
$\omega_e z_e = 3.12 \times 10^{-28}$ joules
$B_e = 3.836439 \times 10^{-23}$ joules
$\alpha_e = 3.4789 \times 10^{-25}$ joules
$\gamma_e = 5.88 \times 10^{-29}$ joules
$D_e = 1.2157 \times 10^{-28}$ joules
$\beta_e = 1.192 \times 10^{-32}$ joules
$H_e = 1.163 \times 10^{-34}$ joules

---

*Simple harmonic oscillator, rigid rotator terms

**First anharmonic term

†Term responsible for R branch rotational bandheads

The overtone P and R branch CO lines have wavelengths given by equations II.D.2 and II.D.3, respectively

$$\lambda_P(v,J) = hc[E(v,J) - E(v-2,J+1)]^{-1} \qquad \text{(II.D.2)}$$

$$\lambda_R(v,J) = hc[E(v,J) - E(v-2,J-1)]^{-1} \qquad \text{(II.D.3)}$$

In spectroscopic notation, equations II.D.2 and II.D.3 correspond to the vP(J+1) and vR(J-1) overtone transitions. The lineshapes are determined by Lorentz and Doppler broadening. The line spacing exceeds the line widths in our experimental conditions by over 3 orders of magnitude, so overlap of lines is improbable.

In the CS_2/O_2 laminar mixing layer flame, there are regions of vibrational nonequilibrium; therefore, a vibrational temperature is not a well defined quantity. In free burning CS_2/O_2 flames the rates for equilibration of the rotational distribution are rapid compared with other flame processes [II.30]. The rotational distributions on all the vibrational levels can be characterized by a single rotational temperature, equal to the gas kinetic temperature. The equilibrium rotational distribution for CO in vibrational level v is given by equation II.D.4 [II.13].

$$N_v(J) = N_v(2J+1)\ \exp(-(E(v,J) - E(v,0))/k_BT)/\ Q_r \qquad \text{(II.D.4)}$$

where

$$N_v = \sum_J N_v(J)$$

and Q_r is the rotational partition function,

$$Q_r = \sum_{J=0}^{\infty} (2J+1)\ \exp(-(E(v,J) - E(v,0))/k_BT)$$

Equations II.D.5 and II.D.6 are expressions for the intensities per unit wavelength as a function of J for the P and R branch CO overtone spontaneous transitions. The P branch transitions have a slightly greater probability than the R branch transitions [II.13],

$$I_{vP}(J) = CN_v A_{v,v-2} \lambda_P(v,J)^{-4} (J+1) \exp\{-(E(v,J) - E(v,0))/k_B T\} \quad (II.D.5)$$

$$I_{vR}(J) = CN_v A_{v,v-2} \lambda_R(v,J)^{-4} (J) \exp\{-(E(v,J) - E(v,0))/k_B T\} \quad (II.D.6)$$

where C is a constant and $A_{v,v-2}$ is the Einstein coefficient for the $v \rightarrow v-2$ overtone transition. Observation of the relative emission intensities of two different rotational lines on the same vibrational transition provides sufficient data to solve for the temperature using equations II.D.5 and II.D.6.

We can predict the spectrum of the CO overtone emission that will be measured assuming a vibrational distribution. The predicted intensity is $I(\lambda)$:

$$I(\lambda) = \eta(\lambda) \sum_{\substack{\text{all} \\ v,J}} [s(\lambda-\lambda_P(v,J)) \times I_{vP}(J) + s(\lambda-\lambda_R(v,J)) \times I_{vR}(J)]$$

where $\eta(\lambda)$ is the efficiency of the detecting optical system, and $s(\lambda-\lambda')$ is the slit function; both $\eta(\lambda)$ and $s(\lambda-\lambda')$ will be discussed further in this section. The intensity contribution due only to the emitting population in a single vibrational level can be predicted by fixing v in the sum above. The intensities can be predicted to within a single normalization constant, C, which enters through $I_{vP}(J)$ and $I_{vR}(J)$.

Figure II-D-2 shows the predicted emission intensities from CO(v=2) in rotational equilibrium at each of three temperatures, 500°K 1000°K, and 2500°K, as would be observed with a monochromator with slits set to allow 5Å resolution. This resolution is about two orders of magnitude larger than the Doppler line width. In Figure II-D-2, the normalization for each curve is arbitrary and different. The emission is over a broader band at elevated temperatures, because higher rotational levels are populated.

The wavelengths of the P branch CO overtone emission spectral lines on a single vibrational band increase with increasing J, and their spacing also increases with increasing J. For R branch lines, the wavelength initially decreases with increasing J. The spacing of the R branch lines decreases with increasing J until the wavelength reaches a bandhead; further increasing J increases both the wavelength and the spacings of successive J lines. The energies of the transitions on the v=2 → v=0 band are plotted as a function of the emitting rotational level in Figure II-D-5. The minimum wavelength found on the R branch marks the bandhead of the vibrational transition. The bandhead of the v=2 → v=0 transition can be seen in Figure II-D-2 to be just above 2.28 μm. Near the bandhead, the lines are finely spaced. The R branch bandheads are a pronounced feature of the CO overtone spectra from our CS_2/O_2 flames. Rotational levels which emit near the bandhead are populated, in evidence of high temperatures, T > 2500°K. The value of J at the bandhead of the R branch transition is found as a function of the vibrational band by solving equation II.D.7; the solution is equation II.D.8.

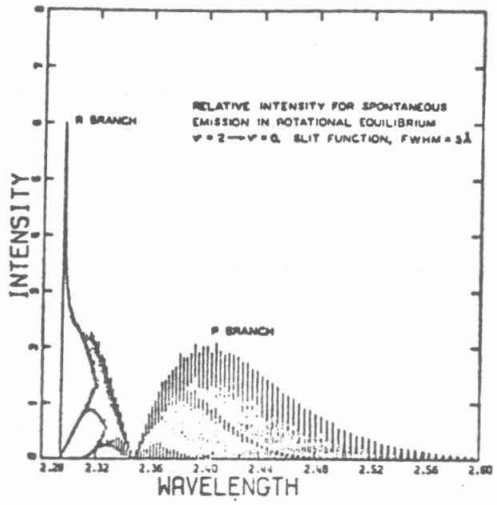

Figure II-D-2
Predicted spectrum due to the v=2 → v=0 band of CO: 5Å resolution

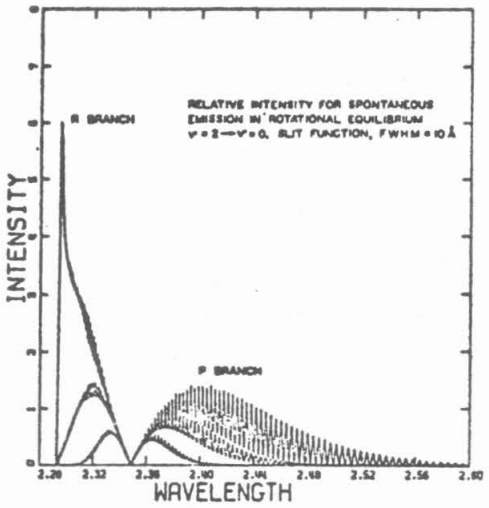

Figure II-D-3
Predicted spectrum due to the v=2 → v=0 band of CO: 10Å resolution

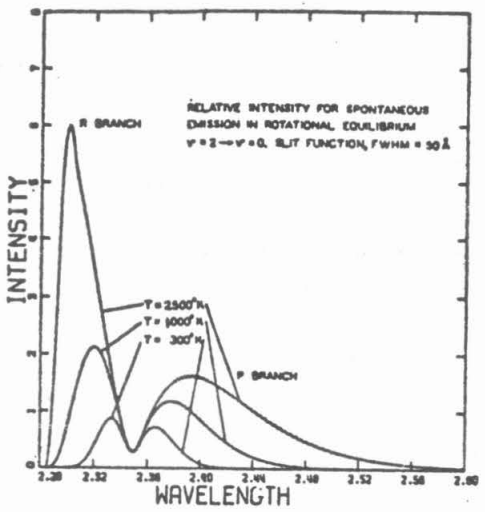

Figure II-D-4
Predicted spectrum to the v=2 → v=0 band of CO: 50Å resolution

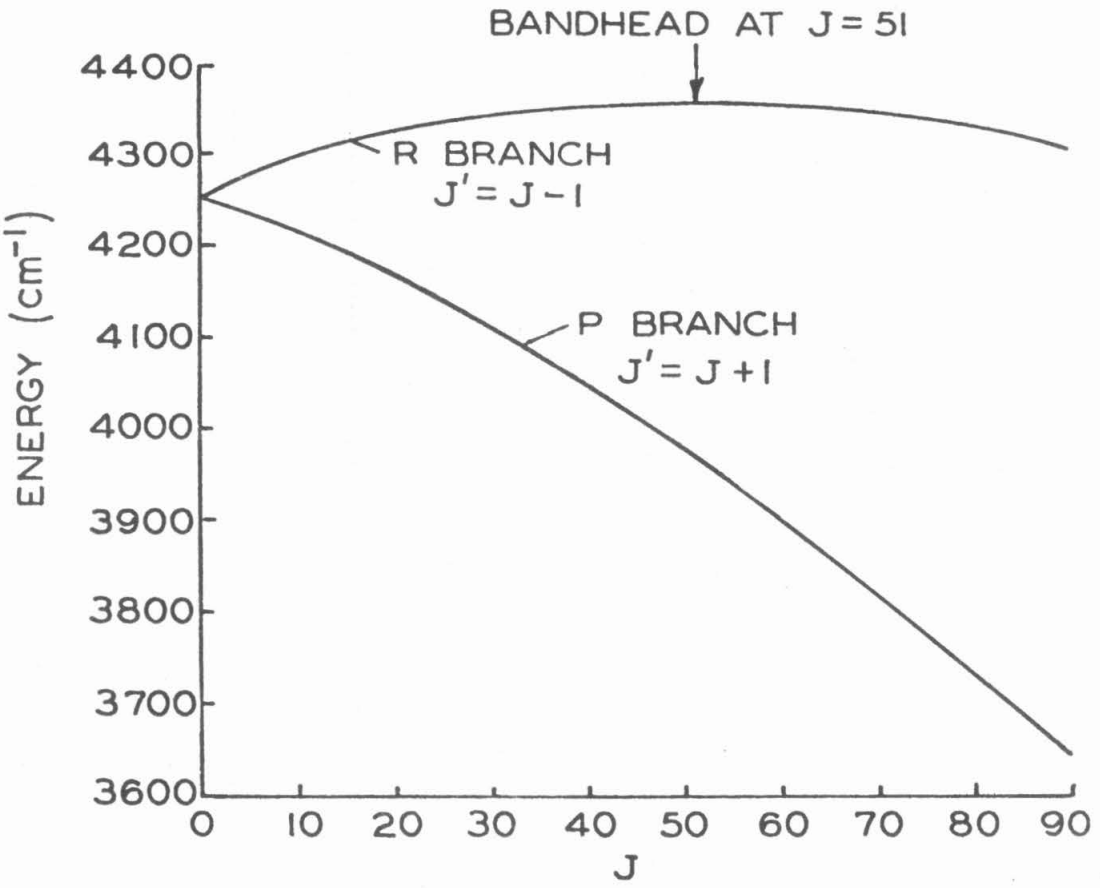

ENERGY OF THE FIRST OVERTONE TRANSITIONS

$(v'' = 2, J) \longrightarrow (v'' = 0, J')$

Figure II-D-5 Energy of the CO overtone transitions, (v=2,J) → (v=0,J) as a function of J

$$\frac{\partial \lambda_R(v,J)}{\partial J} = 0 \qquad \text{(II.D.7)}$$

$$J \simeq (52.5 - .45v) \qquad \text{(II.D.8)}$$

For each vibrational overtone band, the missing spectral line from the overtone Q branch transition, J=0 → J=0, marks the vibrational band origin. In Figure II-D-2 the 2 → 0 band origin is at the intensity minimum just below 2.35 μm. Band origins for successive vibrational transitions are separated by about half the band-origin, bandhead spacing. The lines of different vibrational transitions are consequently interspersed among each other.

Inferring Temperatures, CO Concentrations, and CO Vibrational Populations from Spectra

A McPherson model 2501 scanning monochromator and a lead sulfide infrared detector at ambient temperature were used in taking CO overtone spectra. The experimental apparatus is described in Chapter II, Section A. Calibration with a He-Ne laser line shows the monochromator passes light most efficiently at the wavelength to which it is tuned, λ_o, and with linearly decreasing efficiency as the wavelength varies, as shown in Figure II-D-6. The dependence of the efficiency on wavelength is known as the slit function, $s(\lambda-\lambda_o)$. Using 1.5 mm wide input and output slits, the full width at half maximum of the slit function is about 48Å, and it varies linearly with the slit widths. The narrower the slits, the finer is the resolution, but at the severe penalty of reduced output signal. Experimentally, individual CO spontaneous overtone emission lines were not resolvable.

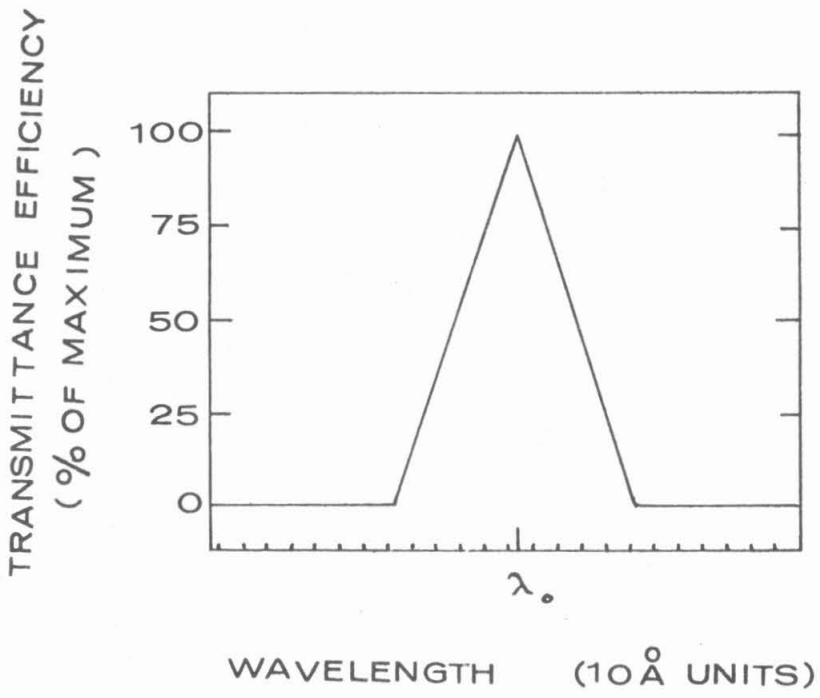

Figure II-D-6 Transmittance efficiency curve for the monochromator tuned to λ_o using 1.5 mm slits and a 300 line/mm grating. The full width at half maximum is 48Å.

Adjacent rotational lines on a CO overtone band are less than 10Å apart, often considerably less, such as near the R branch bandheads. The intensity passed by the monochromator is the sum of the intensities of all the emission lines in the band passed by the monochromator. The CO spectra observed consequently display an intensity continuum. Peaks are found near the R branch bandheads where many lines, finely spaced, are simultaneously passed by the monochromator. These peaks are sharper, and at slightly shorter wavelengths when the CO is at higher temperatures, because the higher rotational levels near the bandheads are populated. Dilution of the combustibles reduces the flame temperatures, resulting in less pronounced peaks near the bandheads. The contrast in the predicted spectra of the $(2 \rightarrow 0)$ band for three gas temperatures and spectral resolutions can be seen in Figures II-D-2, II-D-3, and II-D-4. The normalization of each curve is arbitrary and different.

Emission spectra were taken of CS_2/O_2 flames using the lens-scanning monochromator-detector system. Black body spectra were taken to calibrate the relative efficiency of the optical system as a function of wavelength. Experimental details can be found in Chapter II Section A. Equation II.D.9 gives the theoretical variation of the emission intensity from the black body as a function of wavelength [II.31,II.32],

$$I_{BB}(\lambda) = \frac{C_{BB}}{\lambda^5(\exp(hc/k_B\ 644°K) - 1)} \qquad \text{(II.D.9)}$$

where C_{BB} is a constant independent of λ. The temperature of our black body source is 644°K.

The output signal intensity of the detector when viewing the black body standard will be called $I_{OBB}(\lambda)$. $I_{OBB}(\lambda)$ equals the product

of the emission intensity of the standard, which is assumed to be $I_{BB}(\lambda)$, and the net efficiency of the optical system $\eta(\lambda)$. This is stated in equation II.D.10. $\eta(\lambda)$ accounts for variations with wavelength in losses along the optical path and in the sensitivity of the detector. The net response on the optical system is assumed linear with intensity;

$$I_{OBB}(\lambda) = I_{BB}(\lambda)\ \eta(\lambda) \qquad \text{(II.D.10)}$$

The spectra of the flames were corrected to remove the variations due to the efficiency of the optical system. This efficiency, $\eta(\lambda)$, is determined by equation II.D.10 using our experimental values for $I_{OBB}(\lambda)$, and equation II.D.9 for $I_{BB}(\lambda)$. A corrected spectrum $I_c(\lambda)$ was generated from each observed flame spectrum $I_o(\lambda)$ using equation II.D.11,

$$I_c(\lambda) = I_o(\lambda)/\eta(\lambda) \qquad \text{(II.D.11)}$$

$I_c(\lambda)$ is the corrected flame spectrum, one that would be observed using an optics-detector system with uniform efficiency over all wavelengths. Figure II-D-7 shows an uncorrected experimental spectrum, and Figure II-D-8 shows the corresponding corrected spectrum. Figure II-D-9 shows the theoretically predicted spectrum of CO in vibrational equilibrium. Comparison of Figures II-D-7, II-D-8, and II-D-9 reveals that the vibrational population responsible for the emission intensity shown in Figure II-D-7 must be nearly in equilibrium over the lower levels. The strong band starting at 2.65 μm is discussed in Chapter II Section E; it is due to CO_2.

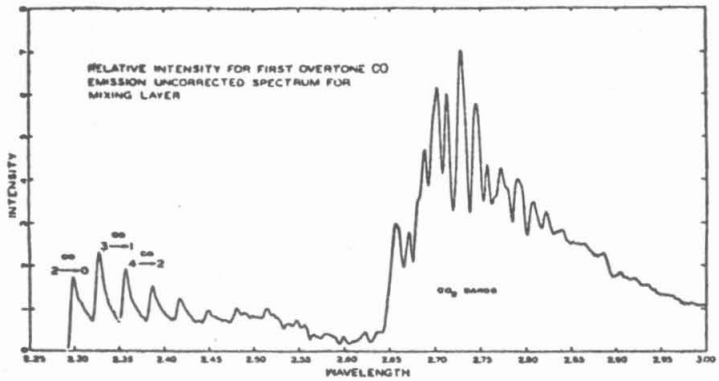

Figure II-D-7 Emission spectrum from a CS_2/O_2 mixing layer flame in the region 3.8 cm downstream of the splitter plate and in the plane of the splitter plate

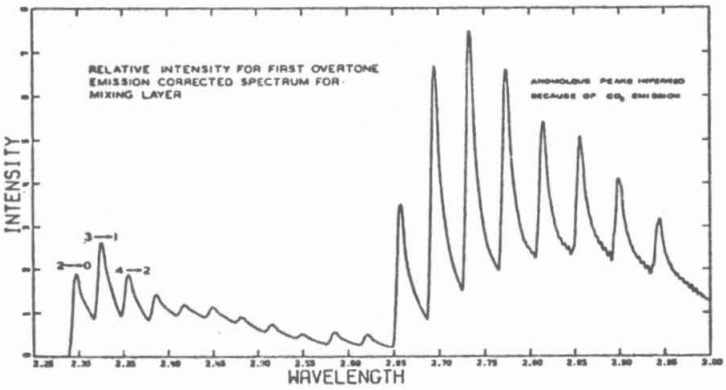

Figure II-D-8 A corrected spectrum corresponding to Figure II-D-7 with efficiency of the optical system accounted for, and assuming CO is the emission source

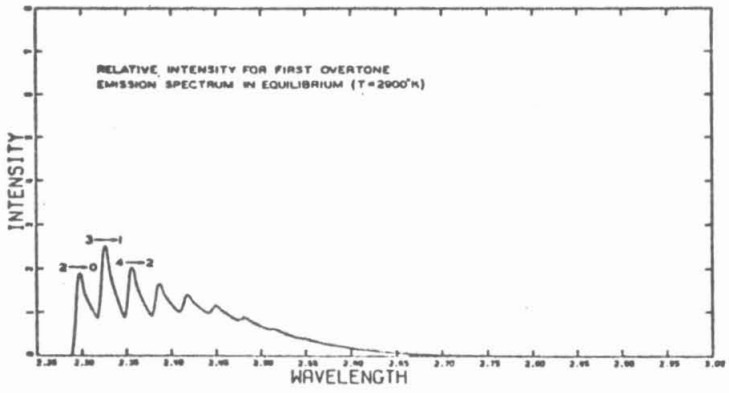

Figure II-D-9 Predicted spectrum of CO in vibrational and rotational equilibrium at 2900°K

The CO rotational temperature is determined from the CO overtone spectra. The technique used is similar to that discussed in References II.19 through II.21. The variation with temperature of the spectra near the bandhead of the v=2 → v=0 vibrational transition can be seen in Figure II-D-4. A sharper peak, shifted slightly to shorter wavelength, indicates an elevated temperature. The rotational temperature is found, as a parameter, by curve fitting to two intensities on the spectrum near the bandhead of the v=2 → v=0 transition. Earlier we saw that this single rotational temperature characterizes the rotational distribution on all the vibrational levels, and equals the gas kinetic temperature.

All the vibrational-rotational state populations can be found after determining the rotational temperature and calculating the corrected CO overtone spectrum. The contribution to the corrected spectrum due to the emission from each vibrational level is isolated; the contribution of individual bands can be seen, comparing Figures II-D-10, II-D-11, and II-D-12. To isolate the contribution of each vibrational band to the spectrum, we began by measuring the intensity from the corrected spectrum at a chosen wavelength near the bandhead of the (2 → 0) transition. This region of the spectrum has no overlap from other vibrational bands. From this intensity and the temperature, the intensity contribution over the whole spectrum of the v=2 → v=0 band is calculated utilizing equations II.D.5 and II.D.6. Sequentially, the intensity contributions of higher vibrational bands (3 → 1, 4 → 2, 5 → 3, ···) are found by measuring the intensities from the corrected spectrum at chosen wavelengths near each vibrational bandhead, and subtracting the calculated

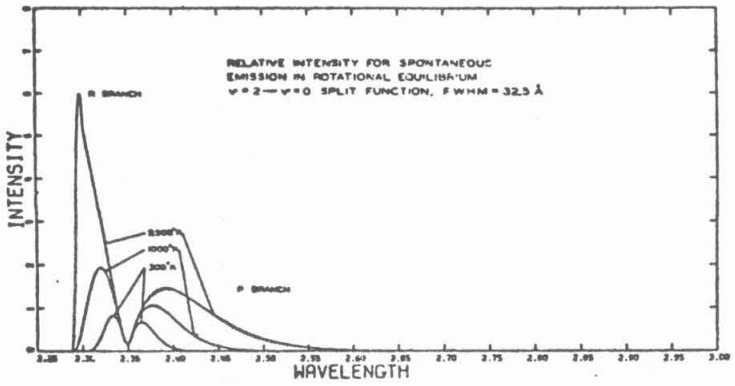

Figure II-D-10 Predicted overtone emission from CO(v=2) in equilibrium at three temperatures

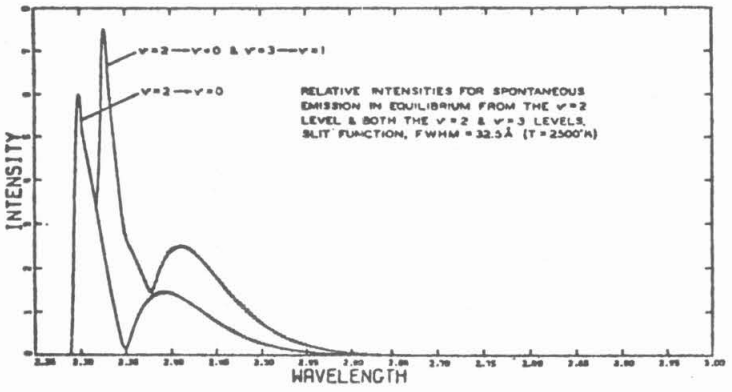

Figure II-D-11 Predicted overtone emission from CO(v=2) and CO(v=3) in equilibrium at 2500°K

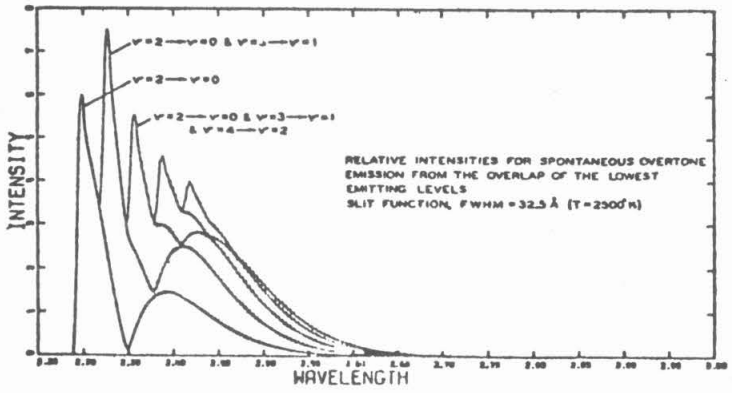

Figure II-D-12 Predicted overtone emission from CO($2 \leq v \leq 6$) in equilibrium at 2500°K

contributions from lower vibrational bands. This works, because near the bandhead of each rotational transition, there is only overlap from lower vibrational bands. Once the intensity contribution to the corrected spectrum from each vibrational band is isolated, the total emission on each vibrational band can be calculated.

The photon flux from an optically thin flame in each vibrational overtone band of carbon monoxide is proportional to the population in the emitting vibrational level, v. The constant of proportionality is the Einstein spontaneous emission coefficient, $A_{v,v-2}$. The total emission intensity on the $(v \rightarrow v-2)$ band, designated $I_c(v)$, is proportional to the rate at which photons are emitted, multiplied by the energy per photon ($E \propto 1/\lambda$). The average photon energy over each band is taken to be the energy of a photon with the band origin wavelength. The relation between the band intensities and the vibrational populations is given in equation II.D.12.

$$\frac{N_v}{N_{v'}} = \frac{I_c(v)\,\lambda_{v'}\,A_{v',v'-2}}{I_c(v')\lambda_v\,A_{v,v-2}} \qquad \text{(II.D.12)}$$

For equation II.D.12 to be useful, (i) the Einstein coefficients must be known (the values from References II.33 and II.34 are used), (ii) the flame must be optically thin, as it is calculated to be, and (iii) the emission intensity must indeed be due to CO, not an anomalous emission source.

By inferring vibrational populations from the spontaneous emission intensity, we find the ratios of populations in vibrational levels, not the absolute populations. The relative CO vibrational populations

across the mixing layer are obtained using equation II.D.13

$$\frac{N_v(z,y)}{N_{v'}(z,y)} = \frac{I_c(v;z,y)\,\lambda_{v'}\,A_{v',v'-2}}{I_c(v';z,y')\,\lambda_v\,A_{v,v-2}} \qquad \text{(II.D.13)}$$

The coordinates (z,y) designate the location in the CS_2/O_2 flame; at (z,y) the corrected total intensity on the ($v \rightarrow v-2$) band is $I_c(v;z,y)$.

Because overtone spectra were observed, no information on the populations in levels v=0 and v=1 was found. The populations in the v=0 and v=1 levels were approximated for each vibrational distribution by assuming that levels v=0, v=1 and v=2 were populated in equilibrium, characterized by the rotational temperature. Nonequilibrium populations were inferred only in the higher vibrational levels. The populations in the v=2,3, and 4 levels were observed to be in equilibrium at temperatures near (±200°K), the rotational temperature. This motivates the assumption of equilibrium on the lowest three levels.

At each location in the mixing layer flame (z,y) the total CO concentration was determined by summing the relative concentrations $N_v(z,y)$ over all v,v = 0,1,2,···. The concentration deduced was a relative concentration. It was useful in comparison to other CO concentrations likewise obtained throughout the flame.

Error Analysis

Experimental variations in the emission or calibration spectra can be due to electrical noise or changes in the optical alignment and flow conditions. These variations lead to uncertainties in the inferred temperatures and CO vibrational populations. Errors in the low

vibrational level populations propagate to the higher levels because of the sequential technique by which the spectra were deconvolved into the contributions from individual vibrational bands. A spurious emission intensity contribution for one vibrational band will induce an error of the opposite sense in the intensity contribution of the next band (as an example, consider the points at v=5 and v=6 on Figure II-E-13). An error bound estimate for the populations in the vibration levels, N_v, is given by equations II.D.14 and II.D.15.

$$N_v(\text{inferred}) - \Delta N_v < N_v(\text{actual}) < N_v(\text{inferred}) + \Delta N_v \qquad \text{(II.D.14)}$$

$$\Delta N_v/N_v \simeq .1\sqrt{1 + \tfrac{1}{2}\,(N_{v-1}/N_v)^2} \qquad \text{(II.D.15)}$$

Equation II.D.15 reflects an uncertainty in emission signal intensity of up to 10%. In practice, we can neglect errors propagating up more than one vibrational level. This bound, ΔN_v, may be excessive for cases in which the emission signal is steady and large; the smoothness of the vibrational population profiles is indicative of the reproducibility of the data.

The temperature was found to within about 5%. Errors again result primarily from fluctuations in the emission signal. We use the rotational temperature in deconvolving the spectra into contributions from individual vibrational bands. However, the inferred relative vibrational level populations are insensitive to small variations in the temperature, and the errors in the vibrational distribution propagated by uncertainties in the temperature are negligible in comparison to the error bound, equation II.D.15.

Summary

A technique for determining the CO rotational temperature, relative vibrational populations, and relative CO total concentration in a CS_2/O_2 flame has been presented. The assumptions used in this analysis are: (i) the medium is optically thin ; (ii) the Einstein coefficients are known; (iii) the emission source is CO; (iv) the response of the optical system does not vary with intensity; and (v) there is rotational equilibrium. In addition, the lowest three vibrational levels, v=0, 1, and 2, are assumed in equilibrium in order to calculate the relative total CO concentration.

E. A Spectroscopic Investigation of the CS_2/O_2 Mixing Layer Flame

The CS_2/O_2 mixing layer flame was examined by use of infrared emission spectroscopy. The pressures were in the range 3 to 20 torr, and the gas flow velocities were typically about 1 m/sec. Upstream, within a centimeter of the leading edge of the flame, there was CO in vibrational nonequilibrium, but not in a vibrational inversion. Downstream, beyond about 2.5 cm, the CO vibrational distribution was relaxed and COS and CO_2 had been formed. The temperatures and CO concentrations were at a maximum a few centimeters downstream. The maximum temperatures in the mixing layer flame were above 2500°K. In the following section, evidence in support of these statements will be presented. The importance of COS in deactivating vibrationally excited CO and the effect of additive N_2O will be discussed.

The distribution of CO vibrational populations in a two-dimensional laminar mixing layer flame was found by means of CO overtone emission spectroscopy. The technique used to deduce the CO vibrational distributions from the infrared spectra is explained in Section D of this chapter. Five assumptions were employed in deducing the CO vibrational distributions: (i) the emitting gas is optically thin; (ii) the Einstein coefficients are known for the observed transitions; (iii) CO is the emitting molecule; (iv) the CO is in rotational equilibrium at the kinetic temperature; and (v) the response of the optical system is linear with the emission intensity.

CO Vibrational Distributions, Variations along the Direction of Flow

CS_2/O_2 laminar mixing layer flames without gas additives were

studied using both the large and small double-slot injectors described in Chapter II, Section A. The pressures ranged from 3 to 20 torr, and the flow velocities at the burner exits ranged from .5 to 5.0 m/sec. Strong vibrational nonequilibrium on the levels $v \geq 5$ was found at the upstream edges of these flames.

Our most exhaustive studies employed the large double-slot injector at pressures 4 torr and above. These flames attached to the splitter plate, and nonequilibrium on the levels $v \geq 5$ was inferred within a centimeter of the edge of the splitter plate. Vibrational levels 2, 3, 4, and 5 were populated in equilibrium with one another, characterized by a vibrational temperature which was measured to equal ±200°K, the rotational temperature. Figure II-E-1 displays a typical spectrum taken from a CS_2/O_2 laminar mixing layer flame within a centimeter of the splitter plate. Figure II-E-2 shows CO vibrational distributions inferred from spectral measurements in a CS_2/O_2 laminar mixing layer flame.

The spectra of the flame 5 to 10 centimeters downstream of the splitter plate differed from the spectra within a centimeter of the splitter plate. Downstream, the spectra exhibited a strong band starting at 2.65 μm and extending past 3.0 μm. Figure II-E-3 displays such a spectrum, and Figure II-E-2 displays a typical downstream vibrational distribution. If CO is the emission source (and keep in mind that we will argue it is due to CO_2) then the emission in the band that started at 2.65 μm and extended out past 3.0 μm was due to populations in the $v = 13,14,15,\cdots$ vibrational levels of CO. Under a variety of flow conditions, the band observed at and above 2.65 μm was always a feature of

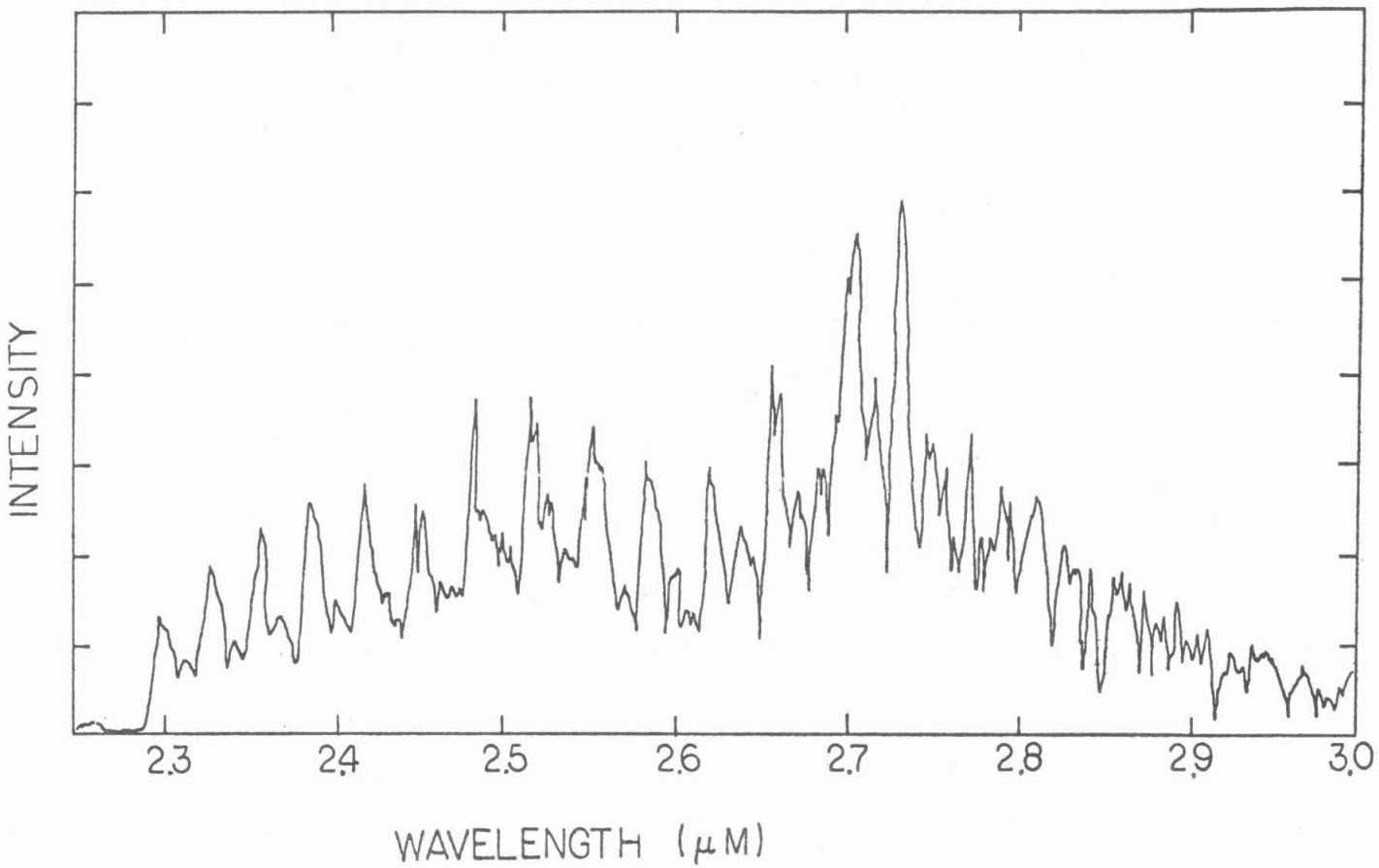

Figure II-E-1 Emission spectrum from a CS_2/O_2 mixing layer flame in the upstream region, 1.3 cm downstream of the splitter plate, and in the plane of the splitter plate. U_{O_2} = 3.4 m/sec; U_{CS_2} = 1.0 m/sec, p = 5.4 torr.

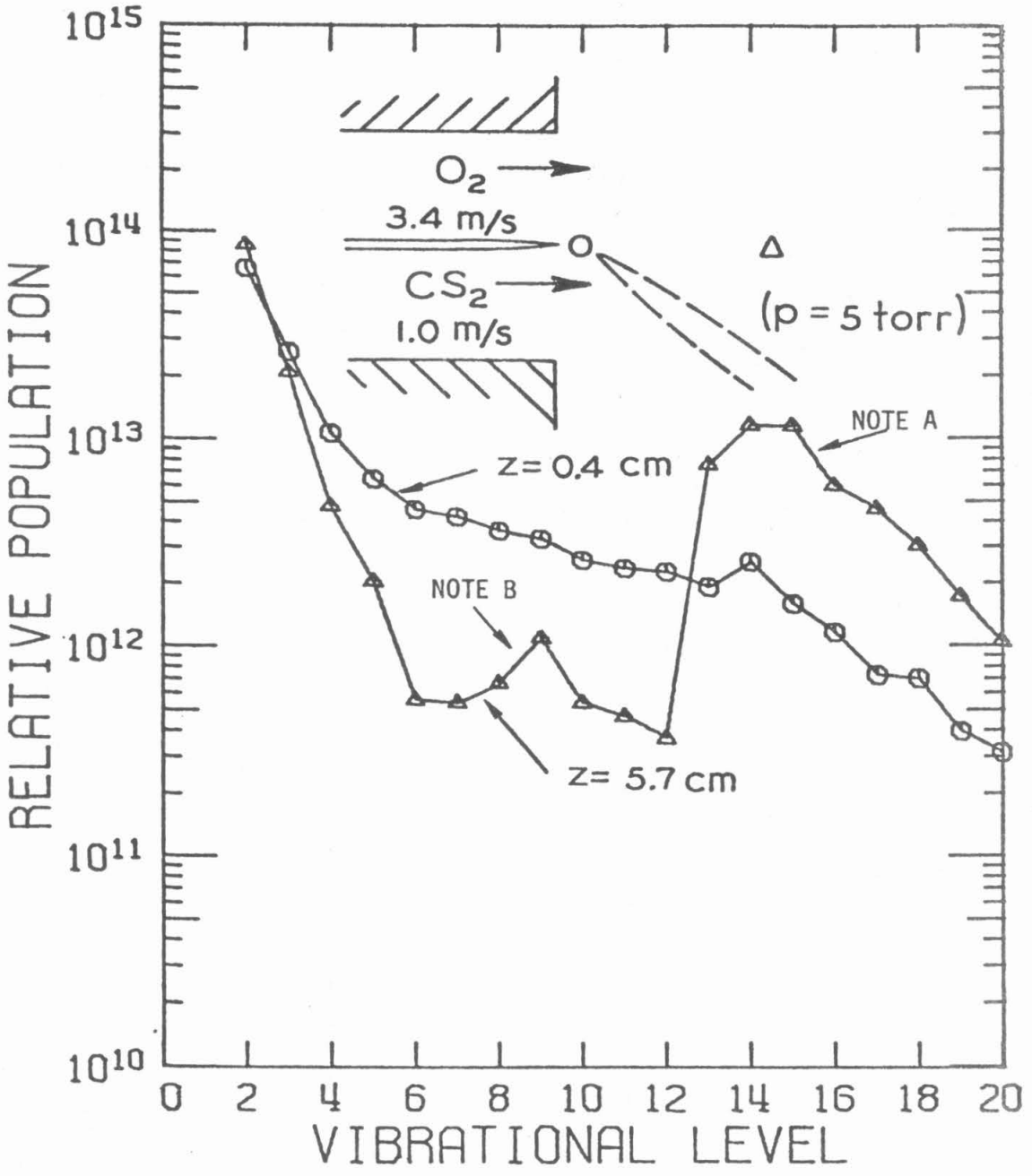

Figure II-E-2 Relative populations of CO(#/cm^3) as a function of vibrational level in a CS_2/O_2 mixing layer flame at .5 torr; U_{O_2} = 3.4 m/sec; U_{CS_2} = 1.0 m/sec.

NOTE A: Anomalous peak due to COS, not CO.
NOTE B: Anomalous peak due to CO_2, not CO.

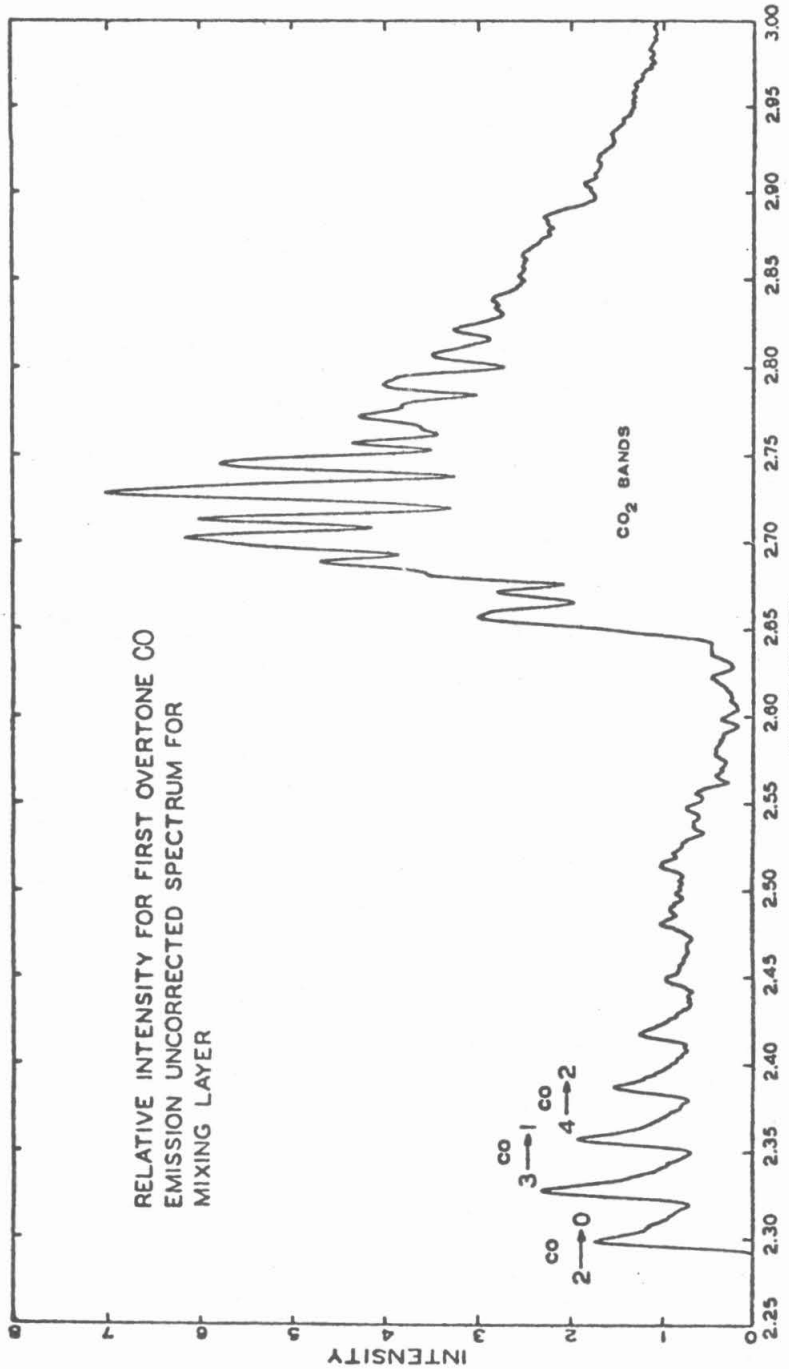

Figure II-E-3 Emission spectrum from a CS_2/O_2 mixing layer flame in the downstream region: 3.8 cm downstream of the splitter plate, and in the plane of the splitter plate. U_{O_2} = 3.3 m/sec; U_{CS_2} = 1.0 m/sec; p = 5.1 torr.

the downstream region in the CS_2/O_2 mixing layer flame. The vibrational distributions also showed a small peak at v = 9, corresponding to emission at about 2.5 μm. This emission was neither as strong, nor as reproducible, as the peak at 2.65 μm.

There were experimental difficulties associated with taking infrared emission spectra at wavelengths near and above 2.6 μm. Molecular absorption bands of H_2O and CO_2, both present in the atmosphere, lie in this region, and they imposed their absorption signatures on the emission of the flame. The entire optical system was never successfully purged of these absorbers. It remained a discomforting feature of the experiment that absorption losses had to be accounted for in the calibration of the response of the optical system, rather than by eliminating the absorbers.

In the spectral region, $\lambda \geq 2.6$ μm, where there were difficulties due to absorption, there were the most striking results. Based on the assumption that CO was the emission source, a total inversion was deduced to exist between vibrational levels 13 and 12, 14 and 13, and sometimes 15 and 14. The small signal gain was less than .25%/cm on all these CO vibrational-rotational transitions; this estimate was based on the measured vibrational populations and temperatures.

Mirrors were installed in order to make a laser with the CS_2/O_2 mixing layer flame. The mirrors were coated for minimum cavity losses on the P branch transitions from upper vibrational level v = 14. The optical cavity, described in Chapter II, Section A, consisted of internally mounted mirrors with a double-pass active length of 40 cm. The

double-pass mirror losses did not exceed 2.5%; consequently, the small signal gain at laser threshold was less than .07%/cm. This was less than the inferred gain. The flame did not operate as a laser.

The $CS_2 + O_2 + N_2O$ Premixed Flame

For comparison with the CS_2/O_2 mixing layer flame, we examined a $CS_2 + O_2 + N_2O$ premixed flame similar to the flames reported in References II.35, II.36, and II.27. A single slot of our large double-slot injector supplied the gas mixture to the chamber. Typically, the pressure was 10 to 15 torr and the gas exited the injector at about 1 m/sec. The gas stream then spread and slowed until the flame-front. The flame speeds were about .6 m/sec under these conditions. The $CS_2:O_2:N_2O$ ratios were about 1:30:5. These flames supported laser action. The laser output was sensitive to the position of the flame in the optical cavity. Moving the injector 4 mm downstream brought the laser output from zero to a maximum, and to zero again. Because of the difficulty in stabilizing the flame to millimeter accuracy, it was not possible to observe if there was any variation in the laser spectrum as the flame was moved through the optical cavity.

An infrared spectrum of a $CS_2/O_2/N_2O$ flame is shown in Figure II-E-4, and the inferred CO vibrational populations are shown in Figure II-E-5. The CO vibrational populations were also inferred from the laser spectrum of the same flame, shown in Figure II-E-6, with the results shown in Figure II-E-7. The technique by which the results in this figure were obtained is explained in the next paragraph. The vibrational populations inferred by spontaneous emission and laser emission

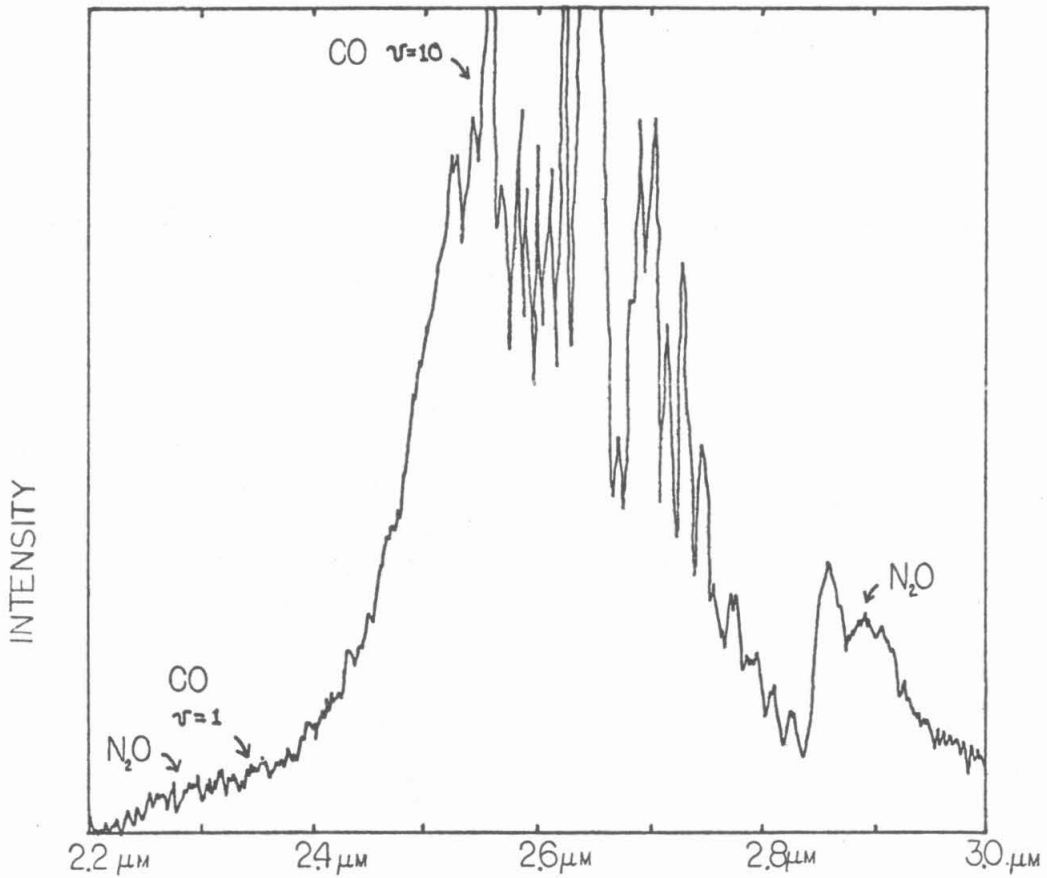

Figure II-E-4 Emission spectrum from the visibly luminescing zone of a premixed $CS_2/O_2/N_2O$ flame; p = 14.6 torr; $CS_2:O_2:N_2O$ ratio = 1:28:7

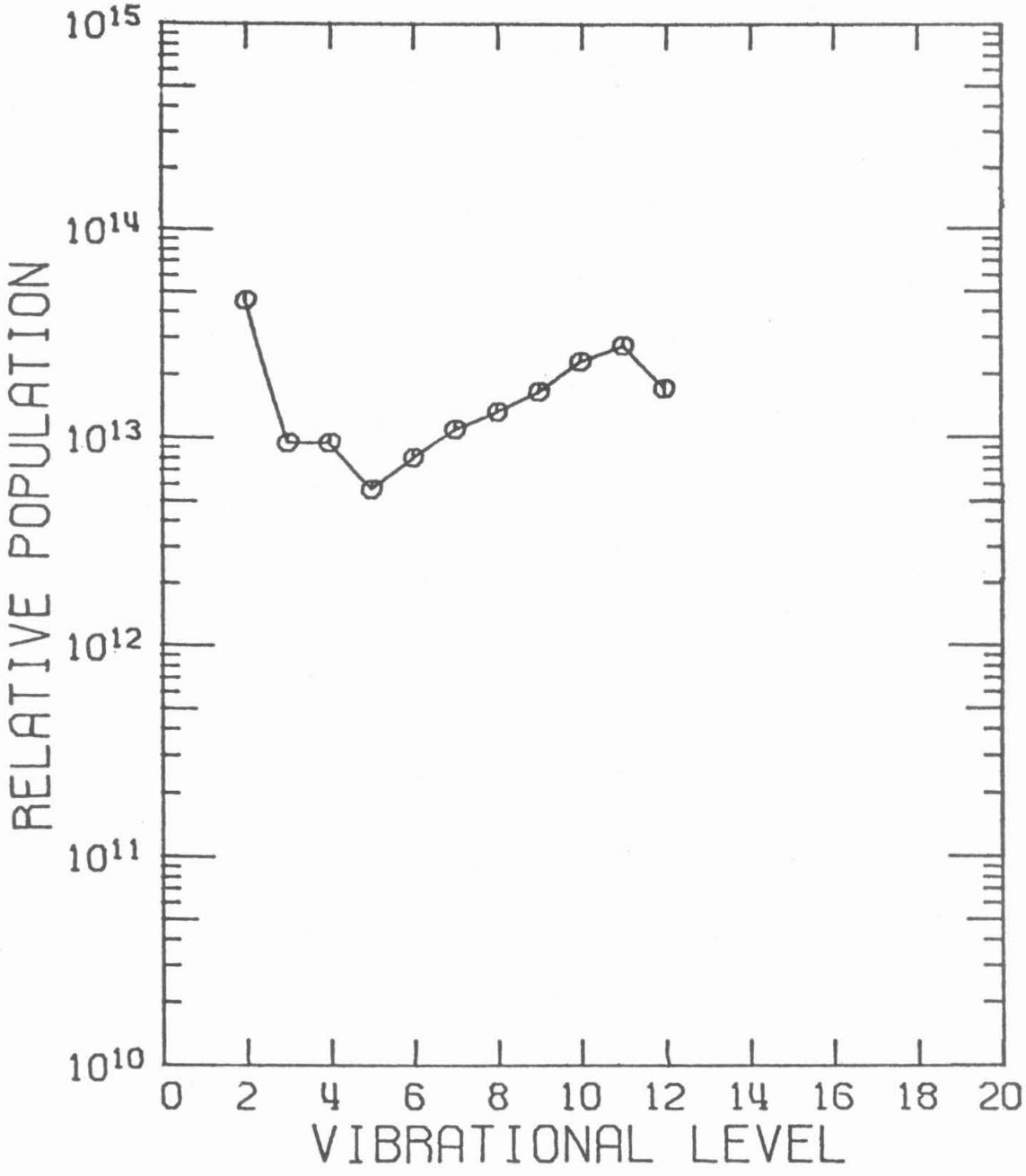

Figure II-E-5 Vibrational populations of CO (#/cm^3) in the visibly luminescing region of a premixed $CS_2/O_2/N_2O$ flame at 14.6 torr; CS_2:O_2:N_2O ratio 1:28:7

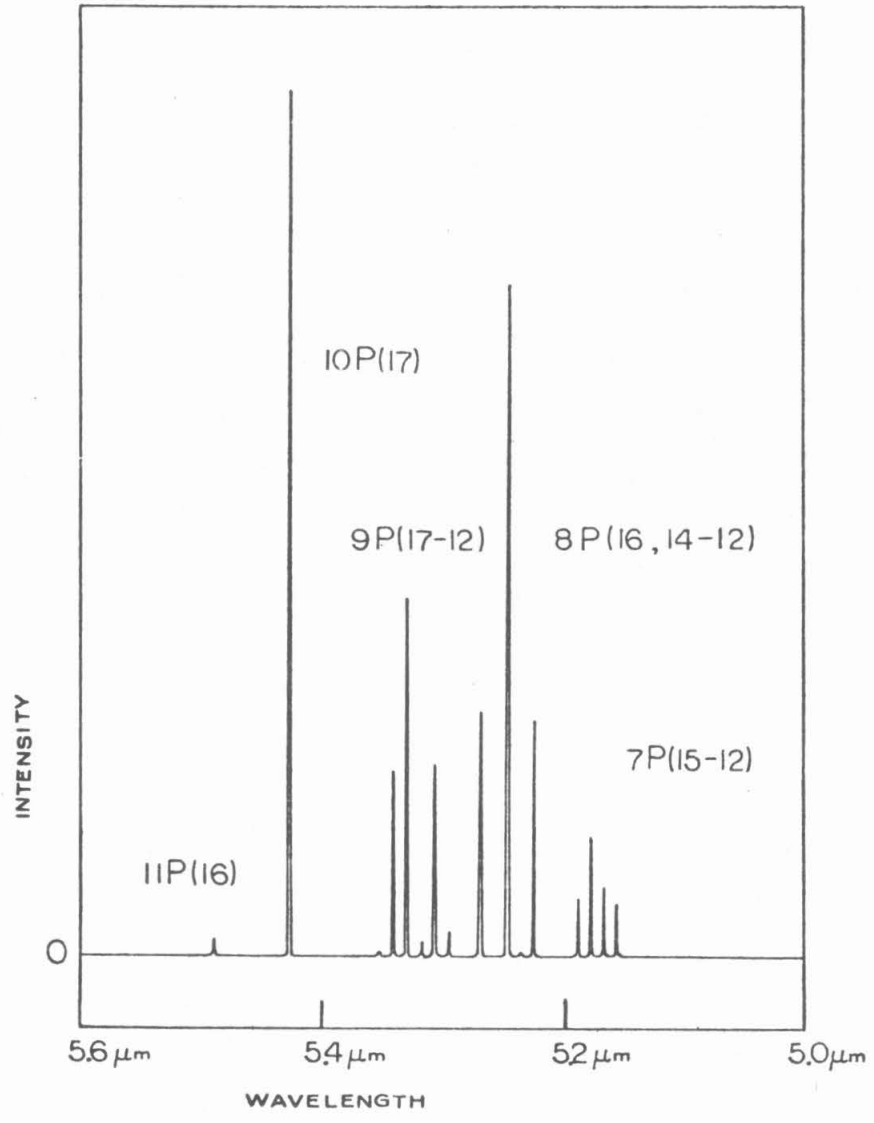

Figure II-E-6 Laser emission spectrum from a premixed $CS_2/O_2/N_2O$ flame at 14.6 torr; $CS_2:O_2:N_2O$ ratio 1:21:4

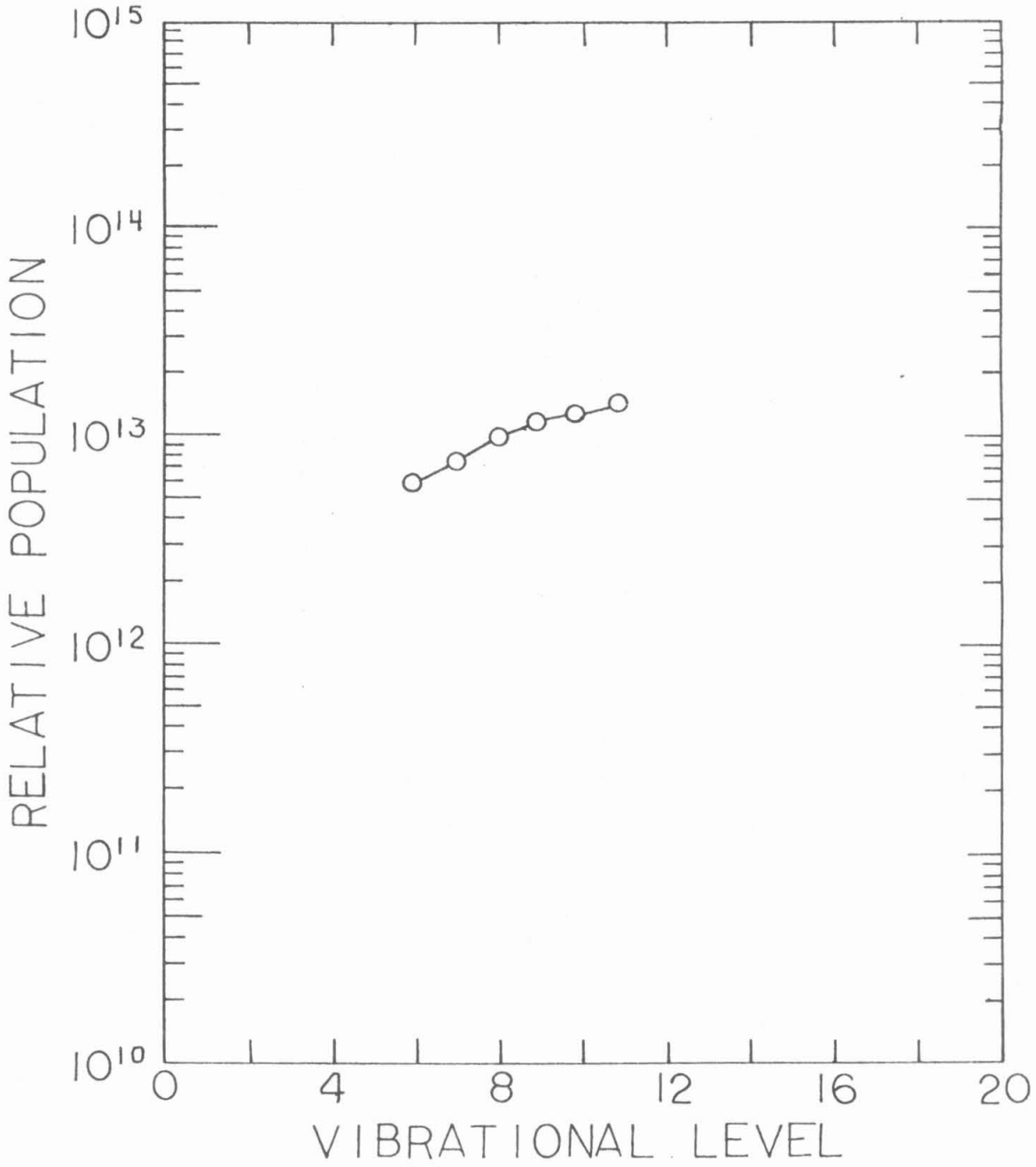

Figure II-E-7 Vibrational populations of CO (#/cm^3) in a premixed $CS_2/O_2/N_2O$ flame at 14.6 torr; CS_2:O_2:N_2O ratio 1:28:4, found from the laser emission spectrum.

measurements, Figures II-E-5 and II-E-7, are in satisfactory agreement.

The ratio of the populations in adjacent vibrational levels, N_v/N_{v-1}, can be found using the laser output spectrum. Assuming the temperature is the rotational temperature, found by emission spectroscopy, and the medium is Doppler broadened, there is a family of curves in the parameter N_v/N_{v-1} representing the dependence of the small signal gain on the transition vP(J) as a function of J. The curves used were from Reference II.37, which is an extension of similar work on CO_2 reported in Reference II.38. The rotational level at which each curve was a maximum, J_m, varied with N_v/N_{v-1}. The rotational level J_m for which the small signal gain on the vP(J) transition was a maximum was approximated to be the transition vP(J), with the maximum measured laser power. The value N_v/N_{v-1} was found by selecting the gain curve with a maximum at J_m, and identifying the parameter N_v/N_{v-1} for that curve.

In the laser spectrum shown in Figure II-E-6 there was laser output on all the vibrational transitions for which an inversion was inferred by emission measurements except the $v=6 \rightarrow v=5$ transition. This can be seen comparing the output spectrum, Figure II-E-6, with the corresponding vibrational level populations, Figure II-E-5. The gain inferred on the $6 \rightarrow 5$ transition, which was not lasing, was less than the gain on the laser transitions, due to both a weaker inversion and smaller Einstein coefficients. Moreover, the mirror losses were a minimum for the v = 14 to v = 13 transition, and were larger for the lower transitions. Agreement between the vibrational populations inferred from spontaneous emission and the laser emission observed in the

$CS_2 + O_2 + N_2O$ premixed flame is evidence of the validity of the technique for inferring vibrational populations from spectra for the levels $v \leq 12$.

Comparison of Mixing Layer and Premixed CS_2/O_2 Flames

CS_2/O_2 laminar mixing layer flame and laminar premixed flames were studied spectroscopically; both flames had no gas additives. The spectra of the mixing layer flame near the splitter plate was similar to the spectra of the premixed flame in the upstream edge of the region of visible emission, and similar CO vibrational populations are inferred. The region 5 cm downstream of the splitter plate in the mixing layer flame produced strong emission bands starting at 2.65 μm --more so than the premixed flames; compare Figures II-E-2 and II-E-12.

The Presence of CO_2

Spectra were taken of COS/O_2, CO/O_2, and H_2S/O_2 laminar mixing layer flames for comparison with the CS_2/O_2 flame. The spectra of both COS/O_2 and CO/O_2 flames have bands starting at 2.65 μm that resemble the band seen in the spectra of the downstream region of the CS_2/O_2 mixing layer flame; this is shown in Figures II-E-8 and II-D-9. The spectra of the COS/O_2 flame has a prominent broad band around 2.5 μm. The infrared spectrum of the H_2S/O_2 flame, shown in Figure II-E-10, differs in form from the spectrum of the CS_2/O_2 laminar mixing layer flame. The bands start at different wavelengths. The oxides of sulfur are among the products of both flames. Therefore, the dissimilarity of the H_2S/O_2 and CS_2/O_2 flame spectra is evidence that the oxides of sulfur are not strong sources contributing to the observed infrared emission spectra of

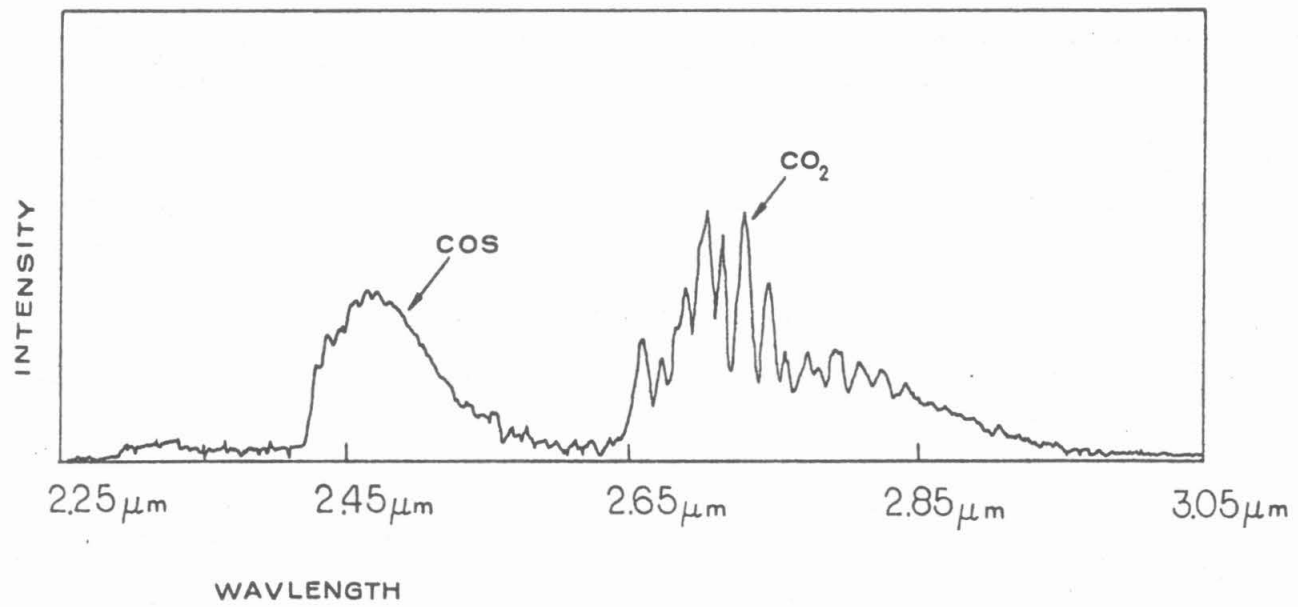

Figure II-E-8 Emission spectrum of a COS/O_2 mixing layer flame at 6.3 torr; U_{COS} = .6 m/sec; U_{O_2} = 2.6 m/sec

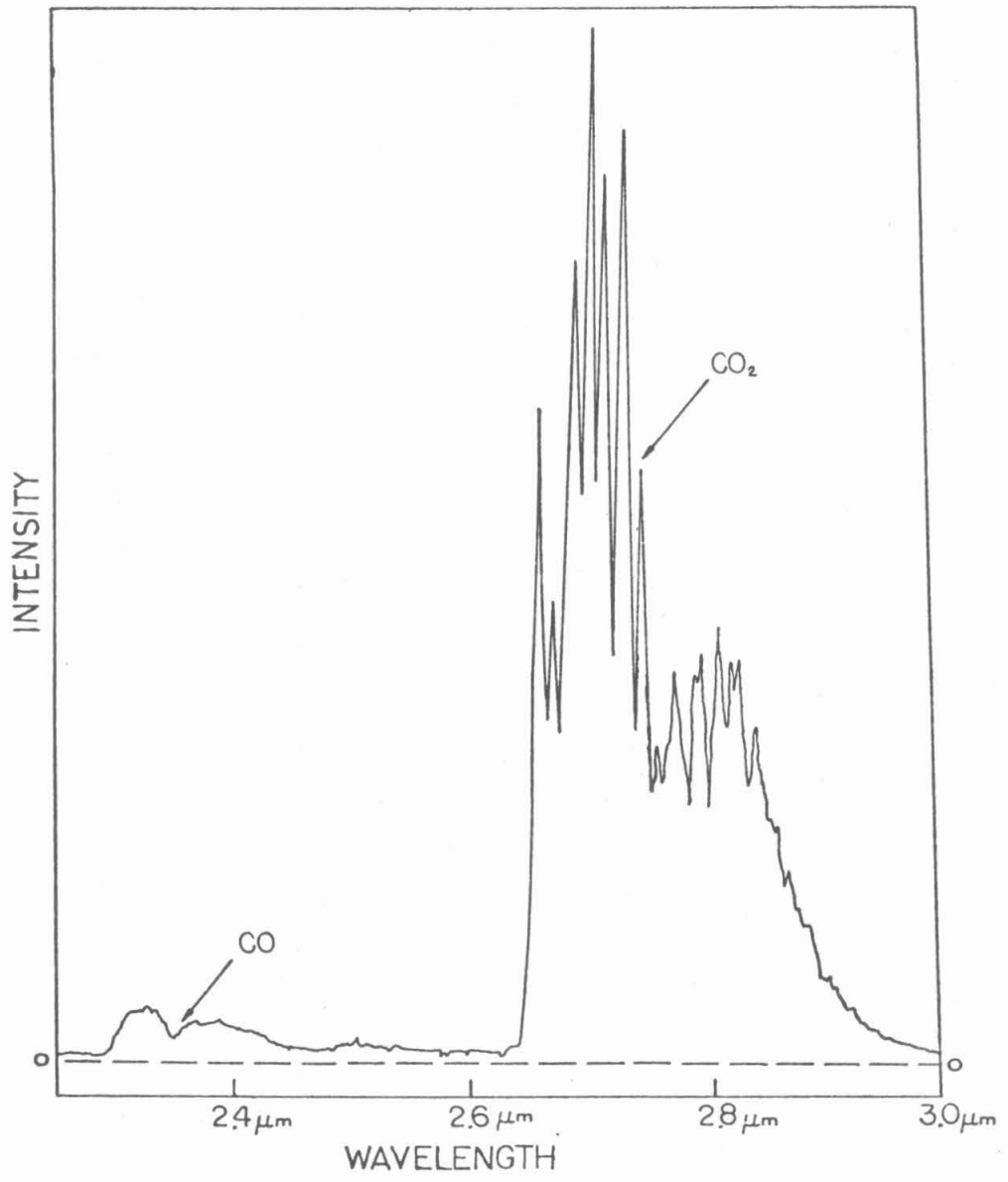

Figure II-E-9 Emission spectrum of a CO/O_2 mixing layer flame at 25 torr; U_{CO} = .2 m/sec; U_{O_2} = .6 m/sec

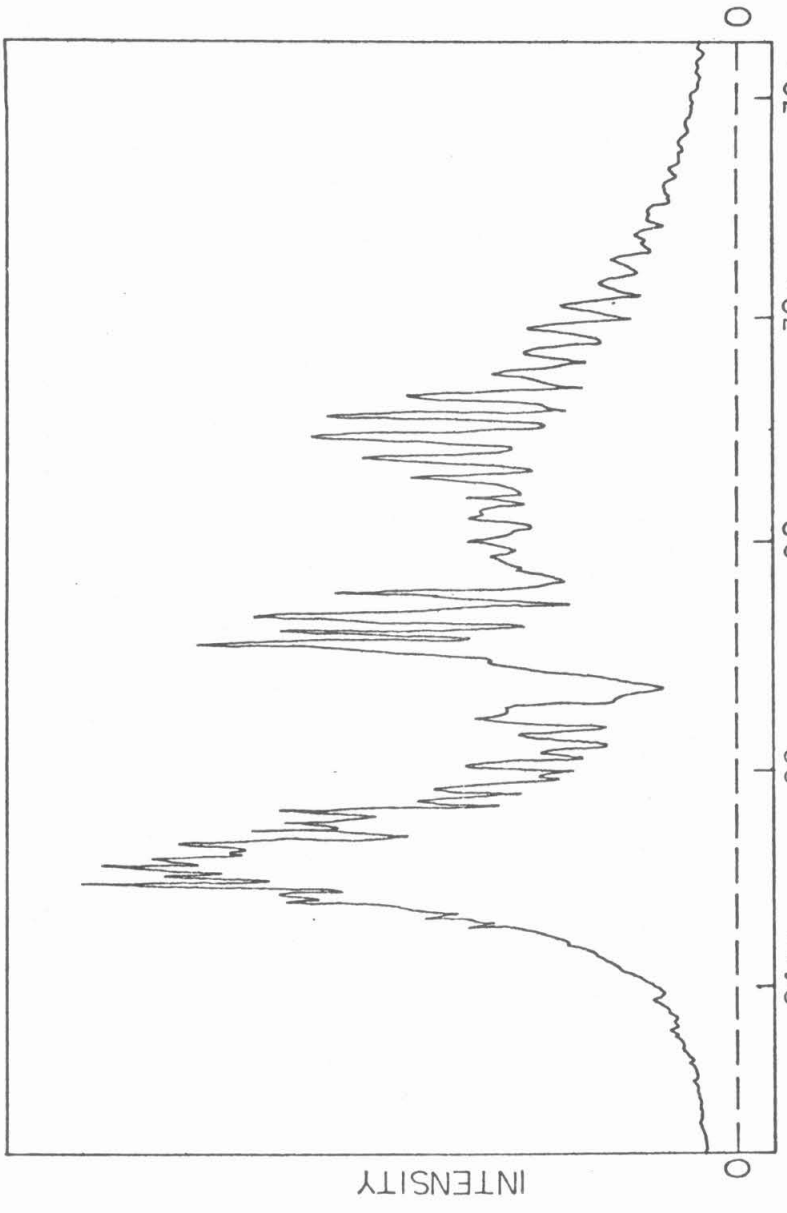

Figure II-E-10 Emission spectrum of a H_2S/O_2 mixing layer flame at 4.4 torr, U_{H_2S} = .3 m/sec; U_{O_2} = 3.6 m/sec

CS_2/O_2 flames.

CO_2 has strong emission bands near 2.7 μm [II.12, II.39, II.40]. The origin of the (1,0,1) → (0,0,0) band is at 2.68 μm, and the origin of the (0,2,1) → (0,0,0) band is at 2.71 μm. We will argue that the emission at and above 2.65 μm, observed from the downstream region of the CS_2/O_2 mixing layer flame, is probably due to these CO_2 bands. If so, the assumption that CO is the molecule emitting is not valid for the downstream region of the CS_2/O_2 laminar mixing layer flame.

To test for CO_2 bands in the CS_2/O_2 mixing layer flame, a 20 cm long absorption cell filled with CO_2 at atmospheric pressure, fitted with NaCl windows, was placed in the optical path between the flame and the monochromator. Due to the low temperature of the gas in the absorption cell relative to the temperature of the combustion gases, we did not expect the CO_2 cell to absorb all of the emission on the CO_2(1,0,1)→ (0,0,0) and (0,2,1) → (0,0,0) bands. In the flame, the range of active vibrational-rotational transitions was broadened relative to the room temperature gas because high rotational levels were populated. Experimentally, we found that the CO_2 absorption cell attenuated the emission around the band origins of the CO_2 (1,0,1) → (0,0,0) and (0,2,1)→(0,0,0) transitions by a factor of more than two. The cell passed unattenuated a narrow band at 2.65 μm, and a broad band starting at 2.73 μm and extending to above 3.0 μm.

The CO_2 oscillator strength for the 2.7 μm bands is about 20-fold larger than that for CO on the 2 → 0 overtone vibrational transition band at 2.3 μm [II.39, II.40], and

$$f \propto A/\lambda^2 \qquad \text{(II.E.1)}$$

$$\text{photon flux} \propto AN^* \qquad \text{(II.E.2)}$$

$$N^{(0)} = N^* e^{hc/\lambda k_B T} \qquad \text{(II.E.3)}$$

$$N \simeq N^{(0)} \qquad \text{(II.E.4)}$$

where f is an oscillator strength, A is the Einstein spontaneous emission coefficient, and λ is the wavelength, for the transition of interest. The excited and ground state populations of the emitting molecule are $N^{(0)}$ and N*, respectively. Equation II.E.3 relates the ground and excited state populations under <u>vibrational equilibrium</u>. Under equilibrium conditions, at temperatures typical of CS_2/O_2 flames, $N^{(0)}$ will be approximately equal to the total species population, N. Using equations II.E.1 through II.E.4, and taking the temperature to be 2500°K,

$$\frac{N_{CO_2}}{N_{CO}} \simeq .1 \frac{\text{photon flux from } CO_2 \ (2.7\ \mu m)}{\text{photon flux from CO} \ \ (2.3\ \mu m)} \qquad \text{(II.E.5)}$$

In the region five centimeters downstream of the splitter plate the CS_2/O_2 laminar mixing layer flame, the measured photon flux from the 2.7 μm bands of CO_2 is about five-fold larger than from the CO (2 → 0) band at 2.3 μm. Therefore, making use of equation II.E.5, we find that the concentration of CO_2 in this region is roughly 50% of the concentration of CO. It is apparent that appreciable CO_2 production occurs.

<u>The Presence of COS</u>

The small peak in the CO vibrational populations centering about level 9 in the downstream region of the CS_2/O_2 laminar mixing layer flame is associated with an intensity peak centered at 2.4 μm. This intensity

peak coincides in wavelength with a prominent peak observed in the COS/O_2 flame, which can be identified with the COS overtone band. The origin of the COS overtone band, (2,0,0) → (0,0,0), is at 2.42 [II.12]. These facts indicate that much emission in the spectrum of downstream region of the CS_2/O_2 mixing layer flame at wavelengths near 2.5 μm is due to COS.

Discussion of the CO, CO_2, and COS Emission Intensities

There is overlap from COS and CO_2 emission on the CO overtone spectra. However, the intensity attributable to the COS band is substantially less than that attributable to the CO overtone bands. Moreover, the smoothness of the inferred CO vibrational distributions for the upstream region of the CS_2/O_2 mixing layer flame lends to their credibility. Within a centimeter of the splitter plate, the emission intensity at 2.6 μm is relatively large (see Figure II-E-1) and has the general structure of the CO overtone spectra. The inferred distributions of the vibrational population are smooth through the corresponding vibrational level, v = 12. This evidence implies that the CO_2 concentrations are low in comparison to the CO concentrations. If the CO_2 concentration exceeds 10% of the CO concentration, the emission intensity on the 2.7 μm CO_2 band would be larger than on the intensity on the 2 → 0 CO vibrational overtone band, and the CO_2 2.65 μm band would be distinguishable. It is not. A few centimeters downstream of the splitter plate the CO_2 concentration grows to approximately 50% of the CO concentration; in Figure II-E-11 we see that in the same region the CO concentration does not fall. The COS emission is always low relative to the emission on the CO overtone bands. In the region by the splitter plate, the COS emission is overwhelmed by

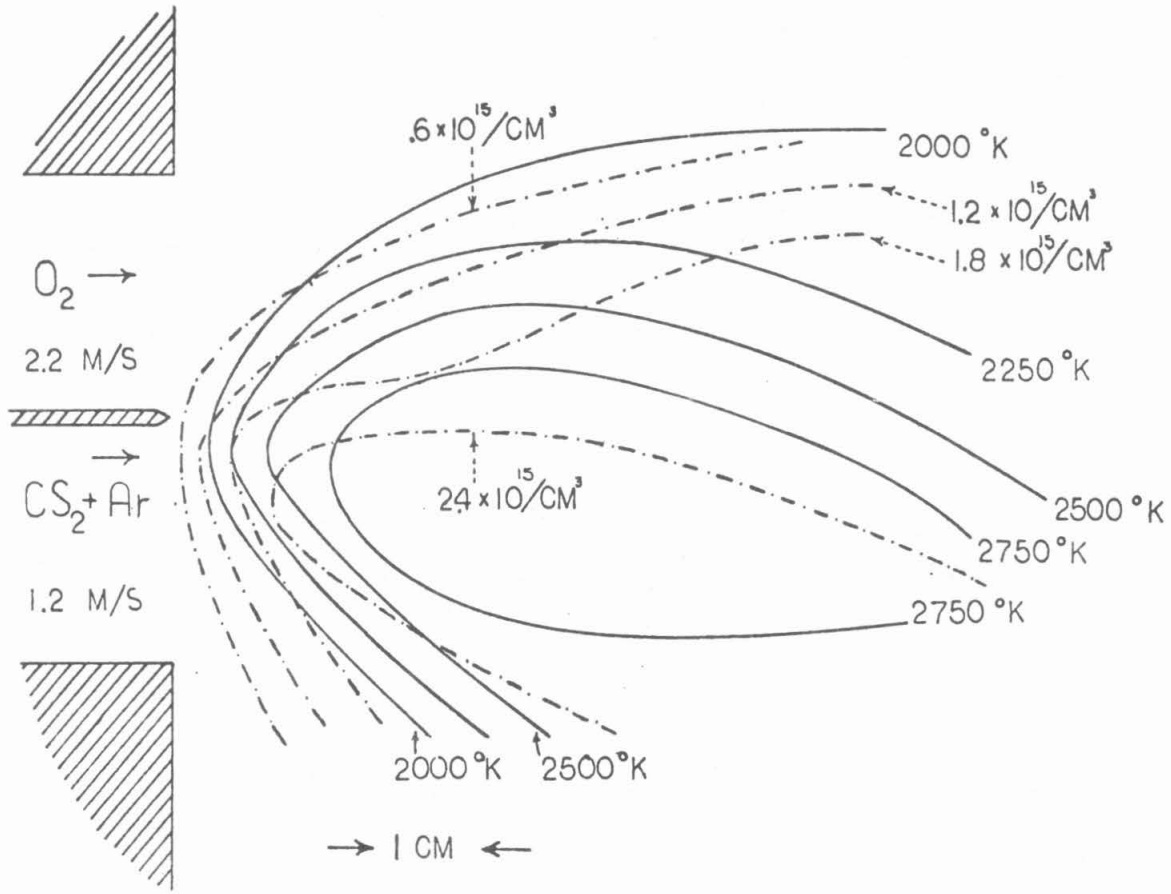

Figure II-E-11 Contours of CO concentrations (dashed lines) and temperatures (solid lines) in a CO_2/O_2 mixing layer flame diluted with Ar. The CS_2:Ar ratio is 1:.8. The special resolution is 1 cm.

the CO emission. Consequently, no estimate can be made of the streamwise variations in the COS concentrations.

The most plausible interpretation of the spectral data taken from the upstream region of the mixing layer flame, within a centimeter of the splitter plate, is that the CO vibrational populations are nonequilibrium, but not inverted. A few centimeters downstream of the splitter plate, the entire vibrational distribution is nearly equilibrated. The amount of vibrationally excited CO chemically produced in this region is either minute in comparison with the equilibrated population, or the deactivation processes are rapid in comparison with the CO production processes.

At 2.6 μm there is a window between the COS and the CO_2 bands. In the downstream region of the CS_2/O_2 mixing layer flame, CO emission at 2.6 μm could imply a population in the 12th vibrational level of CO. A few centimeters downstream of the splitter plate, there is virtually no emission at this wavelength; consequently, there is almost no population in the 12th vibrational level.

The spectral data are evidence that CS_2/O_2 mixing layer flames produce more CO_2 than CS_2/O_2 premixed flames at similar pressures. Comparison of Figures II-E-2 and II-E-12 shows that the inferred vibrational populations for the mixing layer flame have a peak at v = 13, <u>not</u> due to CO (v = 13), but rather due to the 2.7 μm CO_2 bands, while this is not a prominent feature of the premixed flames. The cause for this apparent difference may be that the reaction products, CO and COS, have a long residence time in the mixing layer flame, which extends downstream. The reaction products may again react with unstable reaction intermediates (atomic oxygen) in the flame. This is impossible in the premixed flame,

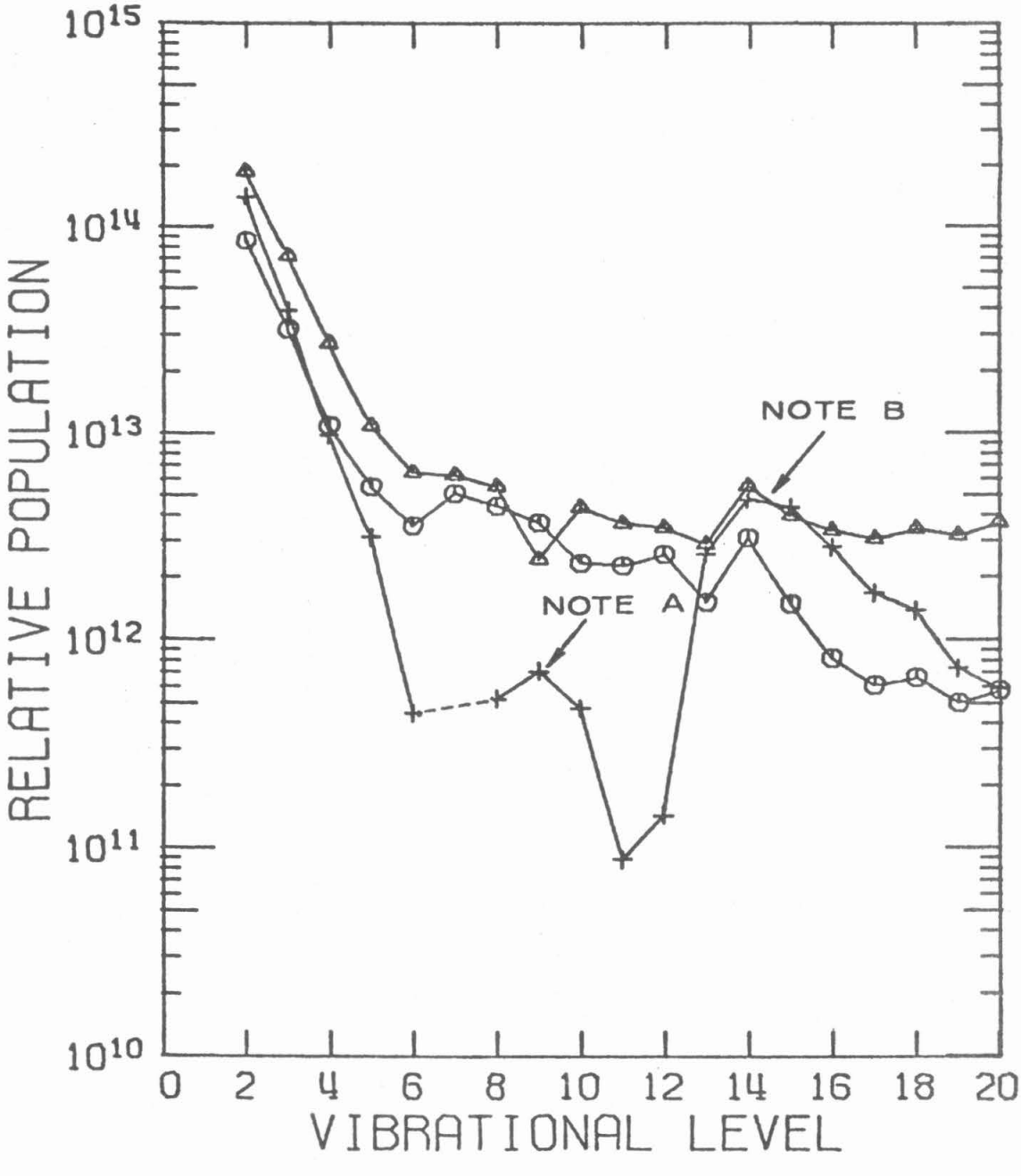

Figure II-E-12 Vibrational populations of CO (#/cm^3) in a premixed CS_2/O_2 flame. CS_2:O_2 ratio 1:2.1; p = 4.9 torr. Distance downstream of the flame front: "o" .0 cm,"Δ".9 cm, "+" 4.3 cm. NOTE A: Anomalous peak due to COS, not CO. NOTE B: Anomalous peak due to CO_2, not CO.

where the reaction products are rapidly convected from the flame front. Chemical processes that lead to CO_2 production were investigated using computer modeling, and they will be discussed in Chapter III. The most important reaction mechanism leading to the production of CO_2 at pressures below 10 torr was found to be the reaction $CS_2 + O \rightarrow COS + S$, followed by $COS + O \rightarrow CO_2 + S$.

CO Vibrational Distributions, Variations Transverse to the Plane of the Splitter Plate

We have discussed variations in the emission of the mixing layer flame along the direction of flow. CO in vibrational nonequilibrium is found within a centimeter of the edge of the splitter plate in flames with pressures 4 to 15 torr and flow velocities approximately 100 cm/sec. Once a few centimeters downstream, the infrared emission varies only slightly as we observe from further downstream.

We would not be surprised if the infrared emission observed from the region of the flame producing blue-white emission differed from the infrared emission elsewhere, considering that the visible emission differs. However, downstream of the splitter plate, the infrared emission spectra and the inferred CO vibrational populations do not vary appreciably, as we observe along a traverse perpendicular to the plane of the splitter plate (see Figure II-E-13). No variation is noted, even when passing through the region of blue-white emission in the flame. We might expect the production of vibrationally excited CO and the resultant CO emission to be located in the same region as the visible emission, because this is the observed behavior in premixed CS_2/O_2 flames [II.35].

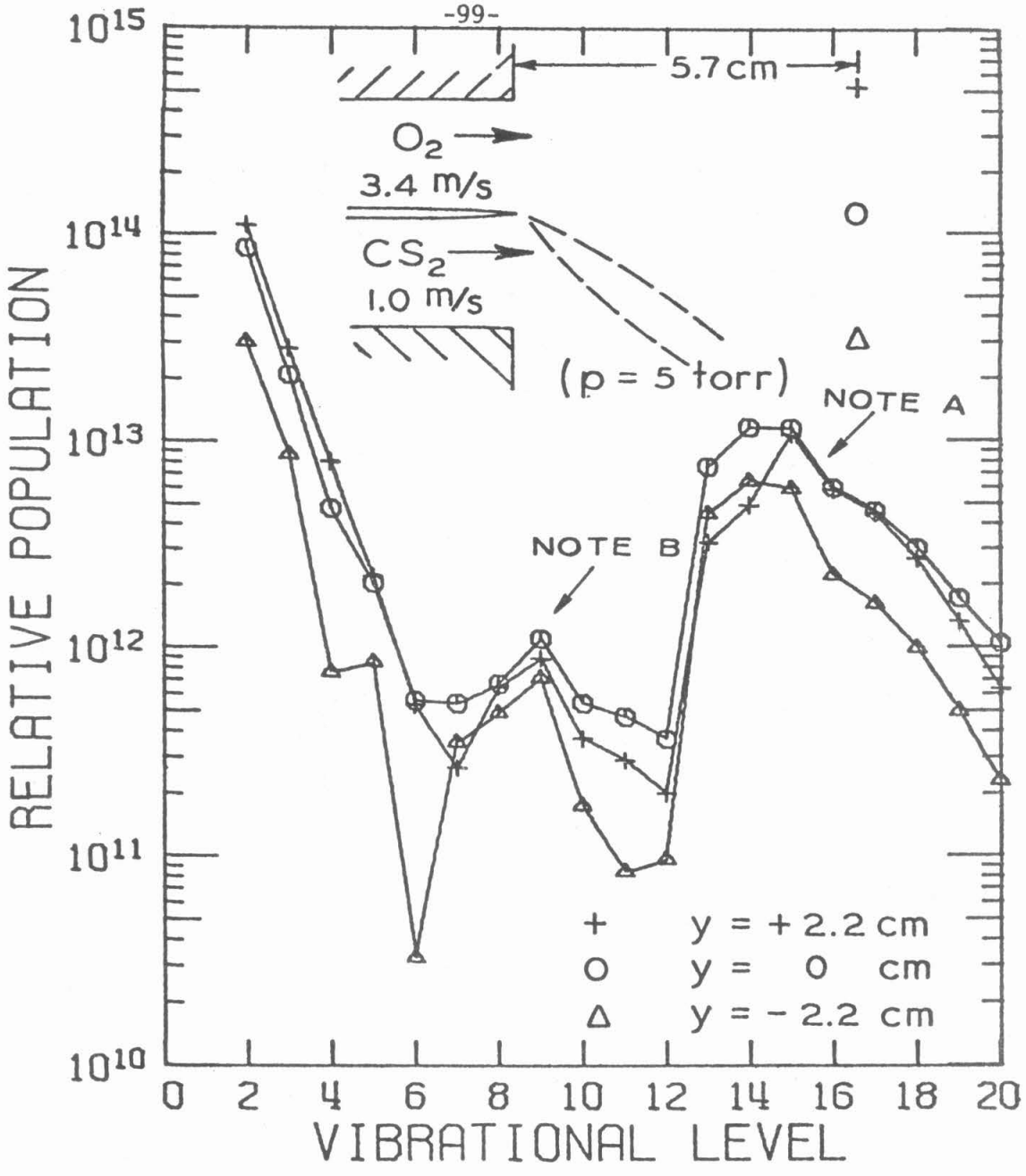

RELATIVE POPULATIONS CO(v') FOR THREE POSITIONS IN A TRANSVERSE PLANE FOR A LAMINAR MIXING LAYER

Figure II-E-13 Relative populations of CO (#/cm^3) as a function of vibrational level in a CS_2/O_2 mixing layer flame at .5 torr; U_{O_2} = 3.4 m/sec; U_{CS_2} = 1.0 m/sec.
NOTE A: Anomalous peak due to CO_2, not CO.
NOTE B: Anomalous peak due to COS, not CO.

From the flame spectra, the CO is inferred to be in vibrational equilibrium throughout the downstream region of the mixing layer. The luminous blue-white region extends from the area by the splitter plate where nonequilibrium CO is found into the downstream region of equilibrium.

Discussion of the CO Vibrational Population Profiles and Equilibration Processes

One cause for the homogeneity of the CO vibrational distributions found downstream in the mixing layer flame could be that CO is not formed vibrationally excited in these regions. However, this supposition implies that the mechanism of the chemical reaction differs downstream from that upstream, where vibrationally excited CO is formed. Another possible cause is that the chemically formed vibrationally excited CO is too rapidly equilibrated to contribute a measurable emission intensity. This is a plausible model if the vibrational relaxation rates are sufficiently large in comparison with the chemical pumping rates, resulting in near equilibrium. This explanation is favored; we will discuss the role COS may play in CO deactivation.

An estimate of the chemical production rate of carbon monoxide, W, (moles/(sec-cm^2)) based on the flame sheet approximation in Appendix A is:

$$W \simeq N_o \sqrt{\mathcal{D}_o/(U_o z)}$$

where N_o, $\mathcal{D}_o$, and U_o are the values at the flame-sheet for the molar density, diffusion constant, and velocity, respectively, and z is the coordinate along the direction of flow. This result is stated in order to

emphasize that the mixing and production is most rapid for small z if the reaction rates are not limiting. Sufficiently far downstream, the production rate must fall off.

Competing with chemical production of CO, which increases the population of vibrationally excited CO, is deactivation by emission processes, vibrational-vibrational energy exchange, and vibrational-to-translational energy exchange. Because of the large number of vibrational exchange processes active in CS_2/O_2 flames, we will not try to elaborate on them here; Reference II.41 carries a survey of the subject. In that reference, the author generalizes: nonresonant transfer probabilities increase exponentially with increasing temperature; resonant transfer probabilities are linear or decrease with increasing temperature.

The exchange reaction COS (1,0,0) + CO(v) $\rightleftarrows$ CO(v-1) + COS (0,0,0) is very nearly resonant for v = 4, with an increasing energy defect as v differs from 4. At 300°K, the vibrational exchange rates for CO ($4 \leq v \leq 13$) with COS are over two orders of magnitude larger than corresponding rates for vibrational transfer to O_2, Ar, He, CO, O_2, N_2, CO_2, SO_2, N_2O, or CS_2 based on the rates in References II.30 and II.42. Consequently, if the mole fraction of ground state COS exceeds about .01, COS will be the dominant quenching agent. With increasing temperature, the net CO quenching will increase as the rates for nonresonant transfer increase, although the relative importance of quenching by COS will decrease. Vibrational relaxation by exchange among CO molecules will generally dominate the equilibration processes if the COS concentration is low [II.43]. If the ground state COS mole fraction is in excess of

.01, with the pressure above 5 torr, the rate for vibrational exchange from CO to COS exceeds the rates for relaxation by vibrational-translational exchange and spontaneous emission. Based on the rates in References II.30, II.33, II.34, II.42, and II.44, when COS is present, the rate limiting step in the relaxation of the CO may be the deactivation of the vibrationally excited quenching agent, COS (1,0,0) [II.45].

Consider the vibrational exchange reaction,

$$\text{COS}\ (0,0,0) + \text{CO}(v=12) \xrightarrow{k} \text{COS}\ (1,0,0) + \text{CO}(v=11)$$

$k \simeq 19.10^{-12} \text{cm}^3/(\text{molecule-sec}))$ at 300°K [II.30]

$$\left(\frac{\partial \text{CO}(v=12)}{\partial t}\right)_{\substack{\text{due only to the} \\ \text{reaction above}}} = k[\text{COS}\ (0,0,0)][\text{CO}(v=12)]$$

If the mole fraction of COS in the ground state is .01 at a pressure of .01 atm, the characteristic time for deactivation by only COS, τ, is

$$\tau \simeq 1/(k[\text{COS}]) = 2 \text{ msec}$$

The sum of the equilibration times for CO deactivating about 10 levels, $v=12 \rightarrow v=11, \cdots, v=3 \rightarrow v=2$, is less than three times τ because the rates for COS (0,0,0) - CO(v) vibrational exchange are larger for lower vibrational levels, reaching a maximum at $v = 5$. In this example, COS will cause the CO distribution to equilibrate in a time τ_E, equal to less than 3τ, about 6 ms. If the flow velocity is 100 cm/sec, the CO distribution will equilibrate in less than 1 cm,

$$\ell_E \simeq U \cdot \tau_E \simeq U\ 3\tau \simeq 6 \text{ mm}$$

We observe nonequilibrium CO vibrational distributions within a centimeter of the splitter plate; this suggests that the COS mole fractions are not in excess of .01 there. Downstream, were the COS mole fraction just a few percent, the deactivation distance for CO(v) would be merely millimeters. Our computer model, to be discussed in Chapter III, predicts the COS mole fraction rises from 0 to about .1 in the first 4 cm of the mixing layer flame under typical conditions, p = .01, U = 200 cm/sec. Downstream of the splitter plate a few centimeters, these sizeable COS concentrations will cause rapid equilibration of the CO vibrational distributions. The equilibrated CO population convected downstream will greatly exceed the population of vibrationally excited CO. This description of the mixing layer flame, and the influence of COS, are consistent with the observation of COS emission bands in the mixing layer flame spectra starting roughly 2 cm downstream of the splitter plate.

Temperature Profiles and CO Concentrations

Profiles of the temperatures and total CO concentrations in the CS_2/O_2 mixing layer flame were found using measurements of the infrared flame emission and the interpretation technique explained in Chapter II, Section D. Figure II-E-14 shows the temperature contour for a CS_2/O_2 flame, and Figure II-E-11 shows the CO concentration contour superimposed on the temperature contour for a CS_2/O_2 flame. The temperature profile has a maximum just to the side of the O_2 stream from the visibly emitting portion of the flame. The temperature profiles are broad, and the maximum temperatures are near the adiabatic flame temperatures [II.46]. Figure

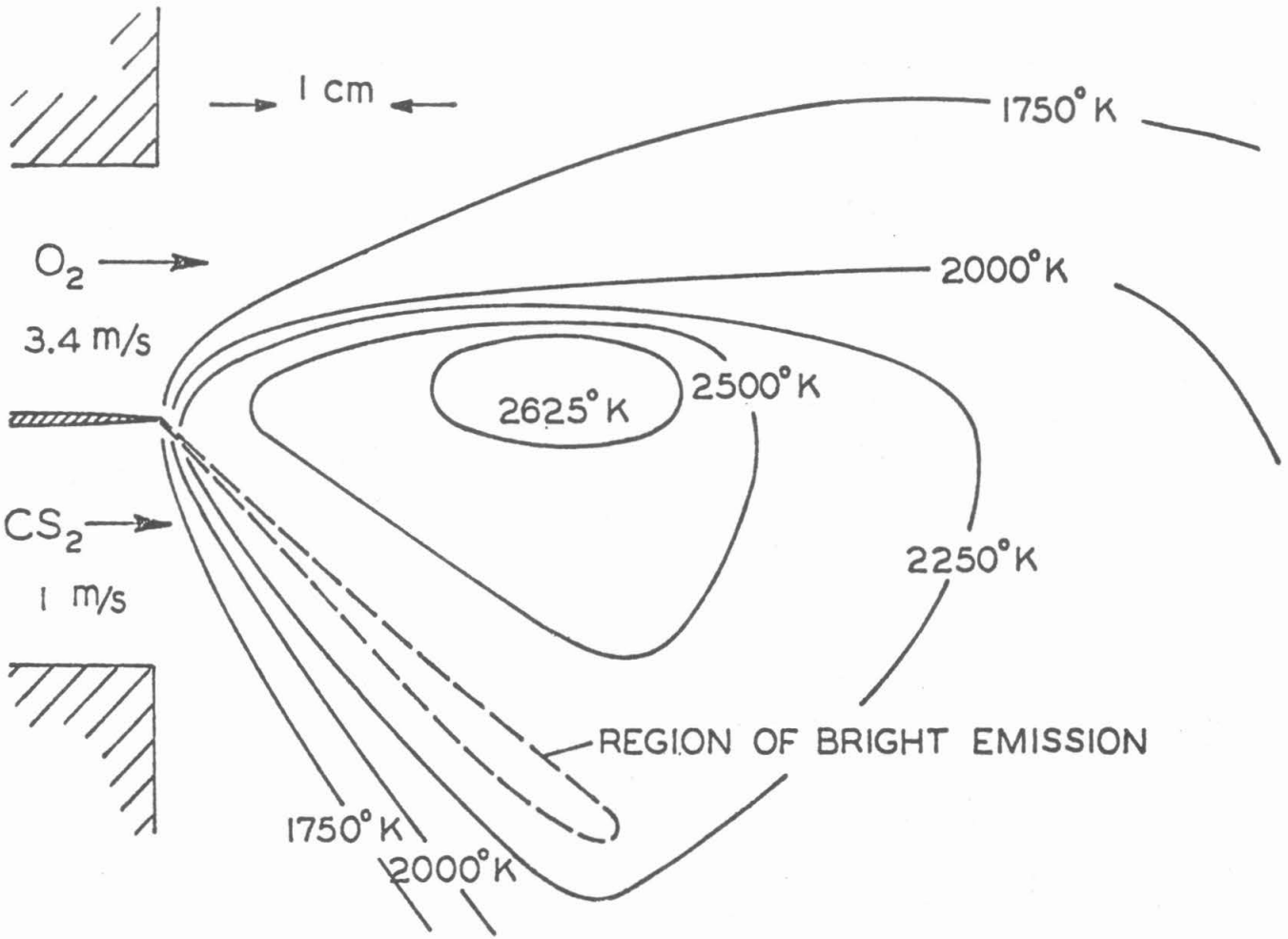

ISOTHERMS IN A 5 TORR CS_2/O_2 REACTING MIXING LAYER FROM CO EMISSION MEASUREMENTS

Figure II-E-14 Isotherms in a CS_2/O_2 laminar mixing layer flame at 5 torr, found using spectroscopic measurements. The special resolution is 1 cm.

II-E-15 presents temperature and CO concentration profiles in a one-dimensional premixed flame: these may be roughly compared to the data on the mixing layer flame in Figures II-E-11 and II-E-14. The temperature profiles will be further discussed after the supporting thermocouple temperature measurements are presented in Chapter II, Section F.

N_2O and COS Additive Flames

The effects of N_2O and CO addition on a CS_2/O_2 laminar premixed flame were briefly investigated. CO overtone spectra were taken of $CS_2/O_2/N_2O$ and $CS_2/O_2/N_2O$ free burning flames to examine the variation in the CO vibrational distributions with changes in the CS_2:O_2:N_2O and CS_2:O_2:COS ratios. This work is similar to the investigation of the effects of N_2O in Reference II.35, in which only qualitative results are presented. N_2O is reported to be an advantageous additive for increasing laser power [II.30, II.35, II.47 to II.50]. COS has generally been found to reduce laser power [II.36, II.47, II.51].

The gas injector used to investigate the effect of COS and N_2O addition to CS_2/O_2 flames was the 240 mm long, multiple-slot injector described in Chapter II, Section A. The results of N_2O addition on the CO vibrational populations are presented in Figure II-E-16. These show the CO vibrational populations at the flame-front with a spatial resolution of less than 1 cm. N_2O depopulates the lower vibrational levels of CO ($v = 4$-10) causing inversions, in agreement with the results in references II.30, II.35, and II.47.

The flame spectra with and without COS addition are indistinguishable, both at the flame front and downstream of it. These experiments were performed at a pressure of 9.5 torr. The CS_2:O_2 ratios varied

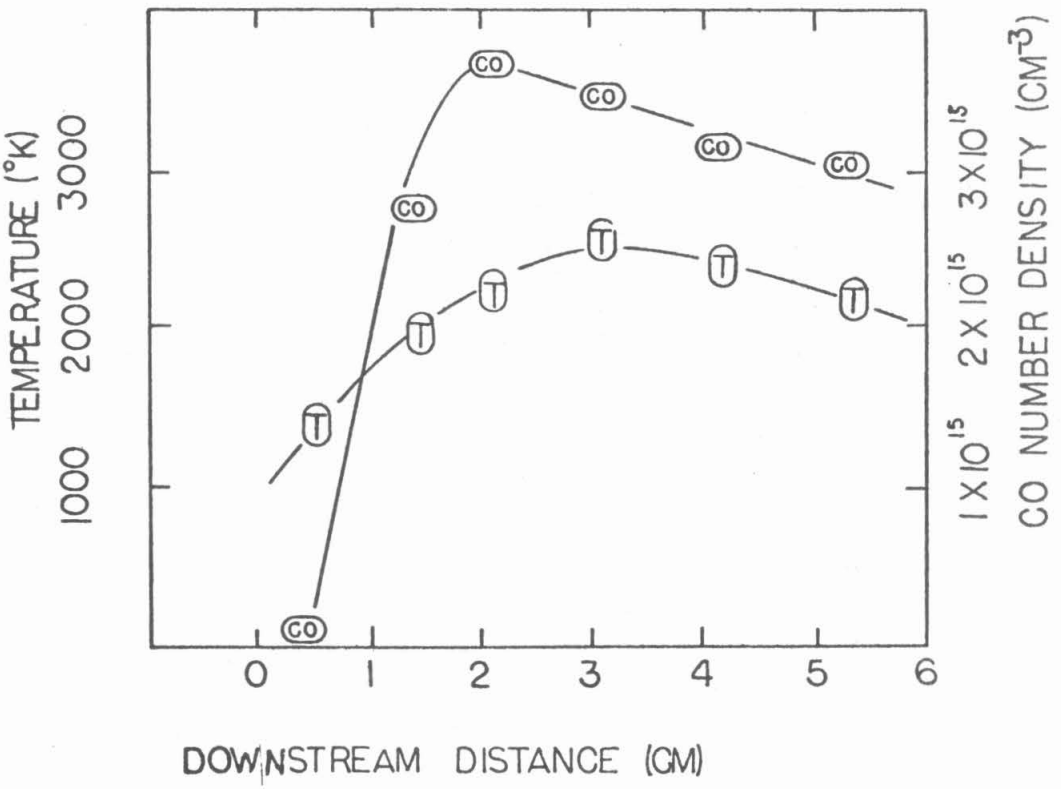

Figure II-E-15 Temperature and CO concentration profiles across a premixed CS_2/O_2 flame at 5.2 torr, found using spectroscopic measurements.

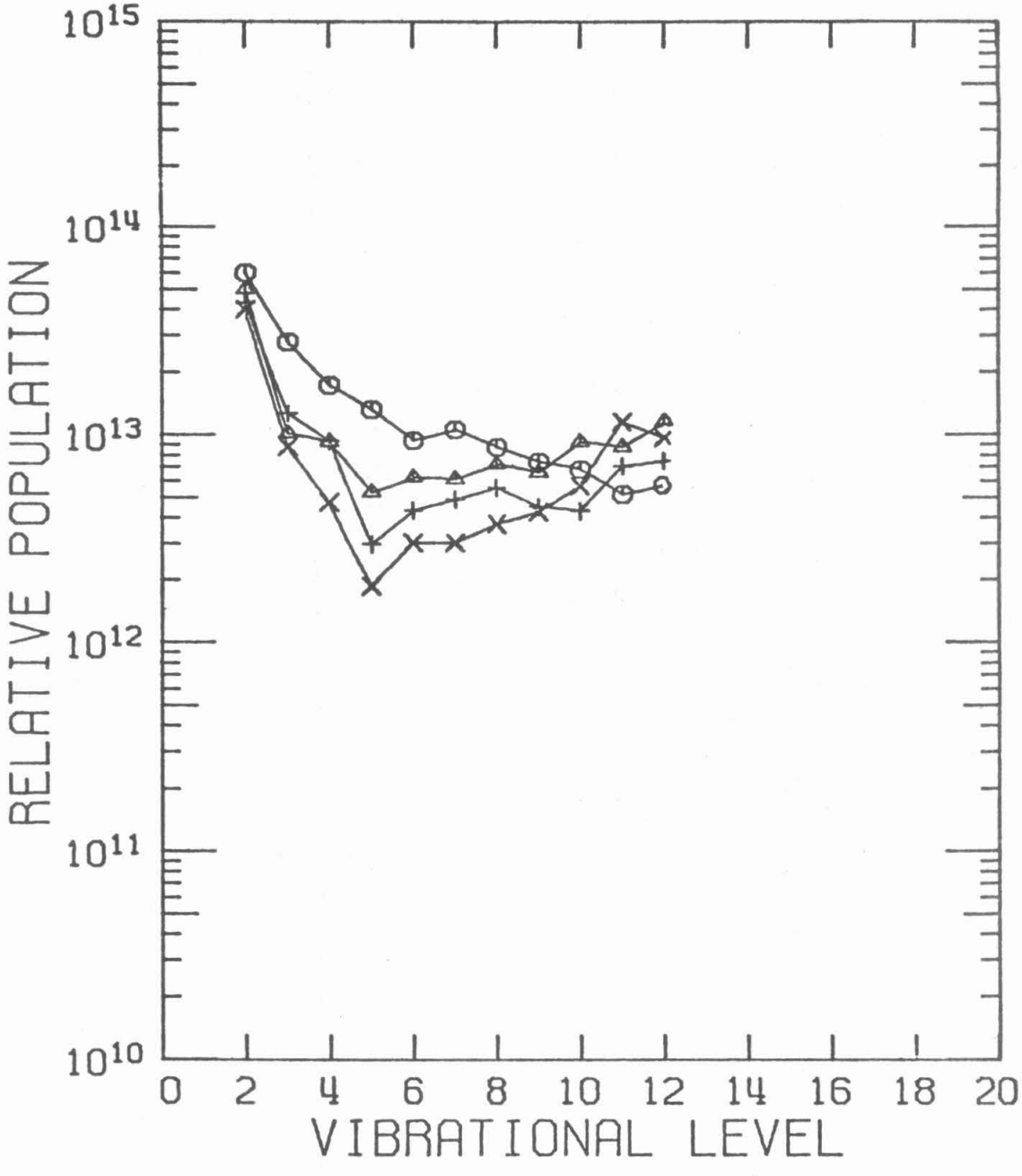

Figure II-E-16 Vibrational populations of CO (#/cm^3) in the visibly luminescing region of a premixed $CS_2/O_2/N_2O$ flames at 7.0 torr; CS_2:O_2:N_2O ratios: "o" 6:36:0, "Δ" 6:36:1, "+" 6:36:3, and "x" 6:36:6.

between 1:10:0 and 1:10:1.3. The lack of influence by COS may be due to rapid COS oxidation, resulting in an equilibrium concentration far below the COS concentration in the precombustion mixture.

In the CS_2/O_2 mixing layer flames, N_2O was added to either, or both, reactant streams. In every case, the CO vibrational populations were inferred not to have inversions. N_2O addition does not affect the CO vibrational distributions near the splitter plate. In these experiments the mole fraction of N_2O in the oxidant stream ($N_2O + O_2$) was varied from 0 to .25; the total oxidant flow, $N_2O + O_2$, was constant; the pressure was about 5 torr; and the flow velocity was about 1.5 m/sec. Downstream of the splitter plate 2.5 cm, the effect of N_2O was to increase the intensity on the 2.7 μm bands of CO_2. The CO_2 emission intensity increased roughly linearly with the N_2O addition over the range of our data. These results are summarized in Table II.E.1. The CO mole fraction is crudely estimated to be .2 on the basis of the reaction stoichiometry [II.1, II.57], and the predicted equilibrium concentrations [II.46].

TABLE II.E.1 $CS_2/(O_2+N_2O)$ Mixing Layer Flame 2.5 cm Downstream of the Splitter Plate

Case	$N_2O/(N_2O+O_2)$	Pressure (torr)	Estimated CO_2/CO	Estimated CO_2 mole fraction
(1)	0	5.0	.2	.04
(2)	.125	5.2	.25	.05
(3)	.25	5.8	.3	.06

In case 1, the upstream region of the $CS_2/(O_2+N_2O)$ mixing layer flame

within 1 cm of the splitter plate, there is emission on the 2.7μm bands of CO_2. In contrast, CO_2 emission is absent upstream in premixed CS_2/O_2 flames.

In Reference II.53 there is an examination of the $CO + N_2O \rightarrow CO_2 + N_2$ gas phase reaction. Rate constants are presented for the temperature range 1169° - 1655°K:

$$CO + N_2O \xrightarrow{k} CO_2 + N_2$$

$$k = 2.1 \cdot 10^{11} e^{-8705/T} \ (cm^3/mole\text{-}sec)$$

At the elevated temperatures typical of CS_2/O_2 flames, often in excess of 2500°K, this rate constant is about 10-fold smaller than the slowest rate in the 4 reaction branching chain mechanism dominant in CS_2/O_2 flames. However, both CO and N_2O may have appreciable mole fractions, exceeding .1, and this reaction will then be important in CO_2 production.

N_2O participates in vibrational exchange with CO. N_2O also appears to oxidize CO to CO_2. In these experiments the CO_2 concentration increased 50% with the addition of N_2O. If the CO_2 is formed in the reaction $CO + N_2O \rightarrow CO_2 + N_2$, the CO concentration will drop about 25% because the concentration of CO_2 is estimated to be 50% of the concentration of CO, as we saw earlier in this section. Then reaction of CO and N_2O may occur in the $CS_2/O_2 + N_2O$ flame, but we have no evidence that N_2O chemistry affects the CO vibrational distributions or laser performance; we have only evidence of the reaction $CO + N_2O \rightarrow CO_2 + N_2$. In Section G of this chapter we will discuss the effects of N_2O on the CS_2/O_2 flame chemistry found by measuring the flame speeds and by making visible observations. The evidence will indicate that N_2O participates in the

flame chemistry by slowing the flame speeds and acting as an oxygen acceptor.

F. Thermocouple Measurements of the Temperature Fields

Thermocouples were used to measure the temperatures in CS_2/O_2 laminar mixing layer flames, providing us with verification of the temperature profiles, independent of those measured using infrared emission spectroscopy. Thermocouples are intrusive probes; they interact with the flow fields, as well as offering a surface on which chemical reactions may occur. The thermocouples were not reliable indicators of the absolute gas temperature; they were cooler than the surrounding gas because of radiative heat losses. However, they did serve for investigating the general form of the temperature fields, locating the regions of maximum temperature.

Temperature measurements using emission spectroscopy were discussed in Chapter II, Section E. The maximum temperatures in the CS_2/O_2 laminar mixing layer flames were shifted to the side of the O_2 stream from the region of blue-white emission. The temperature profiles found using thermocouple measurements are in qualitative agreement with the profiles found using infrared spectroscopy.

Experimental

Chromel-alumel thermocouples were used; these junctions function at temperatures below 1550°C [II.54]. The use of higher temperature thermocouples (platinum-rhodium or platinum-10% rhodium) would have been preferable. The chromel-alumel wires were found to be prone to corrosion. Wires of two diameters were used, .010" and .025". These entered the flames perpendicular to the direction of flow and parallel to the plane of the splitter plate, as shown in Figures II-A-8 and II-F-1. This

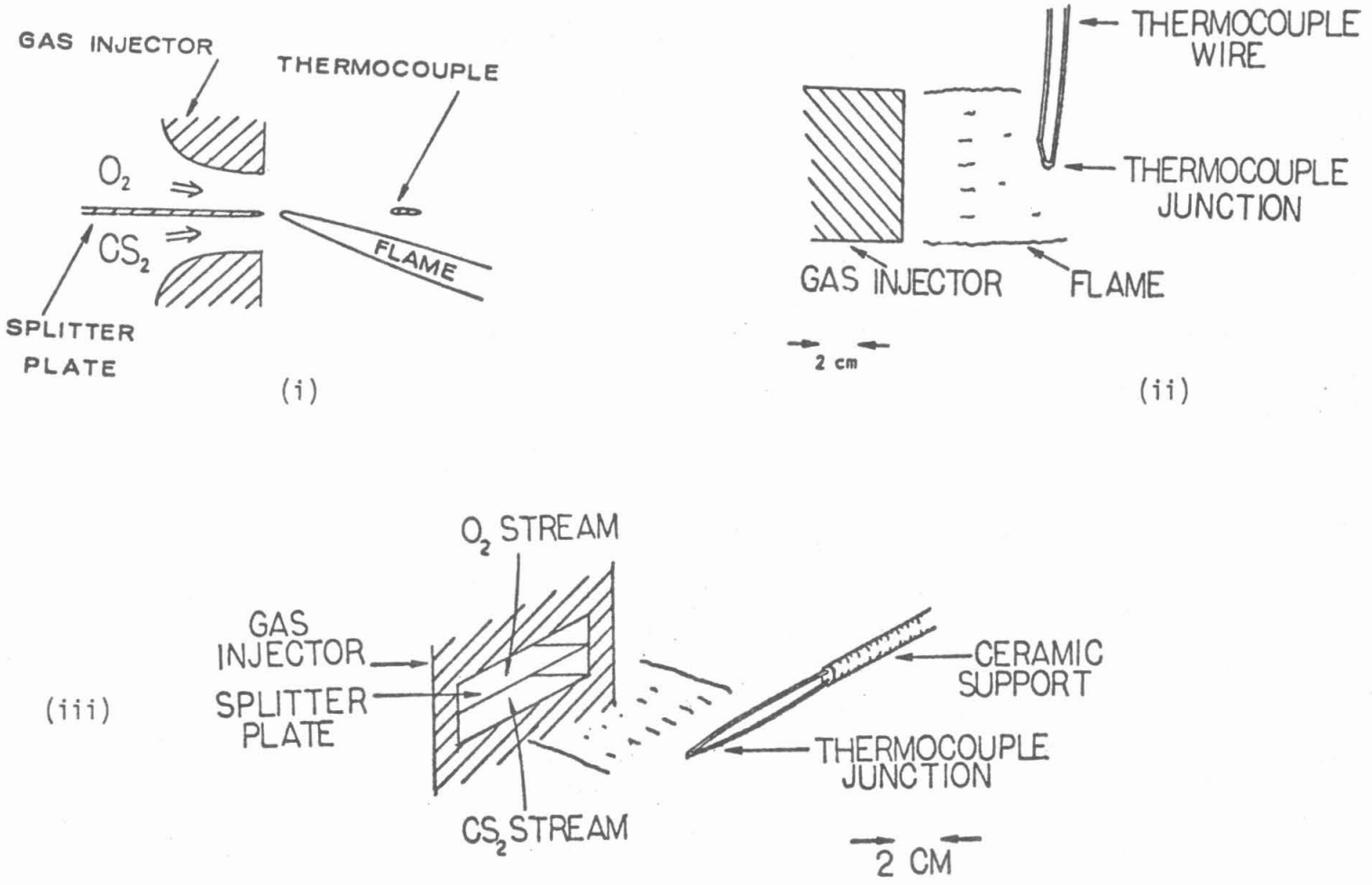

Figure II-F-1 Three views of the positioning of a thermocouple in the flame; (i) a cut-away view, (ii) a top view, (iii) a three-dimensional view

configuration minimized the temperature gradients and heat conduction along the span of the wires [II.55]. The wires were mounted on ceramic supports and extended into the flame, held by their own rigidity. They had no surface protection. The wire of larger diameter (.025") was used to take data because of its durability.

Heat transfer processes controlled the temperatures of the wires; consequently, the temperatures were a function of wire diameter. Two thermocouples of different diameters (.010 and .025") were used simultaneously to calibrate the absolute gas temperature to the thermocouple junction temperature. The two wires were positioned parallel, 3 mm apart, in order to subject them to a similar environment of temperature and flow; however, this calibration was crude.

The low pressure chamber in which the experiments were conducted and the small double-slot gas injector used are shown in Figures II-A-2, II-A-4, and II-A-8. Measurements were taken throughout the mixing layer flame by moving the gas injector, while the thermocouple junction remained fixed. At a series of downstream positions, the injector was moved vertically, perpendicular to the plane of the splitter plate, to gather data at approximately 30 points, 2 mm apart. The maximum junction voltages were found to be about 32 mV, corresponding to a a junction temperature of 1050°K. The junction glowed red at this temperature.

Reduction of Data

Using a thermocouple, an absolute determination of the temperature in a gas was made by finding the junction temperature and then calculat-

ing the gas temperature which would cause the thermocouple junction to attain the observed temperature. This was done, assuming the temperature was steady, by equating the heat transfer losses to the heat transfer gains at the wire, which depended on the junction temperature, and solving for the gas temperature. The solution for the gas temperature will be shown in the analysis to follow.

Equation II.F.1 is the steady state energy balance equation for a unit length of thermocouple wire. The free stream temperature and the stagnation temperature differed negligibly in our low Mach number flows. We neglected any possible effects due to exothermic reactions on the surface of the wire because we had no evidence of their importance.

$$\left(\begin{array}{c}\text{convective transfer}\\ \text{to the wire}\end{array}\right) = \left(\begin{array}{c}\text{net radiative transfer}\\ \text{from the wire}\end{array}\right) + \left(\begin{array}{c}\text{net conductive transfer}\\ \text{down the wire}\end{array}\right) \qquad \text{(II.F.1)}$$

The heat transfer terms are given below in units of power per unit length.

$$\left(\begin{array}{c}\text{convective transfer}\\ \text{to the wire}\end{array}\right) = (.44 \pm .06)\, Re_d^{1/2}\, K_G(T_G - T_W) \qquad \text{(II.F.2)}$$

$$\left(\begin{array}{c}\text{net radiative transfer}\\ \text{from the wire}\end{array}\right) = \sigma\varepsilon\left(\begin{array}{c}\text{configuration}\\ \text{factor}\end{array}\right) \pi d(T_W^4 - T_S^4) \qquad \text{(II.F.3)}$$

$$\left(\begin{array}{c}\text{net conductive transfer}\\ \text{down the wire}\end{array}\right) = \frac{\pi d^2}{4}\, K_W \left(\frac{\partial T_W}{\partial \ell}\right)_{\text{along wire}} \qquad \text{(II.F.4)}$$

The temperature of the gas, thermocouple wire, and surrounding chamber walls are T_G, T_W, and T_S, respectively. The diameter of the wire is d,

and the thermal conductivities of the wire and of the gas are K_W and K_G, respectively. Equation II.F.2 is applicable in the range of Reynolds numbers $100 < Re_d < 10{,}000$ [II.55]. The heat transfer may deviate from this expression in the flows of interest, where Re_d is approximately 0.1. Equation II.F.3 is the Stephan-Boltzmann radiation law, where σ is the Stephan-Boltzmann constant. Because the environment in the flame affects the surface of the thermocouple wire, the composition of its surface is not known, leaving the emissivity, ε, unknown.

Radiative transfer to the thermocouple wire from the surrounding chamber was negligible in our experiments. We will neglect the term T_S^4 in equation II.F.3. The heat transfer due to heat conduction along the wire was estimated to be small in comparison to the convective and radiative transfer. The energy balance equation, ignoring radiative transfer from the chamber and conduction along the wire, is

$$(.44 \pm .06)\ Re_d^{1/2}\ K_G(T_G - T_W) = \sigma\varepsilon\left(\begin{matrix}\text{configuration}\\ \text{factor}\end{matrix}\right)\pi d\ T_W^4 \qquad \text{(II.F.5)}$$

This equation follows from equation II.F.2; consequently, it is valid for $100 < Re_d < 10{,}000$. To allow for a gradual departure from equation II.F.5 at low Re_d, an adjustable heat transfer parameter, a, is inserted into equation II.F.5, yielding equation II.F.6. This crudely extends the applicability of equation II.F.5 into the encountered range of Reynolds numbers.

$$a(.44)\ Re_d^{1/2}\ K_G(T_G - T_W) = \varepsilon\sigma\left(\begin{matrix}\text{configuration}\\ \text{factor}\end{matrix}\right)\pi d\ T_W^4 \qquad \text{(II.F.6)}$$

Measurements were made using two closely spaced thermocouple wires (wires "1" and "2") of different diameters. These provided sufficient information to calculate both the gas temperatures, T_G, and then constant a/ε, eliminating the need for a priori knowledge of the surface emissivity and the coefficient for convector heat transfer. The solution for T_G, equation II.F.7, is derived directly from equation II.F.6.

$$T_G = (bT_{W_2}^4 T_{W_1} - T_{W_2} T_{W_1}^4) / (bT_{W_2}^4 - T_{W_1}^4) \qquad \text{(II.F.7)}$$

T_W = temperature of wire 1

T_W = temperature of wire 2

$$b = \left(\frac{\text{diameter of wire 2}}{\text{diameter of wire 1}}\right)^{1/2} = \left(\frac{d_2}{d_1}\right)^{1/2}$$

Equation II.F.7 is valid over the domain of physically realizable values for T_{W_1} and T_{W_2}. For example, if wire 2 is the thicker, $b > 1$, then T_{W_1} must be larger than T_{W_2}. The denominator in the right hand side of equation II.F.7 vanishes for $bT_{W_2}^4 = T_{W_1}^4$, and is negative for $T_{W_1}^4 > bT_{W_2}^4$. Temperatures in this range correspond to heat transfer terms which disobey the assumed functional behavior of the energy transfer rates in equations II.F.2 and II.F.3. The region of validity of equation II.F.7 is

$$b^{1/4} T_{W_2} > T_{W_1} > T_{W_2} \qquad \text{(for } b > 1\text{)} \qquad \text{(II.F.8)}$$

Some pairs of temperatures were measured which violated this inequality. To realize these pairs of temperatures, the two wires must have been

subject to dissimilar flow and temperature environments at times, contrary to assumptions.

After the gas temperature was calculated using equation II.F.7, the quantity a/ε was calculated using equation II.F.6. We assumed a/ε was constant. From data obtained using a single thermocouple junction, all the gas temperatures were then calculated using equation II.F.6. The calibration to find constant, a/ε, was difficult because of the interaction of the flame and the pair of thermocouples. The shape of the flame generally showed no visible distortion due to a single thermocouple, but was strongly distorted by the pair of thermocouples. Many data points were found to violate inequality II.F.8. The measured values of ε/a ranged over an order of magnitude; a value of .15 was chosen among these values because it caused the maximum temperatures to agree with the spectroscopically inferred values for the .025" diameter wire, the calculated difference between the gas temperature and the wire temperature was about 500°K at the T_W = 800°K, 1000°K at T_W = 1000°K, and 1500°K at T_W = 1100°K. These differences may be inaccurate, but the location of maximum temperature and the qualitative form of the temperature profiles are insensitive to the value of a/ε chosen.

The emissivity of an oxidized metal surface is between .5 and 1 [II.54]. With ε/f chosen to be .15, 'a' must equal about 5. In the flames examined, where Re_d was about .1, the heat transfer to the wires was therefore larger by a factor of about 5 than the value obtained using equation II.F.2, which was applicable over the range $100 < Re_d < 10{,}000$.

This discrepancy is not surprising because the flows around the wires differ at these different Reynolds numbers.

Results

Temperature profiles found from thermocouple measurements in mixing layer flames at pressures of 7.0 and 2.8 torr are shown in Figures II-F-2 and II.F.3, respectively. The generally symmetric form of the temperature contours in Figure II-F-3 is marred by the high temperatures near the injector, on the side of the flow near the CS_2 stream. Although the undisturbed flow might also be hot in this region, the temperatures measured are more likely high because of stabilization of the combustion on the thermocouple wire. The visibly luminescing region of the flame appeared to attach to the thermocouple wire in this region, while elsewhere it did not. Downstream, in the burned gas, there should be no flame stabilization on the wire, so that the temperature profiles should be more reliable.

The thermocouple wires broke when passed through the mixing layer flame about 1.5 cm downstream of the injector. The pressure was about 7 torr; the flow velocities about 1 m/sec. When the wires broke, an unusually high temperature was not being indicated. The thermocouple wires did not break when placed 3 or more centimeters downstream of the injector face, although the flame appeared to luminesce as strongly there, and the thermocouples indicated higher temperatures. This is evidence that upstream the wires were not melted, but were attacked chemically, perhaps by atomic oxygen. Also, we are led to believe atomic oxygen may be the agent attacking the wires because the results of computer modeling of the

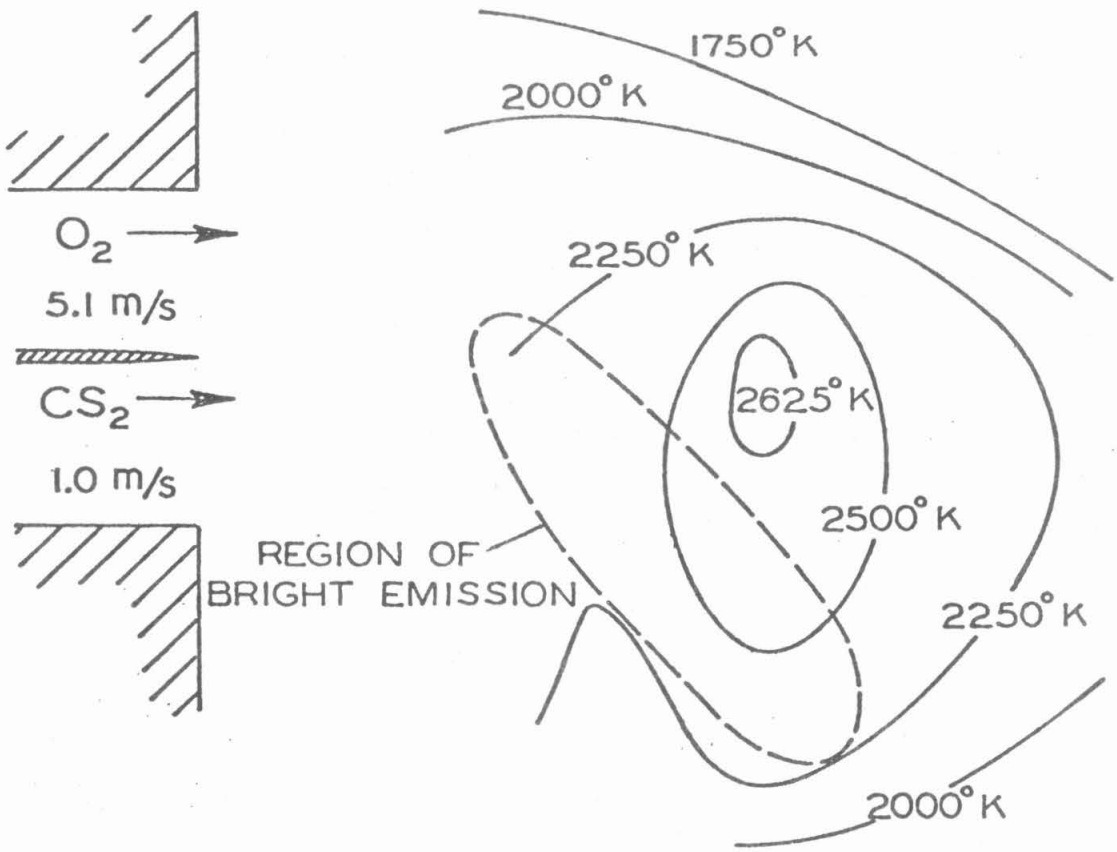

ISOTHERMS IN A CS_2/O_2 REACTING MIXING LAYER FROM THERMOCOUPLE MEASUREMENTS
(p = 2.75 torr)

Figure II-F-2 Isotherms in a 2.75 torr CS_2/O_2 flame

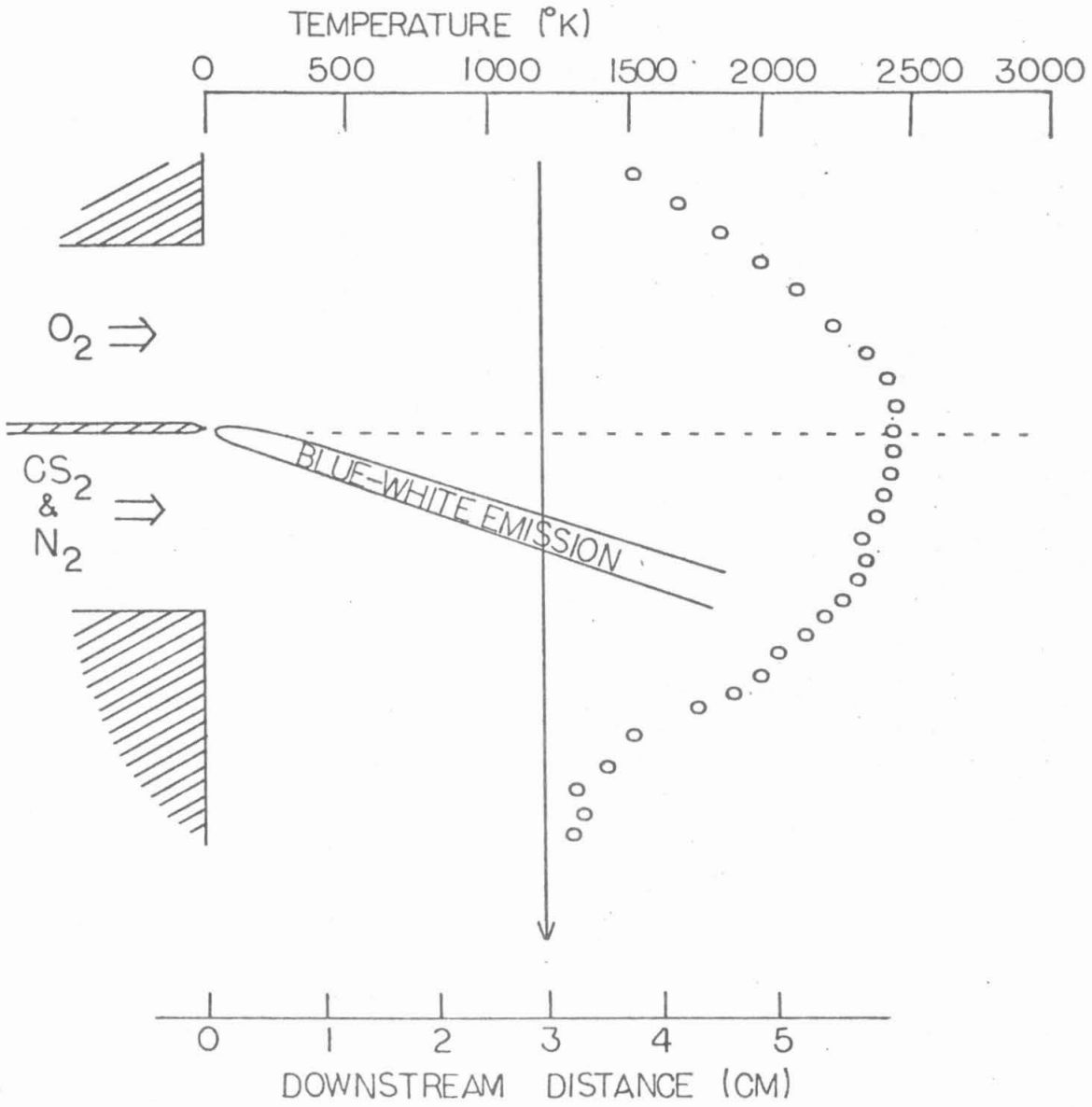

Figure II-F-3 Temperature profile across a 7.0 torr CS_2/O_2 mixing layer flame, taken 3.0 cm downstream of the gas injector

flame (Chapter III) indicate that atomic oxygen has a maximum concentration upstream, in the same regions where the thermocouples broke. The predicted atomic oxygen concentrations are shown in Figure III-B-7.

Error Analysis

The temperature profiles have uncertainties due to the procedure used to estimate the temperature of the gas from the temperature of the thermocouple junction. There are also uncertainties due to possible variations in the surface emissivity and variations in the flow. The following assumptions are needed in order to apply equation II.F.6 to find the gas temperature: (i) K_G is known, (ii) the flow speed is known, and (iii) the functional dependences for the heat transfer terms, specified by equations II.F.2 and II.F.3, are correct. For simplicity, the flow speed is assumed constant. Uncertainties in the configuration factor in equation II.F.3 are inconsequential, because any error there is absorbed in the parameter a.

To compute the gas temperature using the energy balance equation, the conductive heat transfer was assumed to vary as the square root of the Reynolds number, Re. Reference II.56 indicates that for small Re the heat transfer will be linear in Re. However, the experimental data presented in this reference do not fall in the range of interest: $.05 < Re < .2$. We do not know exactly how the heat transfer varies with Re, and this uncertainty in the analysis may induce some inaccuracy in the quantitative, but not the qualitative aspects of the results.

The errors inherent in calculating the temperatures of the gas from the temperatures of the thermocouple junction may be as large as the differences between these two temperatures. Errors due to temporal

fluctuations in the system were estimated on the basis of the observed fluctuations in the voltages of the thermocouples at fixed locations. An error bound of ±5% was found. The calibration error can be approximated to be about $\pm 50 \times (T_G/1000)^4$%. Additionally, the temperature profiles are meaningful only if the thermocouples were not damagingly intrusive to the flow fields, temperature fields, or the chemistry. Combustion stabilization behind the wire, surface catalysis, or reactions consuming the surface of the wire could induce erroneous results. The measured temperature profiles would be distorted if radiative losses from the surface of the wires accounted for a substantial heat loss from the flow. If $T_W = T_G \simeq 1500°K$, the power radiated by the thermocouple wires, given by equation II.F.9, is comparable to the rate of convection of thermal enthalpy to the thermocouple wire, given by equation II.F.10.

$$\text{enthalpy convected / cm-sec} \simeq \rho U C_p T_G d \qquad \text{(II.F.9)}$$

$$\text{radiated energy / cm-sec} \simeq \pi d \sigma \varepsilon T_W^4 \qquad \text{(II.F.10)}$$

We inferred gas temperatures exceeding 2600°K, and corresponding wire temperatures exceeding 1100°K. At these temperatures, the thermal wake of the wire must have been at least ten wire diameters, about 1 cm, just to account for the energy lost by radiation. The interaction of the thermocouples and temperature fields of the gas is substantial, and the spatial resolution achieved is not nearly as fine as the wire diameters. The temperature profiles found using the thermocouple measurements should only be taken as indicative of the general form of the temperature fields of the undisturbed flame.

Conclusions

The temperature measurements using the spectroscopic technique and the thermocouple technique gave qualitatively similar results. The gas temperature was a maximum on the side of the region of the brightest visible emission by the O_2 stream. This result was independent of which stream was on top; buoyancy was not a factor. The temperature profiles were more symmetrical about the plane of the splitter plate than the shape of the visibly emitting region might suggest.

The maximum temperatures are on the O_2 side of the region of brightest visible emission. This may be due to exothermic reactions on the side of the visibly luminescing region by the O_2 stream, or endothermic reactions on the side by the CS_2 stream. On the side by the O_2 stream, any of a number of exothermic oxidation reactions may be occurring without visible chemiluminescence, or there may be vibrational equilibration of the product CO, releasing heat. There may be a component of the flow normal to the highly skewed visible flame. Because of the geometry we would expect the flow to cross from the CS_2 side to the O_2 side of the visibly emitting region, which skews toward the side of the CS_2 stream. The factors influencing the shape of the temperature profiles must be rooted in the flame chemistry. The region in which there is the highest rate for exothermic chemical reactions is not as skewed in the mixing layer as the shape of the visibly emitting region suggests.

G. Diluent and Flame Speeds: The Mixing Layer and Premixed Flames

The kinetic processes in a CS_2/O_2 laminar mixing layer flame determine the vibrational distribution of the CO in the product gas. To predict the CO vibrational distributions, the relative rates of production and deexcitation of vibrationally excited CO are necessary. In this section, the relationship between the rate of CO production and the laminar flame speeds will be discussed. The effect of diluents on the flame speeds has been experimentally investigated, and unexpected flame quenching properties of N_2O were found. The main purpose of this section is to establish that the addition of inert diluent to the reactant gas mixture causes a reduction in the CO production rate in the flame.

For a chemical laser, it is generally preferable to use excess oxidant, rather than an inert gas, when diluting the reactant mixture. Diluting a premixed flame with O_2 can be beneficial to laser performance because the flame temperature is lowered. Similar dilution with an inert gas involves a larger accompanying reduction in flame speed. To reduce the temperature in a mixing layer flame, inert diluent may be added, but not O_2, unlike the premixed flame. It is therefore relevant in contrasting the utility of the premixed and mixing layer CS_2/O_2 flames for use as a laser medium to know the effects of diluent on the flame speeds.

Analysis

The processes that control the CO vibrational populations can be isolated as terms in the rate equation:

$$\frac{dN_v}{dt} = \left(\begin{array}{c}\text{chemical production} \\ \text{in level v}\end{array}\right) + \left(\begin{array}{c}\text{pumping of level v by} \\ \text{transfer from other levels}\end{array}\right)$$

$$- \text{(transfer of CO from level v to other levels)}$$

At the flame front, the chemical production in each vibrational level of CO is proportional to the rate at which CO is produced chemically, which is approximately the flame thickness divided by the flame speed.

The calculation of laminar flame speeds has been a goal of combustion research throughout the years, and has been accomplished by a number of elegant means [II.4]. The simplest of these results, that of dimensional analysis, will be reviewed here. An analysis of flames that propagate by thermal conduction will be presented. An analysis of the flames that propagate by species diffusion will be shown to predict the same flame speeds.

In a premixed flame, the characteristic time for CO production, τ, is approximately equal to the residence time of the gas in the flame. The residence time equals the thickness of the flame, δ, divided by the flame speed, v :

$$\tau \simeq \delta/v \qquad \text{(II.G.2)}$$

To evaluate τ, obviously δ and v must be known.

Flames will propagate by thermal conduction and by the diffusion of reactive intermediate species. Most flames propagate by a combination of both processes. In flames that propagate by thermal conduction, the rate at which heat is conducted across the flame equals the heat production in the flame:

$$W\delta_T q \simeq K\left(\frac{\partial T}{\partial z}\right) \qquad \text{(II.G.3)}$$

In a flame that propagates by species diffusion, the rate at which intermediates produced in the flame diffuse upstream to initiate chemical reactions roughly equals the total chemical production rate for the flame:

$$W\delta_S \simeq \mathcal{D}\left(\frac{\partial N_p}{\partial z}\right) \qquad \text{(II.G.4)}$$

W is the reaction rate (moles-cm^{-3}/sec^{-1}). The subscripts S and T denote the flames that propagate by species diffusion and thermal conduction, respectively. The notation is fully explained in a section preceding Chapter I.

To evaluate the transport terms in equations II.G.3 and II.G.4, the derivatives are approximated:

$$\frac{\partial T}{\partial z} \simeq \frac{T_F - T_I}{\delta_T} \qquad \text{(II.G.5)}$$

and

$$\frac{\partial N_p}{\partial z} \simeq \frac{N_F}{\delta_S} \qquad \text{(II.G.6)}$$

T_I and T_F are the initial temperature and adiabatic flame temperature, respectively. N_F is the molar concentration of the fuel in the unburned gas.

The heat release of the chemical reaction, q, can be estimated, assuming a calorically perfect gas to be:

$$q \simeq C_p(T_F - T_I) \qquad \text{(II.G.7)}$$

where C_p is the molar heat capacity. Assuming complete combustion, conservation of mass requires the fuel consumption in the flame to equal the convection of fuel into the flame, equations II.G.7 and II.G.8,

$$N_F v_T = \delta_T W \qquad \text{(II.G.8)}$$

$$N_T v_S = \delta_S W \qquad \text{(II.G.9)}$$

Equations II.G.3, II.G.5 and II.G.7 are solved for the thickness of the flame propagating by thermal conduction, giving

$$\delta_S^2 = \mathcal{D}N_F/W \quad , \qquad \delta_S = \sqrt{\mathcal{D}N_F/W} \tag{II.G.11}$$

Combining these results with the continuity equation, the flame speeds for the thermal and species diffusion flames are

$$v_T = \sqrt{KW/N_F^2\, C_p} \tag{II.G.12}$$

and

$$v_S = \sqrt{\mathcal{D}W/N_F} \tag{II.G.13}$$

Equations II.G.12 and II.G.13 are similar; II.G.12 can be rewritten as

$$v_T = \sqrt{\mathcal{D}W/(N_F Le)}$$

In the same manner, equations II.G.10 and II.G.11 are similar: II.G.9 can be rewritten as

$$\delta_T = \sqrt{\mathcal{D}N_F/(WLe)}$$

where Le is the Lewis number; $Le = N_F C_p \mathcal{D}/K$. It is a good approximation for most gases to take the Lewis number to be one.

The solution for τ is given by equation II.G.14; τ equals the characteristic time of the reaction, as would have been estimated without considering the fluid processes

$$\tau = \delta/v = \sqrt{\mathcal{D}N_F/W(Le)}\ \sqrt{\mathcal{D}W/N_F(Le)} = N_F/W \tag{II.G.14}$$

For a bimolecular reaction, $W = N_F N_{Ox} k$, where k is the reaction rate constant; N_F and N_{Ox} are the fuel and oxidant concentrations. In the Arrhenius form, the rate constant is $k = A_k e^{-\Delta E_a/k_B T}$. If the reactions in the flames are bimolecular, and Le = 1

$$\delta = (\mathcal{D}^{-1} N_{Ox} A_k e^{-\Delta E_a / k_B T})^{-1/2} \qquad \text{(II.G.15)}$$

$$v = (\mathcal{D} N_{Ox} A_k e^{-\Delta E_a / k_B T})^{1/2} \qquad \text{(II.G.16)}$$

and

$$\tau = (N_{Ox} A_k e^{-\Delta E_a / k_B T})^{-1} \qquad \text{(II.G.17)}$$

In a CS_2/O_2 chemical laser, a large CO production rate is advantageous for high power. From equation II.G.17 we see that high production rates are favored by large concentrations of oxidant, N_{Ox}, and by high temperatures. However, high temperatures are not favorable for achieving high gain. They have a deleterious effect on laser performance because they favor undesirable vibrational transfer processes. High flame temperatures are characteristic of combustion near the stoichiometric ratio. Diluting the reactant mixture with excess O_2 or inert gases reduces the flame temperature, but also reduces the CO production rates. Dilution with excess O_2 is often preferable to dilution with an inert gas, because diluting with O_2 will not lower the production rate of CO as substantially. O_2 also has a relatively low probability to deactivate vibrationally excited CO [II.30].

Consider a premixed CS_2/O_2 flame in which the reactant mixture is oxidant rich, fuel lean. The excess oxygen serves to keep the flame temperatures low. If the mixture is varied by gradually increasing the concentration of diluent at the expense of reducing the oxidant concentration, the concentration of CS in the fuel mixture will remain constant, and the mixture will still be oxidant rich. The concentration of oxidant

N_{Ox} is the difference between the original oxidant concentration, N_{x_I} and the added diluent concentration, N_D:

$$N_{Ox} = N_{x_I} - N_D$$

Equations II.G.15, II.G.16, and II.G.17 can be used to predict the dependence of v, δ, and τ on the concentration of added diluent, giving

$$\delta = (\mathcal{D}/((N_{Ox_I} - N_D)\, A_k e^{-\Delta E_a/k_B T}))^{1/2} \qquad \text{(II.G.18)}$$

$$v = (\mathcal{D}(N_{Ox_I} - N_D)\, A_k e^{-\Delta E_a/k_B T})^{1/2} \qquad \text{(II.G.19)}$$

and

$$\tau = ((N_{Ox_I} - N_D)\, A_k e^{-\Delta E_a/k_B T})^{-1} \qquad \text{(II.G.20)}$$

where τ is the characteristic time for formation of CO in the flame as defined by equation II.G.2, and τ was found to equal the characteristic reaction time for the CO producing reaction mechanism.

Equation II.G.20 implies that boosting concentration of the inert gas in the reactant mixture at the expense of the concentration of O_2 reduces the reaction rates. The flame speed decreases as the flame thickness increases. Measuring the dependence of either v or τ on the concentration of diluent, N_D, can provide an experimental verification of the relationships expressed in equations II.G.15 through II.G.17. In Appendix B, an analysis is carried out showing that to maximize the small signal gain of the product mixture, it is advantageous to have a low temperature flame, fuel lean. In the CS_2/O_2 mixing layer flame, excess oxygen cannot be used as a diluent, and to reduce the temperatures an inert diluent must be used. Consequently, the implications of diluting with an inert

gas rather than O_2 are relevant to evaluating the relative utility of mixing layer and premixed CS_2/O_2 flames for use as laser media.

Experimental Work and Results

The effects of diluent addition on the flame speeds were found and compared with the theoretical results based on dimensional analysis. Rotometer measurements were used to find the gas flow rates, and photographs were taken and used to measure the area of the flames. The flame speeds were then calculated using the law of mass conservation: v = (the gas flow rate)/(the area of the flame). The details of this technique are fully described in Reference II.1. The flow rate of the mixture of O_2 and diluent and the flow rate of CS_2 were individually held constant. The flow rate of the mixture of O_2 and diluent was 30-fold larger than the flow rate of CS_2. Ar or N_2O was added as a diluent at the expense of O_2, and the flame speeds were measured. The results are shown in Figure II-G-1.

The data points in Figure II-G-1 have error bars due to uncertainties in the flow rates and the photographic measurements. The flow rates account for a larger part of the uncertainty. The relative values of the points are considerably more certain than the error bars on their absolute magnitudes indicate.

Results and Conclusions

Dilution with N_2O or Ar causes the flame speed to decrease more rapidly than was predicted by dimensional analysis. Ar or N_2O was added to the reactant mixture at the expense of O_2, comparing heat capacities:

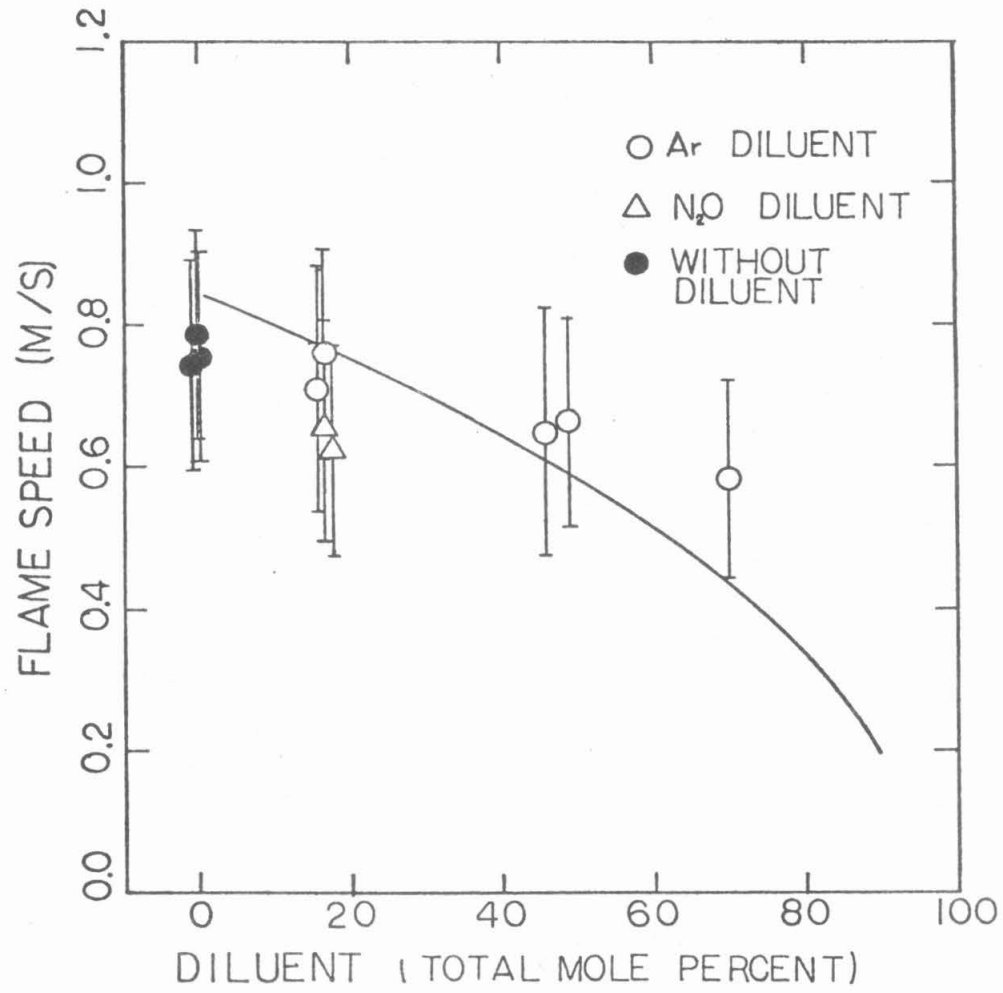

Figure II-G-1 Flame speed as a function of the fraction of diluent gas; p = 14.5 torr; CS_2:(O_2 + diluent) = 1:30. The solid line is a theoretical prediction based on the results of dimensional analysis, equation II.G.19, with arbitrary normalization.

$C_{P_{CS_2}}$ = 14.5, $C_{P_{O_2}}$ = 8.7, $C_{P_{Ar}}$ = 5.0, and $C_{P_{N_2O}}$ = 14.0 (cal/mole-deg K at 1500°K [II.57]). Because N_2O has a larger heat capacity than Ar, N_2O will bring about a greater reduction in flame temperature and reaction rates if the N_2O acts inert chemically. It is therefore not surprising that N_2O reduces the flame speeds more readily than Ar. Even though $C_{P_{Ar}} < C_{P_{O_2}}$, the flame speed with Ar dilution fell slightly below the theoretical curve. The reduction in the flame speeds by dilution, and the consequential decrease in the CO production rate, is greater than predicted by simple dimensional analysis.

It is proposed in Reference II.35 that N_2O may act as an oxygen donor in $CS_2/O_2/N_2O$ flames, increasing the rate at which the mixture reacts. The flame speed measurements are evidence that the more important effect of N_2O is one of reducing the vigour of the reactions, lowering the flame speed.

When N_2O is added to CS_2/O_2 mixtures in concentrations comparable to the CS_2 concentration, a straw-brown colored emission was observed from the region downstream of the flame front. This emission either replaced or overwhelmed the blue SO_2 afterglow. The straw-brown emission was probably due to NO_2 chemiluminescence on the $\tilde{A}(^2B_1) \rightarrow \tilde{X}^2A_1$ transition [II.35]. Producing NO_2 in the $\tilde{A}(^2B_1)$ state requires at least 43 kcal/mole; $NO + O \rightarrow NO_2$ is the only suitably exothermic reaction. The addition of N_2O to the CS_2/O_2 flame affects the vibrational transfer processes and the chemistry. The flame speed measurements presented here are evidence that N_2O is not beneficial in speeding the chemistry, and the observation of NO_2 emission suggests N_2O may even act to reduce the atomic oxygen concentration.

Chapter II References

II.1 A. A. Vetter, Ph.D. thesis: "Kinetics and Structure of the CS_2/O_2 Flame Laser," California Institute of Technology (1975).

II.2 V. A. Dudkin, private communication (1977).

II.3 A. E. Siegman, An Introduction to Lasers and Masers (McGraw-Hill, New York, 1971).

II.4 F. A. Williams, Combustion Theory (Addison-Wesley, Reading, Mass., 1965).

II.5 F. M. White, Viscous Fluid Flow (McGraw-Hill, New York, 1974).

II.6 H. G. Wolfhard and W. G. Parker, "A New Technique for the Spectroscopic Examination of Flames at Normal Pressures," Proceedings of the Physical Society A-62, 722-730 (1949).

II.7 H. G. Wolfhard and W. G. Parker, "A Spectroscopic Investigation into the Structure of Diffusion Flames," Proceedings of the Physical Society A-65, 2-19 (1952).

II.8 P. Dearden and R. Long, "Soot Formation in Ethylene and Propone Diffusion Flames," Journal of Applied Chemistry 18, 243-251 (1968).

II.9 H. F. Sullivan and I. Glassman, "Vapor Phase Diffusion Flames in the Combustion of Magnesium and Strontium," Combustion Science and Technology 4, 241-256 (1972).

II.10 J. A. Barnard and C. F. Cullis, "The Rates of Chemical Reactions in the Diethyl-Ether Diffusion Flame," Eighth Symposium (International) on Combustion, pp. 481-486 (1961).

II.11 R. J. Richardson and T. J. Menne, "Combustor-Driven CO Laser," Laser Focus 14, 50-53 (1978)

II.12 G. Hertzberg, Molecular Spectra and Molecular Structure III. Electronic Spectra and Structure of Polyatomic Molecules (Van Nostrand-Reinhold Co., New York, 1966).

II.13 G. Hertzberg, Molecular Spectra and Molecular Structure I. Spectra of Diatomic Molecules (Van Nostrand-Reinhold Co., New York, 1950).

II.14 E. M. Bulewicz and P. J. Padley, "A Cyclotron Resonance Study of Ionization in Low-Pressure Flames," Ninth Symposium (International) on Combustion, pp. 639-646 (1963).

II.15 G. H. Markstein, "Structure of Low Pressure Trimethylaluminum-Oxide Flat Diffusion Flames," Combustion and Science Technology 3, 245-253 (1971).

II.16 R. M. Osgood, W. C. Eppers, Jr., and E. R. Nichols, "An Investigation of the High Power CO Laser," IEEE Journal of Quantum Electronics QE-6, 145-154 (1970).

II.17 V. N. Ochkin, N. N. Sobolev, and E. A. Trubacheev, "Relaxation of Active Levels in CO Laser Due to CO*-CN Collisions," Soviet Journal of Quantum Electronics 6, 38-43 (1976).

II.18 M. I. Bhaumik, W. B. Lacina, and M. M. Mann, "Characteristics of a CO Laser," IEEE Journal of Quantum Electronics QE-8, 150-160 (1972).

II.19 K. P. Horn and P. E. Oettinger, "Vibrational Energy Transfer in Diatomic Molecules," Journal of Chemical Physics 54, 3040-3046 (1970).

II.20 J. Janin, F. Roux, and J. d'Incan, "Etude thermodynamique de la flamme oxyace´tlénique á partir du spectre de vibration-rotation de OH," Spectrochemica Acta 23A, 2939-2950 (1967).

II.21 G. Hancock, B. A. Ridley, and I.W.M. Smith, "Infrared Chemiluminescence from Vibrationally Excited CO, Part 2.--Product Distribution from the Reaction $O + CS \rightarrow CO + S$," Journal of the Chemical Society, Faraday Transactions II 68, 2117-2126 (1972).

II.22 G. Hancock, C. Morely, and I.W.M. Smith, "Vibrational Excitation of CO in the Reaction: $O + CS \rightarrow CO + S$", Chemical Physics Letters 12, 193-196 (1971).

II.23 K. D. Foster, "Initial Distribution of $CO^{\dagger}$ from the Reaction $O + CS \rightarrow CO^{\dagger} + S$," Journal of Chemical Physics 57, 2451-2455 (1972).

II.24 N. Djeu, "Quantitative Laser Measurements of Very Small Absorptions: Studies of the $O + CS \rightarrow CO(v) + S$ Reaction," Journal of Chemical Physics 60, 4109-4115 (1974).

II.25 H. T. Powell and J. D. Kelly, "Vibrational Distribution of Carbon Monoxide from $O + CS \rightarrow S + CO(v)$," Journal of Chemical Physics 60, 2191-2192 (1974).

II.26 J. D. Kelley, "A Comment on the Vibrational Distribution of CO Produced by the Reaction of O with CS and CS_2," Chemical Physics Letters 41, 7-11 (1976).

II.27 K. D. Foster and G. H. Kimbell, "Characteristics of a CS_2/O_2 Chemical Laser with Flow Transverse to the Optical Axis," Fourteenth Symposium (International) on Combustion, pp. 203-210, The Combustion Institute (1973).

II.28 S. Tsuchiya, N. Neilson, and S. H. Bauer, "Lasing Action and Relative Populations of Vibrationally Excited Carbon Monoxide Produced in Pulse-Discharged Carbon Disulphide-Oxygen-Helium Mixtures," Journal of Physical Chemistry 77, 2455-2464 (1973).

II.29 P. H. Krupenic, The Band Structure of Carbon Monoxide, NSRDS-NBS Circular 5 (1966).

II.30 G. Hancock and I.W.M. Smith, "Quenching of Infrared Chemiluminescence. 1: The Rates of De-Excitation of CO ($4 \leq v \leq 13$) by He, CO, NO, N_2, O_2, OCS, N_2O, and CO_2," Applied Optics 10, 1827-1843 (1971).

II.31 C. Kittle, Thermal Physics (John Wiley and Sons, Inc., New York, 1969).

II.32 J. P. Holman, Heat Transfer (McGraw-Hill Co., New York, 1963).

II.33 A. J. Lightman and E. R. Fisher, "A Coefficient for Spontaneous Emission in $CO^{\dagger}$," Applied Physics Letters 29, 593-595 (1976).

II.34 S. D. Rockwood, J. E. Brau, W. A. Proctor, and G. H. Canavan, "Time Dependent Calculations of Carbon Monoxide Laser Kinetics," IEEE Journal of Quantum Electronics QE-9, 120-129 (1973).

II.35 M. J. Linevsky and R. A. Carabetta, "CW Laser Power from Carbon Bisulfide Flames," Applied Physics Letters 22, 288-291 (1972).

II.36 S. K. Searles and N. Djeu, "Characteristics of a CS CO laser Resulting from a CS_2-O_2 Additive Flame," Chemical Physics Letters 12, 53-56 (1971).

II.37 F.E.C. Culick, private communication (1978).

II.38 C.K.N. Patel, "Interpretation of CO_2 Optical Maser Experiments," Physical Review Letters 12, 588-590 (1964).

II.39 S. S. Penner, Quantitative Molecular Spectroscopy and Gas Emissivities (Addison Wesley Inc., Reading, Mass., 1959).

II.40 C. B. Ludwig, W. Malkmus, J. E. Pearson, and J.A.L. Thompson, Handbook of Infrared Radiation from Combustion Gases, NASA Scientific Publication, NASA SP 3080 (1973).

II.41 N. A. Nielson, Jr., Ph.D. thesis: "An Electrically Discharged Carbon Disulphide-Oxygen Chemical Laser," Cornell University (1975).

II.42 R.W.F. Gross and J. F. Bott, Handbook of Chemical Lasers (Wiley and Sons, New York, 1976).

II.43 N. Djeu, "Quantitative Laser Measurements of Very Small Absorptions: Studies of the O + CS CO(v) + S Reaction," Journal of Chemical Physics 60, 4109-4115 (1974).

II.44 W. Q. Jeffers, "Carbon Monoxide Chemical Laser Research," Report MDC-Q0495, ARPA, McDonnell Douglas Corp., St. Louis, Mo. (1973).

II.45 M. A. Kovacs, "Vibrational Relaxation of Carbon Monoxide by Foreign Gases," Journal of Chemical Physics 58, 4704-4706 (1973).

II.46 W. Grossman, A. A. Vetter, and F.E.C. Culick, "Some Results for the Combustion of CS_2/O_2 in a Laminar Mixing Layer," Proceedings of the 14th JANNAF Conference (1977).

II.47 R. D. Suart, S. J. Arnold, and G. H. Kimbell, "Power Enhancement by the Addition of Vibrationally Cool Gases," Chemical Physics Letters 7, 337-340 (1970).

II.48 W. Q. Jeffers, C.E. Wiswall, and H. Y. Ageno, "Gas Additive Effects in CO Chemical Lasers," IEEE Journal of Quantum Electronics QE-12, 693-697 (1976).

II.49 K. D. Foster, G. H. Kimbell, and D. R. Snelling, "Near Single-Line Operation of a Free Burning $CS_2/O_2/N_2O$ Flame Laser with a Nondispersive Optical Cavity," IEEE Journal of Quantum Electronics QE-11, 253-258 (1975).

II.50 V. A. Dudkin, "Anomalous Effects of Impurities on CS_2-O_2 Flame Laser Emission," Combustion, Explosion, and Shock Waves 9, #3, (English Translation), pp. 398-399 (1975).

II.51 H. V. Lilenfield, R. F. Webbink, W. Q. Jeffers, and J. D. Kelley, "Modelling of the CW CO Chemical Laser," IEEE Journal of Quantum Electronics QE-11, 660-669 (1975),

II.52 G. Hancock and I.W.M. Smith, "Infrared Chemiluminescence from Vibrationally Excited CO, Part 1. --The Reaction of Atomic Oxygen with Carbon Disulphide," Transactions of the Faraday Society 67, 2586-2598 (1971).

II.53 D. Milks and R. A. Matula, "A Single-Pulse Shock-Tube Study of the Reaction between Nitrous Oxide and Carbon Monoxide," Proceedings of the Fourteenth Symposium (International) on Combustion, The Combustion Institute, Pittsburgh, PA (1973).

II.54 R. E. Bolz and G. L. Tuve, CRC Handbook of Applied Engineering Science, CRC Press (1976).

II.55 J. Chedaille and Y. Brand, Measurements in Flames (Edward Arnold, Ltd., 1972).

II.56 C. F. Dewey Jr., "A Correlation of Convective Heat Transfer and Recovery Temperature Data for Cylinders in Compressible Flow," International Journal of Heat and Mass Transfer 8, 245-252 (1965).

II.57 JANAF Thermochemical Tables, Second Edition N SRDS-NBS37 (1971).

Chapter III

COMPUTER MODELING

A. Introduction and Summary

Computer modeling was used to investigate the CS_2/O_2 laminar mixing layer flame. The fluid and chemical behavior of the flame was examined by means of the computer code created by this author, MIXWG, which is listed in Appendix C. The equations governing the flow, as set forth in Appendix A, were solved numerically. The processes of species diffusion, viscous transport of momentum, heat conduction, convective transport of species, momentum and energy, and chemical production of species and heat are incorporated into the model.

The results of this study are summarized here. CS_2 and O_2 mix and react in a low Mach number (velocity $\simeq$ 200 cm/sec) mixing layer flame. In a mixing layer with shear, the reaction zone tends to skew into the reactant stream of lower velocity. The CO production reaches a maximum about 1 cm downstream of the start of the mixing layer, proceeding by the 4 reaction branching chain mechanism discussed in Chapter I:

$$CS_2 + O \rightarrow CS + SO$$
$$CS + O \rightarrow \underline{CO} + S$$
$$S + O_2 \rightarrow SO + O$$
$$SO + O_2 \rightarrow SO_2 + O$$

About 1 cm downstream of the start of the mixing layer, COS formation by the reaction

$$CS_2 + O \rightarrow COS + S$$

completes with the earlier dominant reaction: $CS_2 + O \rightarrow CS + SO$. Subsequent to COS formation, CO_2 is produced by the reaction

$$COS + O \rightarrow CO_2 + S$$

Oxidation of COS is responsible for more CO_2 production than is oxidation of CO.

The gas composition is inhomogeneous in the mixing layer. The CS_2 concentration is appreciable only on the side of the mixing layer by the CS_2 stream, and the atomic oxygen concentration is only appreciable by the O_2 stream. The intermediates, S, SO, and COS, and the products SO_2, CO, and CO_2 are found nested fairly symmetrically between the CS_2 and O_2 streams. Going downstream, the species accumulate in roughly the following sequence: SO_2 and CO, CS, O, SO, COS, and finally CO_2 and S.

B. Chemical and Fluid Processes

CS_2 and O_2 mix and react in a low Mach number laminar mixing layer flame. The governing equations are presented in Appendix A. For simplicity we choose to look for the class of solutions for which there is no net fluid velocity, v, normal to the flame. The Howarth transformed equations of flow, as solved, are

$$\frac{u\partial Y_i}{\partial z} = \mathcal{D}_\infty \frac{\partial^2 Y_i}{\partial y^2} + \frac{W_i}{\rho}$$

where Y_i is the mass fraction of species i, and W_i is the chemical source term for species i, and

$$\frac{u\partial T}{\partial z} = \frac{K_\infty}{\rho_\infty C_p} \frac{\partial^2 T}{\partial y^2} + \frac{\dot{Q}}{\rho C_p}$$

where T is the temperature and Q is the chemical heat source term. Because Mach number of the flow is low, the pressure is taken to be constant. For simplicity, the diffusion constant $\mathcal{D}_\infty$ is taken to be equal in both the CS_2 and the O_2 free streams. The Lewis number is taken to be unity; consequently, $k_\infty/\rho_\infty C_p = \mathcal{D}_\infty$ is constant. C_p is the heat capacity; ρ_∞ and K_∞ are the free stream values for the density and coefficient for heat conduction.

Ten species were considered in the chemistry: O_2, CS_2, CS, S, O, SO, CO, CO_2, COS, and SO_2. The chemical species source terms, $\dot{Q}$, were computed on the basis of the rates for the chemical reactions included in the model. These reactions are listed in Table III.B.1. The first four reactions comprise the branching chain mechanism that is responsible for production of vibrationally excited CO [III.1]. Reactions 5 through

Table III.B.1

	Reaction	Forward Rate[a]	Exothermicity[6]	Ref.
1	$CS_2+O \rightarrow CS+SO$	$5.0 \times 10^{13} \times \exp(-960/T)$	20.1	III.6 III.8
2	$CS+O \rightarrow CO+S$	$2.4 \times 10^{14} \times \exp(-1010/T)$	85.0	III.6
3	$S+O_2 \rightarrow SO+O$	$1.0 \times 10^{13} \times \exp(-2800/T)$	5.9	III.9
4	$SO+O_2 \rightarrow SO_2+O$	$3.5 \times 10^{11} \times \exp(-3280/T)$	12.9	III.6
5	$CO+S+M \rightarrow COS+M$	$2.0 \times 10^{16} \times \exp(-900/T)$	73.4	III.6
6	$CO+O+M \rightarrow CO_2+M$	$1.6 \times 10^{16} \times \exp(-900/T)$	127.5	III.6
7	$CS_2+O \rightarrow COS+S$	$1.0 \times 10^{14} \times \exp(-4040/T)$	54.1	III.6 III.8
8	$CO+O_2 \rightarrow CO_2+O$	$1.7 \times 10^{12} \times \exp(-25700/T)$	2.1	Note c
9	$CO+SO \rightarrow CO_2+S$	$3.5 \times 10^{12} \times \exp(-25700/T)$	18.6	III.10
10	$COS+O \rightarrow CO_2+S$	$4.4 \times 10^{14} \times \exp(-26300/T)$	54.0	III.6

[a]The temperature is in °K, and the reaction rates are in units of moles, cm, and seconds.

[b]A positive exothermicity indicates an exothermic reaction. These values are computed using the data of Reference III.11. The heat of formation of CS is taken from Reference III.12.

[c]Because this rate was not found in the literature, it was chosen to equal the rate of the similar reaction, number 9, divided by a steric factor of 2.

10 in Table III.B.1 are involved in the production of COS and CO_2. These reactions were included in order to investigate the presence of COS and CO_2, and to determine the mechanisms responsible for their formation. Not all of these reactions were found to be important. A number of reactions were eliminated from consideration prior to the analysis using the computer. Those that proceed very slowly due to large endothermicity, large activation energy, or low reactant concentrations were not included.

The heat capacity of the combustion gas increases with temperature. The amount of energy required to raise the temperature of the mixture one unit is larger than the heat capacity of the mixture. This is because adding energy to the mixture drives the endothermic dissociation of molecules in the gas, as well as heating them, for example, $SO_2 \rightarrow SO+O$. In lieu of including a set of dissociation reactions in our model, we chose to simplify the computations by employing an altered heat capacity which sharply increases at the temperatures at which molecular dissociation imposes a restriction on the flame temperature. This approximation should cause the predicted concentrations of free radicals to be too low in regions of high temperatures, because free radicals are not generated by dissociation. The altered heat capacity used is

$$C_p = 10.2 + 2.5 \times 10^9 \times (\exp(17\text{-}50{,}000/T))/T^2 \ \text{(cal/mole-°K)}$$

This is of the form

$$C_p = C_{p_o} + (\Delta H_o/RT)^2 \exp(-\Delta F/RT)$$

where ΔH_o is the endothermicity of the dissociation reaction limiting the flame temperature, and ΔF is the change in the free energy in this reaction, $\Delta F \simeq TS - \Delta H$.

The heat released to the flow from the exothermicity of the chemical reactions was computed ignoring energy trapped in internal degrees of freedom of the molecules. The net reaction in one cycle of the 4 reaction branching chain mechanism for CS_2/O_2 combustion [III.2] is

$$CS_2 + 5/2\ O_2 \rightarrow 2SO_2 + CO + 195\ \text{kcal/mole} \qquad \text{(III.B.1)}$$

The reaction step responsible for the production of vibrationally excited CO in this mechanism is

$$CS + O \rightarrow CO + S + 85\ \text{kcal/mole} \qquad \text{(III.B.2)}$$

About 80% of the exothermicity of reaction III.B.2 is channeled into the vibrational excitation of CO [III.3]. Therefore, about 35% of the exothermicity of the net reaction III.B.1 is channeled into vibrational excitation of CO.

As the CO vibrationally equilibrates, the kinetic temperature of the gas rises. Were the gas temperature to increase linearly with the added heat, this could account for 35% of the increase in temperature. However, because the rise in temperature is nonlinear in the heat added, less than 35% of the increase in temperature during CS_2/O_2 combustion is neglected if we should fail to consider the exothermicity of the vibrational relaxation processes. In Chapter II, Section E, we found that, due to the presence of COS, vibrational equilibration of CO in our CS_2/O_2 flames took place in less than 1 cm. Over this distance, a large portion of the vibrational energy is transferred to kinetic energy. By assuming the energy immediately goes into kinetic energy, the computed temperature rise and reaction progress will be slightly too rapid.

The forward rates for each reaction included are listed in Table II.B.1. The reverse rates were generated by use of detailed balancing for each of the reactions except for the recombination reactions, 5 and 6. These were assumed to proceed only forward because of their large exothermicity. In our computations, the net rates for the remaining 8 reactions were taken to be the difference between the forward and reverse rates.

The species mole fractions, the temperature, and the velocity were calculated on a grid of points in Howarth transformed space by numerical integration of the governing equations, marching downstream. Initially, the reactant streams, CS_2 and O_2, each had uniform velocity, and on the grid point where the streams abut, there was a small mole fraction of reactive intermediates, CS, S, O, and SO, as well as a slightly elevated temperature. This initial condition served to assure ignition. The downstream conditions were insensitive to the details of this initial ignition. The ignition of the flame in this manner was necessary because upstream conduction and diffusion, which are essential to flame propagation, were neglected in this model.

In order to simplify the computational complexity of the problem, the velocity profiles were not computed explicitly. They were determined by assuming a similarity between the species concentration profiles and the velocity profile. This approximation was motivated by the result one finds in the free laminar shear layer without reaction, and the computer generated velocities were found to match analytical solutions within 10% for simple test cases.

The grid used was quite coarse; in the direction normal to the plane of the splitter plate (y axis) there were 9 grid points at each downstream location (z axis). Derivatives in y were approximated by differences along y. The integration downstream was accomplished by use of a numerical routine from the Caltech computer library called "MODDEQ", altered slightly to handle a larger set of equations. This routine automatically adjusts the integration step size along the z axis in order to control truncation errors. The method of Runge-Kutta-Gill is used to start the integration process is also used to restart the integration whenever the step size has been altered. Once the integration has been started, it is continued by the Adams-Moulton predictor-corrector method.

Before presenting results, we should keep in mind that modeling can be no more accurate than the rate constants used in the model. The chemical rate constants are typically measured at temperatures well below the flame temperatures encountered in CS_2/O_2 combustion, and the values at elevated temperatures must be estimated by extrapolation. The rates in Table III.B.1 should be taken as estimates, accurate to one significant figure at best. The flame modeling calculations are meant to aid in the understanding of the processes dominant in the mixing layer flame. In light of the uncertainties in the reaction rate constants, even differences of 25% in the mole fractions of two species should generally be considered insignificant, except for the qualitative trends these differences may suggest.

Results

CS_2 and O_2 mix and react in a low Mach number laminar mixing layer flame. The heat generated in exothermic chemical reactions raises the maximum temperature above 2500°K; the gas expands and the streamlines diverge. In a mixing layer with shear, the reaction zone tends to skew into the stream of lower velocity. The results of several calculations for different flow conditions are presented in this section.

Figures III-B-1 through III-B-17 show the predicted streamlines, concentrations, and temperature field for a mixing layer flame in which the CS_2 free stream velocity, U_{CS_2}, is 100 cm/sec and the O_2 free stream velocity, U_{O_2}, is 300 cm/sec. The pressure is .01 atm (7.6 torr). The contour plots of species and temperature, and the plot of the streamlines are for the region just downstream of where mixing commences, corresponding in experiments to the region starting at the edge of the splitter plate and extending downstream. The upstream boundary conditions at the grid point separating the CS_2 and O_2 streams, which we will call the "central grid point" are:

$X_{O_2} = .90$	$X_{SO} = .01$	$T = 850°K$
$X_{CS_2} = .000033$	$X_{CO} = .03$	
$X_{CS} = .000030$	$X_{CO_2} = 0$	
$X_S = .000330$	$X_{COS} = 0$	
$X_O = .003300$	$X_{SO} = .056307$	

where X_i is the mole fraction of species i. A dashed line across these figures traces the path of the central grid point downstream. It

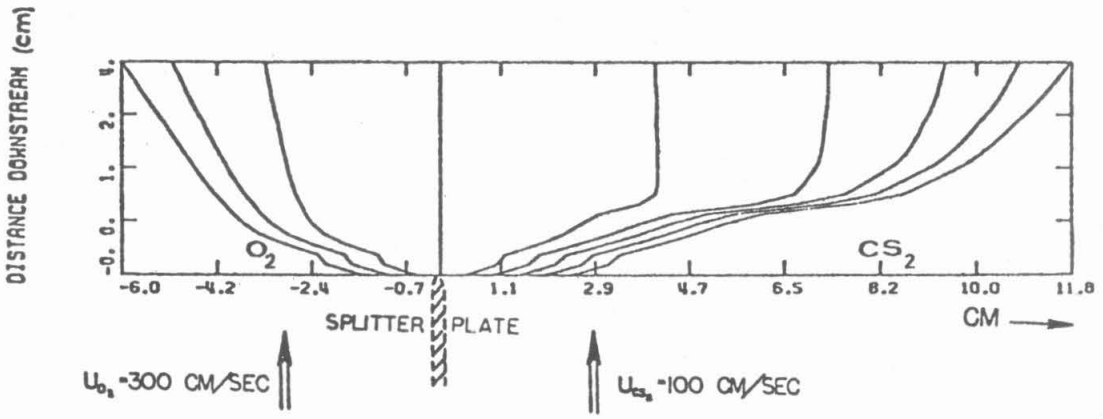

Figure III-B-1 Predicted streamlines in a CS_2/O_2 mixing layer flame with shear at 7.6 torr

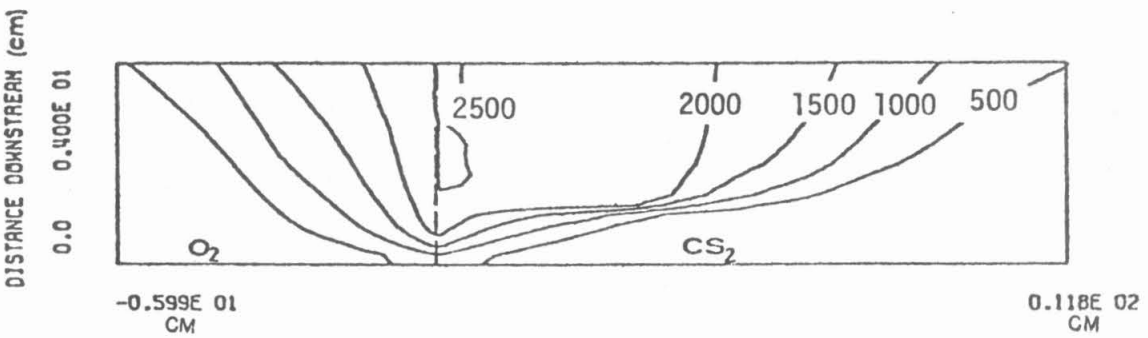

Figure III-B-2 Predicted temperatures (°K) in a CS_2/O_2 mixing layer flame with shear at 7.6 torr

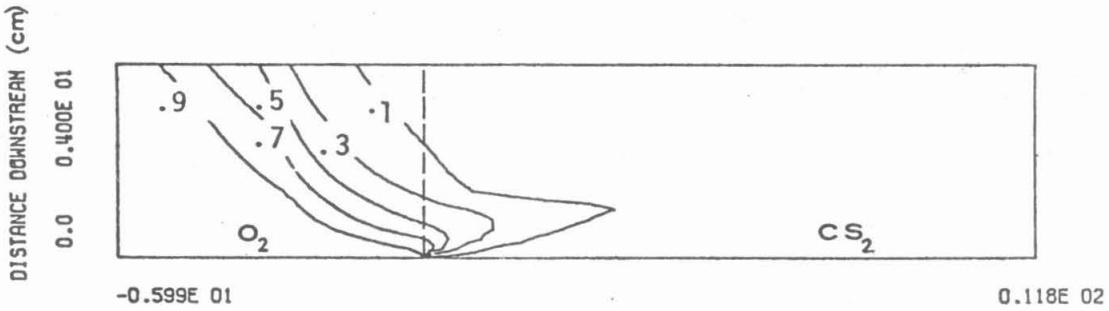

Figure III-B-3 Predicted mole fraction of O_2 in a CS_2/O_2 mixing layer flame with shear A = 7.6 torr

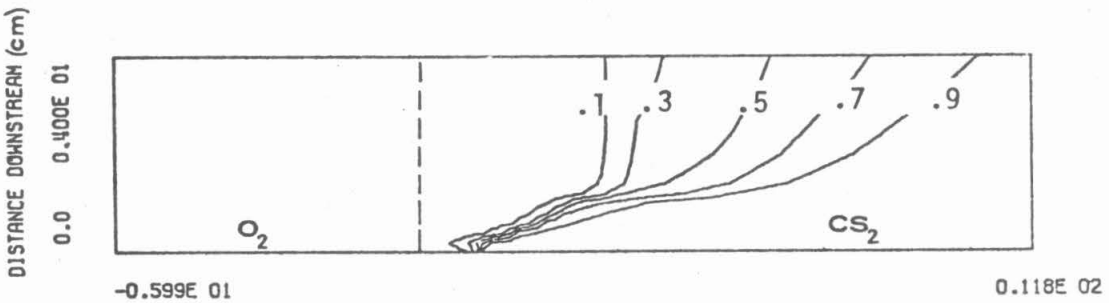

Figure III-B-4 Predicted mole fractions of CS_2 in a CS_2/O_2 mixing layer flame with shear at 7.6 torr

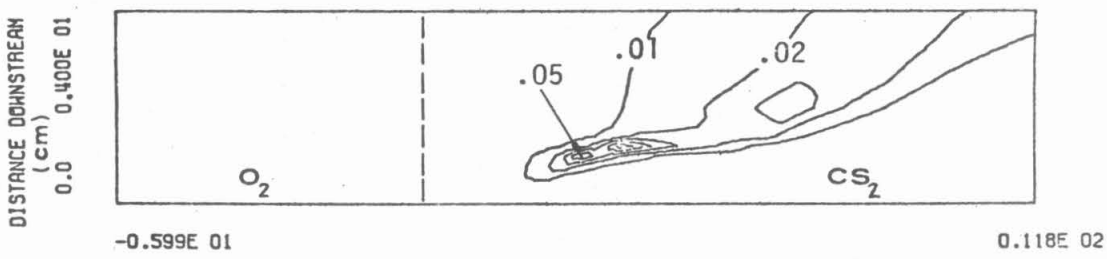

Figure III-B-5 Predicted mole fractions of CS

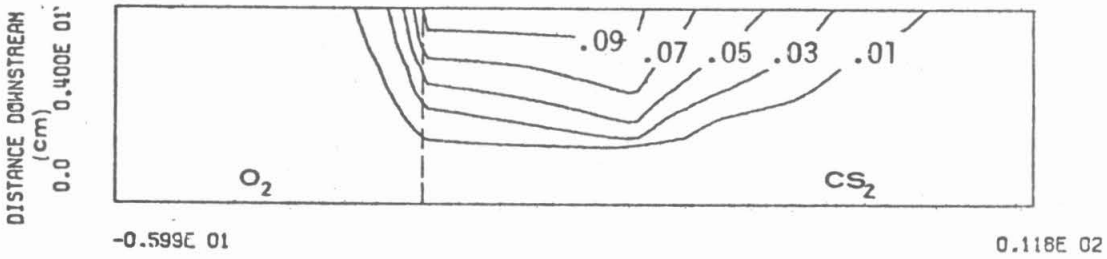

Figure III-B-6 Predicted mole fractions of S

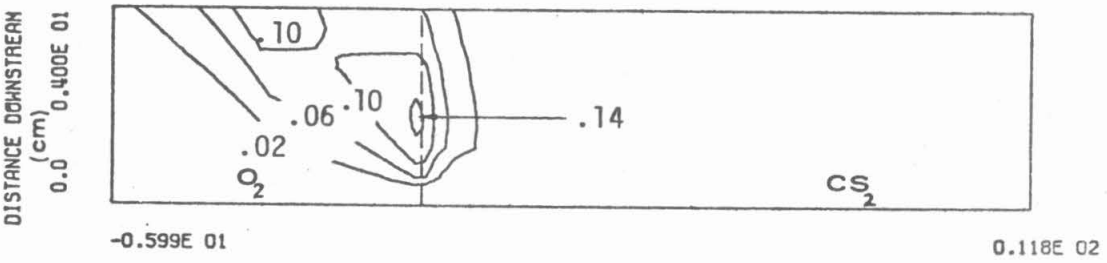

Figure III-B-7 Predicted mole fractions of O

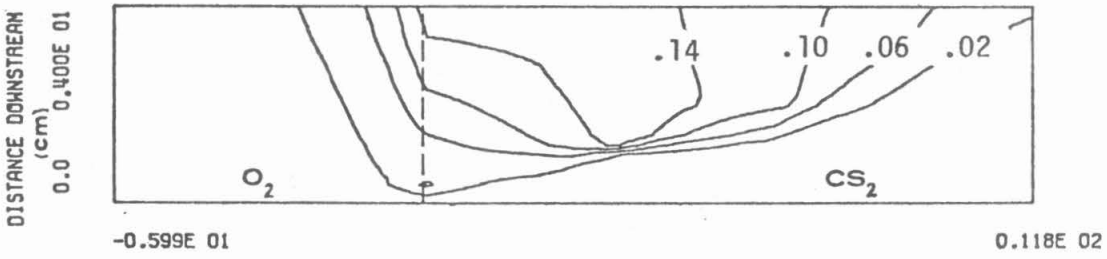

Figure III-B-8 Predicted mole fractions of SO

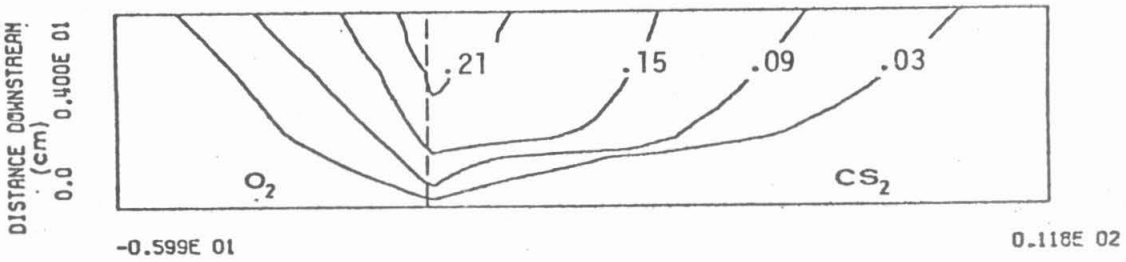

Figure III-B-9 Predicted mole fractions of CO

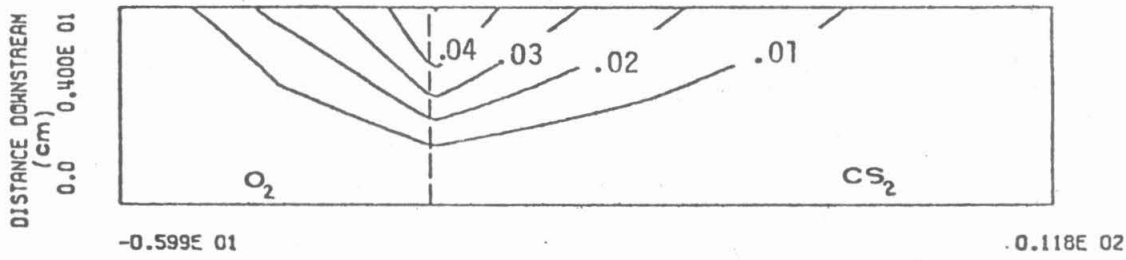

Figure III-B-10 Predicted mole fractions of CO_2

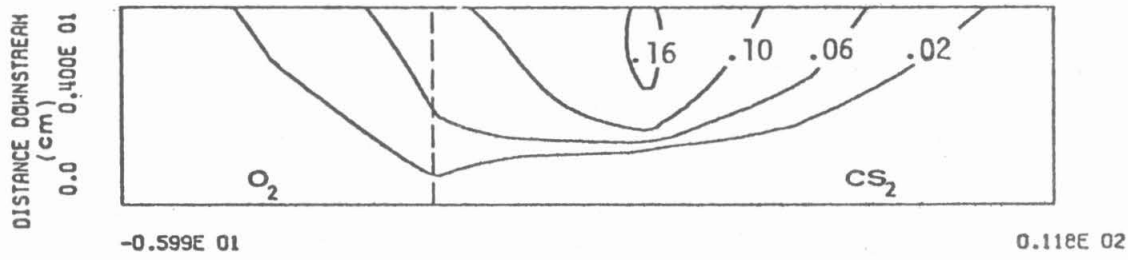

Figure III-B-11 Predicted mole fractions of COS

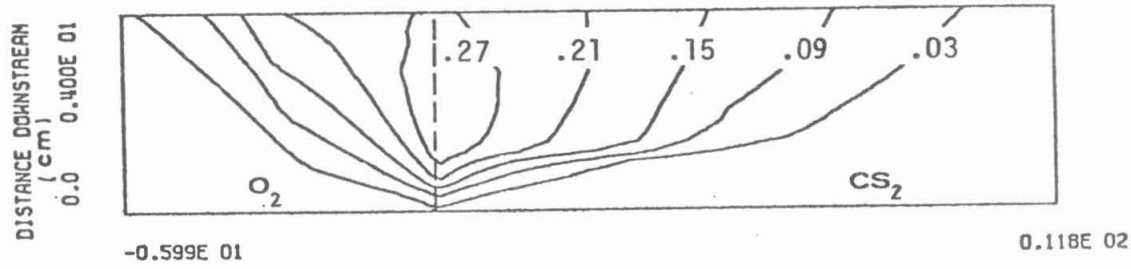

Figure III-B-12 Predicted mole fractions of SO_2

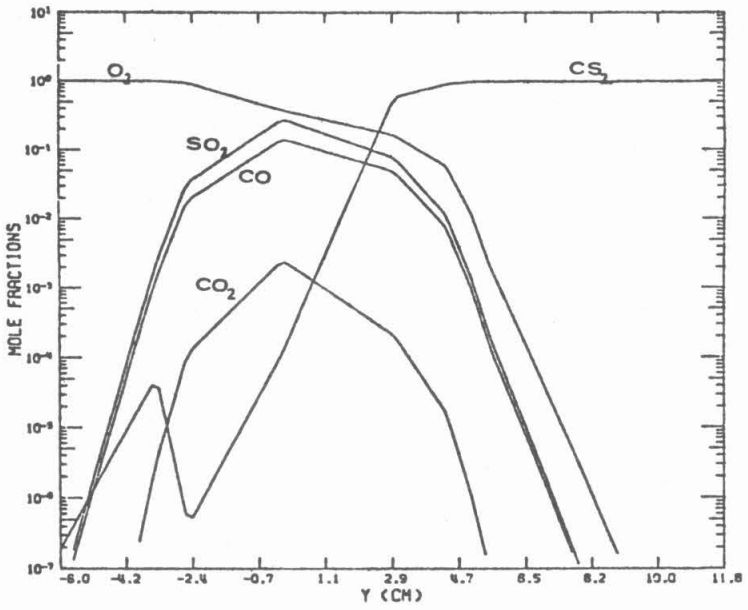

Figure III-B-13 Predicted concentrations of reactants and products in a CS_2/O_2 mixing layer flame 1 cm downstream of a splitter plate. Free stream velocities: U_{O_2} = 300 cm/sec and U_{CS_2} = 100 cm/sec; p = 7.6 torr

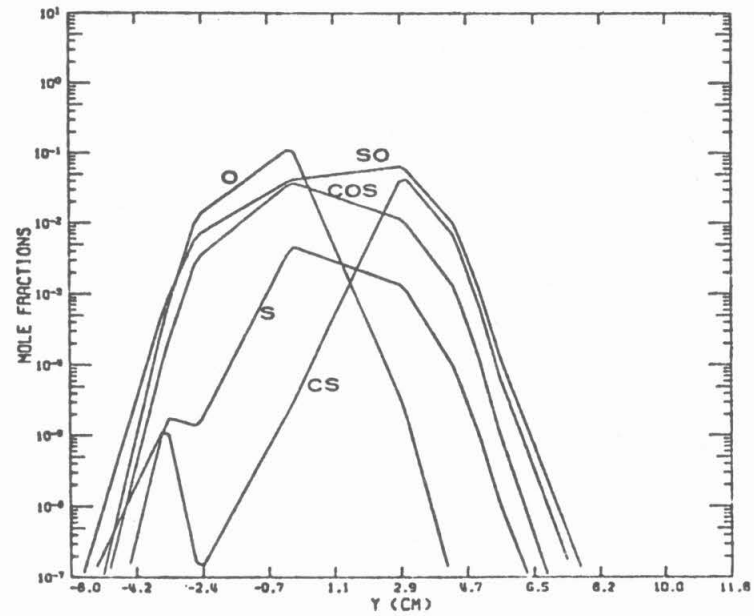

Figure III-B-14 Predicted concentrations of reactive intermediates in a CS_2/O_2 mixing layer flame 1 cm downstream of a splitter plate. Free stream velocities: U_{O_2} = 300 cm/sec and U_{CS_2} = 100 cm/sec; p = 7.6 torr

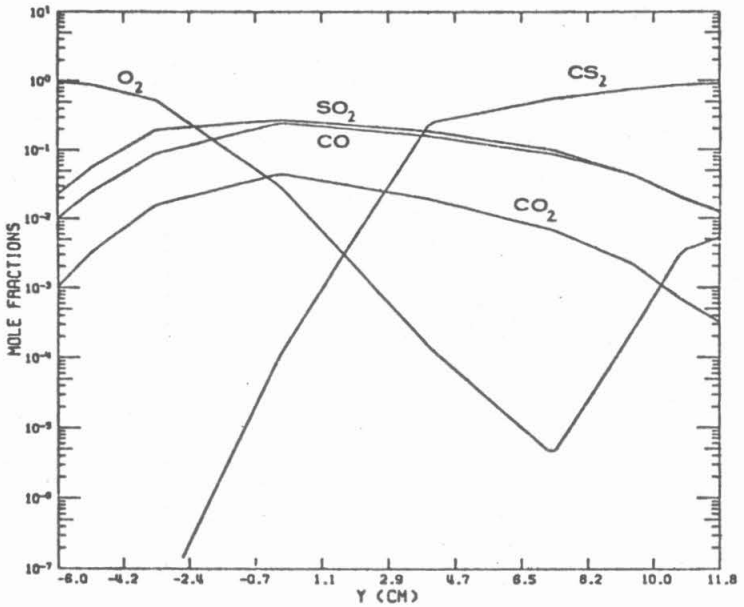

Figure III-B-15 Predicted concentrations of reactants and products in a CS_2/O_2 mixing layer flame 4 cm downstream of a splitter plate. Free stream velocities: U_{O_2} = 300 cm/sec, and U_{CS_2} = 100 cm/sec; p = 7.6 torr

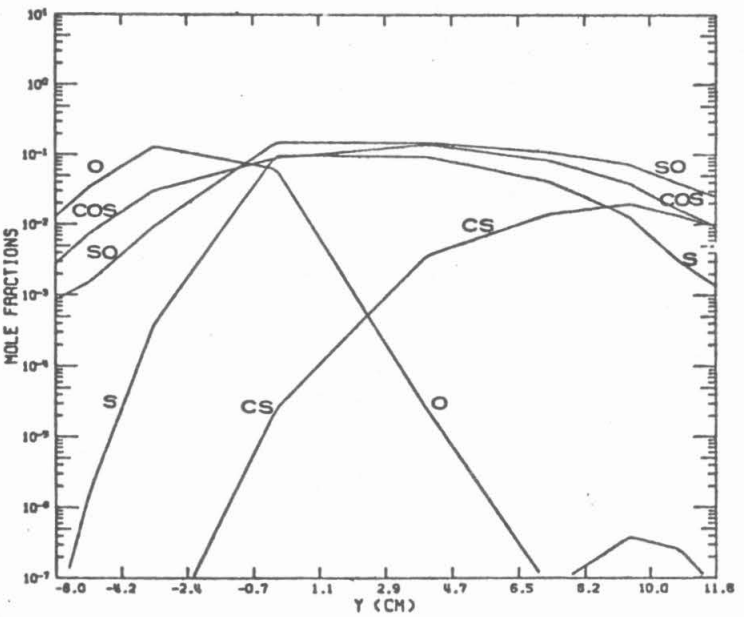

Figure III-B-16 Predicted concentrations of reactive intermediates in a CS_2/O_2 mixing layer flame 4 cm downstream of a splitter plate. Free stream velocities: U_{O_2} = 300 cm/sec, and U_{CS_2} = 100 cm/sec; p = 7.6 torr

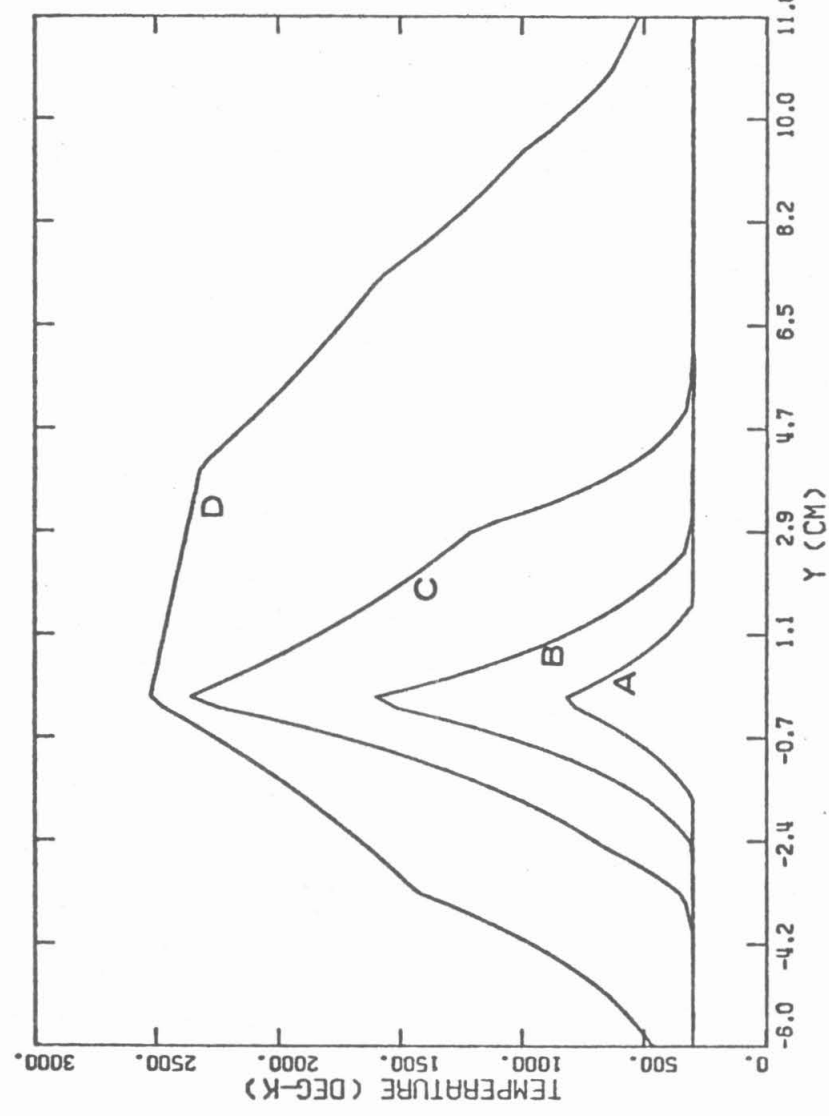

Figure III-B-17 Predicted temperature profiles across a CS_2/O_2 mixing layer flame with shear (U_{O_2} = 300 cm/sec; U_{CS_2} = 100 cm/sec; and p = 7.6 torr). Distance downstream: (A) .1 cm, (B) .4 cm, (C) 1.0 cm, and (D) 4.0 cm.

corresponds to the plane of the splitter plate. For the grid points adjacent to the central grid point on which flame initiation occurs, the temperature was initially 425°K. At all other points the initial temperature was 300°K. The initial values of the species mole fractions on the side of the CS_2 stream are

$$X_{O_2} = 0 \qquad X_{SO} = 0$$
$$X_{CS_2} = 1 \qquad X_{CO} = 0$$
$$X_{CS} = 0 \qquad X_{CO_2} = 0$$
$$X_{S} = 0 \qquad X_{COS} = 0$$
$$X_{O} = 0 \qquad X_{SO_2} = 0$$

and on the side of the O_2 stream they are

$$X_{O_2} = 1 \qquad X_{SO} = 0$$
$$X_{CS_2} = 0 \qquad X_{CO} = 0$$
$$X_{CS} = 0 \qquad X_{CO_2} = 0$$
$$X_{S} = 0 \qquad X_{COS} = 0$$
$$X_{O} = 0 \qquad X_{SO_2} = 0$$

These initial conditions were chosen because they both assured ignition, and did not involve premixing the CS_2 and O_2. Initially, at $z = 0$, the intermediates which cause the flame to propagate are mixed with an abundance of O_2 at the central grid point. The bulk of the remaining gas is product, CO and SO_2. At $z = 0$, at the central grid point, only 1.5% of the gas was reaction intermediates, and elsewhere there were none. A test case was run in which the intermediates were initially in an abundance of CS_2 instead of O_2:

X_{O_2} = .000033		X_{S_2} = .01		T = 850°K
X_{CS_2} = .90		X_{CO} = .03		
X_{CS} = .00033		X_{CO_2} = 0		
X_S = .0033		X_{COS} = 0		
X_O = .000003		X_{SO_2} = .056334		

In spite of these radically different conditions upstream, the results of the modeling calculation exhibited similar behavior with no quantitative differences worthy of note.

In the furthest upstream region of the mixing layer, the CO production is near zero. The production rate as a function of the z coordinate (along the flow) is shown in Figure II-B-18. The production rates plotted are the total production rates at a downstream position, z, in Howarth transformed space:

$$\text{Production} = \left(\int_{-\infty}^{\infty} W_{CO_2} \, dy \right) n_p$$

where W_{CO_2} is the chemical reaction rate for CO_2 such that

$$\left(\frac{\partial X_{CO_2}}{\partial (z/U)} \right)_{\substack{\text{due to particular} \\ \text{reaction only}}} = \left(\frac{\partial X_{CO_2}}{\partial t} \right)_{\substack{\text{due to one} \\ \text{reaction only}}} = W_{CO_2}$$

and n_p is the number of moles per cm^3 at 300°K and pressure p. The results shown in Figure II-B-18 are for the CO production predicted by the modeling calculation without shear, U = 200 cm/sec. They very closely match the results of the modeling calculation with shear: U_{CS_2} = 100 cm/sec, U_{O_2} = 300 cm/sec. Note that the theoretical curve

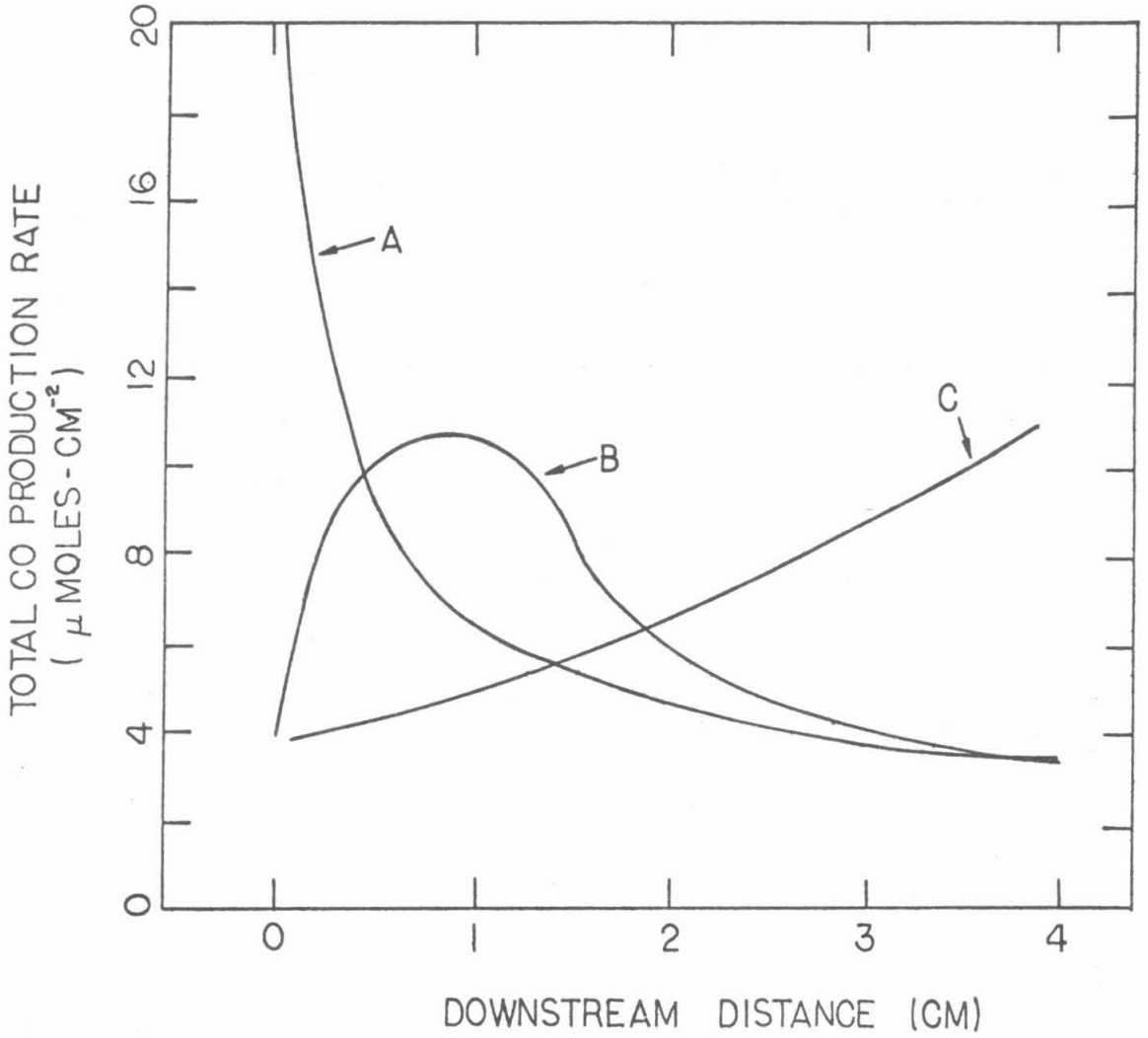

Figure III-B-18 Predicted CO production rate in a CS_2/O_2 mixing layer flame without shear as a function of downstream distance using (A) a flame-sheet approximation, (B) a branching chain reaction mechanism, and (C) a contrived straight chain reaction mechanism

based on the flame sheet approximation displays an integrable $z^{-1/2}$ singularity at z = 0. The CO production predicted by the modeling calculation displays no such singularity. Upstream the chemical production is limited by the low temperature of the reactant gases and the paucity of reactive chemical intermediates, O, S, and SO.

Downstream several centimeters from the start of the mixing layer, the CO production decreases, falling into accord with the prediction of the flame-sheet approximation. Downstream, CO production appears to be limited by the rate at which the reactants, CS_2 and O_2, diffuse toward each other. Upstream the fuel and oxidant species mix, but do not react with the vigor they do downstream where the mixing layer becomes rich in reactive intermediates. Downstream, the reactants are depleted in the central zone.

In Figure III-B-13 we find a small irregular rise in the CS_2 concentration in a region of nearly pure O_2. This CS_2 concentration is established upstream in the flow when the mixing processes are rapid and reactions slow. Flowing downstream the reactions deplete the central region of CS_2. Other examples of this sort of phenomena can be seen in Figures II-B-13 through II-B-16.

In Figures III-B-2, III-B-9, and III-B-12 the temperature CO and SO_2 profiles exhibit maxima which are nested in a generally symmetric manner between the CS_2 and O_2 streams. The temperature and mole fractions of CO and SO_2 rise most rapidly along the flow within 1.5 cm of the start of the mixing layer, and continue to increase downstream. The COS production follows after the temperature rises sufficiently. The reaction dominant in producing COS is reaction 7 in Table III.B.1.

The reaction intermediates fall into three groups, (S, SO, and COS), (CS), and (O); these groups are distinguished by where their concentrations are largest. Atomic oxygen is in abundance only on the side of the mixing layer by the O_2 stream, and reaches a mole fraction of over .15 in our test cases. The region of maximum atomic oxygen concentration shifts to more negative y with flow, as shown in Figure III-B-7. The magnitude of the concentration grows irregularly downstream, and this may be a consequence of the coarse computational grid in y. The other intermediates, CS, S, SO, and COS, do not rise rapidly toward their ultimate maximum mole fractions with flow compared with atomic oxygen. CS differs from S, SO, and COS in that it is concentrated on the side of the CS_2 stream, while the group (S, SO, and COS) is distributed more symmetrically between the CS_2 and O_2 streams.

COS formation is dominated by the reaction $CS_2 + O \rightarrow COS + S$. This reaction competes for CS_2 with the reaction $CS_2 + O \rightarrow CS + SO$, which is a precursor to CO formation. The reaction channel leading to the production of CS and SO has a smaller activation energy than the reaction channel leading to the production of COS and S. Upstream in the mixing layer, the temperature is relatively low; consequently, COS production is not favored. The ratio of the rate for the reaction channel $CS_2 + O \rightarrow COS + S$ to the rate for the reaction channel $CS_2 + O \rightarrow CS + SO$ is $2 \times \exp(-3080/T)$; the rates are taken from Table III-B-1. This ratio is .01 at 580°K and .1 at 1030°K. Because COS rapidly quenches vibrationally excited CO, it is advantageous to avoid COS production. To do so, cool fuel-lean flames, not mixing layer flames, are favored. By comparing Figures III-B-9 and III-B-11, or Figures II-B-13 through II-B-16, we see that the CO and COS

concentrations overlap in the mixing layer flames. COS deactivation of vibrationally excited CO will dominate the CO equilibration according to the estimates made in Chapter II, Section E.

Downstream of the production of COS, CO_2 is formed in the reaction $COS + O \rightarrow CO_2 + S$. The production of CO_2 is delayed downstream of the initial rise in concentration of the products CO and SO_2 because CO_2 production must await the accumulation of COS and O. The reactions $CO + O_2 \rightarrow CO_2 + O$ and $CO + SO \rightarrow CO_2 + S$ are found to contribute less than 10% of the CO_2. The reaction $CO + O + M \rightarrow CO_2 + M$ is found to contribute about 20% of the CO_2 at a pressure of .01 atm (7.6 torr) and 30% at a pressure of .02 atm (15.2 torr). The relative importance of CO_2 production by the four reactions examined, reactions 5, 6, 8, and 9 in Table II.B.1, is shown in Figure II-B-19.

The variations in the computed behavior of the mixing layer flame with pressure are small. When the pressure is increased to .02 atm (15.2 torr) from .01 atm (7.6 torr), the mixing layer thickness decreases slightly due to the reduction in the diffusion constants with increased pressure. The streamlines diverge less abruptly, and the heat addition, per unit downstream distance normalized to the density, decreases. However, the total reactant consumption by the flame is larger at higher pressure. These results are in accord with the trends predicted using the flame-sheet approximation, Appendix A.

The CO_2 mole fraction profile in the mixing layer exhibits a noticeable variation with pressure, and it is the only species to do so. At p = .02 atm, the maximum mole fractions of CO_2 are almost twice those at p = .01. The additional mole fraction of CO_2 is due nearly equally

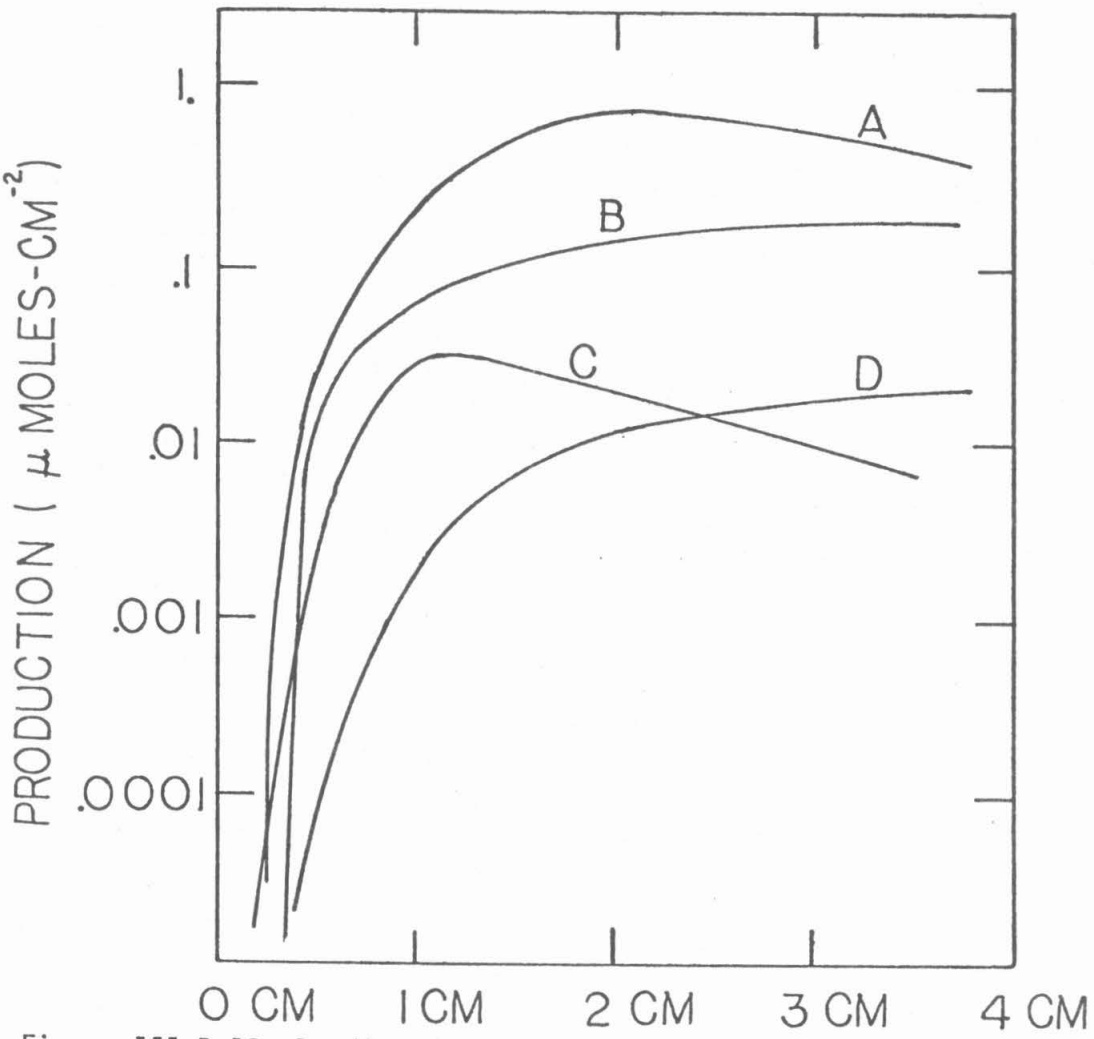

Figure III-B-19 Predicted CO_2 production in a CS_2/O_2 mixing layer flame with shear as a fraction of downstream distance due to the reactions: (A) $COS+O \rightarrow CO_2+S$; (B) $CO+O+M \rightarrow CO_2+M$; (C) $CO+O_2 \rightarrow CO_2+O$, and (D) $CO+SO \rightarrow CO_2+S$

to increased CO_2 production by the reaction $CO + O + M \rightarrow CO_2 + M$ and the reaction $COS + O \rightarrow CO_2 + S$. Because the profile of the COS mole fractions does not vary appreciably with pressure, the COS concentrations are nearly linear with pressure. Consequently, with increasing pressure the COS, along with other molecules, will more rapidly deactivate vibrationally excited CO.

In agreement with our experimental results, an effect of decreasing the velocity of the CS_2 stream relative to the O_2 stream is to cause the region in which the majority of the chemical reactions occur and CO production occurs to skew towards the side of the CS_2 stream. This trend can be seen in the CO concentration and the temperature profiles for two test cases, one in which U_{CS_2} = 100 cm/sec and U_{O_2} = 300 cm/sec, and the other in which U_{CS_2} = 200 cm/sec and U_{O_2} = 200 cm/sec. These are shown in Figures III-B-2, III-B-9, III-B-20, and III-13-21.

At low pressures, $p \leq .01$ atm, the CO_2 production is dominated by the reaction $COS + O \rightarrow CO_2 + S$. At higher pressures the three-body recombination of CO and O must be considered. COS formation by the three-body recombination of CO and S is found to be negligible compared with the production by the reaction $CS_2 + O \rightarrow COS + S$. If we restrict our attention to low pressures, $p \tilde{<} .01$, the flame model can be simplified by eliminating reactions 5 and 6 found in Table III.B.1. Examining Figure II-B-19, it is apparent that reactions 8 and 9 are relatively unimportant and can be eliminated as well. When this is done, the computed temperatures and flow velocities change less than 3% from the values computed using the full 10 reaction model. Some of the

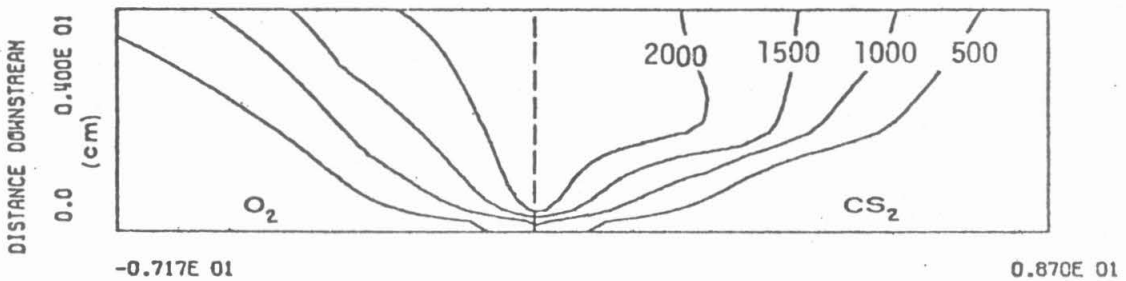

Figure III-B-20 Predicted temperatures in a CS_2/O_2 mixing layer flame without shear (U = 200 cm/sec) at 7.6 torr (°K)

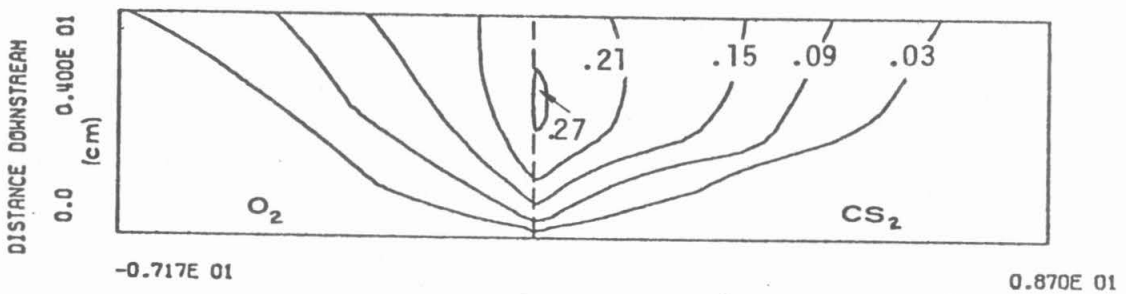

Figure III-B-21 Predicted CO mole fractions in a CS_2/O_2 mixing layer flame without shear (U = 200 cm/sec) at 7.6 torr

species mole fractions change by as much as 30%, while most remain within 10% of values predicted by the 10 reaction model. The qualitative form of the species profiles did not vary with the simplification of the model. The six reaction simplified model is

$$\left.\begin{aligned} CS_2 + O &\rightarrow CS + SO \\ CS + O &\rightarrow CO + S \\ S + O_2 &\rightarrow SO + O \\ SO + O_2 &\rightarrow SO_2 + O \end{aligned}\right\} \text{ CO production}$$

$$\left.\begin{aligned} CS_2 + O &\rightarrow COS + S \\ COS + O &\rightarrow CO_2 + S \end{aligned}\right\} \begin{matrix} CO_2 \text{ and COS} \\ \text{production} \end{matrix}$$

The reactions we are proposing for CO_2 production in the CS_2/O_2 mixing layer flame, $CS_2 + O \rightarrow COS + S$ followed by $COS + O \rightarrow CO_2 + S$, have been studied in relation to the CS_2/O_2 premixed gas flame [III.4 - III.7].

The four reaction mechanism for CS_2/O_2 combustion is a branching mechanism. Consider S, O, and SO to be chain carriers. In this case the reactions can be labeled as follows:

$$\begin{aligned} CO_2 + \underline{O} &\rightarrow CS + \underline{SO} && \text{propagating} \\ CS + \underline{O} &\rightarrow CO + \underline{S} && \text{propagating} \\ S + O_2 &\rightarrow \underline{SO} + \underline{O} && \text{branching} \\ \underline{SO} + O_2 &\rightarrow SO_2 + \underline{O} && \text{propagating} \end{aligned}$$

The underlined species are chain carriers. Including the two reactions,

$$\begin{aligned} CS_2 + \underline{O} &\rightarrow COS + \underline{S} && \text{propagating} \\ COS + \underline{O} &\rightarrow CO_2 + \underline{S} && \text{propagating} \end{aligned}$$

does not change the branching nature of the mechanism.

Hydrogen-halide chemical lasers have straight chain chemistry. This motivates us to question how the branching chain mechanism in the CS_2/O_2 mixing layer causes this flame to differ. Although in the laboratory it is impossible to switch the reaction mechanism from a branching to a straight chain, in the computer model we are not so constrained. In the computer model the branching step was altered to

$$S + O_2 \rightarrow SO^* + O$$

where SO* is a chemical species with all the properties of SO except that it does not react with O_2 as SO does: $SO + O_2 \rightarrow SO_2 + O$. Consequently, SO* is a product, not a chain carrier.

When the CS_2/O_2 mixing layer is modeled by this contrived straight chain chemistry, but the same upstream conditions, the reactions proceed with far less vigor than before. There is considerable mixing before the middle of the reaction zone nears the adiabatic flame temperature. Compared to the flame with the branching chain chemistry, the concentration of atomic oxygen is low relative to S and SO, due to the initial dominance of the reactions $O + CS_2 \rightarrow CS + SO$ and $O + CS \rightarrow CO + S$. Progressing downstream, the temperature rises, and the reaction rates increase driving the combustion rapidly in spite of the low concentration of intermediates.

Comparing the production of carbon monoxide for the straight chain and branching chain cases, shown in Figure III-B-18, we see that the branching chain mechanism is very important in determining the

chemical production in the mixing layer.

With a straight chain mechanism the progress of the chemical reactions is limited by the initial temperature and the initial concentration of chain carriers. The total number of chain carriers remains constant with flow. This is one reason most hydrogen-halide chemical lasers run lean; they require an abundance of the chain carriers, typically atomic fluorine. A system with a branching chain mechanism should be able to support efficient combustion with a less lean mixture, because the initial concentration of chain carrier is not limiting.

C. Chemical and Vibrational Processes

MIX60 is a computer code created by this author to predict the CO vibrational distributions as a function of downstream distance in a flow with production of vibrationally excited CO. The rate of CO production is calculated using a simple two-dimensional laminar mixing layer flame model. This code, therefore, can be used to predict crudely the CO vibrational distributions along the plane of the splitter plate as a function of the distance downstream.

The computer code GKAP [III.13] is a commercially available program. GKAP was used to perform a similar calculation to the one performed using MIX60. GKAP is used to solve the equations governing the flow in a one-dimensional stream tube with entrainment of reactants. The conditions in the stream tube are assumed to be homogeneous in the direction normal to the flow. The equations governing the CO vibrational kinetics are solved. One inadequacy of the code GKAP is that the reactant entrainment rates must be prespecified; growth rates based on the well known behavior of the laminar nonreacting mixing layer were used. Also, the methods by which the chemical reaction rates are handled in GKAP are complex, and leave obscure some of the basic aspects of the problem. In the code MIX60, the equations governing the chemistry and fluid mechanics are grossly simplified; however, the mixing is treated by a two-dimensional calculation. The code MIX60 is listed and briefly documented in Appendix C.

In solving for the vibrational distributions, the formulation of GKAP and MIX60 included the same vibrational kinetic processes. Reactions III.C.2 through III.C.5 were included.

$$CO(v) \rightarrow CO(v-1) + h\nu \qquad \text{(III.C.1)}$$

$$CO(v) + CO(v') \rightarrow CO(v+1) + CO(v'-1) \qquad \text{(III.C.2)}$$

$$CO(v) + M \rightarrow CO(v-1) + M + \text{kinetic energy} \qquad \text{(III.C.3)}$$

$$CO(v) + M(v') \rightarrow CO(v\pm1) + M(v'\mp1) \qquad \text{(III.C.4)}$$

$$CS + O \rightarrow CO(v) + S \qquad \text{(III.C.5)}$$

Multiquanta exchanges and stimulated emission processes were ignored. In MIX60 and GKAP reaction III.C.1 (radiative losses) was neglected because radiative losses were estimated to be minor with respect to the other loss processes. For simplicity, reactions III.C.3 and III.C.4 were combined to give

$$CO(v) + M \rightarrow CO(v-1) + M \qquad \text{(III.C.6)}$$

Still, a large number of processes were involved, and we chose to consider only a representative set of them, preserving the qualitative behavior of the system. In lieu of including all reactions of the form of reaction III.C.2, we included only the reactions:

$$CO(v) + CO(v) \rightleftarrows CO(v+1) + CO(v-1) \qquad \text{(III.C.7)}$$

The forward rates were adjusted from the literature values, [III.14] so as to compensate for the neglected reactions.

Rates for reaction 6 are found in Reference III.15. The reverse rates for reactions 6 and 7 are computed from forward rates on the basis of detailed balancing. Considering only these processes, the pumping and loss mechanisms affecting each vibrational level are shown in Figure III-C-1. With at least 20 vibrational levels involved, the calculation remains nontrivial.

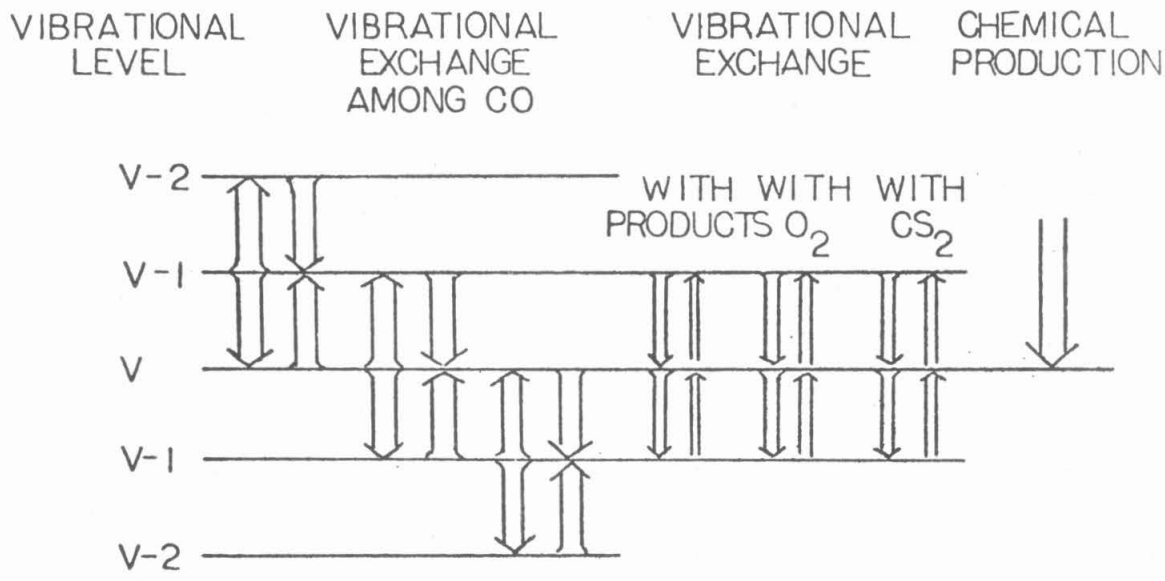

Figure II-C-1 Processes affecting the vibrational population of CO in level v considered in the computer code MIX60

Typical vibrational profiles predicted by using the code MIX60 are shown in Figure III-C-2. The upstream flow velocities are U_{CS_2} = 100 cm/sec and V_{O_2} = 300 cm/sec. The pressure is .01 atm (7.6 torr), the deactivation rates were chosen assuming that COS is present in a fixed mole fraction of .045, and that COS is the dominant partner in collisional deactivation with a nonreactant species. The CO vibrational populations are pumped by chemical production in the upper levels and equilibrated by collisional processes. Farther downstream the predicted CO vibrational distributions become successively more relaxed. These results are in agreement with experiment in that no inversion is predicted. However, there is evidence presented in Chapter II that the CO vibrational distributions relax more rapidly than is predicted by this calculation. MIX60 overestimates the equilibration time for the CO, possibly because the COS concentration chosen in order to calculate the deactivation rates is too low.

The vibrational distributions predicted using the computer code GKAP are shown in Figure III-C-3. The flow velocity is about 300 cm/sec The abscissa is time in the flow; 0.1 sec corresponds to about 30 cm downstream. The vibrational distribution equilibrates downstream, but not as rapidly as was found experimentally. The deactivation rates are not sufficient to duplicate experimental results. However, quenching by COS is not included in the GKAP calculations.

The code, GKAP, has a number of complex as well as unsatisfying features. The predicted species concentrations are at odds with the results found using the code MIXWG, and the calculated equilibrium composition. The predicted vibrational distributions remain strongly

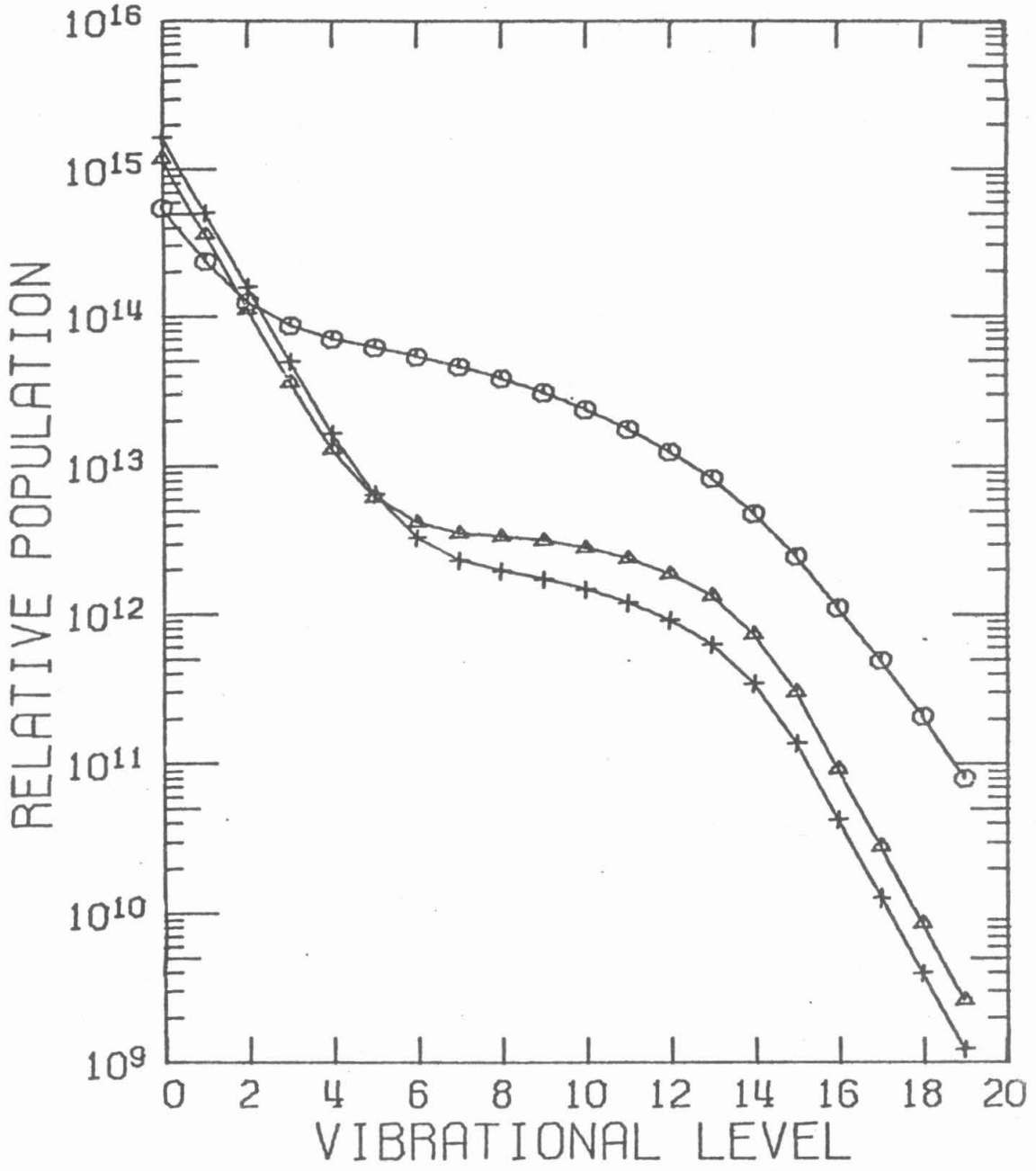

Figure III-C-2 Predictions by the computer code MIX60 of the concentrations of CO (cm^{-3}) in vibrational levels v = 0 through v = 19 at locations (o) .4, (Δ) 1.0, and (+) 3.8 cm downstream of the start of the mixing layer

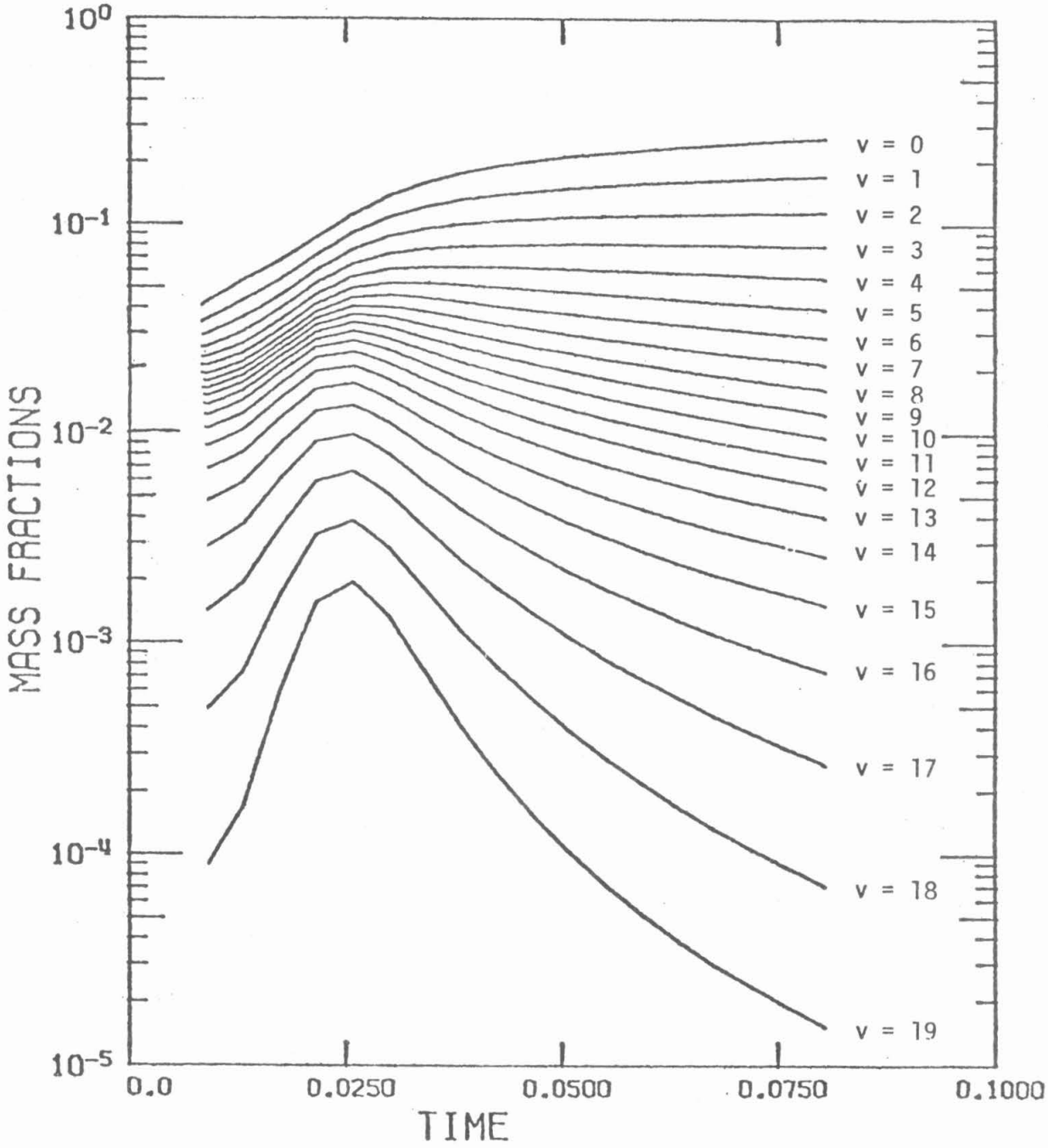

Figure III-C-3 Populations of CO in vibrational levels 0-19 as predicted using the code GKAP for a CS_2/O_2 flame with entrainment; p = 7.6 torr; u ≈ 300 cm/sec.

nonequilibrium farther downstream than was experimentally observed. For each reaction, the rate for the reverse reaction is automatically computed in the code GKAP. Consequently, the reaction producing vibrationally excited CO, CS+O → CO(v) + S is driven backwards in most of the regions of flow, for vibrational levels for which the forward reaction is only marginally exothermic, $v \gtrsim 15$. This is the most novel and interesting result of these calculations. In the presence of sulfur atoms, the reaction

$$CO(v) + S \rightarrow CS + O$$

is predicted to offer a sink for highly vibrationally excited CO.

We have no experimental evidence which supports this mechanism, and only mention it as a possibly important process which we have not seen discussed elsewhere. In a fuel lean CS_2/O_2 flame, the equilibrium products are lacking in unoxidized species. There is a scarcity of atomic sulfur, and the reaction CO(v) + S → CS + O is improbable. The role of this reaction in mixing layer flames and near stoichiometric or rich premixed flames may be more important and warrant further study.

Chapter III References

III.1 J. Janin, F. Roux, and J. d'Incan, "Etude thermodynamique de la flamme oxyacétlénique á partir du spectre de vibration-rotation de OH," Spectrochemica Acta 23A, 2939-2950 (1967).

III.2 A. A. Vetter, Ph.D. thesis: "Kinetics and Structure of the CS_2/O_2 Flame Laser," California Institute of Technology (1975).

III.3 G. Hancock, G. A. Ridley, and I.W.M. Smith, "Infrared Chemiluminescence from Vibrationally Excited CO, Part 2 --Product Distribution from the Reaction O + CS → CO + S," Journal of the Chemical Society, Faraday Transactions II 68, 2117-2126 (1972).

III.4 I. Glassman, Combustion (Academic Press, New York, 1977).

III.5 W. Q. Jeffers and C. E. Wiswall, "A Transverse Flow CO Chemical Laser," Applied Physics Letters 17, 67-69 (1970).

III.6 D. W. Howgate and T. A. Barr, Jr., "Dynamics of a CS_2-O_2 Flame," Journal of Chemical Physics 59, 2815-2829 (1973).

III.7 V. N. Kondrat'ev, "The Mechanism of Carbon Disulfide Oxidation," Kinetics and Catalysis 13, 1223-1229 (1972).

III.8 I. R. Slagle, J. R. Gilbert, and D. Gutman, "Kinetics of the Reaction between Oxygen Atoms and Carbon Disulfide," Journal of Chemical Physics 61, 704-709 (1974).

III.9 Von K. H. Howmann, G. Krowe, and H. G. Wagner, "Schwefelfuhlen-Stoff Oxidation, Geschwindigket von Elementarreakionen," Berichte der Bunsengesellschaft für Physik Alische Chemie 72, 998-1004 (1968).

III.10 K.G.P. Sulzmann, B. F. Myers, and E. R. Bartle, "CO Oxidation. I. Induction Period Preceding CO_2 Formation in Shock Heated CO-O_2-Ar Mixtures," Journal of Chemical Physics 42, 3969-3979 (1965).

III.11 JANAF Thermochemical Tables, Second Edition, NSRDS-NBS37 (1971).

III.12 H. Okabe, "Photodissociation of CS_2 in the Vacuum Ultraviolet; Determination of D_0^o(SC-S)," Journal of Chemical Physics 56, 4381-4384 (1972).

III.13 G. R. Nickerson, H. M. Frey, and D. E. Coats, "GKAP, Generalized Kinetics Analysis Program," (The Users Manual) A Computer Code Written at Dynamic Science Corp., Irvine, CA (1971).

III.14 N. A. Nielson, Jr., Ph.D. thesis: "An Electrically Discharged Carbon Disulphide-Oxygen Chemical Laser," Cornell University (1975).

III.15 G. Hancock and I.W.M. Smith, "Quenching of Infrared Chemiluminescence. 1: The Rates of De-Excitation of CO ($4 \leq v \leq 13$) by He, CO, NO, N_2, O_2, OCS, N_2O, and CO_2," Applied Optics 10, 1827-1843 (1971).

Chapter IV

CONCLUSIONS

A. Conclusions Based on the Experimental and Analytical Studies

CS_2/O_2 laminar mixing layer flames were investigated experimentally and theoretically. The temperatures and CO vibrational populations in the CS_2/O_2 mixing layer flames were measured. Computer modeling was used to investigate in detail the behavior of this mixing layer flame. The fluid, chemical, and vibrational kinetic processes in the flame were considered in constructing the computer model. Some of our experimental effort focused on investigating the presence of species other than CO, such as COS and CO_2, because of their importance to the chemistry and vibrational kinetics of this flame.

Measurements were made on CS_2/O_2 laminar mixing layer flames over the pressure range 2.5 torr to 25 torr, and with flow speeds .5 to 5.0 m/sec. The CO vibrational populations were determined from measurements of the CO vibrational overtone spectra. At the upstream edge of the mixing layer flame, the CO was found in nonequilibrium distributions, but not in vibrationally inverted populations. A few centimeters downstream, the CO vibrational distributions were relaxed to near equilibrium, and there was no evidence of production of vibrationally excited CO.

In Figures IV-A-1 and IV-A-2 we see CO concentration and temperature profiles, both as measured experimentally and as predicted using computer modeling, with corresponding conditions. The computer modeling calculation reproduces the qualitative aspects of the experimental results. The maximum predicted concentrations of S, O, SO, CO, CO_2, and SO_2 are within a factor of two of the equilibrium concentrations produced using a

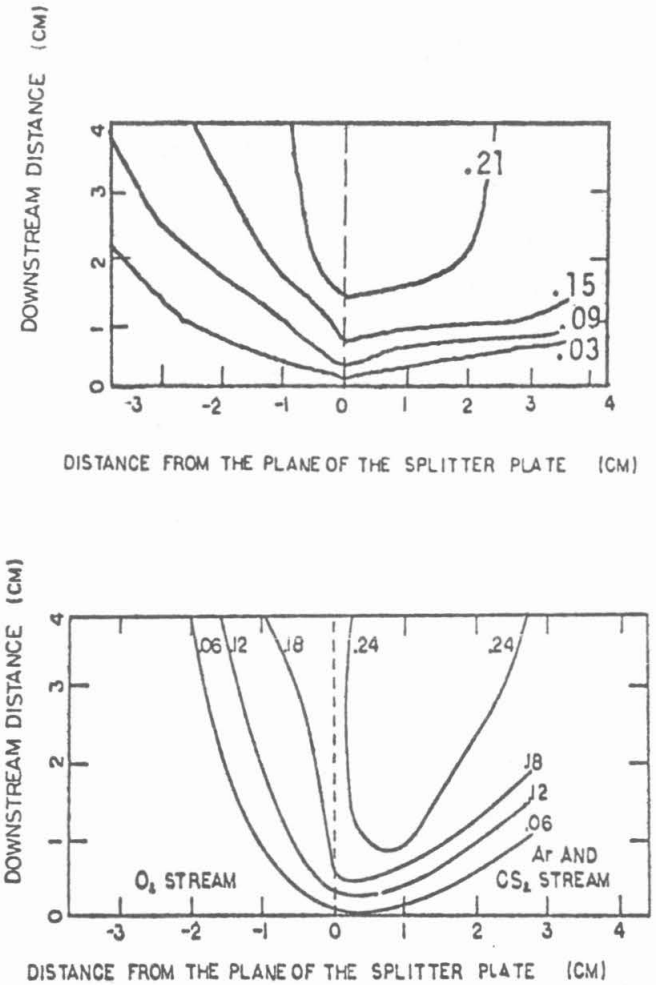

Figure IV-A-1 Predicted (top) and measured (bottom) concentrations of CO in a CS_2/O_2 mixing layer flame at 5 torr

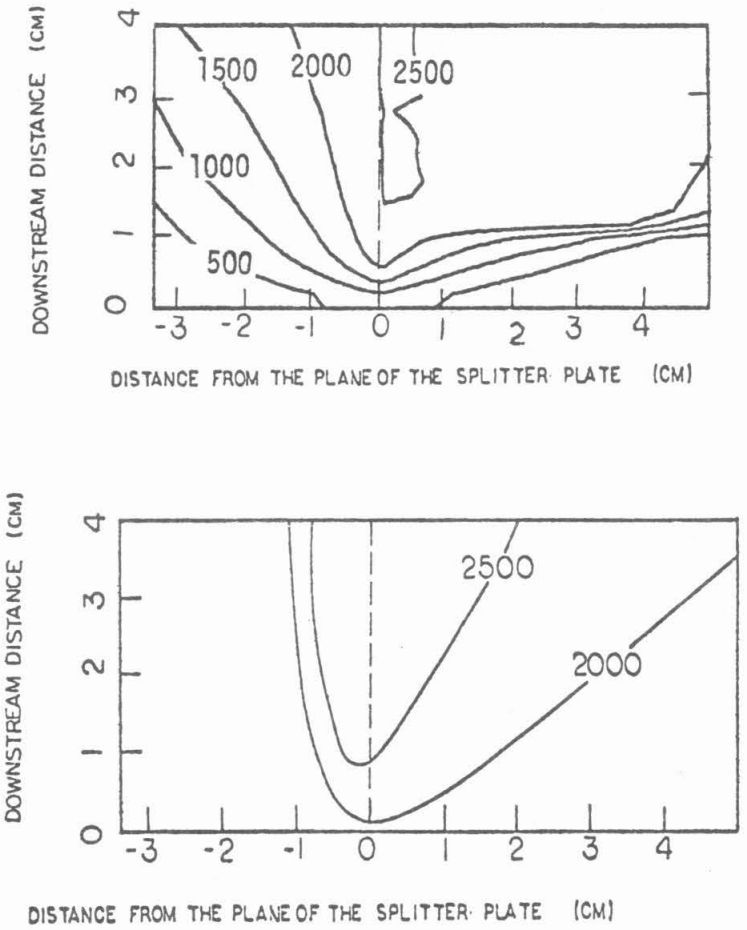

Figure IV-A-2 Predicted (top) and measured (bottom) temperatures in a CS_2/O_2 mixing layer flame at 7.6 torr

stoichiometric ratio of CS_2 and O_2 ($CS:O_2$ 1:3). The equilibrium concentration can be found in reference IV.1. COS and CS are reaction intermediates and have predicted concentrations that exceed the equilibrium values.

Both in experiments and in the predictions by computer modeling, the flames were often skewed into the CS_2 stream, generally with increasing angle as the velocity of the O_2 stream increased relative to the velocity of the CS_2 stream. The computer predictions indicate that the reaction intermediates are stratified in the mixing layer, a feature unparalleled in the premixed flame. CS is localized toward the CS_2 stream, and O is localized toward the O_2 stream. Nested more symmetrically between the two streams are the other intermediates and products. It is therefore not surprising that the visible emission from the mixing layer flame was found to vary across the mixing layer, as discussed in Chapter II, Section B.

A strong emission band starting at 2.65 μm and extending past 3.0 μm was observed when surveying CS_2/O_2 mixing layer flames a few centimeters downstream of the leading region of the flame (the flame attaches to the splitter plate for $p \gtrsim 4$ torr). The source of this band was identified to be CO_2. A weaker COS overtone band was also observed. On the basis of the spectral observations, the CO_2 concentrations in the flame were calculated to be about one-half the CO concentrations. The CO_2 emission observed from the CS_2/O_2 mixing layer flames was about five-fold more intense than was observed from premixed CS_2/O_2 flames at similar pressures and flow velocities, indicating higher CO_2 concentrations.

Our computer model predicts the appearance of COS followed by the production of CO_2 further downstream, in agreement with the experimental observations. The CO_2 mole fractions reach only about .05 in the first

4 cm of a typical flame, or about 20% of the maximum CO mole fraction there, which is about .25. This is in quantitative disagreement with the experimental result; the CO_2 mole fraction grows to 50% of the CO mole fraction. A discrepancy of this magnitude is not surprising because so many of the reaction rates are poorly known at the temperatures found in the CS_2/O_2 flames.

The computer model predicts that the CO production is a maximum within about 1 cm of the upstream edge of the mixing layer. The production is limited by the rate at which the chemical processes proceed, as in a premixed flame, and additionally limited by the rate of diffusive mixing. The mixing is most vigorous upstream in the mixing layer because of the steep gradients in the concentrations of reactants there. Downstream, the gas in the mixing layer is at an elevated temperature and there is an abundance of chemically reactive species. These conditions favor rapid consumption of the reactants. Upstream the production of CO is limited by the rates of the chemical process, and downstream by the rate of mixing.

By use of the computer models, the reaction scheme for the CS_2/O_2 mixing layer flame was investigated. The chemical mechanism producing CO is the same as in the premixed CS_2/O_2 flame:

$$CS_2 + O \rightarrow CS + SO \qquad \text{(IV.A.1)}$$

$$CS + O \rightarrow CO + S \qquad \text{(IV.A.2)}$$

$$S + O_2 \rightarrow SO + O \qquad \text{(IV.A.3)}$$

$$2(SO + O_2 \rightarrow SO_2 + O) \qquad \text{(IV.A.4)}$$

This is a branching chain mechanism. If we regard S, O, and SO as chain

carriers, the branching step is $S + O_2 \rightarrow SO + O$.

The production of CO_2 and COS at low pressures, $p \lesssim .01$ atm, was calculated to be dominated by the reactions:

$$CS_2 + O \rightarrow COS + S \qquad \text{(IV.A.5)}$$

$$COS + O \rightarrow CO_2 + S \qquad \text{(IV.A.6)}$$

The production of COS and the oxidation of COS to CO_2 affects the efficiency with which this flame can supply vibrationally excited CO to a chemical laser, because COS is a powerful deactivating agent of vibrationally excited CO. The addition of reactions IV.A.5 and IV.A.6 to the four reaction mechanism of CS_2 combustion leaves the resultant six reaction sequence still a branching chain mechanism. The two additional reactions are both chain propagating.

Because the combustion of CS_2 proceeds by a branching chain mechanism, there is a large production of chain carriers (S, O, and SO); with identical upstream conditions, the combustion was calculated to be severely limited by the chemical reaction rates, not the rate of mixing, when the chemical mechanism was, instead, modeled by a contrived straight chain. However, because the combustion actually proceeds by a branching mechanism, a low upstream concentration of intermediates does not severely limit the rate of combustion. Hydrogen-halide chemical lasers, in which combustion proceeds by a straight chain mechanism, must for this reason among others, have a large chain carrier concentration in the oxidant.

The high temperatures observed in the CS_2/O_2 mixing layer flames and the species profiles predicted by computer modeling indicate that the mixing layer flame burns near stoichiometric. The flame is hot, with maximum

temperatures in excess of 2500°K. High temperatures influence the suitability of the CS_2/O_2 mixing layer flame for use in a chemical laser in many ways, all of them bad.

At elevated temperatures, the reaction $CS_2+O \rightarrow COS+S$ competes more favorably with the reaction $CS_2+O \rightarrow CS+SO$. More COS is produced. COS is the most powerful deactivating agent among the molecules present in CS_2/O_2 flames. Along with increased production of COS, increasing the temperature directly affects the vibrational transfer rates. Off resonant exchange probabilities generally grow exponentially with temperature, resulting in increased deactivation by almost all the species present in the flame. Additives such as N_2O are beneficial to increasing laser power because they selectively deactivate the lower vibrational levels of CO by near resonant exchange, resulting in stronger inversions. With increasing temperature, the off-resonant exchange probabilities grow more rapidly than the near-resonant exchange probabilities, causing the vibrational exchange to lose its selectivity for the lower levels, and reducing the beneficial effect of the additive.

If the combustion product gas has positive gain on some vibrational-rotational transitions, increasing the temperature will tend to reduce the gain, as is discussed in Appendix B. Increasing the temperature causes a decrease in gain due to three effects: the density of the gas is reduced; the population in each vibrational-rotational static decreases because the rotational distribution broadens; and the lineshapes broaden and flatten.

To achieve combustion at reduced temperatures, supersonic expansion has been used in some hydrogen-halide chemical lasers. In chemical lasers

utilizing free burning flames, the mixture must be diluted in order to keep the temperatures down. This can be achieved either by the introduction of an inert diluent gas or by the addition of excess oxidant. The advantage of using an excess of oxidant is that the reaction rates remain larger than they would if the flame was diluted with an inert gas. This result was verified experimentally; see Chapter II, Section G.

It is important to keep the production rates for vibrationally excited CO high in comparison with the deactivation rates in order to produce an efficient chemical laser. For this reason, free burning CS_2/O_2 additive flames used in chemical lasers have always burned a fuel lean, excess oxidant, mixture. This is impossible in a mixing layer flame where the CS_2 can only be diluted with an inert gas.

Nitrous oxide was used as an additive in a number of CS_2/O_2 flames. The N_2O was found to participate in vibrational energy transfer with CO, increasing laser power, and straw-brown visible emission was seen from N_2O additive flames indicative of the NO+O recombination reaction. These well known results are presented in Chapter II, Sections B and E. Two unexpected effects of the additive N_2O were found: N_2O reduces the flame speeds when substituted for O_2 in fuel lean CS_2/O_2 flames; and N_2O addition results in an increase in production of CO_2, probably by the reaction $CO+N_2O \rightarrow CO_2+N_2$. These results are presented in Chapter II, Sections G and E. The N_2O is active chemically, as well as in vibrational exchange. It lowers the flame speeds; it does not speed the chemistry as has been conjectured [IV.2]. In addition to oxidizing CO, N_2O appears to have a reaction quenching effect, probably taking up free oxygen to form N_2+O_2 or 2NO. NO reacting with O will produce the observed straw-brown N_2O emission.

There are advantages to the mixing layer configuration that make it attractive. The CS_2/O_2 mixing layer flames were generally more stable than the corresponding premixed flames. They cannot flash back upstream as a premixed flame may, and they are not inclined to blow off. Moreover, the length of the flame can be increased with no noticeable scaling difficulties.

We had anticipated differences between the reaction mechanism in the premixed flames and the mixing layer flames. One possibility was that as the CS_2 diffused toward the oxidant, opposing outward diffusion of products, and heated, it might thermally dissociate: $CS_2 \rightarrow CS+S$. If this were to happen, the COS producing step $CS_2+O \rightarrow COS+S$ would be eliminated. The evidence of COS and CO_2 production suggests that this was not the case. Moreover, in the mixing layer flame, because of the high temperatures in the region where CS_2 is oxidized, the reaction producing COS, $CS_2+O \rightarrow COS+S$, competes more favorably with the more probable reaction channel, $CS_2+O \rightarrow CS+SO$, than in the premixed flame. In the mixing layer, the fuel and oxidant only meet and react after reaching nearly their adiabatic flame temperature. Consequently, conditions are perfect for maximal COS production. The COS production is followed by oxidation of COS to CO_2. In the premixed flame, the fuel and oxidant are in contact and react over the full range of temperatures from the upstream gas temperature to the flame temperature. Consequently, even in premixed flames burning CS_2 and O_2 at their stoichiometric ratio, the reaction channel producing COS and CO_2 will be less important than in mixing layer flames. Also, in a fuel lean premixed flame the flame temperatures will be reduced, suppressing the COS production.

The main reaction mechanism responsible for the production of CO was found to be the same in the mixing layer and premixed CS_2/O_2 flames. This is the 4 reaction branching chain mechanism that we have discussed. In the mixing layer flames, a secondary mechanism competing for the reactant CS_2 producing COS and CO_2 has greater importance than in the premixed flames. The sizeable concentrations of COS and CO_2 in the mixing layer flames in comparison with the premixed flames is evidence of this influence of the mixing process on the chemistry.

The CS_2/O_2 mixing layer flame was found to differ from the premixed CS_2/O_2 flame because the relative probability of the reaction channels $CS_2+O \rightarrow CS+SO$ and $CS_2+O \rightarrow COS+S$ varies with temperature. There is no corresponding situation in the hydrogen-halide chemical laser systems. The observation of CO_2 emission in the CS_2/O_2 mixing layer flames is important because it has led us to understand that there is considerable production of COS. The importance of COS is that it is a strong quenching agent for CO; again, this is unique to the CS_2/O_2 system.

Chapter IV References

IV.1 W. Grossman, A. A. Vetter, and F.E.C. Culick, "Some Results for the Combustion of CS_2/O_2 in a Laminar Mixing Layer," Proceedings of the Fourteenth JANNAF Conference (1977).

IV.2 M. J. Linevsky and R. A. Carabetta, "CW Laser Power from Carbon Bisulfide Flames," Applied Physics Letters 22, 288-291 (1972).

Appendix A

THE LAMINAR MIXING LAYER FLAME

Introduction

In this appendix, the laminar diffusion flame will be analyzed. The governing equations of the flame will be presented in the form that they were numerically solved (see Chapter III). An approximate formulation based on flame-sheet chemistry will be discussed. Flame-sheet chemistry is not expected to give a precise or complete description of CS_2/O_2 flames; rather, it is included in this appendix so that it may serve to illustrate some basic physical properties of the diffusion flame. A minor extension of previous flame-sheet analyses [A.1] is included, in which the diffusion constants for the product gases with the fuel (CS_2) and oxidant (O_2) are not assumed equal. In this situation, the bimolecular diffusion constants for the product gases changes discontinuously across the flame-sheet where the diffusion partners change abruptly from fuel to oxidant. This alters the species balance condition at the flame-sheet, tending to skew the flame-sheet into the stream of the reactant with lesser diffusivity. The results will be extended to predict the qualitative behavior of flames in which the free stream velocities of fuel and oxidant are unequal.

The Equations Governing a Laminar Mixing Layer Flame

Consider the mixing layer flame pictured in Figure A-1. Two uniform gas streams of infinite extent, one fuel and the other oxidant, flow separated by a splitter plate until the termination of the plate at $\tilde{z} = 0$. The gases react in a mixing layer of finite thickness downstream of the splitter plate. For simplicity, the wake of the splitter plate will be

ignored, and uniform velocity profiles will be assumed on either side of the plate for $\tilde{z} < 0$. For a discussion of reactive mixing in the wake of a plate, consult Reference A.2.

The main assumptions used in analyzing this flame are the following:

(i) The flow is steady, laminar, and two-dimensional.

(ii) The flow is at low Mach number; the pressure is constant, and the kinetic energy terms are negligible in the energy equation.

(iii) The boundary layer assumption is used; v and derivatives along the flow are taken to be small in comparison with u and derivatives perpendicular to the boundary layer.

(iv) The gas is perfect: $p = \rho RT$.

In addition, for convenience, we will make two assumptions regarding the properties of the gas:

(v) The gas is calorically perfect ($de = C_v dT$), with constant uniform heat capacity ($h = C_p T$).

(vi) The gas has constant uniform molecular weight.

The equations governing the flow are presented below; these equations are derived in a similar form in Reference A.3:

$$\frac{\partial \rho \tilde{u}}{\partial \tilde{z}} + \frac{\partial \rho \tilde{v}}{\partial \tilde{y}} = 0 \qquad \text{conservation of mass} \qquad (A.1)$$

$$\rho_i \tilde{u}_i \frac{\partial \tilde{u}}{\partial \tilde{z}} + \tilde{v} \frac{\partial \tilde{u}}{\partial \tilde{y}} = \frac{\partial}{\partial \tilde{y}} \left(\mu \frac{\partial \tilde{u}}{\partial \tilde{y}} \right) \qquad \text{momentum} \qquad (A.2)$$

$$\frac{\partial \rho_i \tilde{u}_i}{\partial \tilde{z}} + \frac{\partial \rho_i \tilde{v}_i}{\partial \tilde{y}} = W_i \qquad \text{species balance} \qquad (A.3)$$

$$\rho\tilde{u}\frac{\partial h}{\partial \tilde{z}} + v\frac{\partial h}{\partial \tilde{y}} = \frac{\partial}{\partial \tilde{y}}\left(\frac{K\partial T}{\partial \tilde{y}}\right) + \dot{Q} \qquad \text{energy balance} \qquad (A.4)$$

The meaning of the coordinates $\tilde{z}$ and $\tilde{y}$ can be gathered from Figure A-1; ρ_i and v_i are the density and velocity along y of species i, and W_i and $\dot{Q}$ are species and heat source terms, respectively; h is the enthalpy; μ is the viscosity, and K is the thermal conductivity. The nomenclature used here is explained in a section preceding Chapter I. In this Appendix only, the coordinates and velocities carrying the tilda, $\tilde{z}$, $\tilde{y}$, $\tilde{u}$, and $\tilde{v}$, are in the laboratory reference frame; z, y, u and v will later be introduced as the Howarth transformed coordinates and velocities. The subscripts ∞, $+\infty$ and $-\infty$ refer to initial free stream conditions at $y = \infty$, $+\infty$, or $-\infty$. The subscripts i and j are used in place of the formal chemical species names. The chemical species considered include CS_2, O_2, and reaction intermediates and products.

The initial upstream conditions and boundary conditions follow. We assume that for $\tilde{z} > 0$ all the thermodynamic and fluid mechanical variables are continuous, and

for $\tilde{z} > 0$ and $\tilde{y} \to -\infty$ or $\tilde{z} < 0$ and $\tilde{y} < 0$:	for $\tilde{z} > 0$ and $\tilde{y} \to +\infty$ or $\tilde{z} < 0$ and $\tilde{y} > 0$:
$\rho = \rho_{CS_2}$	$\rho = \rho_{O_2}$
$Y_{O_2} = 0$	$Y_{O_2} = \rho_{O_2}/\rho = 1$
$Y_{CS_2} = \rho_{CS_2}/\rho = 1$	$Y_{CS_2} = 0$
$\tilde{u} = u_{-\infty}$	$\tilde{u} = u_{+\infty}$
$T = T_\infty$	$T = T_\infty$

and $\tilde{v} = 0$ for $\tilde{z} < 0$

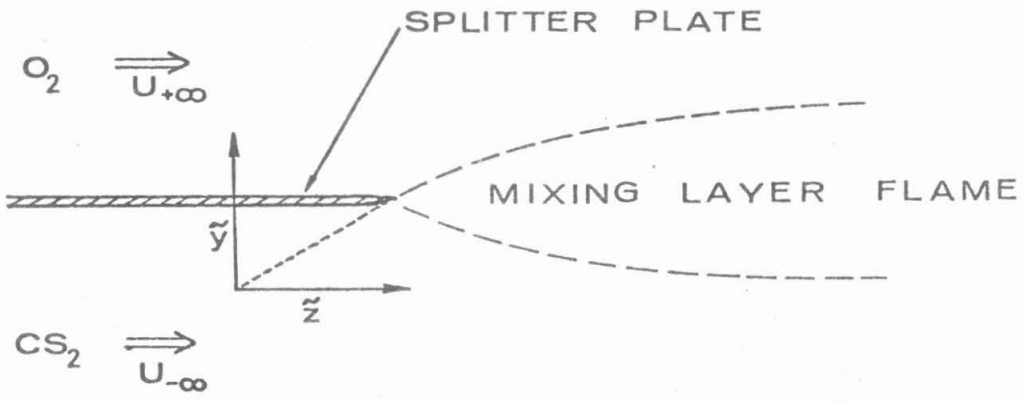

Figure A-1 A mixing layer flame burning downstream of a splitter plate

where Y_i is the mass fraction of species i .

The Diffusion Terms

The difference between the mean velocity of species i, v_i, and the mean gas veolcoty, v, along the y coordinate is the diffusion velocity of species i,

$$\tilde{v}_i = \tilde{v} + \tilde{v}_{iD} \tag{A.5}$$

where

$$\tilde{v} = \sum Y_i \tilde{v}_i$$

The diffusion velocity is

$$\tilde{v}_{iD} = - \frac{\mathcal{D}_i}{Y_i} \frac{\partial Y_i}{\partial \tilde{y}} \tag{A.6}$$

Equations A.5 and A.6 can be found in Reference A.3. Equation A.3 can be manipulated into a more illuminating form using equations A.5 and A.6:

$$\frac{\partial \rho_i \tilde{u}}{\partial \tilde{z}} + \frac{\partial \rho_i \tilde{v}}{\partial \tilde{y}} = \frac{\partial}{\partial \tilde{y}} \left(\frac{\rho_i \mathcal{D}_i}{Y_i} \frac{\partial Y_i}{\partial y} \right) + W_i$$

Substituting $\rho_i = \rho Y_i$ gives

$$\frac{\partial Y_i \rho \tilde{u}}{\partial \tilde{z}} + \frac{\partial Y_i \rho \tilde{v}}{\partial \tilde{y}} = \frac{\partial}{\partial \tilde{y}} \left(\rho_i \frac{\partial Y_i}{\partial \tilde{y}} \right) + W_i \tag{A.7}$$

Subtracting equation A.1 multiplied by Y_i from equation A.7 gives:

$$\rho \tilde{u} \frac{\partial Y_i}{\partial \tilde{z}} + \rho \tilde{v} \frac{\partial Y_i}{\partial \tilde{y}} = \frac{\partial}{\partial \tilde{y}} \left(\rho \mathcal{D}_i \frac{\partial Y_i}{\partial \tilde{y}} \right) + W_i \tag{A.8}$$

By using assumption (v), $h = C_p T$ we may write the energy equation as

$$\rho C_p \left(\tilde{u} \frac{\partial T}{\partial \tilde{z}} + \tilde{v} \frac{\partial T}{\partial \tilde{y}}\right) = \frac{\partial}{\partial \tilde{y}} \left(\frac{K \partial T}{\partial \tilde{y}}\right) + \dot{Q} \tag{A.9}$$

The set of equations governing the flow are rewritten together below. They follow from equations A.1, A.3, A.8 and A.9.

$$\frac{\partial \rho \tilde{u}}{\partial \tilde{z}} + \frac{\partial \rho \tilde{v}}{\partial \tilde{y}} = 0 \qquad \text{conservation of mass} \tag{A.10}$$

$$\rho \tilde{u} \frac{\partial \tilde{u}}{\partial \tilde{z}} + \rho \tilde{v} \frac{\partial \tilde{u}}{\partial \tilde{y}} = \frac{\partial}{\partial \tilde{y}} \left(\mu \frac{\partial \tilde{u}}{\partial \tilde{y}}\right) \qquad \text{conservation of momentum} \tag{A.11}$$

$$\tilde{u} \frac{\partial Y_i}{\partial \tilde{z}} + \tilde{v} \frac{\partial Y_i}{\partial \tilde{y}} = \frac{1}{\rho} \frac{\partial}{\partial \tilde{y}} \left(\rho \mathcal{D}_i \frac{\partial Y_i}{\partial \tilde{y}}\right) + \frac{W_i}{\rho} \qquad \text{species balance} \tag{A.12}$$

$$\tilde{u} \frac{\partial T}{\partial \tilde{z}} + \tilde{v} \frac{\partial T}{\partial \tilde{y}} = \frac{1}{\rho C_p} \frac{\partial}{\partial \tilde{y}} \left(\frac{K \partial T}{\partial \tilde{y}}\right) + \frac{\dot{Q}}{\rho C_p} \qquad \text{energy balance} \tag{A.13}$$

The Howarth Transformed Equations

Equations A.10 through A.13 are a coupled set because of the density, ρ. A Howarth transformation [A.4] removes this coupling. Use of the transform follows the discussion in References A.3 and A.5. The Howarth transformed coordinates are (z,y) where

$$dz = d\tilde{z} \qquad z = \tilde{z} \tag{A.14}$$

and

$$\rho_\infty \, dy = \rho d\tilde{y} \; ; \quad y = \int_0^{\tilde{y}} \frac{\rho(\tilde{z},\tilde{y}')}{\rho_\infty} d\tilde{y}' \; ; \quad \tilde{y} = \int_0^{y} \frac{\rho_\infty}{\rho(z,y')} dy' \tag{A.15}$$

The subscripts, ∞, refer to conditions at $y = \infty$. It can be shown [A.3, A.5] that the transformed velocities and equations governing the flame are:

$$u = \tilde{u} \tag{A.16}$$

$$v = \frac{\rho}{\rho_\infty}\tilde{v} + \tilde{u}\int_0^{\tilde{y}} \frac{\partial(\rho/\rho_\infty)}{\partial\tilde{z}}\, dy' \tag{A.17}$$

$$\frac{\partial u}{\partial z} + \frac{\partial v}{\partial y} = 0$$

$$\frac{u\partial u}{\partial z} + v\frac{\partial u}{\partial y} = \frac{1}{\rho_\infty}\frac{\partial}{\partial y}\left(\frac{\rho\mu}{\rho_\infty}\frac{\partial u}{\partial y}\right)$$

$$\frac{u\partial Y}{\partial z} + v\frac{\partial Y}{\partial y} = \frac{1}{\rho_\infty}\frac{\partial}{\partial y}\left(\frac{\rho^2\mathcal{D}_i}{\rho_\infty}\frac{\partial Y_i}{\partial y}\right) + \frac{W_i}{\rho}$$

$$\frac{u\partial T}{\partial z} + v\frac{\partial}{\partial y} = \frac{1}{\rho_\infty}\frac{\partial}{\partial y}\left(\frac{\rho}{\rho_\infty}\frac{K}{C_p}\frac{MT}{My}\right) + \frac{\dot{Q}}{\rho C_p}$$

A common assumption made for boundary layers in low Mach number flows is that μ varies inversely as T and ρ vary linearly with T, so that $\rho\mu$ is constant:

$$\rho\mu = \text{constant} = \rho_\infty \mu_\infty$$

The Prandtl (Pr) and Schmidt (Sc) numbers will be assumed constant as well:

$$Pr = \mu C_p/K = \text{constant}$$

$$Sc = \mu/\rho\mathcal{D} = \text{constant}$$

With the three assumptions above, the equations of the flame in the Howarth transformed space are:

$$\frac{\partial u}{\partial z} + \frac{\partial v}{\partial y} = 0 \qquad \text{continuity} \tag{A.18}$$

$$\frac{u\partial u}{\partial z} + \frac{v\partial u}{\partial y} = \nu_\infty \frac{\partial^2 u}{\partial y^2} \qquad \text{momentum conservation} \tag{A.19}$$

$$\frac{u\partial Y_i}{\partial z} + \frac{v\partial Y}{\partial y} = \mathcal{D}_\infty \frac{\partial^2 Y_i}{\partial y^2} + \frac{W_i}{\rho} \qquad \text{species balance} \qquad (A.20)$$

$$\frac{u\partial T}{\partial z} + \frac{v\partial T}{\partial y} = \frac{K_\infty}{\rho_\infty C_p} \frac{\partial^2 T}{\partial y^2} + \frac{\dot{Q}}{\rho C_p} \qquad \text{energy balance} \qquad (A.21)$$

In addition, using equations A.14 through A.17 we can transform the boundary conditions on the flow. Note that in the Howarth transformed space there is no longer a boundary condition on the density. We assume that for $z > 0$ all the thermodynamic and fluid mechanical variables are continuous, and

for $z > 0$ and $y \to -\infty$ or $z < 0$ and $y > 0$	for $z > 0$ and $y \to +\infty$ or $z < 0$ and $y > 0$
$Y_{O_2} = 0$	$Y_{O_2} = 1$
$Y_{CS_2} = 1$	$Y_{CS_2} = 0$
$U = U_{-\infty}$	$U = U_{+\infty}$
$T = T_\infty$	$T = T_\infty$

and

$$v = 0 \quad \text{for} \quad z < 0$$

A notable accomplishment of the Howarth transform is that the continuity and momentum equations are in the form of the equations governing an <u>incompressible</u> low Mach number viscous mixing layer. They can be solved apart from the species balance and energy balance equations. An approximate solution of equation A.19 for u was found assuming v to be small; for $z < 0$, $v = 0$. In the case of small shear,

$|(\nu_\infty/u^2)(\partial u/\partial y)| << 1$, the condition $|v/u| << 1$ is satisfied. Equations A.20 and A.21 were solved numerically in Chapter III assuming v to be negligibly small. Examining the results of the numerical calculation, we find v is only appreciable near z = 0. Neglecting v in equations A.20 and A.21 will cause the solutions to be transformed in y toward the stream of higher velocity, because convection in y is being neglected with respect to convection in z. The numerical solutions to equations A.19, A.20, and A.21 were found in Howarth transformed space. To compare these solutions with experimental flame measurements, the solutions were inverse transformed. This procedure was accomplished numerically using equations A.14 through A.17.

The Flame-Sheet Approximation

In the flame-sheet approximation, the chemical reactions in the flame proceed instantaneously upon the mixing of the reactants. Consequently, the chemical reactions occur only on a two-dimensional sheet (a sheet of zero thickness). The flame is limited in its consumption of reactants solely by the rate at which the reactants diffuse into the flame-sheet.

We will show that when u varies sufficiently slowly, the energy and species balance equations, A.20 and A.21, exhibit a similarity, only destroyed by the chemical source terms, W_i and $\dot{Q}$. In the flame-sheet approximation there are no sources off the flame sheet, and a similarity solution is permitted. This solution will be presented in the fashion of Reference A.1, and has been extended to include the effects of a discontinuity in the bimolecular diffusion constants at the flame sheet. In Reference A.1, the Schmidt number ($Sc = \mu/\rho\mathcal{D}$) and the quantity $\rho\mu$ were taken as constant.

This forced the bimolecular diffusion constant to be dependent on the temperature, but independent of the local gas composition. The bimolecular diffusion constants for the product gases may change discontinuously across flame sheet where the diffusion partners change abruptly from fuel oxidant:

$$\mathcal{D}_{P,Ox} \neq \mathcal{D}_{P,F}$$

$$Sc_{+} = \text{constant} \neq Sc_{-} = \text{constant}$$

The subscript + refers to the region above the flame (the oxidant stream), and - refers to the region below the flame (the fuel stream). For simplicity only three species will be considered; these are fuel (F), oxidant (Ox), and combustion product (P). All the combustion products will be lumped under the single label "product". The Lewis number ($Le = \rho\mathcal{D}C_p/K$) will be assumed to be one throughout, so that K, like $\mathcal{D}$, will be discontinuous at the flame sheet.

Let the location of the flame-sheet define the origin of the y axis, $y = 0$; then the equations governing the flame for $y \neq 0$ are

$$\frac{u\partial Y_i}{\partial z} + \frac{v\partial Y_i}{\partial y} = \mathcal{D}_{0\pm} \frac{\partial^2 Y_i}{\partial y^2} \tag{A.22}$$

and

$$\frac{u\partial T}{\partial z} + \frac{v\partial T}{\partial y} = \frac{K_{0\pm}}{\rho_o C_p} \frac{\partial^2 T}{\partial y^2} \tag{A.23}$$

Because the flame sheet defines the origin of the y axis, we cannot neglect the convective terms, $v\partial Y_i/\partial y$ and $v\partial T/\partial y$. The subscripts 0- and 0+ refer to the limits of the variables as y approaches zero, the flame-sheet, from below and above respectively. The 0+ value is to be used

when $y > 0$ and the 0- value when $y < 0$.

Matching Conditions at the Flame-Sheet

The boundary conditions presented in the previous section on T, u, Y_{O_2} and Y_{CS_2} still apply. At the flame-sheet the reactants diffuse toward each other, and are consumed in their stoichiometric ratio, f*. Both the fuel and oxidant concentrations must vanish at $y = 0$, because the fuel and oxidant are assumed to react instantly upon meeting, and the concentrations must be continuous. Assuming no net molar production, we have the condition

$$(\text{fuel}) + f^*(\text{oxidant}) \rightarrow (1+f^*)(\text{product})$$

The equations for the matching conditions at $y = 0$ follow.

$$Y_{Ox}(y = 0) = Y_F(y = 0) = 0$$

and

$$f^*\Gamma_{F(y=0^-)} = -\Gamma_{Ox(y=0^+)}$$

where Γ_i is the flux of species i, and

$$\Gamma_i = \rho_i v_i = \rho Y_i v_i$$

$$v_i = v + v_{iD}$$

consequently,

$$f^*(\rho Y_i(v + \frac{\mathcal{D}}{Y_F}\frac{\partial Y_F}{\partial y})_{y=0} = -(\rho Y_{Ox}(v + \frac{\mathcal{D}}{Y_{Ox}}\frac{\partial Y_{Ox}}{\partial y})_{y=0^+} \qquad (A.24)$$

In the limit as y goes to zero, Y_{Ox} and Y_F are zero; therefore, the convective terms vanish from equation A.24, leaving

$$f^* \mathcal{D}_{0-}\left(\frac{\partial Y_F}{\partial y}\right)_{0-} + \mathcal{D}_{0+}\left(\frac{\partial Y_{Ox}}{\partial y}\right)_{0+} = 0 \qquad \text{(A.25)}$$

The energy matching condition at the flame-sheet expressed in units of [energy/time] is

(heat produced at y = 0) = [(heat conducted away at y = 0)
+ (heat convected away at y = 0)]

and

$$\text{(heat produced at } y = 0 = -(q\Gamma_F)_{0-} = -q\rho\mathcal{D}_{0-}\left(\frac{\partial Y_F}{\partial y}\right)_{0-}$$

where q is the heating constant based on fuel mass for the stoichiometric fuel-oxidant reaction.

$$\text{(heat conducted away at } y = 0) = \left(\frac{K\partial T}{\partial y}\right)_{0-} - \left(\frac{K\partial T}{\partial y}\right)_{0+}$$

(heat convected away at y = 0)

$$= \lim_{\varepsilon \to 0} \left[(\rho C_p v T)_{y=\varepsilon} - (\rho C_p v T)_{y=-\varepsilon}\right] = 0$$

Convection will not remove a finite amount of heat from an infinitesimal volume because ρ, C_p, v, and T are continuous. Conduction will remove a finite amount of heat from an infinitesimal volume if the derivative of the temperature is discontinuous there, which will be the case. The energy matching condition is equation A.26:

$$\left(\frac{K\partial T}{\partial y}\right)_{0-} - \left(\frac{K\partial T}{\partial y}\right)_{0+} = -\rho q\left(\mathcal{D}\frac{\partial Y_F}{\partial y}\right)_{0-} \qquad \text{(A.26)}$$

The Similarity Transformed Equations

Consider the similarity transformation:

$$\chi = z$$

$$\eta = y/\sqrt{\mathcal{D}_{0\pm} z/u}$$

If u varies sufficiently slowly with both x and y, then

$$\frac{\partial}{\partial z} = \frac{\partial}{\partial \chi} - \frac{\eta}{2z}\frac{\partial}{\partial \eta}$$

$$\frac{\partial}{\partial y} = \frac{1}{\sqrt{\mathcal{D}_{0\pm} z/u}}\frac{\partial}{\partial \eta}$$

with the constraints on the variation in u being

$$\left|\frac{y}{u}\frac{\partial u}{\partial y}\right| << 1 \qquad \text{and} \qquad \left|\frac{z}{u}\frac{\partial u}{\partial z}\right| << 1$$

These inequalities hold under conditions of low shear: $\Delta u/u_{min} << 1$, where u_{min} is the minimum of $u_{+\infty}$ and $u_{-\infty}$, and $\Delta u = |u_{+\infty} - u_{-\infty}|$.

With the similarity transformation, the species and energy conservation equations become:

$$\frac{u\partial Y_i}{\partial \chi} + \left(\frac{-u\eta}{2\chi} + \frac{v}{\sqrt{\mathcal{D}_{0\pm}\chi u}}\right)\frac{\partial Y_i}{\partial \eta} = \frac{u}{\chi}\frac{\partial^2 Y_i}{\partial \eta^2} \tag{A.27}$$

and

$$\frac{u\partial T}{\partial \chi} + \left(\frac{-u\eta}{2\chi} + \frac{v}{\sqrt{\mathcal{D}_{0\pm}\chi u}}\right)\frac{\partial T}{\partial \eta} = \frac{u}{\chi}\frac{K_{0\pm}}{\mathcal{D}_{0\pm}\rho_o C_p}\frac{\partial^2 T}{\partial \eta^2} \tag{A.28}$$

For a similarity solution to exist ($Y_i = Y_i(\eta)$), $v/\sqrt{\mathcal{D}_{0\pm}\chi u}$ must have the same dependence on χ and $\mathcal{D}_{0^+}$ as the other coefficients of $(\partial Y_i/\partial \eta)$ and

$\partial^2 Y_i/\partial\eta^2$ in equation A.27. We require

$$Y_i = Y_i(\eta)$$

$$v/\sqrt{\mathcal{D}_{0^\pm} x/u} = \alpha_\pm u/x$$

and

$$v = \alpha_\pm \sqrt{\mathcal{D}_{0^\pm} u/x}$$

where α_+ and α_- are dimensionless constants to be determined from the matching conditions. Because v is continuous

$$\alpha_+ \sqrt{\mathcal{D}_{0+}} = \alpha_- \sqrt{\mathcal{D}_{0-}}$$

Equations A.27 and A.28 reduce to equations A.29 and A.30 under the similarity transformation

$$(\alpha_\pm - \eta/2) \frac{\partial Y_i}{\partial \eta} = \frac{\partial^2 Y_i}{\partial \eta^2} \qquad \text{(A.29)}$$

$$(\alpha_\pm - \eta/2) \frac{\partial T_i}{\partial \eta} = \frac{\partial^2 T}{\partial \eta^2} \qquad \text{(A.30)}$$

In passing from equation A.28 to equation A.30, we have used the assumption $Le = \rho \mathcal{D} C_p/K = 1$.

Solutions

The solutions to these equations satisfying the boundary conditions can be seen to be:

$$Y_{0x} = \begin{cases} \dfrac{\operatorname{erf}(\frac{\eta}{2} - \alpha_+) + \operatorname{erf}(\alpha_+)}{1 + \operatorname{erf}(\alpha_+)} & \eta \geq 0 \\ 0 & \eta \leq 0 \end{cases}$$

$$Y_F = \begin{cases} 0 & \eta \geq 0 \\ \dfrac{\operatorname{erf}(-\frac{\eta}{2} + \alpha_-) - \operatorname{erf}(\alpha_-)}{1 - \operatorname{erf}(\alpha_-)} & \eta \leq 0 \end{cases}$$

$$Y_P = 1 - Y_F - Y_{Ox}$$

The chemical production rate at the flame-sheet, W (moles/cm^2-sec) is proportional to the fuel consumption there. In the reaction scheme (fuel) + f*(oxidant) → (r+f*)(product), this constant of proportionality is (1+f*). The fuel is consumed at the flame sheet at the rate it arrives; therefore,

$$\text{Chemical production at the flame sheet} = W = (1+f^*)(-\Gamma_F)_{y=0-}$$

$$= (1+f^*)\rho_{o\ 0-}\left(\frac{-\partial Y_F}{\partial y}\right)_{y=0-}$$

$$= \frac{(1+f^*)\rho_{o}\mathcal{D}_{0-}}{(1 - \operatorname{erf}\alpha_-)}\left(\left(\frac{\partial(\frac{\eta}{2})}{\partial y}\right)\left(\frac{\partial \operatorname{erf}(\frac{\eta}{2} + \alpha_-)}{\partial(\eta/2)}\right)\right)_{\eta/2 = 0-}$$

$$= \frac{(1+f^*)}{2(1 - \operatorname{erf}\alpha_-)}\rho_o\sqrt{\mathcal{D}_{0-}(U/z)}$$

The chemical production varies inversely with the square root of z; consequently,it has an integrable singularity at z = 0. Because ρ_o is linear in pressure and $1/\mathcal{D}_0$ is approximately linear in pressure, W varies as the square root of the pressure.

Using the energy balance, equation A.30, and assuming Le = 1, the solution for the temperature field satisfying the boundary and matching

conditions at $y = -\infty, 0$, and ∞ can be shown to be:

$$T = (T_f - T_\infty)Y_p + T_\infty$$

where

$$T_f = \frac{q}{(1+f^*)C} + T_\infty$$

We see from the previous equation that T_f is the adiabatic flame temperature for the fuel and oxidant burning in their stoichiometric ratio.

By the species matching condition, equation A.25,

$$\frac{f^* \mathcal{D}_{0-}}{(1 + \mathrm{erf}(\alpha_-))} = \frac{\mathcal{D}_{0+}}{(1 - \mathrm{erf}(\alpha_+))} \tag{A.31}$$

Recall that

$$\alpha_- \mathcal{D}_{0-} = \alpha_+ \mathcal{D}_{0+} \tag{A.32}$$

so α_- and α_+ must have the same sign. We can define

$$\alpha \equiv \alpha_- \mathcal{D}_{0-} = \alpha_+ \mathcal{D}_{0+}$$

The sign of α_+ determines the sense of the mean velocity along the y axis. Equation A.17 will transform this velocity into the velocity in the laboratory frame. In the laboratory frame, this fluid velocity normal to the flame-sheet will be called V(z):

$$V(z) = \alpha\sqrt{\mathcal{D}_0 u/z}$$

V(z) is defined in the coordinate system in which the flame-sheet is at $y = 0$. In a laboratory reference frame, the velocity v can be fixed by walls to be near zero, but there is a mean velocity, V(z), normal to the

flame sheet. V(z) can be interpreted as the negative of the downstream velocity, u, multiplied by the slope along the flame sheet. This slope corresponds to dh(z)/dz, where h(z) is identified in Figure A-2. On the basis of this argument and equations A.31 and A.32, the followirg conclusions were found:

If (i) The fuel is used in excess: $f^* < 1$ and $\mathcal{D}_{0+} = \mathcal{D}_{0-}$,

or

(ii) $f^* = 1$ and the products diffuse more readily into the oxidant: $\mathcal{D}_{0+} > \mathcal{D}_{0-}$,

then $\alpha < 0$, $V(z) < 0$, and the flame skews down into the fuel.

If (i) The oxidant is used in excess: $f^* < 1$ and $\mathcal{D}_{0+} = \mathcal{D}_{0-}$,

or

(ii) $f^* = 1$ and the products diffuse more readily into the fuel: $\mathcal{D}_{0+} < \mathcal{D}_{0-}$,

then $\alpha > 0$, $V(z)$, and the flame skews up into the oxidant.

Skewing of the Flame

The flame is driven to skew into the stream of the reactant which is consumed by the flame in a larger proportion, and into the stream with the smaller bimolecular diffusion constant. The quantitative statements of these trends are given by equations A.31 and A.32. In CS_2/O_2 premixed flames the stoichiometric ratio, f*, is about 2.5 [A.6]. The bimolecular diffusion constants for the reactant-product pairs $CO-O_2$, $CO-CS_2$, SO_2-O_2, and SO_2-CS_2 obtained using the tables for prediction of transport properties in Reference A.7 are

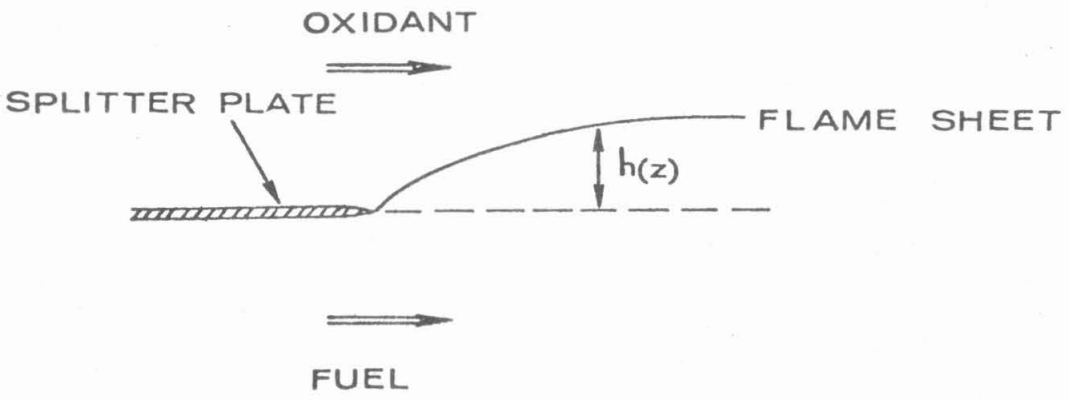

Figure A-2 A flame-sheet burning downstream of a splitter plate

$$\mathcal{D}_{O_2,CO} / \mathcal{D}_{CS_2,CO} = 1.9$$

$$\mathcal{D}_{O_2,SO_2} / \mathcal{D}_{CS_2,SO_2} = 2.0$$

We know

$$f^* \simeq 2.5$$

The ratio of the bimolecular diffusion constants for O_2-product pairs to the bimolecular diffusion constants for CS_2-product pairs, $\mathcal{D}_{O-} / \mathcal{D}_{O+}$, is about

$$\mathcal{D}_{O-} / \mathcal{D}_{O+} \simeq 1/2$$

Consequently

$$f^* \mathcal{D}_{O-} / \mathcal{D}_{O+} \simeq 1.25 > 1$$

If $f^* \mathcal{D}_{O-} / \mathcal{D}_{O+} > 1$, then using equations A.31 and A.32 we find that α_+ and α_- are positive; the flame skews up into the oxidant. This result follows using the flame-sheet approximation when the fuel and oxidant free stream velocities are equal. The stoichiometric ratio is large: $f^* > 2$. This predicted skewing is not observed; rather, the flames normally skew into the CS_2 stream. This may be due to the differing stream velocities often present in our experiments, or to the mixing layer flames having a smaller actual stoichiometric ratio than the value of 2.5, which is based on the 4-reaction branching chain mechanism for CS_2/O_2 combustion.

The flame-sheet solution presented in this appendix follows Reference A.1, and was modified to include the effects of unequal diffusion constants on the two sides of the flame sheet. To arrive at the similarity

solution, u was assumed to vary slowly with z and y; it was essentially taken to be constant; consequently the solution for v does not include the effects of a velocity gradient. A simple qualitative argument will be made to show that the flame will tend to skew into the stream with lower velocity in the absence of other effects ($\mathcal{D}_{0^+} = \mathcal{D}_{0^-}$ and f*= 1).

Consider a flow with a step in velocity at $\tilde{y} = 0$, $u = U_{+\infty}$ for $\tilde{y} > 0$ and $u = U_{-\infty}$ for $\tilde{y} < 0$. Suppose we observe two fluid elements, one above $\tilde{y} = 0$, one below, both at $z = \tilde{z}_1$ at time = 0. At time = Δt, we will see them displaced as shown in Figure A-3. At the flame-sheet, an equal quantity of reactants 1 and 2 must be consumed per unit length because f* = 1. However, because the lower stream moves more rapidly, fluid element 2 spends a time of only $(\ell_1/\ell_2)\Delta t$ in passing from $\tilde{z}_1$ to $\tilde{z}_1+\ell$, while fluid element 1 spends a time of Δt. Consequently, the fluid element in stream 1 (as shown in Figure A-3) will be depleted of reactant molecules as it flows downstream at a rate that is larger by a factor of $U_{-\infty}/U_{\infty}$ than the depletion rate for the fluid element in stream 2. For predicting the skewing of the flame, this has the same effect as changing the stoichiometric ratio by the ratio of the velocities, and the flame will have the tendency to skew into the slower stream. This result, expressed in equation A.33, is a simple extension of equation A.31,

$$\frac{f^*(U_{-\infty}/U_{+\infty})}{1+\mathrm{erf}(\alpha_-)}\ \mathcal{D}_{0^-} = \frac{0^+}{(1+\mathrm{erf}(\alpha_+))} \qquad (A.33)$$

The flame is not skewed (v=0) when $f^*U_{-\infty}\ \mathcal{D}_{0^-}/U_{+\infty}\ \mathcal{D}_{0^+} = 1$. We should bear in mind that this result is approximate, and was derived using a step function velocity profile (viscosity ignored); consequently, it should be

regarded only as qualitative.

The solution to the flame-sheet problem presented here follows as in Reference A.1, but it has been extended to include some of the effects of having a discontinuity in $\mathcal{D}$ or in velocity at the flame-sheet. The flame tends to skew into the gas stream with (i) a lower bimolecular diffusion constant, or (ii) a lower velocity, or (iii) the gas that is consumed in greater proportion by the chemical reaction.

Comments on the Applicability of the Flame-Sheet Approximations

For the flame-sheet approximation to be valid, the width of the zone in which chemical reactions occur must be substantially smaller than the downstream distance. This is not the case very near to the splitter plate. However, the results of the analysis using the mixing layer approximation provide simple scaling laws which are a general basis for predicting the behavior of mixing layer flames sufficiently far downstream. The behavior of a laminar mixing layer flame with viscous shear may even depart qualitatively from the behavior predicted using the flame-sheet analysis, because the flame-sheet analysis did not include the details of the growth of a viscous shear layer.

The zone of bright visible emission in the CS_2/O_2 laminar mixing layer flames is a region in which chemical reactions occur. It is not a flame-sheet of zero thickness; however, under many experimental conditions the zone of visible emission was suggestively narrow compared with the distance downstream over a large portion of the flame. We were motivated to seek an explanation for some of the behavior of the flame within the scope of flame-sheet theory. In particular, we use the

results of the flame-sheet theory in discussing the skewing of the CS_2/O_2 flame in Chapters II and III.

Appendix A References

A.1 F. E. Marble, from unpublished class lectures on the laminar diffusion flame, California Institute of Technology, Pasadena, California (1975).

A.2 S. I. Cheng and A. A. Kovitz, "Mixing and Chemical Reaction in a Laminar Wake of a Flate Plate," Journal of Fluid Mechanics 4, 64-80 (1958).

A.3 F. A. Williams, Combustion Theory (Addison-Wesley, Reading, Mass. (1965).

A.4 P. L. Howarth, "Concerning the Effect of Compressibility on Laminar Boundary Layers and Their Separation," Proceedings of the Royal Society, London 194, Series A, 16-42 (1948).

A.5 F. E. Marble and T. C. Adamson, Jr., "Ignition and Combustion in a Laminar Mixing Zone," Jet Propulsion 24, 85-94 (1954).

A.6 A. A. Vetter, Ph.D. thesis, "Kinetics and Structure of the CS_2/O_2 Flame Laser," California Institute of Technology (1975).

A.7 R. B. Bird, W. E. Stewart, and E. N. Lightfoot, Transport Phenomena (John Wiley and Sons, New York, 1960).

Appendix B

THE OPTIMAL CS_2:O_2 RATIO FOR THE PERFORMANCE OF A CO CHEMICAL LASER

Introduction

In the reaction zone of the laminar two-dimensional CS_2/O_2 mixing layer, the ratio of the concentration of CS_2 to O_2 is locally determined by competing processes. Diffusion replenishes the reactants as the chemical reactions deplete them. As mentioned in Appendix A, the mixing layer flame will tend to consume its reactants in their stoichiometric ratio, and burn at the corresponding adiabatic flame temperature. In contrast, the CS_2:O_2 ratio in a premixed flame can be varied to optimize chemical laser performance.

In this appendix, the optimal CS_2:O_2 ratio for maximizing the gain in a CS_2/O_2 free burning flame is estimated to be about 1:80. This is fuel lean compared with the stoichiometric ratio which is about 1:2.5 [B.1]. The optumum ratio for maximum laser power, not gain, has been measured to be about 30:1 [B.2]. The mixing layer flame, burning at the stoichiometric ratio, is far too fuel rich for optimal chemical laser performance. The calculation presented in this appendix is intended to point out that fuel lean combustion is advantageous to laser performance, and to identify the physical processes which cause this to be so.

Analysis

In a premixed CS_2/O_2 flame, the ratio of the concentrations of CS_2 to O_2 may be chosen over a wide range of values by the experimenter. This ratio will be defined as r :

$$r \equiv X_{CS_2}/X_{O_2} \tag{B.1}$$

where X_{CS_2} and X_{O_2} are the mole fractions of CS_2 and O_2 in the reactant gas mixture. Varying r will cause the composition and temperature of the combustion products to vary, as well as affecting the detailed kinetics of the flame. One combustion product is vibrationally excited CO. The following calculation estimates the optimal value for r to achieve the maximum small signal gain on the vibrational-rotational transitions of CO. The combustion will be assumed to proceed in the manner outlined in Figure B-1. In this figure, the subscripts "I" and "∞" refer to the initial conditions and conditions subsequent to combustion, respectively. We will find the value of r which maximizes the small signal gain on the CO vibrational-rotational transition with the largest gain.

The combustion will be assumed fuel lean so that

$$X_{O_2} >> X_{CS_2} \tag{B.2}$$

or, equivalently,

$$1 >> r \qquad \text{and} \qquad r \simeq X_{CS_2} \tag{B.3}$$

because in the reactant gas

$$X_{CS_2} + X_{O_2} = 1 \tag{B.4}$$

Examining the full set of kinetic processes governing the CO vibrational-rotational populations in time and space for a CS_2/O_2 flame is an extensive problem, and will be drastically simplified by two

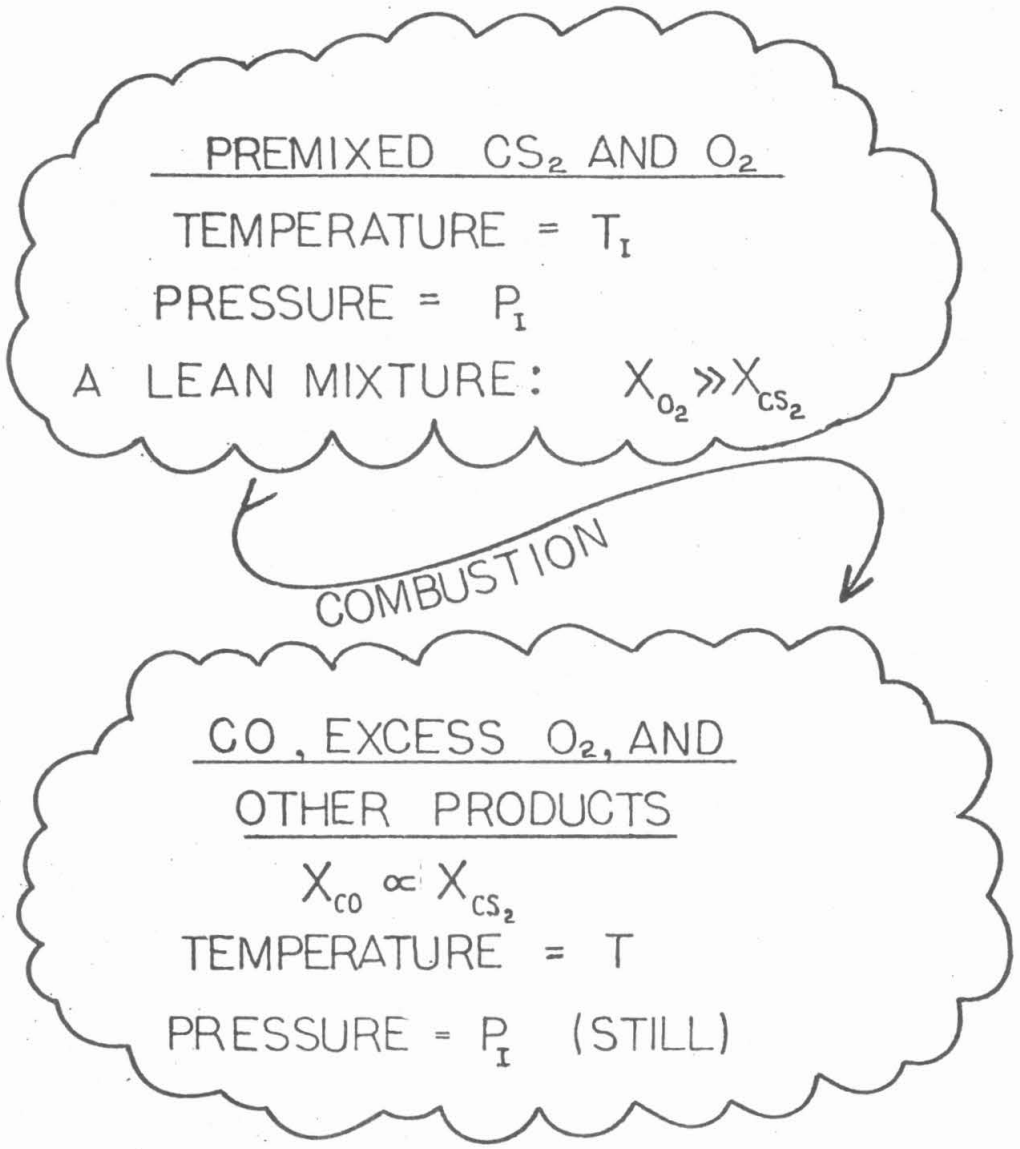

Figure B-1 A simple model of fuel lean combustion

assumptions. (i) The CO will be assumed to be in equilibrium at the kinetic temperature. This is an excellent assumption in free burning flames [B.3]. (ii) A total vibrational inversion will be assumed to exist in the flame with the maximum gain on the $v \rightarrow v\text{-}1$ transition. Moreover, in the flame, the mole fraction of CO in each vibrational level, X_v, will be assumed to vary linearly with r, and the ratio X_v/X_{v-1} will be assumed to be independent of r. These assumptions are expressed in equations B.5 and B.6:

$$X_v \propto X_{CO} \tag{B.5}$$

$$\partial(X_v/X_{v-1})/\partial r = 0 \tag{B.6}$$

These assumptions are discussed at the end of this appendix. There, it is shown that they are expected to apply when: (1) the pumping rate for each vibrational level (in mole fraction-sec^{-1}) due to chemical production is linear in r; and (2) the rate constants for the deactivation processes (in sec^{-1}) are all independent of r.

The mole fraction of CO in the combustion products, X_{CO}, is assumed proportional to the mole fraction of CS_2 in the reactant gas mixture, X_{CS_2},

$$X_{CO} \propto X_{CS_2} \tag{B.7}$$

We are assuming that all the fuel is consumed, and the reactions go to completion, because a fuel lean flame is being considered. Chemical consumption of CO is neglected for simplicity. The CO is assumed

to be produced in an inverted vibrational distribution $\{N_v\}_{v=0,1,2,\cdots}$ subject to assumptions i and ii. Because the flame is assumed lean, the change in gas composition and temperature during combustion is taken to be sufficiently small so that the heat capacity and reaction exothermicity do not vary. Consequently, the heat release (per mole of gas) and temperature rise in combustion is linear in X_{CS_2}, but by equation B.3, $X_{CS_2} \simeq r$, so that

$$(T - T_I) \simeq (T_F - T_I)r \tag{B.8}$$

where T and T_I are the temperatures in the flame and reactant gas, respectively, and T_F is a parameter. We can evaluate the constant of proportionality $(T_F - T_I)$ and the parameter, T_F, in particular, by

$$T_F = \left(\frac{\partial T}{\partial X_{CS_2}}\right) + T_I \tag{B.9}$$

The problem reduces to finding both the optimum value of r and the rotational transition on the v^{th} vibrational band that will yield the largest gain. The gain on a particular vibrational-rotational transition is [B.4]

$$\gamma(\nu) = \frac{(N_{v,J} - (g_{v,J}/g_{v-1,J'})N_{v-1,J'})\lambda^2 \, g(\nu)}{8\pi n^2 \, t_{spont}} \tag{B.10}$$

where $\gamma(\nu)$ is the gain at frequency ν for the vibrational-rotational transition $(v,J) \rightarrow (v-1,J')$; $\nu = c/\lambda$. N_{vJ} is the number density in the vibrational-rotational level (v,J), and $g_{v,J}$ is the degeneracy of that level. For carbon monoxide, $g_{v,J} = 2J+1$. The spontaneous emission

lifetime for the transition $(v,J) \rightarrow (v-1,J')$ is t_{spont}; $t_{spont} = A^{-1}_{(v,J) \rightarrow (v-1,J')}$. $A_{(v,J) \rightarrow (v-1,J')}$ is the Einstein A coefficient for the transition, and $g(\nu)$ is the lineshape. The real part of the index of refraction of the gas, n, can be taken to be one for the flames of interest.

Only P branch fundamental transitions will be considered, because in rotational equilibrium, for each upper laser level (v,J), the gain on the P branch transition, $(v,J) \rightarrow (v-1,J+1)$, is greater than the gain on the R branch transition, $(v,J) \rightarrow (v-1,J-1)$. Equation B.11 gives the dependence of the gain on T and J. Equation B.11 follows from equation B.10 by inserting the degeneracies and neglecting λ and n; λ and n vary negligibly with T and J:

$$\gamma(\nu) \propto N_{v,J} \left(1 - \frac{N_{v-1,J+1}}{N_{v,J}} \frac{(2J+3)}{(2J+1)}\right) g(\nu)/(8\pi t_{spont}) \quad (B.11)$$

Assuming rotational equilibrium, the rotational distribution is

$$N_{v,J}/N_v = (2J+1) \exp(-E_J/k_B T)/Q_r \quad (B.12)$$

where T is the gas temperature, k_B is Boltzmann's constant, and N_v is the number density in vibrational level v. If the temperature is high, $T >> hcB/k_B$, the partition function, Q_r, can be approximated [B.5]:

$$Q_r \simeq k_B T/hcB \quad (B.13)$$

where h is Planck's constant, c is the speed of light, and B is the rotational constant for CO, often written B_e. In the rigid rotar

approximation, the rotational energy of CO, E_J, is

$$E_J \simeq J(J+1)hcB/k_BT \tag{B.14}$$

The Einstein coefficients are independent of T and vary with J as [B.5]:

$$A_{(v,J) \rightarrow (v-1,J+1)} \propto 2(J+1)/2J+1) \tag{B.15}$$

Hence, using equations B.11 through B.15, we find

$$\gamma(\nu) \propto N_v \left(1 - \frac{(2J+3)N_{v-1}\exp(-J(J+1)hcB/k_BT)}{(2J+1)N_v \exp(-J(J-1)hcB/k_BT)} \right) \times \frac{(J+1)\exp(-J(J+1)hcB/k_BT)}{k_BT/hcB} g(\nu) \tag{B.16a}$$

implying

$$\gamma(\nu) \propto N_v \left(1 - \frac{(2J+3)N_{v-1}\exp(-2JhcB/k_BT)}{(2J+1)\ N_v} \right) \times \frac{(J+1)\exp(-J(J+1)hcB/k_BT)}{T} g(\nu) \tag{B.16b}$$

From equations B.3, B.5, and B.7, we find

$$X_v \propto r \tag{B.17}$$

Multiplying by the number density, N, implies

$$N_v \propto rN \tag{B.18}$$

If we assume the mixture behaves as a perfect gas at constant pressure, then

$$N_v \propto r/T \tag{B.19}$$

Using equations B.8 and B.19, we find

$$N_v \propto (T-T_I)/T \tag{B.20}$$

Consider the gain at linecenter, $\nu = \nu_o$, for a transition $v \rightarrow v-1$. In the Doppler broadened limit, $g(\nu_o)$ is independent of J and varies linearly with the square root of T:

$$g(\nu_o) \propto T^{-1/2} \tag{B.21}$$

The explicit dependence of γ on J and T follows from equations B.16, B.20, and B.21:

$$\gamma \propto \frac{(T-T_I)}{T^{5/2}} \left(1 - \frac{N_{v-1}(2J+3)}{N_v(2J+1)} \exp(-2JhcB/k_BT) \right) (J+1)\exp(-J(J+1)hcB/k_BT) \tag{B.22}$$

There is a maximum in gain with respect to both variables, T and J. If J is treated as a continuous variable, the gain is a maximum with respect to J when

$$\left(\frac{\partial \gamma}{\partial J}\right)_T = 0 \tag{B.23}$$

and the gain is a maximum with respect to T when

$$\left(\frac{\partial \gamma}{\partial T}\right)_J = 0 \tag{B.24}$$

Working from equations B.22 and B.23 to find the rotational transition with the maximum gain with respect to J yields

$$0 = (T-T_I)T^{-5/2}\left\{1 - \frac{N_{v-1}(2J+3)\exp(-2hcB/k_BT)}{N_v(2J+1)}\right\}(1 - (2J+1)(J+1)hcB/k_BT) \times \exp(-J(J+1)hcB/k_BT)$$

$$+ (T-T_I)T^{-5/2}\left(\frac{N_{v-1}}{N_v}\left(\frac{2}{2J+1} - \frac{2(2J+1)}{(2J+1)^2} - \frac{2hcB}{k_BT}\right)\exp(-2JhcB/k_BT\right) \times (J+1)\exp(-J(J+1)hcB/k_BT)$$

which can be rearranged to give

$$0 = \left\{1 - \frac{N_{v-1}(2J+3)}{N_v(2J+1)}\exp(-2JhcB/k_BT)\right\}(1 - (2J+1)(J+1)\ hcB/k_BT) + \frac{N_{v-1}}{N_v}\exp(-2JhcB/k_BT)\left(\frac{4}{(2J+1)^2} + \frac{2hcB}{k_BT}\right)(J+1) \qquad (B.25)$$

Instead of solving exactly for J, a good approximate solution, $J^{(0)}$, will be found by solving equation B.25, while neglecting the second term on the right hand side with respect to the first. Setting the first term to zero implies

$$0 = (1 - (2J^{(0)} + 1)(J^{(0)} + 1)\ hcB/k_BT)$$

or

$$0 = 2J^{(0)2} + 3J^{(0)} + (1 - k_BT/hcB)$$

This gives

$$J^{(0)} = \frac{-3 \pm \sqrt{9 + 8(k_B T/hcB - 1)}}{4}$$

We are interested only in the positive solution for $J^{(0)}$ so that

$$J^{(0)} \quad -3/4 + \sqrt{1/16 + k_B T/2hcB} \tag{B.26}$$

or

$$(J^{(0)} + 1)(J^{(0)} + 1/2) \simeq k_B T/2hcB$$

so that

$$J^{(0)}(J^{(0)} + 1) \simeq k_B T/2hcB \tag{B.27}$$

For carbon monoxide, B = 1.9 [B.5], so that

$$k_B/hcB = .36°K^{-1}$$

At temperatures above 300°K,

$$k_B T/hcB > 100 >> 1 \tag{B.28}$$

implying

$$J^{(0)} \gtrsim 10 >> 1 \tag{B.29}$$

We will refer to the difference between the exact solution to equation B.25 and $J^{(0)}$ as $J^{(1)}$. $J^{(1)}$ was approximated from equation B.25 by assuming $J^{(0)} >> 1$ and $k_B T/hcB >> 1$, the result being

$$J^{(1)} \simeq (N_v/N_{v-1} - 1)^{-1} \tag{B.30}$$

where

$$J = J^{(0)} + J^{(1)}$$

Combining equations B.29 and B.30

$$J^{(1)}/J^{(0)} \lesssim .025\ (N_v/N_{v-1} - 1)^{-1} \qquad (B.31)$$

we find that $J^{(1)}$ will be an important correction only when N_v/N_{v-1} differs just fractionally from 1. Consequently, we will assume N_v/N_{v-1} is large enough so that $1 >> J^{(1)}/J^{(0)}$. By examining equation B.31 we see that if $N_v/N_{v-1} \gtrsim 1.2$, then $J^{(0)}$ is a good approximate solution to equation B.25, and we will take this to be the case.

Working from equations B.22 and B.24 to find the temperature at which the maximum gain with respect to T occurs, yields the equation

$$0 = T^{-5/2}\ \{\ 1 - \frac{N_{v-1}(2J+3)}{N_v(2J+1)} \exp(-2JhcB/k_BT)\}\{(J+1)\exp(-J(J+1)hcB/k_BT)\}$$

$$- \frac{5}{2}\ (T-T_I)T^{-7/2}\ \{1 - \frac{N_{v-1}(2J+3)}{N_v\ (2J+1)} \exp(-2JhcB/k_BT)\}$$

$$\times\ \{(J+1)\exp(-J(J+1)hcB/k_BT)\}$$

$$+ (T-T_I)T^{-5/2}\ \frac{2hcB}{k_BT^2}\ \frac{(2J+3)}{(2J+1)} \exp(-2JhcB/k_BT)\{(J+1)\exp(-J(J+1)hcB/k_BT)\}$$

$$+ (T-T_I)T^{-5/2}\{1 - \frac{N_{v-1}(2J+3)}{N_v\ (2J+1)} \exp(-2JhcB/k_BT)\}$$

$$\times\ \{\frac{(J+1)J(J+1)hcB}{k_BT^2} \exp(-J(J+1)hcB/k_BT)\}$$

which can be rearranged to give

$$0 = \{1 - \frac{N_{v-1}(2J+3)}{N_v(2J+1)} \exp(-2JhcB/k_BT)\}\{1 - \frac{5}{2}\frac{(T-T_I)}{T} + \frac{(T-T_I)J(J+1)hcB}{k_BT^2}\}$$

$$+ \frac{(T-T_I)}{T}\frac{N_{v-1}(2J+3)}{N_v(2J+1)}\frac{2hcB}{k_BT}\exp(-2JhcB/k_BT) \qquad (B.32)$$

Instead of solving exactly for T, a very good approximate solution, $T^{(o)}$, will be found by solving equation B.32 while neglecting the second term on the right hand side with respect to the first. Setting the first term to zero implies

$$0 = \{1 - \frac{5}{2}\frac{(T^{(0)} - T_I)}{T^{(0)}} + \frac{(T^{(0)} - T_I)\,J(J+1)\,hcB}{k_BT^2}\} \qquad (B.33)$$

This gives

$$T^{(0)} = \frac{5}{6}T_I + \frac{J(J+1)hcB}{3k_B} \pm \frac{1}{3}\sqrt{((\frac{5}{2}T_I)^2 - \frac{T_IJ(J+1)hcB}{k_B} + (\frac{J(J+1)hcB}{k_B})^2}$$

We will refer to the difference between the exact solution to equation B.32 and $T^{(0)}$ as $T^{(1)}$. $T^{(1)}$ was approximated from equation B.32 by assuming (i) we are interested in values of J nearly satisfying equation B.26, and (ii) inequality B.29 holds so that $2JhcB/k_BT \simeq 1/J^{(0)} << 1$, the result being

$$T^{(1)} \simeq T^{(0)}/J^2$$

where

$$T = T^{(0)} + T^{(1)}$$

For the values of J in the range of interest, it follows that $T^{(1)} << T^{(0)}$, and $T^{(1)}$ is a negligible correction.

The maximum gain occurs when both $(\partial\gamma/\partial T)_J = 0$ and $(\partial\gamma/\partial J)_T = 0$. Substituting the value of $J^{(0)}(J^{(0)}+1)$ from equation B.27 for $J(J+1)$ (with $T = T^{(0)}$) into equation B.33 determines the condition on $T^{(0)}$ for optimum gain:

$$0 = \{1 - \frac{5}{2}\frac{T^{(0)} - T_I}{T^{(0)}} + (T^{(0)} - T_I)(\frac{k_B T^{(0)}}{2hcB})\frac{hcB}{k_B T^{(0)2}}\}$$

which simplifies to give

$$T^{(0)} = 2T_I \qquad (B.34)$$

Substituting $T = T^{(0)} = 2T_I$ into equation B.26 results in the approximate solution for $J^{(0)}$ at optimum gain:

$$J^{(0)} \simeq \sqrt{k_B T/hcB} - 1$$

From equations B.8 and B.34 we can find r in terms of T_I:

$$r \simeq (T^{(0)} - T_I)/(T_F - T_I) = T_I/(T_F - T_I)$$

T_F is defined by equation B.9. To evaluate T_F we must first approximate $(\partial T/\partial X_{CS_2})$; we will take T to equal the adiabatic flame temperature and evaluate this derivative for small r. From Reference B.6, we see that T is linear in X_{CS_2} for small X_{CS_2}, and $(\partial T/\partial X_{CS_2}) \simeq 25{,}000°K$. Using equation B.3, $r \simeq X_{CS_2}$, we find that for maximum gain

$$r \simeq T_I/T_F \simeq 300°K/25{,}000°K = .012$$

Conclusions

Equation B.34 states that the optimum ratio of fuel to oxidant is the one that causes the gas in the flame to be twice its initial

temperature. If more fuel is added, the combustion gases become too hot. This lowers the density of the gas, flattens the lineshapes, and spreads the rotational distributions, countering the increase in product (CO) mole fractions, and lowering the gain. If less fuel is added, too little product (CO) is formed and the gain is less than maximal. In deriving this simple result, no particular features of the CS_2/O_2 system were used; the result is general to this model of the chemical laser processes. Note that altering the gas temperature by some special means, such as supersonic expansion, was not considered, and would present a more complex problem.

The optimal value of r (fuel:oxidant ratio) computed is approximate. Later in this appendix we will see that this analysis ignored nonlinearities in the chemical production rates with r, and this will cause an underestimate of the optimal value of r, because the calculation does not include the effect of the decrease in reactivity of the gas as r decreases.

The computed value of r was .012 as compared with the experimentally determined value for optimal power output (not small signal gain) of about .03 [B.2]. It is not surprising that the value of r at which there is maximum power output is above optimal value for small signal gain. The power extraction from a gain saturated medium does not necessarily decrease as rapidly as the small signal gain of the medium when, with increasing r and increasing temperature, the rotational distribution is broadened and the lineshapes flattened.

In Appendix A we saw that in a mixing layer flame the fuel and oxidant will tend to burn at nearly their stoichiometric ratio and

corresponding adiabatic flame temperature. The CS_2:O_2 stoichiometric ratio is about .35 [B.1], which will result in combustion at too high a temperature for maximal gain. Diluting the mixing layer flame with an inert gas to reduce its temperature has a detrimental effect, slowing the chemical reactions (refer to Chapter II, Section G); consequently, the mixing layer flame should be expected not to perform as well as a premixed flame.

Assumptions Concerning the CO Vibrational Populations

The following discussion is concerned with the applicability of the assumptions expressed in equations B.5 and B.6

$$X_v \propto X_{CO} \tag{B.5}$$

$$\partial(X_v/X_{v-1})/\partial r = 0 \tag{B.6}$$

The processes affecting the mole fractions of CO in vibrational levels v-1 and v are outlined in Figure B-2. Chemical production of CO pumps both levels, v and v-1. Also, there is pumping into the levels and deactivation of these levels by vibrational energy transfer processes. We will motivate the use of equations B.5 and B.6 to estimate the dependence of X_{v-1} and X_v on r, and then clarify the meaning of these assumptions in terms of the processes involved in determining X_{v-1} and X_v.

We are interested in when equations B.5 and B.6 hold. Using equations B.3 and B.7, equation B.5 can be put into the equivalent form:

$$X_{v'} \propto r \qquad v' = v-1, v \tag{B.35}$$

If the proportionality, B.35, holds, then X_v/X_{v-1} will be independent of r, and X_{v-1} and X_v will satisfy equation B.6. Consequently equation B.35 is sufficient to establish equations B.5 and B.6.

Motivating the Approximation: $X_{v'} \propto r$

In a fuel lean CS_2/O_2 premixed flame, increasing the mole fraction of CS_2 in the reactant gas increases the mole fraction of CO in the product gas. The most simple assumption is that the mole fraction of CO produced is linear in the initial CS_2 mole fraction, and this was stated earlier in equation B.7:

$$X_{CO} \propto X_{CS_2} \tag{B.7}$$

and because of equation B.3, this implies

$$X_{CO} \propto r \tag{B.36}$$

The distribution of the CO among vibrational levels may be nonequilibrium. In the absence of a detailed analysis of the carbon monoxide vibrational kinetics in the CS_2/O_2 flame, we find no obvious a priori basis for assuming the normalized distribution over vibrational levels varies with the initial fuel mole fraction (or r). Consequently, the most simple estimate is that the fraction of CO in each vibrational level remains a constant fraction of the total CO population:

$$X_v \propto X_{CO} \tag{B.6}$$

Equations B.6 and B.36 imply

$$X_v \propto r \tag{B.37}$$

With this result, we have covered the motivating factor for assuming equations B.5 and B.6, assumptions made in lieu of a detailed analysis of the vibrational kinetics. We have chosen to make such an estimate because it rewards us with the ability to rapidly estimate the optimum CS_2/O_2 ratio for maximal gain in a CS_2/O_2 premixed flame laser, as was shown in the first part of this appendix.

Analysis of the Assumptions

Foregoing lengthy calculations, we will consider the processes in a CS_2/O_2 flame that are compatible with the relation $X_{v'} \propto r$ that we would like to assume. To do this, consider the rate equations governing the mole fractions in the levels v-1 and v; they are

$$\frac{dX_v}{dt} = (R_v^P + R_v^a) - X_v(k_{v,v-1} + k_v^d) + X_{v-1}k_{v-1,v} \tag{B.38}$$

and

$$\frac{dX_{v-1}}{dt} = (R_{v-1}^P + R_{v-1}^a) - X_{v-1}(k_{v-1,v} + k_{v-1}^d) + X_v k_{v,v-1} \tag{B.39}$$

Figure B-2 displays the rate processes considered in equations B.38 and B.39; R_v^P and R_v^a are the rates for pumping by vibrational transfer and chemical addition to level v. The rate constants k_v^d and $k_{v,v'}$ are for deactivation from level v and transfer from level v to level v'. For simplicity, stimulated emission processes are ignored. Chemical sinks for CO may be incorporated into the addition terms R_{v-1}^a and R_v^a.

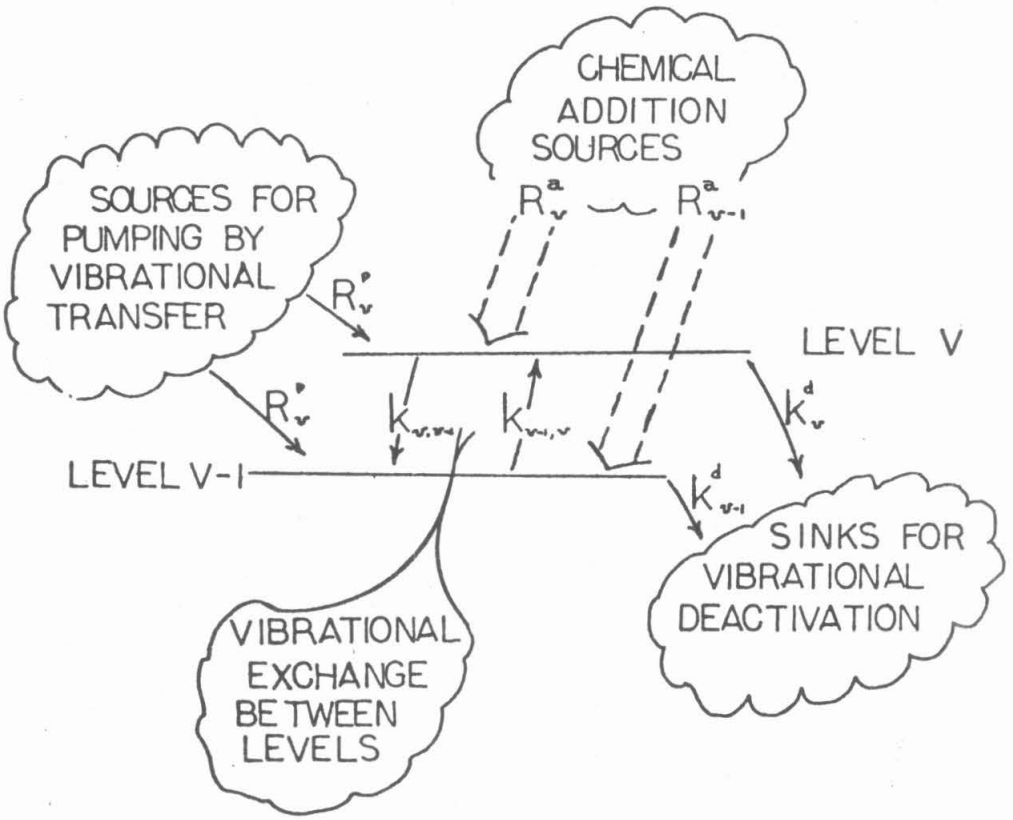

Figure B-2 Processes affecting the relative populations of two adjacent vibrational levels of CO

Spontaneous emission may be included in the deactivation terms $k_{v,v-1}$ and k^d_{v-1}. Fluid, mixing, and flame properties implicitly determine these rates, but will not be elaborated upon here.

If the nonsteady terms in equations B.38 and B.39, dX_v/dt and dX_{v-1}/dt, are negligible, X_{v-1} and X_v will be linear in r if the pumping rates and the rate constants have the following forms:

R^P_v R^a_v R^P_{v-1} and R^a_{v-1} are all proportional to $rf(r)$;

k^d_v k^d_{v-1} $k_{v-1,v}$ and $k_{v,v-1}$ are all proportional to $f(r)$,

where $f(r)$ is some function of r. Because the temperature in the product gas is a function of the initial CS_2 mole fraction, $f(r)$ can carry a general temperature dependence for the rates, but it must be the same for all processes.

The pumping rates, R^a_v, R^P_v, R^a_{v-1}, and R^P_{v-1}, can each be written in the form:

$$R = \sum_{\alpha} k_\alpha X_\alpha + \sum_{\alpha,\beta} k_{\alpha\beta} X_\alpha X_\beta + \cdots$$

That is, each pumping term is the sum of unimolecular, bimolecular, and higher order pumping terms. If the rate constants here too are proportional to $f(r)$, then equation B.37 will be satisfied if $X_\alpha \propto r$ for the unimolecular processes, and $X_\alpha X_\beta \propto r$ for the bimolecular processes. This is approximately true for chemical pumping processes ($X_{CS_2} \cdot X_{O_2} \simeq r \cdot 1 = r$), and unimolecular vibrational decays, but not for vibrational-vibrational exchanges.

If the nonsteady terms in equations B.38 and B.39 cannot be neglected, then $X_{v'} \propto r$ only if both $f(r) = 1$, and the previous discussion holds. Most generally, $X_{v'} \propto r$ if all the rate processes are strictly linear in r; the temperature dependence in the rates is ignored.

We have motivated the choice of equations B.5 and B.6 as approximations to describe the vibrational distributions. These approximations can be rigorously justified only if all the rate processes that influence the mole fraction of CO in each vibrational level are linear processes. This means the relevant reaction rates vary little with temperature and the dominant processes are first order in fuel and product species.

Appendix B References

B.1 A. A. Vetter, Ph.D. thesis: "Kinetics and Structure of the CS_2/O_2 Flame Laser," California Institute of Technology (1975).

B.2 S. K. Searles and N. Djeu, "Characteristics of a CW CO Laser Resulting from a CS_2-O_2 Additive Flame," Chemical Physics Letters 12, 53-56 (1971).

B.3 G. Hancock and I.W.M. Smith, "Quenching of Infrared Chemiluminescence. 1: The Rates of De-Excitation of CO ($4 \leq v \leq 13$) by He, CO, NO, N_2, O_2, OCS, N_2O, and CO_2," Applied Optics 10, 1827-1843 (1971).

B.4 A. Yariv, Quantum Electronics, Second Edition (Wiley and Sons, New York, 1975).

B.5 G. Hertzberg, Molecular Spectra and Molecular Structure I. Spectra of Diatomic Molecules (Van Nostrand Reinhold Co., New York, 1950).

B.6 W. Grossman, A. A. Vetter, and F.E.C. Culick, "Some Results for the Combustion of CS_2/O_2 in a Laminar Mixing Layer," Proceedings of the Fourteenth JANNAF Conference (1977).

Appendix C

COMPUTER CODES

1. A Description of the Computer Codes for the Two-Dimensional CS_2/O_2 Laminar Mixing Layer Flame, "MIXWG"

The computer code "MIXWG" was constructed to investigate the behavior of the CS_2/O_2 laminar mixing layer flame. The Fortran IV source deck for this program is listed in this appendix. A brief description of the main part of the program and the subprograms is given. The program has been run on an IBM 370 computer.

MIXWG is a code used to model a mixing layer downstream of a splitter plate. The streams of the reactant, CS_2 and O_2, each have uniform velocity, UO2 and UCS2, prior to mixing. The computation proceeds from initial values at the start of the mixing layer, and marches downstream, typically for 4 cm, computing the values of the temperature, velocity, and concentrations of O_2, CS_2, CS, S, O, SO, CO, CO_2, COS, and SO_2. The computation is on a two-dimensional grid, (z,y); z is the coordinate in the direction of flow, and y is the coordinate normal to the plane initially separating the CS_2 and O_2. There are nine grid locations in y.

The Limitations of the Code MIXWG

The computer code MIXWG models a system in which there is no net molar production. The mole fraction of one species, SO_2, is calculated by using the constraint that the mole fractions sum to unity. This simplifies the computations by replacing the differential equations for the

mole fractions of SO_2 by a simple algebraic formula. In the chemical reaction sequences, the reactions are automatically balanced, by assuming SO_2 is present to maintain the sum of the mole fractions to unity. If recombination reactions, such as $CO + O + M \rightarrow CO_2 + M$ are included, the computed forward rates are correct and may be used to decide the importance of these reactions relative to others. However, if reactions in which there is a net molar production or loss are important (and they were found not to be) then the computation must be reformulated in order to satisfy species conservation. Difficulties arise because this computer code conserves moles; hence, it will read $CO + O + M \rightarrow CO_2 + M$, and infer $CO + O + M \rightarrow CO_2 + SO_2 + M$ in order to allow no net molar production. This computer code is adequate to fulfill our needs, but would be an inaccurate model of flames at higher pressures, where three-body reactions are expected to become increasingly important.

Main

The main block of MIXWG accepts initial values for the flow parameters at z = 0 in a working vector "X" of dimension 90. In the listing of the program, there is a table presenting the correspondences between the indices on X and the variables O_2, CS_2, CS, S, O, SO, CO, CO_2, and COS (mole fractions) and temperature at nine locations in y. The mole fraction of a tenth species, SO_2, is found by using the fact that the mole fractions must sum to unity. Each set of calls to the numerical integration routine, "MODWMG", replaces X with its value at a distance DZ (2 cm) further downstream. These values are stored in the matrix "A". The integrations are taken 4 cm downstream, and the values of X are

recorded at each of 21 locations, z = .2 cm, z = .4 cm, ···, z = 4.0 cm. After each call to the numerical integration, the calculated data are printed.

Subroutine DIFFY

This subroutine is used to calculate the derivatives of the temperature and species mole fractions for use in the numerical integrations. These derivatives are contained in the vector XDOT. The reaction source terms RW(I,J)/V and the diffusion source terms, $D(X(K+1)+X(K-1)-2X(K))/(V\cdot\Delta y^2)$, sum to give XDOT(K). The indexing system is such that K = 9x I+ J where I is the index identifying the species and J is the index identifying the grid point in y. The spacing in the y grid is Δy, the velocity along the flow is V, and the diffusion constant is D. The Lewis number is assumed one; consequently the transport coefficient for temperature $K/(\rho C_p)$ equals D.

Subroutine WRATE

This subroutine is used to calculate the chemical source terms for each species at each y location, and returns these terms to the subroutine DIFFY in the matrix "RW". RW carries derivatives for the 10 variables, 9 species and temperature, at nine locations in y. In WRATE the matrix "R" contains the individual rates for each chemical reaction included at each of the nine y locations.

Subroutine HWARTH

This subroutine follows the calculation of the temperature field. The y values for the grid on which the numerical integrations were per-

formed are inverse Howarth transformed. The output is a matrix "Y" carrying the values of y in the laboratory coordinates of the 9 streamlines at each of the 21 locations in z; z = 0.0 cm, z = 0.2 cm, ···, z = 4.0 cm.

Function VEL

The function VEL is used to compute the velocity on the basis of a mass weighted average of the species. The free stream velocity for the O_2 stream is UO2 and free stream velocity for the CS_2 streams is UCS2. The variable MI is the molecular weight of species I. In addition to the usual 10 species, O_2, CS_2, CS, S, O, SO, CO, CO_2, COS, and SO_2, atomic carbon is included, with M11 being its molecular weight. The formulas used in computing the velocity can be found in the program listing.

Subroutine WRITE

This subroutine merely serves to print data and punch cards containing the final results.

Subroutines MODWMG, MADAM, MGILL, and MREST

These subroutines together perform the numerical integration in z. The method of Runge-Kutta-Gill is used to start the integration process, and is used to restart the integrations whenever the step size has been altered. Once the integration has been started, it is continued by the Adams-Moulton predictor-corrector method.

This numerical integration code was adapted from the subroutine MODDEQ in the Caltech computer library. The dimensions of the variables have been increased to allow the solution of a system of 90 variables,

the temperature and mole fractions of 9 species at nine y locations. MODDEQ receives a value of the vector X from the main block of MIXWG. It then calls the subroutine DIFFY which computes XDOT, the vector of the derivatives dX/dz. After the numerical integration, MODWMG returns the revised vector, X, to the main block.

2. The Computer Code "MIX60"

The following is a brief description of the computer code MIX60. It was written to model CS_2/O_2 reactive mixing. The chemistry is simplified, considering only a single overall reaction: $CS_2 + O_2 \rightarrow$ product. The species equations are solved. The solutions for the velocity profiles and temperature profiles are approximated by assuming a similarity between the species, temperature, and velocity profiles. The purpose of this part of the calculation was to find an approximate solution for the production of CO in the flame. This part of the calculation is followed by a second calculation, a one-dimensional kinetics program used to predict the carbon monoxide vibrational distribution as a function of the downstream coordinate. The numerical subroutine used, MODDEQ, differs only in the dimensions of the variables from the subroutine MODWMG in the code MIXWMG. MODDEQ is used first to solve the equations of flow, with a procedure similar to that used in the code MIXWMG. Subsequently, MODDEQ is used to solve for the CO vibrational distributions. The listing of MIX60 follows.

```
      EXTERNAL DIFFY
      DIMENSION A(10,9,21), XDOT(90),Y(9,21),X(90), TEMP(9,21),TEMDOT(9)
     +  ,ZDIS(21),IPS(21),VLCT(9,21),ZZ(21),YY(9),DXS02(9),IMINUS(21)
     + ,R(10,9),RR(10,21)
      COMMON/RATE2/DY,TO
      COMMON/RATES/P,DO
      COMMON/WRT2/NZ1,NY,TEMP
      COMMON/WRTE/IPUNCH,YY,ZZ,VLCT,A
      COMMON/RRRR/RR
      COMMON/HWTH/Y
      COMMON/REACT/R
      COMMON/SPEED/U02,UCS2
C
C
C     MAP OF X(J), J=1,2,... 90
C
C             Y=  -2.0  -1.5  -1.0  -0.5   0.0   0.5   1.0   1.0   2.0
C                 ----  ----  ----  ----  ----  ----  ----  ----  ----
C     1   02    :  01    02    03    04    05    06    07    08    09
C     2   CS2   :  10    11    12    13    14    15    16    17    18
C     3   CS    :  19    20    21    22    23    24    25    26    27
C     4   S     :  28    29    30    31    32    34    35    36    37
C     5   O     :  37    38    39    40    41    42    43    44    45
C     6   SO    :  46    47    48    49    50    51    52    53    54
C     7   CO    :  55    56    57    58    59    60    61    62    63
C     8   CO2   :  64    65    66    67    68    69    70    71    72
C     9   COS   :  73    74    75    76    77    78    79    80    81
C         TEMP  :  82    83    84    85    86    87    88    89    90
C
      NY=9
C
C     CGS UNITS.  NZSTEP IS THE NUMBER OF Z STEPS.  NZSTEP=1 IS INITIAL.
C     SPECIES 1  IS  02
C     SPECIES 2  IS  CS2
C     SPECIES 3  IS  CS
C     SPECIES 4  IS  S
C     SPECIES 5  IS  O
C     SPECIES 6  IS  SO
C     SPECIES 7  IS  CO
C     SPECIES 8  IS  CO2
C     SPECIES 9  IS  COS
C     SPECIES 10 IS  SO2
C
C     A(I,J,NZSTEP) IS THE MOLE FRACTION OF SPECIES I AT Y LOCATION J.
C     TEMP(J,NZSTEP)
C     THE STREAMWISE COORDINATE IN SPACE IS Z.
C     NY=THE NUMBER OF Y LOCATIONS.
C     X(1,2,3... N) ARE O2 CONCENTRATIONS.              (IN MOLE FRACTION)
C     X(N+1,N+2,N+3... 2*N) ARE CS2 CONCENTRATIONS=     (IN MOLE FRACTION)
      NZ=20
      ZRO=0.0
      READ (5,65) DO
      WRITE (6,65) DO
      READ (5,64) EPS
      WRITE (6,64) EPS
      READ (5,63) IPUNCH,P,          U02,UCS2
      WRITE (6,63) IPUNCH,P,          U02,UCS2
      TO=300.0
```

Figure C-1 Coding for the computer program MIXWG

```
      HEIGHT=4.0
      ZLENGH=4.0
      DZ=ZLENGH/NZ
      DY=HEIGHT/(NY-1)
      MIDY=(NY+1)/2
      DO 510 I=1,NY
      YY(I)=(I-MIDY)*DY
510   CONTINUE
      Z=0.0
      NZ1=NZ+1
C     KIK=1 IMPLIES STEP ONE. MODDEQ RESETS IT TO 2 LATER.
C     AND -1 TO INDICATE ERRORS.
      KIK=1
      NEQNS=90
      DO 500 I=1,NZ1
      IPS(I)=I+1
      IMINUS(I)=I-1
      ZZ(I)=IMINUS(I)*DZ
500   CONTINUE
      NCUT=10
      D2=DZ/NCUT
      NZSTEP=1
      READ (5,66)     (TEMP(J,1),J=1,9)
      WRITE (6,66)     (TEMP(J,1),J=1,9)
      DO 505 J=1,9
      J1=J+NY
      J2=J1+NY
      J3=J2+NY
      J4=J3+NY
      J5=J4+NY
      J6=J5+NY
      J7=J6+NY
      J8=J7+NY
      J9=J8+NY
      READ (5,62) X(J),X(J1),X(J2),X(J3),X(J4),X(J5),X(J6),X(J7),X(J8)
      WRITE (6,62) X(J),X(J1),X(J2),X(J3),X(J4),X(J5),X(J6),X(J7),X(J8)
C     THERE ARE NO CARDS SEQUENCED 68 THROUGH 75
      A(1,J,NZSTEP)=X(J)
      A(2,J,NZSTEP)=X(J1)
      A(3,J,NZSTEP)=X(J2)
      A(4,J,NZSTEP)=X(J3)
      A(5,J,NZSTEP)=X(J4)
      A(6,J,NZSTEP)=X(J5)
      A(7,J,NZSTEP)=X(J6)
      A(8,J,NZSTEP)=X(J7)
      A(9,J,NZSTEP)=X(J8)
      A(10,J,NZSTEP)=1.-X(J)-X(J1)-X(J2)-X(J3)-X(J4)-X(J5)-X(J6)-X(J7)
     *   -X(J8)
      VLCT(J,1)=VEL(X(J),X(J1),X(J2),X(J3),X(J4),X(J5),X(J6),X(J7),X(J8)
     *    ,ZRO)
      X(J9)=TEMP(J,NZSTEP)
505   CONTINUE
      DO 205 L=1,10
      WRITE (6,21) L,(A(L,K,1),K=1,9)
205   CONTINUE
      WRITE (6,54) (VLCT(J,1),J=1,NY)
      WRITE (6,20) (TEMP(J,1),J=1,9)
      DO 100 I=1,NZ1
```

Figure C-2 Coding for the computer program MIXWG

```
      NZSTEP=I
      IF (I.EQ.1)
     *CALL MODWMG(DIFFY,KIK,NEQNS,Z,X,XDOT,D2,EPS)
      IF (I.EQ.1) GO TO 160
      DO 150 J=1,NCUT
150   CALL MODWMG(DIFFY,KIK,NEQNS,Z,X,XDOT,D2,EPS)
C     * * * * * * * * * * * * * * * * * * * * * * * * * * * * * * * * * * * * *
160   DO 210 J=1,NY
      J1=J+NY
      J2=J1+NY
      J3=J2+NY
      J4=J3+NY
      J5=J4+NY
      J6=J5+NY
      J7=J6+NY
      J8=J7+NY
      J9=J8+NY
      A(1,J,NZSTEP)=X(J)
      A(2,J,NZSTEP)=X(J1)
      A(3,J,NZSTEP)=X(J2)
      A(4,J,NZSTEP)=X(J3)
      A(5,J,NZSTEP)=X(J4)
      A(6,J,NZSTEP)=X(J5)
      A(7,J,NZSTEP)=X(J6)
      A(8,J,NZSTEP)=X(J7)
      A(9,J,NZSTEP)=X(J8)
      A(10,J,NZSTEP)=1.-X(J)-X(J1)-X(J2)-X(J3)-X(J4)-X(J5)-X(J6)-X(J7)
     *   -X(J8)
      TEMP(J,NZSTEP)=X(J9)
      TEMDOT(J)=XDOT(J9)
      VLCT(J,NZSTEP)=VEL(X(J),X(J1),X(J2),X(J3),X(J4),X(J5),X(J6),
     *     X(J7),X(J8),ZRO)
C     TEMP IS THE TEMPERATURE IN DEGREES KELVIN.
210   CONTINUE
      DO 235 J=1,10
      RR(J,I)=0.0
      DO 240 K=1,9
      RR(J,I)=RR(J,I)+R(J,K)
240   CONTINUE
235   CONTINUE
       WRITE (6,11)
      WRITE (6,26) NZSTEP,Z
      WRITE (6,20) (TEMP(K,NZSTEP),K=1,9)
      WRITE (6,19) (TEMDOT(K),K=1,9)
      DO 215 L=1,9
      WRITE (6,21) L,(A(L,K,NZSTEP),K=1,9)
      KT=9*L
      KB=9*(L-1)+1
      WRITE (6,23) L,(XDOT(K),K=KB,KT)
215   CONTINUE
      MNM=10
      WRITE (6,21) MNM,(A(MNM,K,NZSTEP),K=1,9)
      DO 220 J=1,9
      DXSD2(J)=0.0
      DO 225 K=1,9
      KS=J+(K-1)*9
      DXSD2(J)=DXSD2(J)-XDOT(KS)
225   CONTINUE
```

Figure C-3 Coding for the computer program MIXWG

```
220   CONTINUE
      WRITE (6,23) MNM,(DXSQ2(K),K=1,9)
      WRITE (6,54) (VLCT(J,I),J=1,NY)
      WRITE (6,11)
      WRITE (6,12)
      WRITE (6,11)
      DO 230 J=1,9
      WRITE (6,13) (R(K,J),K=1,10)
230   CONTINUE
100   CONTINUE
      CALL HWARTH
      CALL WRIGHT
C     FORMATS
C     * * * * * * * * * * * * * * * * * * * * * * * * * * * * * * * * * * * *
11    FORMAT (' ')
12    FORMAT (' REACTION RATES')
13    FORMAT (5X,1P10E12.5)
19    FORMAT (' TEMDOT',9F12.5)
20    FORMAT (' TEMP  ',9F12.5)
21    FORMAT (' ',I2,'    ',9(1PE12.5))
23    FORMAT (' ',I2,'DOT',9(1PE12.5))
26    FORMAT (4X,'STEP NUMBER ',I2,'      Z=',F7.4,'CM.')
54    FORMAT (' VLCTY',9F12.5)
62    FORMAT (2X,9(1PE8.1))
63    FORMAT (2X,I1,2X,3F10.4)
64    FORMAT (5X,F15.7)
65    FORMAT (5X,F10.4)
66    FORMAT (5X,9(3X,F5.0))
      RETURN
      END
      SUBROUTINE DIFFY(N,Z,X,XDOT)
C     * * * * * * * * * * * * * * * * * * * * * * * * * * * * * * * * * * * *
      DIMENSION X(90),XDOT(90),DUDY(9),RW(10,9),V(9)
      COMMON/RATES/P,DO
      COMMON/RATE2/DY,TO
      CALL WRATE(RW,X)
      NY=9
      ZRO=0.0
      D=DO/P
      DO 100 J=1,9
      J1=J+NY
      J2=J1+NY
      J3=J2+NY
      J4=J3+NY
      J4=J3+NY
      J5=J4+NY
      J6=J5+NY
      J7=J6+NY
      J8=J7+NY
      V(J)=
     *  VEL(X(J),X(J1),X(J2),X(J3),X(J4),X(J5),X(J6),X(J7),X(J8),ZRO)
      DUDY(J)=(D/(DY*DY))/V(J)
100   CONTINUE
      DO 110 I=1,10
      N8=I*9-8
      NP=I*9
      N81=N8+1
      NP1=NP-1
```

Figure C-4 Coding for the computer program MIXWG

```
          XDOT(NB)=2.0*DUDY(1)*(X(NB1)-X(NB))+RW(I,1)/V(J)
          XDOT(NP)=2.0*DUDY(9)*(X(NP1)-X(NP))+RW(I,9)/V(J)
110   CONTINUE
      DO 120 I=1,10
      DO 130 J=2,8
      K=9*(I-1)+J
      KP=K+1
      KM=K-1
          XDOT(K)=DUDY(J)*(X(KP)+X(KM)-2.0*X(K))+RW(I,J)/V(J)
130   CONTINUE
120   CONTINUE
C     SIZ=40.
      SIZ=100.0
      DO 140 I=1,81
      BO=-(X(I)*SIZ+1.0E-34)
      IF (XDOT(I).LT.BO) XDOT(I)=BO
140   CONTINUE
C     THE PREVIOUS LIMITS THE DERIVATIVES IF THEY ARE HUGE AND NEGATIVE.
C     SO THAT A SPECIES WILL HAVE ITS CONCENTRATION DROP TO ZERO IN
C     NO LESS THAN 1/SIZ CM.  IF THE CALCULATION GOES WRONG, AND THE
C     CONCENTRATIONS ARE GOING NEGATIVE, REDUCE SIZ? IF THE SPECIES ARE
C     NOT PROPERLY CONSERVED. INCREASE SIZ, REDUCE THE STEP SIZES BY
C     MAKING MORE CALLS TO MODWMG PER UNIT LENGTH, AND BE PREPARED
C     FOR AN INCREASED COPUTATIONAL COST.  TO BOOST THE NUMBER OF
C     CALLS PER STEP, DZ, INCREASE THE VARIABLE, 'NCUT' IN MAIN.
      RETURN
      END
      SUBROUTINE WRATE (RW,X)
      DIMENSION RW(10,9),       RK(10), DH(10), L(10), X(90), ARG(10)
     *     ,R(10,9)
C     * * * * * * * * * * * * * * * * * * * * * * * * * * * * * * * * * * *
      COMMON/RATE2/DY,TO
      COMMON/RATES/P,DO
      COMMON/REACT/R
C     IF NTST=0 IT IS A 1 REACTION TEST.
C     RUN CASE REACTIONS.
C     CS2 + O   => CS +  SO  REACTION 1
C     CS  + O   => CO +  S   REACTION 2
C     S   + O2  => SO +  O   REACTION 3
C     SO  + O2  => SO2 + O   REACTION 4
C     CO  + S + M   => COS + M  REACTION 5
C     CO  + O + M   => CO2 + M  REACTION 6
C     CS2 + O   => COS + S   REACTION 7
C     CO  + O2  => CO2 + O   REACTION 8
C     CO  + SO  => CO2 + S   REACTION 9
C     COS + O   => CO2 + S   REACTION 10
      ZRO=0.0
      DH(1)=10500.0
      DH(2)=42750.0
      DH(3)= 3000.0
      DH(4)= 6250.0
      DH(5)=37000.
      DH(6)=64100.
      DH(7)=27200.
      DH(8)= 4025.
      DH(9)=  800.
      DH(10)=27100.
      DO 100 I=1,9
```

Figure C-5 Coding for the computer program MIXWG

```
      DO 110 J=1,10
      L(J)=I+(J-1)*9
110   CONTINUE
C     WRITE (6,1) I,(X(L(K)),K=1,10)
      T=X(L(10))
      CP=10.0+2.5E09*(EXP(17.0-50000.0/T))/(T*T)
C     CP=CP0 + (((DH0)**2)/(T**2))*EXP((S0*T-DH0)/RT)
C     R IS A GAS CONSTANT.  S IS AN ENTROPY- LIKE QUANTITY.
      DO 120 N=1,10
      ARG(N)=DH(N)/T
      IF (ARG(N).GT.40.0) ARG(N)=40.0
120   CONTINUE
      RK(1)=5.0E13*EXP(-960./T)
      RK(2)=2.4E14*EXP(-1010./T)
      RK(3)=1.0E13*EXP(-2800./T)
      RK(4)=3.5E11*EXP(-3280./T)
      RK(5)=2.0E16*EXP(-900./T)
      RK(6)=1.6E16*EXP(-900./T)
      RK(7)=1.0E14*EXP(-4040./T)
      RK(8)=3.5E12*EXP(-25700./T)
      RK(9)=1.7E12*EXP(-25700./T)
      RK(10)=4.4E14*EXP(-26300./T)
      RH0=4.08E-5*(P*T0/T)
      XTEN  =1.-X(L(1))-X(L(2))-X(L(3))-X(L(4))-X(L(5))-X(L(6))-X(L(7))
     *     -X(L(8))-X(L(9))
      R(1,I)=  (X(L(2))*X(L(5))-EXP(-ARG(1) )*X(L(3))*X(L(6)))*RH0*RK(1)
      R(2,I)=  (X(L(5))*X(L(3))-EXP(-ARG(2) )*X(L(7))*X(L(4)))*RH0*RK(2)
      R(3,I)=  (X(L(4))*X(L(1))-EXP(-ARG(3) )*X(L(6))*X(L(5)))*RH0*RK(3)
      R(4,I)=  (X(L(6))*X(L(1))-EXP(-ARG(4) )*XTEN    *X(L(5)))*RH0*RK(4)
      R(5,I)=      X(L(4))*X(L(7))*RH0*RH0*RK(5)
      R(6,I)=      X(L(5))*X(L(7))*RH0*RH0*RK(6)
      R(7,I)=(X(L(2))*X(L(5))-EXP(-ARG(7))*X(L(9))*X(L(4)))*RH0*RK(7)
      R(8,I)=(X(L(7))*X(L(1))-EXP(-ARG(8))*X(L(8))*X(L(5)))*RH0*RK(8)
      R(9,I)=(X(L(7))*X(L(6))-EXP(-ARG(9))*X(L(8))*X(L(4)))*RH0*RK(9)
      R(10,I)=(X(L(9))*X(L(5))-EXP(-ARG(10))*X(L(4))*X(L(8)))*RH0*RK(10)
      DO 130 J=1,10
      IF (R(J,I).LT.0.0) R(J,I)=0.0
130   CONTINUE
      RW(1,I)=-(R(3,I)+R(4,I)+R(8,I))
      RW(2,I)=-(R(1,I)+R(7,I))
      RW(3,I)=R(1,I)-R(2,I)
      RW(4,I)=R(2,I)+R(7,I)+R(9,I)+R(10,I)-R(3,I)-R(5,I)
      RW(5,I)=R(4,I)+R(3,I)+R(8,I)-R(1,I)-R(7,I)-R(2,I)-R(6,I)-R(10,I)
      RW(6,I)=R(1,I)        -R(4,I)-R(9,I)
      RW(7,I)=R(2,I)-R(5,I)-R(6,I)-R(8,I)-R(9,I)
      RW(8,I)=R(6,I)+R(8,I)+R(9,I)+R(10,I)
      RW(9,I)=R(5,I)+R(7,I)-R(10,I)
      RW(10,I)=1.98*(R(1,I)*DH(1)+R(2,I)*DH(2)+R(3,I)*DH(3)+
     *     R(4,I)*DH(4)+R(5,I)*DH(5)+R(6,I)*DH(6)+R(7,I)*DH(7)+
     *     R(8,I)*DH(8)+R(9,I)*DH(9)+R(10,I)*DH(10))/CP
C     WRITE (6,3) I,(RW(K,I),K=1,10)
C     WRITE (6,2) I, (R(K,I),K=1,10)
100   CONTINUE
1     FORMAT (' J=',I2,'  X    ',10(2X,1PE10.3))
2     FORMAT (' J=',I4,'  R    ',10(2X,1PE10.3))
3     FORMAT (' J=',I3,'  RW   ',10(2X,1PE10.3))
      RETURN
      END
```

Figure C-6 Coding for the computer program MIXWG

```
      SUBROUTINE HWARTH
C     * * * * * * * * * * * * * * * * * * * * * * * * * * * * * * * * * * * *
      DIMENSION TEMP(9,21),Y(9,21)
      COMMON/HWTH/Y
      COMMON/WRT2/NZ1,NY,TEMP
      COMMON/RATE2/DY,TO
C     THERE IS NO NET VERTICAL VELOCITY.
      MIDY=(NY+1)/2
      MIDYM=MIDY-1
      DYT   =DY/(2*TO)
C     THIS WILL WORK ONLY IF TEMP=TO INITIALLY EVERYWHERE EXCEPT
C      AT THE MID Y POINT.
      DO 160 I=1,NZ1
      Y(MIDY,I)=0.0
      DO 150 J=1,MIDYM
      JDN=MIDY-J
      JUP=MIDY+J
      JUPM=JUP-1
      JDNP=JDN+1
      Y(JUP,I)=Y(JUPM,I)+    (TEMP(JUP,I)+TEMP(JUPM,I))*DYT
      Y(JDN,I)=Y(JDNP,I)-    (TEMP(JDN,I)+TEMP(JDNP,I))*DYT
150   CONTINUE
160   CONTINUE
      RETURN
      END
      FUNCTION VEL(X1,X2,X3,X4,X5,X6,X7,X8,X9,X10)
C     * * * * * * * * * * * * * * * * * * * * * * * * * * * * * * * * * * * *
      REAL*4   M2,M3,M4,M5,M6,M7,M8,M9,M10,M11,MAV,M1
      COMMON/SPEED/U02,UCS2
      IF (U02.NE.UCS2) GO TO 100
      VEL=U02
      RETURN
100   CONTINUE
      X10=1.-X1-X2-X3-X4-X5-X6-X7-X8-X9
C     SPECIES:  02,CS2,CS,S,0,S0,C0,C02,COS,S02
      M1  =32.
      M2  =76.
      M3  =44.
      M4  =32.
      M5  =16.
      M6  =48.
      M7  =28.
      M8  =44.
      M9  =60.
      M10 =64.
      M11 =12.
      MAV=X1*M1+X2*M2+X3*M3+X4*M4+X5*M5+X6*M6+X7*M7+X8*M8+X9*M9+X10*M10
      VEL=(U02*M5*(2.0*X1+X5+X6+X7+2.0*X8+X9+2.0*X10)
     * +  UCS2*M4*(2.*X2+X3+X4+X6+X9+X10)
     * + UCS2*M11*(X2+X3+X7+X8+X9))/MAV
      RETURN
      END
      SUBROUTINE WRIGHT
C     WRITE STATEMENTS
C     * * * * * * * * * * * * * * * * * * * * * * * * * * * * * * * * * * * *
      DIMENSION YY(9),ZZ(21),VLCT(9,21),TEMP(9,21),Y(9,21),A(10,9,21)
     * ,RR(10,21)
      COMMON/WRT2/NZ1,NY,TEMP
```

Figure C-7 Coding for the computer program MIXWG

```
      COMMON/HWTH/Y
      COMMON/WRTE/IPUNCH,YY,ZZ,VLCT,A
      COMMON/RRRR/RR
C     TO WRITE THE TEMPERATURE.
      WRITE (6,11)
      WRITE(6,12)
      WRITE(6,4)
      WRITE(6,5)
      WRITE(6,16) (YY(I),I=1,NY)
      WRITE(6,11)
      DO 540 I=1,NZ1
      WRITE(6,17) ZZ(I),(TEMP(J,I),J=1,NY)
540   CONTINUE
C     THE FOLLOWING PRINTS OUT AN ARRAY OF Y VALUES FROM THE INVERSE
C     HOWARTH TRANSFORM BACK.  THESE VALUES TRACE STREAMLINES ALONG
C     THE FLOW. DESINNATING THE Y VALUE AS WE MOVE IN Z.
      DO 435 M=1,10
      WRITE (6,11)
      WRITE(6,43) M
      WRITE(6,4)
      WRITE(6,5)
        WRITE(6,18) (YY(I),I=1,NY)
      WRITE(6,11)
      DO 434 I=1,NZ1
      WRITE(6,19) ZZ(I),(A(M,J,I),J=1,NY)
434   CONTINUE
435   CONTINUE
      WRITE (6,11)
      WRITE(6,6)
      WRITE(6,16) (YY(I),I=1,NY)
      WRITE (6,11)
      DO 560 I=1,NZ1
      WRITE(6,17) ZZ(I),(Y(J,I),J=1,NY)
560   CONTINUE
      WRITE (6,11)
      WRITE (6,57)
      WRITE (6,11)
      WRITE (6,4)
      WRITE (6,5)
      WRITE (6,11)
      DO 655 I=1,NZ1
      WRITE (6,58) I,(VLCT(J,I),J=1,NY)
655   CONTINUE
      IF (IPUNCH.EQ.1) GO TO 580
      WRITE (7,60) (YY(J),J=1,5)
      WRITE (7,61) (YY(J),J=6,9)
      DO 895 K=1,10
      WRITE (7,73) (RR(K,J),J=1 ,7 )
      WRITE (7,73) (RR(K,J),J=8,14 )
      WRITE (7,73) (RR(K,J),J=15,21)
      DO 890 J=1,9
      WRITE (7,73) (A(K,J,I),I=1,7  )
      WRITE (7,73) (A(K,J,I),I=8,14 )
      WRITE (7,73) (A(K,J,I),I=15,21)
890   CONTINUE
895   CONTINUE
      DO 891 I=1,NZ1
      WRITE (7,60) (Y(J,I),J=1,5)
```

Figure C-8 Coding for the computer program MIXWG

```
      WRITE (7,61) (Y(J,I),J=6,9)
      WRITE (7,60) (TEMP(J,I),J=1,5)
      WRITE (7,61) (TEMP(J,I),J=6,9)
      WRITE (7,60) (VLCT(J,I),J=1,5)
      WRITE (7,61) (VLCT(J,I),J=6,9)
891   CONTINUE
580   CONTINUE
4     FORMAT ('0           Z IN
     *            Y IN CM')
5     FORMAT ('              CM')
6     FORMAT ('1Z IN CM.          Y VALUES AS A FUNCTION OF INITIAL Y')
11    FORMAT ('0')
12    FORMAT ('1         TEMPERATURE IN DEGREES KELVIN')
16    FORMAT (16X,9F10.3)
17    FORMAT (3X,F10.3,3X,9F10.3)
18    FORMAT (16X,9F12.3)
19    FORMAT (4X,F10.3,4X,1P9E12.5)
43    FORMAT (' SPECIES',2X,I2)
57    FORMAT ('1VELOCITIES')
58    FORMAT (4X,I4,9X,9E12.3)
60    FORMAT (4X,5E12.5)
61    FORMAT (4X,4E12.5)
73    FORMAT (3X,7(1PE11.4))
      RETURN
      END
      SUBROUTINE MODWMG(FUNC,K,N,T,Y,YDOT,DELT,EBAR)
C     * * * * * * * * * * * * * * * * * * * * * * * * * * * * * * * * * * * * * * * *
C MODDEQ                                    DATE OF OBJECT DECK 09-09-76
C     MODIFIED SEPTEMBER. 1976 BY ALBERT CHANG
      DIMENSION Y(90),YDOT(90)
      DOUBLE PRECISION TO,TA,TB,YDP
      COMMON /SAVDEQ/ TA,YDPA(90),YDOTA(90),TB,YDPB(90),YDOTB(90),
     1 YDP(90  ),F(90,4),YP(90)
      LOGICAL SIGN
      GO TO (10,100),K
C
C FIRST TIME
   10 IF(K.EQ.1) GO TO 20
      WRITE (6,615) K
  615 FORMAT(/1X 'K NOT VALID',I10/)
      STOP
C
   20 CONTINUE
      SIGN = .TRUE.
      MU = 1
      TIME = T
      TO = T
C     DO 25 I=1,N
C  25 YDP(I  ) = Y(I)
      IF(DELT.LT.0.) SIGN = .FALSE.
      IF(EBAR.NE.0.) GO TO 30
      DT = DELT
      GO TO 40
C VARIABLE MODE
C
   30 CONTINUE
      NOSTEP = 4
      DT = DELT/FLOAT(NOSTEP)
```

Figure C-9 Coding for the computer program MIXWG

```
      EUP = EBAR
      ELO = 0.02*EUP
      DTMAX = DELT
      DTMIN = DTMAX/FLOAT(2**10)
      TM = TIME + DTMAX
   40 CONTINUE
C
C COMPUTE DERIVATIVES INITIALLY
      CALL FUNC(N,T,Y,YDOT)
      J = 1
      DO 44 I=1,N
   44 F(I,J) = YDOT(I)
      K = 2
      RETURN
C
C
  100 CONTINUE
C
C INTEGRATE TO NEXT INTERVAL
      IF(EBAR.NE.0.) GO TO 130
C
C FIXED MODE
  110 IF(J.GT.3) GO TO 120
      CALLMGILL (FUNC,N,DT,T,Y,YDOT,TD)
       J = J+1
      DO 115 I=1,N
115   F(I,J) = YDOT(I)
      RETURN
C
C     CALL ADAM
120   CONTINUE
      CALLMADAM (FUNC,N,DT,T,Y,YDOT,TD)
      DO 125 M=1,3
      DO 125 I=1,N
  125 F(I,M) = F(I,M+1)
      DO 129 I=1,N
  129 F(I,4) = YDOT(I)
      RETURN
C
C VARIABLE MODE
  130 CONTINUE
      TIME = T
      IF(J.GT.3) GO TO 170
      CALL MGILL (FUNC,N,DT,T,Y,YDOT,    TD)
      J = J+1
      DO 137 I=1,N
  137 F(I,J) = YDOT(I)
      TIME = T
      GO TO (140,150,160,170),J
C
C 2A  J = 1
  140 CONTINUE
      IF(SIGN) GO TO 142
      IF(TIME+.50*DT .LE. TM) GO TO 145
      GO TO 130
  142 CONTINUE
      IF(TIME+.50*DT .GE. TM) GO TO 145
      GO TO 130
```

Figure C-10 Coding for the computer program MIXWG

```
  145 TM = TIME + DTMAX
      RETURN
C
C J = 2
  150 CALL MSAVE(MU,N,TIME,Y,YDOT,TD)
      GO TO 140
C
C J = 3
  160 L = 1
      GO TO 130
C
C J .GE. 3
  170 CONTINUE
      GO TO (180,250,280),L
C
C 38
  180 MU = -MU
C
C 3C
  185 CONTINUE
      CALL MSAVE(MU,N,TIMF,Y,YDOL,TD)
  187 CALL MADAM(FUNC,N,DT,T,Y,YDOT,TD)
C
C COMPUTE E(N+1)
  190 EN1 = 0.0
      TIME = T
      DO 195 M=1,3
      DO 195 I=1,N
  195 F(I,M) = F(I,M+1)
      DO 196 I=1,N
  196 F(I,4) = YDOT(I)
      DO 200 I=1,N
      DT = AMAX1 (ABS(Y(I)),.001)
      EN1 = AMAX1 (ABS(YP(I)-Y(I))/(14.0*DT),EN1)
  200 CONTINUE
C
C TEST E(N+1) .GE. EPSIL
      IF(EN1 .GE. EUP) GO TO 220
      IOOD = ABS((TIME-TM)/DT) + 0.1
      IF(MOD(IOOD,2) .NE. 0) GO TO 210
C EVEN
      IF(EN1 .GE. ELO) GO TO 210
        IF(ABS(2.0*DT) .GT. ABS(     DTMAX)) GO TO 210
      NU = 0
      L = 2
      GO TO 140
C 38
  210 L = 1
      GO TO 140
C EN1 .GE. EPSIL
C
  220 IF(ABS(.25*DT).GE. ABS(DTMIN)) GO TO 230
C GO TO ERROR
      K = -1
      WRITE (6,610) T
  610 FORMAT(/1X 'ERROR RETURN AT T =',E15.7/)
      RETURN
C
```

Figure C-11 Coding for the computer program MIXWG

```
C REDUCE STEP
  230 CONTINUE
      NOSTEP = NOSTEP+4
      DT = DELT/FLOAT(NOSTEP)
      CALL MRESTC-MU,N,TIME,Y,YDOT,TD)
      T = TIME
  232 CONTINUE
      IJ = 1
      DO 233 I=1,N
  233 F(I,1) = YDOT(I)
  235 CONTINUE
      CALL MGILL(FUNC,N,DT,T,Y,YDOT,TD)
      IJ = IJ+1
      DO 242 I=1,N
  242 F(I,IJ) = YDOT(I)
      IF(IJ .LE. 3) GO TO 235
      TIME = T
      CALL MSAVEC-MU,N,TIME,Y,YDOT,TD)
      CALL MADAM(FUNC,N,DT,T,Y,YDOT,TD)
      DO 243 M=1,3
      DO 243 I=1,N
  243 F(I,M) = F(I,M+1)
      DO 244 I=1,N
  244 F(I,4) = YDOT(I)
      GO TO 185
C
C 4A
  250 MU = -MU
      TIME = T
      CALL MSAVE(MU,N,TIME,Y,YDOT,TD)
  255 CALL MADAM(FUNC,N,DT,T,Y,YDOT,TD)
  260 EN1 = 0.
      TIME = T
      DO 265 M=1,3
      DO 265 I=1,N
  265 F(I,M) = F(I,M+1)
      DO 266 I=1,N
  266 F(I,4) = YDOT(I)
      DO 270 I=1,N
      DI = AMAX1(ABS(Y(I)),.001)
      EN1 = AMAX1(ABS(YP(I)-Y(I))/(14.0*DI),EN1)
  270 CONTINUE
      IF(EN1 .GE. ELO) GO TO 210
      NU = NU+1
      IF(NU .LT. 2) GO TO 130
      IF( ABS(AMOD(TM-T,2*DT)) .GT. ABS(DTMIN)) GO TO 130
      NOSTEP = NOSTEP/2
      DT = DELT/FLOAT(NOSTEP)
      TIME = T
      CALL MSAVE(MU,N,TIME,Y,YDOT,TD)
      II = 0
      L = 3
      GO TO 140
C
C 4B
  280 CALL MGILL(FUNC,N,DT,T,Y,YDOT,TD)
      II = II+1
      DO 295 I=1,N
```

Figure C-12 Coding for the computer program MIXWG

```
  295 F(I,II) = YDOT(I)
      TIME = T
      IF(II .GT. 3) GO TO 210
      IJIJ=0
      IF (IJIJ.EQ.1) GO TO 625
      GO TO 140
625   CONTINUE
      STOP
      END
      SUBROUTINE MADAMK(FUNC,N,DT,T,Y,YDOT,TO)
C     * * * * * * * * * * * * * * * * * * * * * * * * * * * * * * * * * * * *
      DOUBLE PRECISION TA,TB
      DOUBLE PRECISION DP,TO,YDP,YDC(90)
      COMMON /SAVDEQ/ TA,YDPA(90),YDOTA(90),TB,YDPB(90),YDOTB(90),
     1 YDP(90  ),F(90,4),YP(90)
      DIMENSION Y(90),YDOT(90)
      TO =TO+DT
      T = TO
      DO 40 LSTEP=1,2
      DO 30 I=1,N
      GO TO (10,15),LSTEP
   10 DP = Y(I)+(DT/24.DO)*(55.DDO*F(I,4)-59.DDO*F(I,3)+37.DDO*F(I,2)
     1 -9.DDDO*F(I,1))
C     YDP(I,1) = DP
      GO TO 20
   15 DP = YP(I)+(DT/24.DDO)*(9.DDO*YDOT(I)+19.DDO*F(I,4)-5.DDO*F(I,3)+
     1 F(I,2))
C     YDC(I) = DP
   20 CONTINUE
      YP(I) = Y(I)
      SP = DP
      D1 = DP-SP
      Y(I) = DP+D1
   30 CONTINUE
      CALL FUNC(N,T,Y,YDOT)
   40 CONTINUE
      RETURN
      END
      SUBROUTINE MGILL(FUNC,N,DT,T,Y,YDOT,TO)
C     * * * * * * * * * * * * * * * * * * * * * * * * * * * * * * * * * * * *
      DIMENSION C(3),B(3),Q(90),Y(90),YDOT(90)
      DOUBLE PRECISION TA,TB
      DOUBLE PRECISION DP,YDP,TO,T1,K,B,C
      COMMON /SAVDEQ/ TA,YDPA(90),YDOTA(90),TB,YDPB(90),YDOTB(90),
     1 YDP(90  ),F(90,4),YP(90)
      DATA B,C/0.DDO, .58578643800, 3.41421356200, 0., .12132034300,
     1 -4.121320343/
      T1 = TO
      TO = TO+.5DO*DT
      DO 60 LSTEP=1,4
      DO 50 I=1,N
      K = DT*YDOT(I)
      GO TO (10,20,20,30),LSTEP
   10 YDP(I       ) = Y(I)+.5DO*K
      Q(I) = K
      GO TO 40
   20 YDP(I       )=YDP(I       )+.5DO*B(LSTEP)*(K-Q(I))
      Q(I) = B(LSTEP)*K+C(LSTEP)*Q(I)
      GO TO 40
   30 YDP(I       )=YDP(I       )+(K*.5DO-Q(I))/3.DDO
   40 DP = YDP(I)
```

Figure C-13 Coding for the computer program MIXWG

```
      SP = DP
      D1 = DP-SP
      Y(I) = DP+D1
   50 CONTINUE
      IF(LSTEP .EQ. 3) TO=T1+DT
      T = TO
      CALL FUNC(N,T,Y,YDOT)
   60 CONTINUE
      RETURN
      END
      SUBROUTINE MREST(MU,N,TIME,Y,YDOT,TO)
C     * * * * * * * * * * * * * * * * * * * * * * * * * * * * * * * * * *
      DOUBLE PRECISION TO,TA,TB,YDP
      COMMON /SAVDEQ/ TA,YDPA(90),YDOTA(90),TB,YDPB(90),YDOTB(90),
     1 YDP(90   ),F(90,4),YP(90)
      DIMENSION Y(90),YDOT(90)
      IF(MU .GT. 0) GO TO 30
      DO 20 I=1,N
      Y(I) = YDPB(I)
   20 YDOT(I) = YDOTB(I)
      TO = TB
      TIME = TB
      RETURN
C
C MU .GT. 0
   30 CONTINUE
      DO 40 I=1,N
      Y  (I) = YDPA(I)
   40 YDOT(I) = YDOTA(I)
      TO = TA
      TIME = TA
      RETURN
C
C SAVE
      ENTRY MSAVE(MU,N,TIME,Y,YDOT,TO)
      IF(MU .GT. 0) GO TO 70
      TB = TO
      DO 60 I=1,N
      YDPB(I) = Y  (I)
   60 YDOTB(I) = YDOT(I)
      RETURN
   70 CONTINUE
      TA = TO
      DO 80 I=1,N
      YDPA(I) = Y  (I)
   80 YDOTA(I) = YDOT(I)
      RETURN
      END
C     DATA DECK
          0.1590
                 00.01
 0          .01      300.0     100.0
        300.     300.     425.     850.     425.     300.     300.     300.
   1.0E 00 0.0E 00 0.0E 00 0.0E 00 0.0E 00 0.0E 00 0.0E 00 0.0E 00 0.0E
   1.0E 00 0.0E 00 0.0E 00 0.0E 00 0.0E 00 0.0E 00 0.0E 00 0.0E 00 0.0E
   1.0E 00 0.0E 00 0.0E 00 0.0E 00 0.0E 00 0.0E 00 0.0E 00 0.0E 00 0.0E
   9.0E-01 3.3E-05 3.0E-05 3.3E-04 3.3E-03 1.0E-02 3.0E-02 0.0E 00 0.0E
   0.0E 00 1.0E 00 0.0E 00 0.0E 00 0.0E 00 0.0E 00 0.0E 00 0.0E 00 0.0E
   0.0E 00 1.0E 00 0.0E 00 0.0E 00 0.0E 00 0.0E 00 0.0E 00 0.0E 00 0.0E
   0.0E 00 1.0E 00 0.0E 00 0.0E 00 0.0E 00 0.0E 00 0.0E 00 0.0E 00 0.0E
   0.0E 00 1.0E 00 0.0E 00 0.0E 00 0.0E 00 0.0E 00 0.0E 00 0.0E 00 0.0E
   0.0E 00 1.0E 00 0.0E 00 0.0E 00 0.0E 00 0.0E 00 0.0E 00 0.0E 00 0.0E
```

Figure C-14   Coding for the computer program MIXWG

```
      EXTERNAL VVCOX
      EXTERNAL DIFFY
      DIMENSION CO(20),COOOT(20),ZZ(21),IMINUS(21),TAV(21),PRON(21)
      DIMENSION IPS(21),YY(9),CVV(20),COV(20,21),XAV(3,21),XXV(3,21)
      DIMENSION A(3,9,21),XOOT(18),Y(9,21),X(18),TEMP(9,21)
      DIMENSION ZC(21),VLCT(9,21),ZPZN(20)
      COMMON/WRATE/CONST
      COMMON/TRATE/ALPHA
      COMMON/VRATE/KVT1,KVT2,KVT3,KVV
      COMMON/DRATE/DO
      COMMON/SPEED/UO2,UCS2,U
      COMMON/VVCOT/TAV,XXV,PRON
      COMMON/CMIX11/TO,TINF,P,NY,NZ,NZ1
      COMMON/CMIX12/ZLENGH,DZ,HEIGHT,DY,MIDY,MIDYM,MIDYP
      REAL KVT1,KVT2,KVT3,KVV
C     CGS UNITS.  NZSTEP IS THE NUMBER OF Z STEPS.  NZSTEP=1 IS INITIAL.
C     A(I,J,NZSTEP) IS THE MOLE FRACTION OF SPECIES I AT Y LOCATION J.
C     AND NZSTEP.  I=1 => O2.  I=2 => CS2.  I=3 => PRODUCT
C     TEMP(J,NZSTEP)
C     Y HAS DIMENSION = 2*NY
C     NY=THE NUMBER OF Y LOCATIONS.
C     X(1,2,3... N) ARE O2 CONCENTRATIONS.              (IN MOLE FRACTION)
C     X(N+1,N+2,N+3... 2*N) ARE CS2 CONCENTRATIONS.     (IN MOLE FRACTION)
      READ (5,66) DO,ALPHA,CONST,KVT1,KVT2,KVT3
      READ (5,67) KVV
      WRITE (6,65) DO,ALPHA,CONST,KVT1,KVT2,KVT3,KVV
      READ (5,64) CZ,EPS
      READ (5,63) IPUNCH,P,TO,TINF,UO2,UCS2
      READ (5,62) (CO(J),J=1,5)
      READ (5,62) (CO(J),J=6,10)
      READ (5,62) (CO(J),J=11,15)
      READ (5,62) (CO(J),J=16,20)
      WRITE (6,64) CZ,EPS
      WRITE (6,63) IPUNCH,P,TO,TINF,UO2,UCS2
      WRITE (6,62) (CO(J),J=1,5)
      WRITE (6,62) (CO(J),J=6,10)
      WRITE (6,62) (CO(J),J=11,15)
      WRITE (6,62) (CO(J),J=16,20)
      U=(UCS2+UO2)/2.0
      NY=9
      NZ=20
      HEIGHT=4.0
      ZLENGH=4.0
      DZ=ZLENGH/NZ
      DY=HEIGHT/(NY-1)
      Z=0.0
      N=2*NY
      NZ1=NZ+1
C     KIK=1 IMPLIES STEP ONE. MODDEQ RESETS IT TO 2 LATER.
C     AND -1 TO INDICATE ERRORS.
      KIK=1
      NEQNS=N
      DO 500 I=1,NZ1
      IPS(I)=I+1
      IMINUS(I)=I-1
      ZZ(I)=IMINUS(I)+DZ
500   CONTINUE
C     THE STREAMWISE COORDINATE IN SPACE IS Z.
```

Figure C-15 Coding for the computer program MIX60

```
C     NEXT, THE VALUES OF CONCENTRATION ARE INITIALIZED.
      MIDY =(NY+1)/2
      MIDYP=(NY+3)/2
      MIDYM=(NY-1)/2
        NMCSD=MIDY +NY
      D2INT= .40
      CS2INT=.40
      X(NMCSD)=CS2INT
      X(MIDY) =D2INT
      DD 133 I=1,MIDYM
      II=I+NY
      X(I)=0.0
      X(II)=1.0
133   CONTINUE
      DD 510 I=1,NY
      YY(I)=(I-MIDY)*DY
510   CONTINUE
      DD 134 I=MIDYP,NY
      II=I+NY
      X(I)=1.0
      X(II)=0.0
134   CONTINUE
      NZSTEP=1
      DD 209 J=1,NY
      JJ=J+NY
      VLCT(J,1)=VEL(X(J),X(JJ))
      A(1,J,NZSTEP)=X(J)
      A(2,J,NZSTEP)=X(JJ)
      A(3,J,NZSTEP)=1.0-X(J)-X(JJ)
      TEMP(J,NZSTEP)=THAM(X(J),X(JJ))
209   CONTINUE
      DD 100 I=1,NZ1
      NZSTEP=I
C     * * * * * * * * * * * * * * * * * * * * * * * * * * * * * * * * * * * * *
      CALL MDDEQ(DIFFY,KIK,NEQNS,Z,X,XDOT,DZ,EPS)
C     * * * * * * * * * * * * * * * * * * * * * * * * * * * * * * * * * * * * *
      DD 210 J=1,NY
      JJ=J+NY
      A(1,J,NZSTEP)=X(J)
      A(2,J,NZSTEP)=X(JJ)
      A(3,J,NZSTEP)=1.0-X(J)-X(JJ)
      TEMP(J,NZSTEP)=THAM(X(J),X(JJ))
      VLCT(J,I)=VEL(X(J),X(JJ))
C     TEMP IS THE TEMPERATURE IN DEGREES KELVIN.
210   CONTINUE
       WRITE (6,11)
      WRITE (6,26) NZSTEP
      WRITE (6,20) (TEMP(K,NZSTEP),K=1,9)
      WRITE (6,21) (A(3,K,NZSTEP),K=1,9)
      WRITE (6,22) (A(2,K,NZSTEP),K=1,9)
      WRITE (6,23) (XDOT(K),K=10,18)
      WRITE (6,24) (A(1,K,NZSTEP),K=1,9)
      WRITE (6,25) (XDOT(K),K=1,9)
      WRITE (6,54) (VLCT(J,I),J=1,NY)
100   CONTINUE
C      THE HOWARTH TRANSFORM ACCOUNTS FOR THERMAL COMPRESSIBILITY.
C     THERE IS NO NET VERTICAL VELOCITY.
      MIDY=(NY+1)/2
      MIDYM=MIDY-1
```

Figure C-16 Coding for the computer program MIX60

```
      DYT   =DY/(2*TO)
C     THIS WILL WORK ONLY IF TEMP=TO INITIALLY EVERYWHERE EXCEPT
C      AT THE MID Y POINT.
      DO 160 I=1,NZ1
      Y(MIDY,I)=0.0
      DO 150 J=1,MIDYM
      JON=MIDY-J
      JUP=MIDY+J
      JUPM=JUP-1
      JONP=JON+1
      Y(JUP,I)=Y(JUPM,I)+    (TEMP(JUP,I)+TEMP(JUPM,I))*DYT
      Y(JON,I)=Y(JONP,I)-    (TEMP(JON,I)+TEMP(JONP,I))*DYT
150   CONTINUE
160   CONTINUE
C     THIS SECTION FOLLOWS THE FLUIDS AND CHEMISRY.
C     SETS UP AVERAGED CONDITIONS ACROSS A VERTICAL TRAVERSE.
C     HERE THE AVERAGES ARE TAKEN OF THE FLUID AND CHEMICAL PROPERTIES.
C     THESE AVERAGES ARE USED IN THE VIBRATIONAL KINETICS TO FOLLOW.
      DO 166 IZ=1,NZ1
      DO 164 I=1,3
      XAV(I,IZ)=0.0
      DO 165 J=1,NY
      XAV(I,IZ)=A(I,J,IZ)+XAV(I,IZ)
165   CONTINUE
164   CONTINUE
       WRITE (6,11)
      WRITE (6,27)
      WRITE (6,30) IZ,XAV(1,IZ),XAV(2,IZ),XAV(3,IZ)
166   CONTINUE
      DO 167 IZ=1,NZ1
      DO 169 I=1,3
      DO 168 J=1,NY
      XXV(I,IZ)=A(I,J,IZ)*A(3,J,IZ)/XAV(I,IZ)+XXV(I,IZ)
168   CONTINUE
169   CONTINUE
       WRITE (6,11)
      WRITE (6,29)
      WRITE (6,30) IZ,XXV(1,IZ),XXV(2,IZ),XXV(3,IZ)
167   CONTINUE
      BETA=0.2
      DO 170 IZ=1,NZ1
      PRON(IZ)=0.0
170   CONTINUE
      DIV=XAV(3,NZ1)-XAV(3,1)
      DO 161 IZ=1,NZ
      TAV(IZ)=0.0
      PRON(IZ)=0.0
      IZ1=IZ+1
      DO 162 J=1,NY
      TAV(IZ)=TAV(IZ)+TEMP(J,IZ)*A(3,J,IZ)/XAV(3,IZ)
      PRON(IZ)=A(3,J,IZ1)*(A(3,J,IZ1)-A(3,J,IZ))+PRON(IZ)
162   CONTINUE
      PRON(IZ)=BETA*PRON(IZ)/DIV
      IF (PRON(IZ).LT.0.) PRON(IZ)=0.0
       WRITE (6,11)
      WRITE (6,31)
      WRITE (6,32) IZ,TAV(IZ),PRON(IZ)
161   CONTINUE
```

Figure C-17 Coding for the computer program MIX60

```
      GO TO 535
171   CONTINUE
C     XAV(I,IZ) IS A SUM OVER Y STATIONS OF SPECIES I MOLE FRACTIONS.
C     XXV(I,IZ) IS A NORMALIZED MOMENT OF SPECIES I WITH PRODUCT.
C     PRON(IZ) IS THE CO PRODUCTION BETWEEN STATIONS IZ+U AND IZ.
C     BETA TIMES THE TOTAL PRODUCTION = THE CO PRODUCTION.PRON.
C     TAV(IZ) IS A NORMALIZED MOMENT OF T WITH PRODUCT. (T=TEMPERATURE)
C     THE FOLLOWING SECTION CALLS THE ONE DIMENSIONAL VIBRATIONAL
C     KINETICS PROGRAM.
      KIK=1
      NC=20
C     IF YOU CHANGE NC, YOU MUST BE SURE TO CHECK THE WRITE STATEMENTS
C      FOLLOWING STATEMENT 570, AND THAT IMINUS IS DIMENSIONED
C      LARGER THAN NC.
      DO 690 I=1,NZ1
      ZC(I)=CZ*IMINUS(I)
690   CONTINUE
      Z=0.0
      NZN=20
      C2=CZ/NZN
      DO 900 I=1,NZ
C     * * * * * * * * * * * * * * * * * * * * * * * * * * * * * * * * * *
      IF (I.EQ.1) GO TO 905
      DO 905 J=1,NZN
905      CALL MODEEQ(VVCOX,KIK,20,Z,CO,CDOT,C2,EPS)
C     * * * * * * * * * * * * * * * * * * * * * * * * * * * * * * * * * *
      DENSTY=P*300.0*6.02E 23/(TAV(I)*24500.)
      DO 910 J=1,20
      COV(J,I)      =COK(J)*DENSTY
910   CONTINUE
C          COV STORES THE CO NUMBER DENSITY IN UNITS OF INVERSE
C     CENTIMETERS CUBED AND MOLES.
C     COV(J,NZSTEP) IS THE CO POPULATION IN LEVEL J-1 AT Z INDEX NZSTEP
       WRITE (6,11)
      WRITE (6,40) I,(COK(K),K=1,10)
      WRITE (6,41) (CDOT(K),K=1,10)
      WRITE (6,41) (COK(K),K=11,20)
      WRITE (6,41) (CDOT(K),K=11,20)
      IF (KIK.LT.0) GO TO 810
      GO TO 900
810   WRITE (6,50)
900   CONTINUE
      GO TO 570
C     REFERENCES
C     * * * * * * * * * * * * * * * * * * * * * * * * * * * * * * * * * *
C     THE DECAY VV RATES ARE FROM W. Q. JEFFERS. 'CARBON MONOXIDE
C     CHEMICAL LASER RESEARCH.' FINAL TECHNICAL REPORT, CONTRACT
C     DAAH01-72-C-0578 (1973).
C     THE VT DECAY RATES WERE FROM G. HANCOCK AND I. W. SMITH,
C     'QUENCHING OF INFRARED CHEMILUMINESCENCE. 1: THE RATES OF
C     DE-EXCITATION OF CO(3<V<14) BY HE, CO, NO, N2, 02, OCS, N20,
C     AND C02.' 'JOURNEL OF APPLIED PHYSICS.' VOL. 10, PP 1827-1842
C     (1971)
C     THE RATES FOR THE PRODUCT DISTRIBUTION WERE TAKEN FROM
C     G. HANCOCK, B. A. RIDLEY, AND I. M. SMITH, 'INFRARED CHEM-
C     ILUMINESCENCE FROM VIBRATIONALLY EXCITED CO,' 'JOURNEL OF
C     THE CHEMICAL SOCIETY, FARADAY TRANSACTIONS II,' VOL. 68 .
C     PP 2117-2126 (1972).
```

Figure C-18 Coding for the computer program MIX60

```
C     THE CHEMICAL RATES WERE FROM A. A. VETTER, 'PHD THESIS,'
C     CALIFORNIA INSTITUTE OF TECHNOLOGY (1975), AND FROM R. W. GROSS
C     AND J. F. BOTT, 'THE HANDBOOK OF CHEMICAL LASERS,' JOHN WILEY AND
C     SONS (1976).
C     * * * * * * * * * * * * * * * * * * * * * * * * * * * * * * * * * *
C     FORMATS
1     FORMAT (4X,I4,4X,10E10.3)
2     FORMAT (4X,I4,4X,11E10.3)
3     FORMAT (4X,F10.3,4X,9E10.3)
4     FORMAT ('0          Z IN
     +          Y IN CM')
5     FORMAT ('           CM')
6     FORMAT ('1Z IN CM.          Y VALUES AS A FUNCTION OF INITIAL Y')
7     FORMAT ('1VIBRATIONAL                              Z IN CENTIMETERS')
8     FORMAT ('    LEVEL')
9     FORMAT (8X,10F10.3)
10    FORMAT (12X,11F10.3)
11    FORMAT ('0')
12    FORMAT ('1        TEMPERATURE IN DEGREES KELVIN')
13    FORMAT ('1        CS2      MOLE FRACTIONS')
14    FORMAT ('1        O2       MOLE FRACTIONS')
15    FORMAT ('1        PRODUCT  MOLE FRACTIONS')
16    FORMAT (16X,9F10.3)
17    FORMAT (3X,F10.3,3X,9F10.3)
18    FORMAT (16X,9F12.3)
19    FORMAT (4X,F10.3,4X,9F12.5)
20    FORMAT (' TEMP ',9F12.5)
21    FORMAT (' PROD ',9F12.5)
22    FORMAT (' CS2  ',9F12.5)
23    FORMAT (' CSDOT',9F12.5)
24    FORMAT (' O2   ',9F12.5)
25    FORMAT (' O2DOT',9F12.5)
26    FORMAT (4X,I4)
27    FORMAT (' POSITION     SUMS:              O2          CS2
     * PROD')
29    FORMAT (' POSITION  MOMENTS:              O2          CS2
     * PROD')
30    FORMAT (4X,I4,20X,3F12.5)
31    FORMAT (' POSITION   AVERAGES:          TEMP            PRODUCTION')
32    FORMAT (4X,I4,20X,2F12.5)
40    FORMAT (2X,I4,2X,10E12.5)
41    FORMAT (8X,10E12.5)
50    FORMAT (' ERROR? ERROR? ERROR?  KIK<0')
54    FORMAT (' VLCTY',9F12.5)
57    FORMAT (' VELOCITIES')
58    FORMAT (4X,I4,9X,9E12.3)
60    FORMAT (4X,9F8.4)
61    FORMAT (4X,9F8.1)
62    FORMAT (5X,5E12.5)
63    FORMAT (2X,I1,2X,5F10.4)
64    FORMAT (5X,2F15.7)
65    FORMAT (5X,7E12.5)
66    FORMAT (5X,6E12.5)
67    FORMAT (5X, E12.5)
70    FORMAT (9X,5E14.4)
C     TO WRITE CO(V) FOR V=0.... 19 AT  NZSTEP = 1,2.... 10:
C     WRITE STATEMENTS
C     * * * * * * * * * * * * * * * * * * * * * * * * * * * * * * * * * *
```

Figure C-19 Coding for the computer program MIX60

```
535   CONTINUE
C     TO WRITE THE TEMPERATURE.
      WRITE (6,11)
      WRITE(6,12)
      WRITE(6,4)
      WRITE(6,5)
      WRITE(6,16) (YY(I),I=1,NY)
      WRITE(6,11)
      DO 540 I=1,NZ1
      WRITE(6,17) ZZ(I),(TEMP(J,I),J=1,NY)
540   CONTINUE
C     THE FOLLOWING PRINTS OUT AN ARRAY OF Y VALUES FROM THE INVERSE
C     HOWARTH TRANSFORM BACK.  THESE VALUES TRACE STREAMLINES ALONG
C     THE FLOW, DESINNATING THE Y VALUE AS WE MOVE IN Z.
      M=1
      WRITE (6,11)
      WRITE(6,14)
      WRITE(6,4)
      WRITE(6,5)
        WRITE(6,18) (YY(I),I=1,NY)
      WRITE(6,11)
      DO 433 I=1,NZ1
      WRITE(6,19) ZZ(I),(A(M,J,I),J=1,NY)
433   CONTINUE
      M=2
      WRITE (6,11)
      WRITE(6,13)
      WRITE(6,4)
      WRITE(6,5)
        WRITE(6,18) (YY(I),I=1,NY)
      WRITE(6,11)
      DO 434 I=1,NZ1
      WRITE(6,19) ZZ(I),(A(M,J,I),J=1,NY)
434   CONTINUE
      M=3
      WRITE (6,11)
      WRITE (6,15)
      WRITE(6,4)
      WRITE(6,5)
        WRITE(6,18) (YY(I),I=1,NY)
      WRITE(6,11)
      DO 435 I=1,NZ1
      WRITE(6,19) ZZ(I),(A(M,J,I),J=1,NY)
435   CONTINUE
      WRITE (6,11)
      WRITE(6,6)
      WRITE(6,16) (YY(I),I=1,NY)
      WRITE (6,11)
      DO 560 I=1,NZ1
      WRITE(6,17) ZZ(I),(Y(J,I),J=1,NY)
560   CONTINUE
      WRITE (6,11)
      WRITE (6,57)
        WRITE(6,18) (YY(I),I=1,NY)
      DO 655 I=1,NZ
      WRITE (6,58) I,(VLCT(J,I),J=1,NY)
655   CONTINUE
      IF (IPUNCH.EQ.1) GO TO 580
```

Figure C-20 Coding for the computer program MIX60

```
      WRITE (7,60) (YY(J),J=1,NY)
      DO 890 I=1,NZ1
      WRITE (7,60) (A(1,J,I),J=1,NY)
      WRITE (7,60) (A(2,J,I),J=1,NY)
      WRITE (7,60) (A(3,J,I),J=1,NY)
      WRITE (7,60) (Y(J,I),J=1,NY)
      WRITE (7,61) (TEMP(J,I),J=1,NY)
      WRITE (7,61) (VLCT(J,I),J=1,NY)
890   CONTINUE
580   CONTINUE
      GO TO 171
570   CONTINUE
      WRITE (6,11)
      WRITE(6,7)
      WRITE(6,8)
      WRITE(6,9) (ZC(I),I=1,10)
      WRITE(6,11)
      DO 520 I=1,20
      WRITE(6,1) IMINUS(I),(COV(I,NZSTEP),NZSTEP=1,10)
520   CONTINUE
C     TO WRITE COV(V) FOR V=0.1,... 19 AT NZSTEP=11,12,... 21.
      WRITE(6,11)
      WRITE(6,7)
      WRITE(6,8)
      WRITE(6,9) (ZC(I),I=11,20)
      WRITE(6,11)
      DO 525 I=1,20
      WRITE(6,2) IMINUS(I),(COV(I,NZSTEP),NZSTEP=11,20)
525   CONTINUE
      IF (IPUNCH.EQ.1) GO TO 585
      DO 895 I=1,NZ
      WRITE (7,70) (COV(J,I),J=1,5)
      WRITE (7,70) (COV(J,I),J=6,10)
      WRITE (7,70) (COV(J,I),J=11,15)
      WRITE (7,70) (COV(J,I),J=16,20)
895   CONTINUE
585   CONTINUE
      RETURN
      END
      FUNCTION VEL(XSA,XSB)
C     * * * * * * * * * * * * * * * * * * * * * * * * * * * * * * * * * * *
      COMMON/SPEED/U02,UCS2,U
      VEL=U02*XSA+UCS2*XSB+U*(1.0-XSA-XSB)
C     VEL COMPUTES THE VELOCITY PURELY FROM THE SPECIES CONCENTRATIONS.
      RETURN
      END
      FUNCTION W(XSA,XSB)
C     * * * * * * * * * * * * * * * * * * * * * * * * * * * * * * * * * * *
      COMMON/WRATE/CONST
      COMMON/CMIX11/TO,TINF,P,NY,NZ,NZ1
      COMMON/CMIX12/ZLENGH,DZ,HEIGHT,DY,MIDY,MIDYM,MIDYP
C     W(XSA,XSB) IS THE NET MOLAR FRACTION REACTION RATE.
C     A FUNCTION OF THE COMPOSITION CHEMICALLY AND THE TEMPERATURE,
C     AND THE TEMPERATURE DEPENDS SOLELY ON THE CHEMICAL COMPOSITION.
C     J=I+NY
C     TMP  IS THE TEMPERATURE IN DEGREES K. P IS THE PRESSURE IN ATM.
C      RHO IS THE DENSITY IN MOLES/CC.   CONST IS THE THE REACTION RATE
C     ASSUMING THAT THE RATE LIMITING REACTION IS SO+O2 => SO2+O
```

Figure C-21 Coding for the computer program MIX60

```
      TMP =THRM(XSA,XSB)
      RHO=(1.22E-2)*P/TMP
      AHRR=-14600./TMP
      UU=VEL(XSA,XSB)
      W=-CONST*RHO*XSA*XSB*EXP(AHRR)/UU
C     START SECTION A2  MIX1.   THE FUNCTION THRM
      RETURN
      END
      FUNCTION THRM(XSA,XSB)
C     * * * * * * * * * * * * * * * * * * * * * * * * * * * * * * * * * * * *
      COMMON/TRATE/ALPHA
      COMMON/CMIX11/TO,TINF,P,NY,NZ,NZ1
      COMMON/CMIX12/ZLENGH,DZ,HEIGHT,DY,MIDY,MIDYM,MIDYP
C     THRM COMPUTES THE TEMPERATURE GIVEN THE CHEMICAL COMPOSITION.
C     THRM HAS A NONLINEAR DEPENDENCE ON PRODUCT CONCENTRATION.
C     THRM TAKES THE TEMPERATURE TO ASYMPTOTICALLY APPROACH THE
C     ADIABATIC FLAME TEMPERATURE  MAXIMUM AS THE PRODUCT MOLE
C     FRACTION APPROACHES UNITY.
C     J=1+NY
      PROD=1.0-XSA-XSB
      IF (PROD.GT.1.0) PROD=1.0
      IF (PROD.LT.0.0) PROD=0.0
      SORM=(1.0-EXP(-ALPHA))
      ALPROD=-ALPHA*PROD
      THRM=TO+(TINF-TO)*(1.0-EXP(ALPROD))/SORM
C     XSA IS THE 02 CONCENTRATION? XSB IS THE CS2 CONCENTRATION.
C     BOTH IN MOLE FRACTIONS.
C     THRM IS IN DEGREES K  -NOT-  A NORMALIZED TEMPERATURE.
      RETURN
      END
      SUBROUTINE DIFFY(N,Z,X,XDOT)
C     * * * * * * * * * * * * * * * * * * * * * * * * * * * * * * * * * * * *
      DIMENSION DUDY(9)
      DIMENSION X(18),XDOT(18)
      COMMON/DRATE/DO
      COMMON/CMIX11/TO,TINF,P,NY,NZ,NZ1
      COMMON/CMIX12/ZLENGH,DZ,HEIGHT,DY,MIDY,MIDYM,MIDYP
      D=DO/P
C     D IS THE DIFFUSION CONSTANT IN (CM*CM/SEC).
          DO 75 J=1,NY
      JJ=J+NY
      DUDY(J)=(D/(DY*DY))/VEL(X(J),X(JJ))
75    CONTINUE
      XDOT(1)=2.0*DUDY(1)*(X(2)-X(1))+W(X(1),X(10))
      XDOT(9)=2.0*DUDY(9)*(X(8)-X(9))+W(X(9),X(18))
      XDOT(10)=2.0*DUDY(1)*(X(11)-X(10))+W(X(10),X(1))
      XDOT(18)=2.0*DUDY(9)*(X(17)-X(18))+W(X(18),X(9))
      DO 73 L=2,8
      LS=L-1
      LG=L+1
      KG=LG+9
      KS=LS+9
      K=L+9
      XDOT(K)=DUDY(L)*(X(KS)+X(KG)-2.0*X(K))+W(X(L),X(K))
      XDOT(L)=DUDY(L)*(X(LS)+X(LG)-2.0*X(L))+W(X(L),X(K))
73    CONTINUE
      RETURN
      END
      SUBROUTINE VVCOX(N,Z,CO,CODOT)
C     * * * * * * * * * * * * * * * * * * * * * * * * * * * * * * * * * * * *
      DIMENSION CO(20), CODOT(20), TAV(21), XXV(3,21), PRDN(21), COO(20)
      COMMON/VRATE/KVT1,KVT2,KVT3,KVV
```

Figure C-22 Coding for the computer program MIX60

```
      COMMON/CMIX11/TO,TINF,P,NY,NZ,NZ1
      COMMON/SPEED/UO2,UCS2,U
      COMMON/CMIX12/ZLENGH,DZ,HEIGHT,DY,MIDY,MIDYM,MIDYP
      COMMON/VVCOT/TAV,XXV,PRON
      REAL KVT1,KVT2,KVT3,KVV
11    FORMAT ('0')
42    FORMAT (' V, CO(V), CODOT(V), VT1, VT2, VT3, VVCOVV, COADD, EPXFO1
     +,EPXFO2, EPXPR1, EPXPR2')
43    FORMAT (' Z STATION=',I4,'   Z=',E10.3,'   V=',I4,'   CO(V)=',E12.
     *5,'   CODOT(V)=',E12.5)
44    FORMAT (' IZ=',I4,' Z=',E10.4,' V=',I4,' CO=',E12.5,' CODOT=',
     + E12.5,5E12.5)
45    FORMAT (1X,9E12.5)
C      WRITE (6,11)
C     WRITE (6,42)
C     COO IS THE INITIAL DISTRIBUTION OF CO FROM THE PUMPING
C     REACTION, CS + O => CO(V) + S.
      DO 815 I=1,7
      COO(I)=0.0
815   CONTINUE
      DO 816 I=17,20
816   COO(I)=0.0
      COO(8)=.012
      COO(9)=.053
      COO(10)=.119
      COO(11)=.129
      COO(12)=.157
      COO(13)=.170
      COO(14)=.196
      COO(15)=.125
      COO(16)=.039
C     THESE NUMBERS INDICATE THE RELATIVE PUMPING RATES TO  THE
C     DIFFERENT VIBRATIONAL LEVELS BY CHEMICAL  PRODUCTION.
C     END PG1, SECT. A4 MIX1,  SUBROUTINE VVCOT TO SET UP THE VIB D.E.
C     START PG2,SEC A4  MIX1,  SUBROUTINE VVCOT TO SET UP THE VIB D.E.
      DO 400 I=1,20
      IU=I+1
      IUU=I+2
      IO=I-1
      IOO=I-2
      J1=I-5
      J2=I-4
C     LATER, ONE MIGHT ALTER THIS SECTION SO THAT INTERPOLATED AVERAGE
C     VALUES ALONG Z WERE USED INSTEAD OF TRUNCATING Z/DZ TO USE
C     THE VALUES AT LATTICE POINTS ON Z.
      ZDZ=Z/DZ
      MZ=AINT(ZDZ)+1
      COADD=(PRON(MZ)/DZ)*COO(I)*U
      ARGFO1=-.75*(24-I)  *300.0/TAV(MZ)
      ARGFO2=-.75*(23-I)  *300.0/TAV(MZ)
      ARGPR1=-.34*IABS(J1)*300.0/TAV(MZ)
      ARGPR2=-.34*IABS(J2)*300.0/TAV(MZ)
      EPXFO1=EXP(ARGFO1)
      EPXFO2=EXP(ARGFO2)
      EPXPR1=EXP(ARGPR1)
      EPXPR2=EXP(ARGPR2)
      S=EXP(-2800.0/TAV(MZ))
      IF (I.NE.20)
     *COVOIU=CO(IU)-S*CO(I)
      IF (I.NE.1)
     *COVOI=CO(I)-S*CO(IO)
      IF (I.EQ.20) GO TO 707
```

Figure C-23 Coding for the computer program MIX60

```
      IF (I.EQ.1) GO TO 706
      RHO=1.22E-2*P/TAV(MZ)
      VT1=RHO*KVT1   *XXV(1,MZ)*(C0V0IU*EPXF02-C0V0I*EPXF01)
      VT2=RHO*KVT2   *XXV(2,MZ)*(C0V0IU*EPXF02-C0V0I*EPXF01)
      VT3=RHO*KVT3   *XXV(3,MZ)*(C0V0IU*EPXPR2-C0V0I*EPXPR1)
C     VT1, VT2, VT3, ARE THE V-T ONE QUANTA DECAY RATES WITH SPECIES
C     02,CS2, AND PRODUCT RESPECTIVELY.  THE FIRST TERM IS TRANSFER IN
C     FROM THE LEVEL ABOVE (NOTE THE TERM C0(IU)), AND THE
C     SECOND TERM IS LOSS FROM THE LEVEL I (NOTE THE TERM WITH -C0(I)).
      ARGG=-27.0/TAV(MZ)
      R=EXP(ARGG)
C     R IS THE RATIO OF REVERSE TO FORWARD VV PUMPING RATES.
      GO TO 701
707   CONTINUE
C     I=20 CASE FOLLOWS? NO HIGHER VIBRATIONAL LEVELS.
      VT1=  KVT1*XXV(1,MZ)*(-C0V0I*EPXF01*RHO)
      VT2=  KVT2*XXV(2,MZ)*(-C0V0I*EPXF01*RHO)
      VT3=  KVT3*XXV(3,MZ)*(-C0V0I*EPXPR2*RHO)
            VVC0VV=KVV    *(     C0(ID)*ID*C0(ID)-C0(I)*ID*C0(IDD)*R)
      GO TO 710
706   CONTINUE
C     I=1 CASE FOLLOWS, NO LOWER LEVELS.
      VT1=RHO*KVT1   *XXV(1,MZ)*C0V0IU*EPXF02
      VT2=RHO*KVT2   *XXV(2,MZ)*C0V0IU*EPXF02
      VT3=RHO*KVT3   *XXV(3,MZ)*C0V0IU*EPXPR2
      VVC0VV=KVV    *(C0(IU)*IU*C0(IU)     -C0(I)*(       R*IU*C0(IUU)))
      GO TO 710
701   CONTINUE
      IF (I.EQ.2) GO TO 705
      IF (I.EQ.19) GO TO 708
      VVC0VV=6.0E12*(C0(IU)*(     IU*C0(IU)+I*R*C0(ID))
     *  +C0(ID)*(I*R*C0(IU)+     ID*C0(ID))
     *   -C0(I)*(2.0+I*C0(I)+R*(IU*C0(IUU)+ID*C0(IDD))))
      GO TO 710
708   CONTINUE
      VVC0VV=KVV    *(C0(IU)*(                 I*R*C0(ID))
     *  +C0(ID)*(I*R*C0(IU)+     ID*C0(ID))
     *   -C0(I)*(2.0+I*C0(I)+R*(                ID*C0(IDD))))
C      THE INDEX I WAS 19 JUST NOW
      GO TO 710
705   CONTINUE
      VVC0VV=KVV    *(C0(IU)*(     IU*C0(IU)+I*R*C0(ID))
     *  +C0(ID)*(I*R*C0(IU)                  )
     *   -C0(I)*(2.0+I*C0(I)+R*(IU*C0(IUU)            )))
C     I WAS JUST 2 ABOVE
      GO TO 710
710   CONTINUE
C     C0 AND C0D0T ARE IN MOLE FRACTIONS.
      VVC0VV=VVC0VV*RHO
      C0D0T(I)=(VT1+VT2+VT3+VVC0VV+C0ADD)/U
C     WRITE (6,44) MZ,Z,ID,C0(I),C0D0T(I),VT1,VT2,VT3,VVC0VV,C0ADD
400   CONTINUE
      RETURN
      END
C     DATA DECK
      0.15900E 00 0.50000E 01 0.97000E 14 0.48000E 13 0.48000E 13 0.6000
      0.60000E 13
                  .20            0.001
  0           .01     300.0    2700.0     300.0     100.0
      0.25000E-05 0.25000E-05 0.25000E-05 0.25000E-05 0.25000E-05
      0.25000E-05 0.25000E-05 0.25000E-05 0.25000E-05 0.25000E-05
      0.25000E-05 0.25000E-05 0.25000E-05 0.25000E-05 0.25000E-05
      0.25000E-05 0.10000E-05 0.40000E-06 0.15000E-06 0.60000E-07
```

Figure C-24 Coding for the computer program MIX60